

# POLITECNICO DI TORINO

Department of Structural, Building and Geotechnical Engineering



Master of Science in Civil Engineering

Master Thesis

## *Strategic Infrastructures' Resilience: Case Study of Wireless Telecom Network*

**Advisor:**

Prof. Gian Paolo Cimellaro

**Co-Advisor:**

Ing. Alessandro Cardoni

Dott. Ing. Francesco Malandrino

Dott. Ing. Sebastiano Marasco

**Candidate**

Lucco Borlera Simone



*To my father Piero,  
and his sacrifices*





# Abstract

Telecommunication infrastructures provide essential services to urban communities. During an emergency caused by a seismic event, their functionality is essential to facilitate search and rescue operations. The aim of this study is to introduce a simplified method for assessing the vulnerability of a wireless telecommunication network under seismic action. The case study is a virtual city called Ideal City and part of a larger project on assessing the resilience of vital infrastructure in an urban environment. The wireless network composed of three operators is built starting from information on the real wireless network of the city of Turin. Some simplifications and assumptions are introduced due to the confidentiality of the data, as communications networks are strategic infrastructures. This defines a complete parameter database necessary to describe the various components of the network. Each component is then modeled through equivalent simplified models (SDOF). Once the results of the structural simulations are known, the vulnerability of the individual components is assessed, also considering the interdependence with the built environment that the various elements may have. For example, the BTS on residential buildings will certainly be affected by the behavior of the building under seismic action. Three resilience indices based on failed telecommunication towers, throughput, and number of users per base station were defined and calculated after four different seismic scenarios. It has been found that the topology and vulnerability of base controller stations are key aspects in the resilience of an urban wireless network.

**Keywords:** Wireless Telecom network, cellular network, Resilience, Interoperability, Urban Scale modelling, Telecommunications engineering, Earthquake and Structural engineering, BTS, Python, Strategic Infrastructure, 3G and 4G, Seismic Emergency.

# List of Figures

FIGURE 1-1, A HOME IN GILCHRIST, TEXAS, DESIGNED TO RESIST FLOOD WATERS SURVIVED HURRICANE IKE IN 2008 .....	2
FIGURE 1-2, CITY'S INFRASTRUCTURES.....	3
FIGURE 1-3, SCHEMATIC REPRESENTATION OF DISASTER RESILIENCE (CIMELLARO, REINHORN ET AL. 2010). ....	4
FIGURE 1-4, CRITICAL INFRASTRUCTURES FOR A CITY AND A COMMUNITY .....	7
FIGURE 2-1, IDEALIZATION OF A VIRTUAL CITY MODEL.....	11
FIGURE 2-2, IDEAL CITY' MODELS DEVELOPED .....	13
FIGURE 2-3, IDEAL CITY'S LAYER OF BUILT ENVIRONMENT (MARASCO, CARDONI ET AL. 2020) .....	15
FIGURE 2-4, TRANSPORT NETWORK' LAYER (RTN) (MARASCO, CARDONI ET AL. 2020) .....	17
FIGURE 2-5, ELECTRICAL INFRASTRUCTURE' LAYER (PG) (MARASCO, CARDONI ET AL. 2020) .....	19
FIGURE 2-6, WATER DISTRIBUTION NETWORK' LAYER (WDN) (MARASCO, CARDONI ET AL. 2020).....	20
FIGURE 2-7, VIEW OF THE MAIN SCREEN OF THE PLATFORM (MARASCO, CARDONI ET AL. 2020) .....	22
FIGURE 3-1, DIFFERENT TYPES OF TELECOMMUNICATION NETWORKS CONNECTED TO EACH OTHER .....	24
FIGURE 3-2, POPULATION COVERAGE BY TYPE OF MOBILE NETWORK, 2020, ITU SOURCE .....	24
FIGURE 3-3, PRINCIPAL COMPONENT OF PRINCIPAL TYPES OF TELECOMMUNICATION NETWORK.....	25
FIGURE 3-4, 33 THOMAS STREET INTERNATIONAL GATEWAY LOCATED IN NYC,.....	26
FIGURE 3-5, THE AT&T MADISON COMPLEX TANDEM OFFICE IS A 17-STORY, BUILDING IN LOS ANGELES, CALIFORNIA.....	27
FIGURE 3-6, HARBOUR CENTRE IS LOCATED AT 555 WEST HASTINGS STREET IN DOWNTOWN VANCOUVER. ....	27
FIGURE 3-7, EXAMPLE OF THE COMPONENTS WITHIN A LOCAL EXCHANGE .....	27
FIGURE 3-8, EXAMPLE OF CROSS CONNECTION BOX .....	28
FIGURE 3-9, HIERARCHY IN THE FIXED TELECOMMUNICATIONS NETWORK.....	28
FIGURE 3-10 AN EXAMPLE OF A MSC LOCATED IN GRODZISK MAZOWIECK,.....	30
FIGURE 3-11 EXAMPLE OF MSC SERVICE ROOM .....	30
FIGURE 3-12 EXAMPLE OF MSC SERVER ROOM.....	30
FIGURE 3-13 AN EXAMPLE OF A BSC LOCATED IN TURIN CITY.....	31
FIGURE 3-14 AN EXAMPLE OF BSC LOCATED IN SPAIN INTO THE CITY OF BARCELONA .....	31
FIGURE 3-15, EXAMPLE OF ROOF TOP BTS .....	33
FIGURE 3-16, EXAMPLE OF RAW LAND BTS .....	33
FIGURE 3-17, EXAMPLE OF LATTICE TOWER .....	33
FIGURE 3-18, EXAMPLE OF MONOPOLE TOWER .....	33
FIGURE 3-19, EXAMPLE OF PYRAMID LATTICE TOWER .....	33
FIGURE 3-20, EXAMPLE OF 4 SIDES LATTICE TOWER.....	33
FIGURE 3-21, EXAMPLE OF 3 SIDES LATTICE TOWER.....	33
FIGURE 3-22, EXAMPLE OF POLYGONAL MONOPOLE TOWER.....	33
FIGURE 3-23, EXAMPLE OF FLANGED MONOPOLE TOWER .....	33
FIGURE 3-24, AN OVERVIEW OF THE ELEMENTS OF A BTS.....	34
FIGURE 3-25, SYSTEM ARCHITECTURE FOR A WIRELESS NETWORK.....	35
FIGURE 3-26, DEFINITION OF WHAT IS A ACCESS NETWORK AND A CORE NETWORK IN A CELLULAR NETWORK .....	36
FIGURE 3-27, NETWORK' TOPOLOGY .....	38
FIGURE 3-28, STAR TYPE FOR THE LINK BETWEEN BTS-BSC .....	39
FIGURE 3-29, ASSIGNMENT OF THE PORTIONS OF BAND 1 FOR THE DIFFERENT MNOS .....	41
FIGURE 3-30, EXAMPLE OF A COVERAGE AREA OF A REAL CELL .....	42
FIGURE 3-31, SCHEMATIZATION OF THE COVERAGE OF A CELL.....	42
FIGURE 3-32, EXAMPLE OF THE REUSE FREQUENCY .....	43

FIGURE 3-33, CELL SECTORING EXAMPLE WITH 120° SECTORIAL ANTENNAS .....	43
FIGURE 3-34, TRI-CELLULAR SECTORING EXAMPLE .....	44
FIGURE 3-35, SCALING THE CELL FROM MACRO CELL TO PICO CELL.....	44
FIGURE 3-36, ILLUSTRATION ABOUT WHAT IT IS D .....	46
FIGURE 3-37, CELL WITH THE SAME FREQUENCIES .....	47
FIGURE 3-38, VISUALIZATION ABOUT THE CALCULATION OF THE CRITICAL DISTANCE .....	47
FIGURE 3-39, A SECTOR BTS CAN COVER THREE CELLS.....	48
FIGURE 3-40, ACCESS METHODS.....	50
FIGURE 3-41, EXAMPLE OF SATELLITE GROUND STATION, CENTRO SPAZIALE DEL FUCINO .....	51
FIGURE 3-42, EXAMPLE OF PARABOLIC ANTENNA .....	51
FIGURE 3-43, EXAMPLE OF TELECOMMUNICATION SATELLITE .....	52
FIGURE 3-44, DISASTERS THAT CAN DAMAGE THE NETWORK.....	52
FIGURE 3-45, INCREASING THE RESILIENCE FOR THE NETWORK TOPOLOGY (ALVES, RODRIGUES ET AL. 2017) .....	54
FIGURE 3-46, BASE STATION CONTROLL IN ONAGAWA DESTROYED BY EARTHQUAKE-TSUNAMI, JAPAN 2011.....	54
FIGURE 3-47, BSC COMPONENTS DAMAGE LOCATED IN IWATE PREFECTURE AFTER JAPAN 2011 EARTHQUAKE.....	54
FIGURE 3-48, TRAFFIC NETWORK INCREASE AFTER THE EARTHQUAKE JAPAN 2011 .....	55
FIGURE 3-49, CELL SITE DESTROYED BY THE TSUNAMI IN RIKUZENTAKA .....	55
FIGURE 3-50, A COLLAPSED TOWER OF A BASE STATION LOCATED IN THE KARAKUWA PENINSULA. ....	55
FIGURE 4-1, AN OVERVIEW ON THE CELLMAPPER.COM SITE .....	58
FIGURE 4-2, A ZOOM ON THE CELLMAPPER.COM SITE' MAP .....	58
FIGURE 4-3, MAP FORM GEOPORTALE SITE.....	58
FIGURE 4-4, EXAMPLE OF LOCATION KNOWLADGE ABOUT BTS .....	59
FIGURE 4-5, BTS WITH MANY LEVEL OF WORK FREQUENCY RANGE .....	61
FIGURE 4-6, GROUPING OF BTS, WHICH HAVE BEEN VERIFIED IN PERSON.....	63
FIGURE 4-7, PROSPECT EXAMPLE OF RAW LAND TOWER .....	64
FIGURE 4-8, SECTION EXAMPLE OF LATTICE RAW LAND TOWER.....	64
FIGURE 4-9, PRINCIPAL STRUCTURAL CONFIGURATION FOR TELECOM TOWERS .....	67
FIGURE 4-10, ELEMENTS HIERARCHY FOR THE TOWERS .....	68
FIGURE 4-11, TYPICAL TYPES OF FOUNDATION USED FOR TELECOM TOWERS .....	71
FIGURE 4-12, TYPICAL TYPES OF ANCHOR SYSTEM USED FOR ROOF TOP TELECOM TOWERS .....	71
FIGURE 4-13, EXAMPLES OF TYPICAL CONNECTIONS FOR TELECOM TOWERS .....	72
FIGURE 4-14, DIFFERENT TYPES OF PORTAL BASE FOR LATTICE TOWERS.....	72
FIGURE 4-15, GALVANIZATION PROCESS THAT THE ELEMENTS THAT COMPOSE A TOWER HAVE TO NEED TO DO .....	73
FIGURE 4-16 VISUALIZATION OF THE WINDOW FROM CELLMAPPER.COM .....	75
FIGURE 4-17, ADMINISTRATIVE DISTRICTS AND NEIGHBORHOODS OF <i>IDEAL CITY</i> (BASED ON .....	76
FIGURE 4-18, PHOTO TAKEN FORM THE OUTSIDE AND FROM SATELLITE FOR THE BSC LOCATED IN THE FIGURE 4-16 .....	77
FIGURE 4-19, EXAMPLE OF LOCATION KNOWLADGE ABOUT BSC .....	77
FIGURE 4-20, , EXTERNAL WALL TYPE BY CORRADO ET. AL. (2012) .....	79
FIGURE 4-21, FLOOR TYPES BY CORRADO ET. AL. (2012) .....	79
FIGURE 4-22, VORONOI'S AREA SUDDIVISION ILLUSTRATION (YU AND KIM 2013) .....	80
FIGURE 4-23, BUILDING PORTFOLIO DEVELOPED BY NOORI, MARASCO ET. AL. (2017) .....	81
FIGURE 4-24, USER CLUSTER DEFINED FOR IDEAL CITY .....	82
FIGURE 4-25, MARKET SHARE BY MNO AGCOM (2020) .....	83
FIGURE 4-26, ILLUSTRATION SHOWING SOME CHECKS WITH PICTURES TAKEN IN PERSON OF SOME BTS AND BSC.....	85
FIGURE 4-27, SUMMARY DIAGRAM FOR THE STRUCTURAL CONFIGURATIONS OF THE RAWLAND TOWERS.....	87
FIGURE 4-28, SUMMARY DIAGRAM FOR THE STRUCTURAL CONFIGURATIONS OF THE ROOFTOP TOWERS.....	87
FIGURE 4-29, SCHEMATIZATION OF RAWLAND MONOPOLE TOWER .....	90

FIGURE 4-30, ILLUSTRATION OF THE LOADS CONCERNED THE TOWER .....	96
FIGURE 4-31, SUMMARY DIAGRAM OF THE STRUCTURAL AND NON-STRUCTURAL PARAMETERS THAT CHARACTERIZE THE RAWLAND TOWERS .....	98
FIGURE 4-32, SUMMARY DIAGRAM OF THE STRUCTURAL AND NON-STRUCTURAL PARAMETERS THAT CHARACTERIZE THE ROOFTOP TOWERS .....	99
FIGURE 4-33, EXTRAPOLATION OF THE SHAPEFILE WITH ATTRIBUTE TABLE OF TURIN BUILDINGS .....	100
FIGURE 4-34, SUMMARY OF THE VARIOUS VALUES OF THE PARAMETERS TO CHARACTERIZE THE REINFORCED CONCRETE BUILDINGS DEFINED BY MARASCO ET. TO THE. (2018) .....	101
FIGURE 4-35, VORONOI'S SUDDIVISION FOR BSC .....	102
FIGURE 4-36, RAW DATA ABOUT THE BSC FROM QGIS .....	104
FIGURE 4-37, ILLUSTRATION OF THE STAR TOPOLOGY BETWEEN BTS AND BSC.....	106
FIGURE 4-38, SCHEME OF FAT-TREE TOPOLOGY .....	106
FIGURE 4-39, STAR LINKS BETWEEN THE FIRST MNO'S BTS AND THE BSC .....	107
FIGURE 4-40, STAR LINKS BETWEEN ALL THE BTS AND THE BSC.....	108
FIGURE 4-41, HIERARCHICAL LEVELS FOR THE BSCs FOR THE CONSTRUCTION OF THE TOPOLOGY BETWEEN THEM .....	109
FIGURE 4-42, LINK OBTAIN BETWEEN THE BSCs USING THE FAT-TREE TOPOLOGY .....	109
FIGURE 4-43, SUMMARY DIAGRAM OF THE NETWORK TOPOLOGY.....	110
FIGURE 4-44, SUMMARY MAP OF NETWORK'S TOPOLOGY.....	110
FIGURE 4-45, SCHEME FOR A FRF EQUAL TO ONE .....	111
FIGURE 5-1, PATH LOSS'S FREE SPACE MODEL .....	114
FIGURE 5-2, PATH LOSS AS DISTANCE AND FREQUENCY CHANGE .....	114
FIGURE 5-3, EXAMPLES OF LOS AND NLOS PATHS.....	117
FIGURE 5-4, CASES BY ITU MODEL.....	118
FIGURE 5-5, PATH LOSS FOR A CLUSTER USER RELATIVE TO THE BTS OF THE MACRO CELL TYPE OF THE FIRST PROVIDER .....	120
FIGURE 5-6, PATH LOSS FOR A CLUSTER USER RELATIVE TO THE BTS OF THE MICRO CELL TYPE OF THE FIRST PROVIDER .....	120
FIGURE 5-7, RSSI FOR A CLUSTER USER RELATIVE TO THE BTS OF THE MACRO CELL TYPE OF THE FIRST PROVIDER .....	121
FIGURE 5-8, RSSI FOR A CLUSTER USER RELATIVE TO THE BTS OF THE MICRO CELL TYPE OF THE FIRST PROVIDER .....	122
FIGURE 5-9, EXAMPLE OF INTERFERENCE FOR A USER CLUSTER - BTS PAIR .....	123
FIGURE 5-10, GENERAL ILLUSTRATION OF THE SINR'S TREND .....	124
FIGURE 5-11, SINR FOR CLUSTER USER SELECTED FROM BTS MACRO-CELL.....	125
FIGURE 5-12, SINR FOR CLUSTER USER SELECTED FROM BTS MICRO-CELL.....	125
FIGURE 5-13, STRUCTURE OF A RESOURCE BLOCK (RB).....	127
FIGURE 5-14, SCHEMATIZATION OF CHANNEL BANDWIDTH .....	127
FIGURE 5-15, BLOCK DIAGRAM OF THE OFDM MODULATION.....	129
FIGURE 5-16, .....	130
FIGURE 5-17, ILLUSTRATION OF THE DIFFERENCE BETWEEN FDD AND TDD MODE .....	130
FIGURE 5-18, DIFFERENT MODULATIONS.....	132
FIGURE 5-19, ARTISTIC RAPRESENTATION OF THE MODULATION WITH RESPECT THE DISTANCE THAT THERE IS BETWEEN BTS AND USER.....	132
FIGURE 5-20, AN EXTRAPOLATION OF TABLES TO DEFINE THE $N_{PRB}$ .....	133
FIGURE 5-21, DIFFERENT TYPOLOGIES OF TECHNIQUES TO IMPROVE OF THE BITS TRANSMITTED .....	134
FIGURE 5-22, EXCHANGE OF INFORMATION BETWEEN BTS AND USER .....	134
FIGURE 5-23, EXPERIMENTAL CURVES FOR EACH MODULATION SCHEME .....	135
FIGURE 5-24, THR-SINR RESULT CURVE .....	136
FIGURE 5-25, THR VALUE FOR USER CLUSTER GIVEN BY THE FIRST MNO FOR A PORTION OF IDEAL CITY' DOWNTOWN.....	136
FIGURE 5-26, THR BY MNO 1 FOR WHOLE USER CLUSTER.....	137
FIGURE 6-1, MDOF MODEL FOR RC BUILDINGS USED TO DEFINE THE PHYSICAL PROPERTIES .....	140

FIGURE 6-2, PROPOSED FOUR-LINEAR BACKBONE CURVE, REPRESENTATIVE OF THE GLOBAL .....	141
FIGURE 6-3, GLOBAL (A) AND LOCAL (B) COLLAPSE MECHANISM OF A RC BUILDING (MARASCO AND CIMELLARO 2018).....	143
FIGURE 6-4, ILLUSTRATIVE SCHEME OF THE PHYSICAL ASSUMPTIONS (MARASCO AND CIMELLARO 2018).....	145
FIGURE 6-5, INPUT AND OUTPUT DATA FLOW (MARASCO AND CIMELLARO 2018).....	146
FIGURE 6-6, PROPOSED PHYSICAL BUILDING MODEL BY (MARASCO AND CIMELLARO 2018) FOR THE BUILDINGS OF THE IDEAL CITY .....	147
FIGURE 6-7, SDOF MODEL FOR SUPPORT TOWER USED TO DEFINE THE PHYSICAL PROPERTIES.....	148
FIGURE 6-8, , PROPOSED TRI-LINEAR BACKBONE CURVE, REPRESENTATIVE OF THE GLOBAL CAPACITY OF THE BTS TOWERS .....	148
FIGURE 6-9, APPROXIMATION OF THE BEHAVIOR OF THE TOWERS IN A CANTILEVER BEAM.....	150
FIGURE 6-10, GENERALIZED CANTILEVER SYSTEM EQUAL TO THE TOWER (CIMELLARO AND MARASCO 2018).....	151
FIGURE 6-11, EXAMPLE OF CROSS SECTION OF A LATTICE TOWER TO CALCULATE THE INERTIA OF THE SECTION.....	152
FIGURE 6-12, EXAMPLE OF PUSHOVER ANALYSIS OF LATTICE TOWER WITH THE FORMATION OF THE FIRST HINGES, THAT IT CORRESPONDS TO THE FIRST POINT OF THE CAPACITY CURVE.....	154
FIGURE 6-13, PROPOSED PHYSICAL MODEL FOR THE SUPPORT TOWERS OF THE BTSS .....	155
FIGURE 6-14, CASE STUDIES .....	156
FIGURE 6-15, EXAMPLES OF THE SECTIONS USED TO BUILD THE TELECOM TOWERS OF THE CASE STUDIES .....	157
FIGURE 6-16, SET UP OF THE HINGES FOR THE LEGS OF THE TOWER.....	157
FIGURE 6-17, CAPACITY CURVE OBTAINED FOR RAWLAND LATTICE TOWER CASE STUDY .....	158
FIGURE 6-18, CAPACITY CURVE OBTAINED FOR RAWLAND MONOPOLE TOWER CASE STUDY .....	158
FIGURE 6-19, EXAMPLES OF DIFFERENT TIME STEPS OF THE HINGES FOR THE LATTICE TOWER CASE STUDY.....	159
FIGURE 6-20, DEFINITION OF THE CONDITION ON THE CAPACITY CURVE .....	159
FIGURE 6-21, COMPARISON BETWEEN THE CAPACITY CURVES FROM SAP2000 FEM MODEL AND SDOF EQUIVALENT MODEL FOR THE RAWLAND LATTICE TOWER .....	160
FIGURE 6-22, COMPARISON BETWEEN THE CAPACITY CURVES FROM SAP2000 FEM MODEL AND SDOF EQUIVALENT MODEL FOR THE RAWLAND MONOPOLE TOWER.....	160
FIGURE 8-1, DAMAGE STATES FROM HAZUS (FEMA 2011) .....	163
FIGURE 8-2, WINDOW TO SET THE TIME HISTORY ANALYSIS IN SAP2000 (CSI. 2018) .....	164
FIGURE 8-3, FROM 3D MDOF MODELS TO LINKS SDOF ELEMENTS .....	165
FIGURE 8-4, LINKS ELEMENTS FOR BTS TOWERS (RAWLAND TOWERS + ROOFTOP TOWERS) DISCRETIZED BY THE HEIGHT .....	165
FIGURE 8-5, EDITING DATABASE FOR ASSIGNING COORDINATES TO LINKS ELEMENTS IN SAP2000 (CSI. 2018) .....	166
FIGURE 8-6, GENERAL SETTING WINDOW TO DEFINE THE SDOF LINKS (CSI. 2018) .....	166
FIGURE 8-7, SETTING PHYSICAL PROPERTY WINDOW FOR THE SDOF LINKS FOR THE BTS TOWERS.....	167
FIGURE 8-8, SCHEMATIZATION OF THE TIME HISTORY APPLICATION FOR RAWLAND TOWERS.....	168
FIGURE 8-9, ILLUSTRATION OF SOME NSE CONSIDERED FOR A BUILDING (MURTY, GOSWAMI ET AL. 2012).....	168
FIGURE 8-10, DECOMPOSITION OF THE STRUCTURE INTO THE STRUCTURAL AND NON-STRUCTURAL COMPONENT .....	169
FIGURE 8-11, VARIOUS VIBRATIONS AND INTERACTIONS BETWEEN SEs AND NSE (MURTY, GOSWAMI ET AL. 2012).....	170
FIGURE 8-12, SCHEMATIZATION OF THE TIME HISTORY APPLICATION FOR ROOFTOP TOWERS.....	170
FIGURE 8-13, EXAMPLES OF THE HISTORY OF TOP DISPLACEMENT FOR A LINK ELEMENT THAT RAPRESENTS A RAWLAND TOWER IN THE NORTHRIDGE CASE .....	171
FIGURE 8-14, VIEW EXAMPLE OF THE WINDOW WITH THE TOP ABSOLUTE MAXIMUM AND MINIMUM DISPLACEMENT FOR DIRECTION 1 FOR THE RAWLAND TOWERS.....	171
FIGURE 8-15, ELASTIC AND PLASTIC DISPLACEMENTS DISTRIBUTIONS (MARASCO AND CIMELLARO 2018).....	172
FIGURE 8-16, PROCEDURE PROPOSED BY (MARASCO AND CIMELLARO 2018) TO ASSESS THE DAMAGE TO THE BUILDINGS OF THE IDEAL CITY .....	173

FIGURE 8-17, DEFINITION OF DAMAGE LEVELS FOR TOWERS BASED ON THE CAPACITY CURVE (CIMELLARO, DOMANESCHI ET AL. 2017) .....	174
FIGURE 8-18, PROCEDURE PROPOSED TO ASSESS THE DAMAGE TO THE TELECOM TOWERS OF THE IDEAL CITY .	174
FIGURE 9-1, OUTLINE OF THE POSSIBLE SCENARIOS THAT CAN TAKE A ROOFTOP BTS OUT OF SERVICE .....	176
FIGURE 9-2, OUTLINE OF THE POSSIBLE SCENARIOS THAT CAN TAKE A RAWLAND BTS OUT OF SERVICE .....	177
FIGURE 9-3, LOCALITAZION OF THE EPICENTER FOR THE SIMULATIONS .....	180
FIGURE 9-4, 3D DAMAGE VISUALIZATION OF THE IDEAL CITY DOWNTOWN AFTER FIRST SCENARIO .....	181
FIGURE 9-5, DAMAGE STATE FOR THE BUILDINGS FOR THE FIRST SCENARIO BASED ON THE YEAR OF COSTRUCTION .....	181
FIGURE 9-6 BSC' DAMAGE DISTRIBUTION WITHIN <i>IDEAL CITY</i> FOR EL CENTRO SCENARIO .....	182
FIGURE 9-7, BSC STATE AFTER EL CENTRO SCENARIO .....	182
FIGURE 9-8, CONCEPT OF WHY SOME BSCs ARE OUT OF ORDER EVEN THOUGH THEIR STRUCTURE SUFFERS MINOR DAMAGE .....	183
FIGURE 9-9, DAMAGE STATE FOR THE RAW LAND TOWERS FOR THE FIRST SCENARIO.....	183
FIGURE 9-10 DAMAGE STATE FOR THE ROOF TOP TOWERS FOR THE FIRST SCENARIO .....	184
FIGURE 9-11, BTS OUT OF ORDER FOR THE MNO1 FOR THE FIRST SCENARIO.....	184
FIGURE 9-12, BTS OUT OF ORDER FOR MNO2 FOR THE FIRST SCENARIO .....	185
FIGURE 9-13, BTS OUT OF ORDER FOR MNO3 FOR THE FIRST SCENARIO .....	185
FIGURE 9-14, ABSTRACT OF THE DAMAGED BTS VALUES FOR EACH CONDITION FOR THE FIRST SCENARIO .....	186
FIGURE 9-15, THR VALUE FOR USER CLUSTER GIVEN BY THE FIRST MNO FOR A PORTION OF IDEAL CITY' DOWNTOWN AFTER FIRST CASE SCENARIO .....	186
FIGURE 9-16, 3D DAMAGE VISUALIZATION OF THE IDEAL CITY DOWNTOWN FOR THE SECOND SCENARIO.....	187
FIGURE 9-17, 3D DAMAGE VISUALIZATION OF THE IDEAL CITY FOR THE SECOND SCENARIO .....	187
FIGURE 9-18, DAMAGE STATE FOR THE BUILDINGS FOR THE SECOND SCENARIO BASED ON THE YEAR OF COSTRUCTION .....	188
FIGURE 9-19, BSC' DAMAGE DISTRIBUTION WITHIN IDEAL CITY FOR KOBE SCENARIO .....	188
FIGURE 9-20, BSC STATE AFTER KOBE SCENARIO .....	189
FIGURE 9-21, DAMAGE STATE FOR THE RAW LAND TOWERS FOR SECOND SCENARIO .....	189
FIGURE 9-22, DAMAGE STATE FOR THE ROOF TOP TOWERS FOR SECOND SCENARIO .....	190
FIGURE 9-23, BTS OUT OF ORDER FOR THE MNO1 FOR SECOND SCENARIO.....	190
FIGURE 9-24, BTS OUT OF ORDER FOR THE MNO2 FOR SECOND SCENARIO.....	191
FIGURE 9-25, BTS OUT OF ORDER FOR THE MNO3 FOR SECOND SCENARIO.....	191
FIGURE 9-26, ABSTRACT OF THE DAMAGED BTS VALUES FOR EACH CONDITION FOR THE SECOND SCENARIO .....	192
FIGURE 9-27, THR VALUE FOR USER CLUSTER GIVEN BY THE FIRST MNO FOR A PORTION OF IDEAL CITY' DOWNTOWN AFTER SECOND CASE SCENARIO.....	192
FIGURE 9-28, 3D DAMAGE VISUALIZATION OF THE DOWNTOWN FOR THE THIRD SCENARIO WITH PYTHON TOOL .....	193
FIGURE 9-29, 3D DAMAGE VISUALIZATION OF A BUILDING WITH A TOWER FOR THE THIRD SCENARIO WITH PYTHON TOOL .....	193
FIGURE 9-30, DAMAGE STATE FOR THE BUILDINGS FOR THE THIRD SCENARIO BASED ON THE YEAR OF COSTRUCTION .....	194
FIGURE 9-31, BSC' DAMAGE DISTRIBUTION WITHIN IDEAL CITY FOR HACHINOHE SCENARIO .....	194
FIGURE 9-32, BSC STATE AFTER HACHINOHE SCENARIO.....	195
FIGURE 9-33, DAMAGE STATE FOR THE RAW LAND TOWERS FOR THIRD SCENARIO .....	195
FIGURE 9-34, DAMAGE STATE FOR THE ROOF TOP TOWERS FOR THIRD SCENARIO .....	196
FIGURE 9-35, BTS OUT OF ORDER FOR THE MNO1 FOR THIRD SCENARIO .....	196
FIGURE 9-36, BTS OUT OF ORDER FOR THE MNO2 FOR THIRD SCENARIO .....	197
FIGURE 9-37, BTS OUT OF ORDER FOR THE MNO3 FOR THIRD SCENARIO .....	197
FIGURE 9-38, ABSTRACT OF THE DAMAGED BTS VALUES FOR EACH CONDITION FOR THE THIRD SCENARIO .....	198
FIGURE 9-39, THR VALUE FOR USER CLUSTER GIVEN BY THE FIRST MNO FOR A PORTION OF IDEAL CITY' DOWNTOWN AFTER THIRD CASE SCENARIO .....	198

FIGURE 9-40, 3D DAMAGE VISUALIZATION OF THE DOWNTOWN FOR THE FOURTH SCENARIO WITH PYTHON TOOL .....	199
FIGURE 9-41, 3D DAMAGE VISUALIZATION OF THE SOUTH OF THE CITY FOR THE FORUTH SCENARIO WITH PYTHON TOOL .....	199
FIGURE 9-42, DAMAGE STATE FOR THE BUILDINGS FOR THE FOURTH SCENARIO BASED ON THE YEAR OF COSTRUCTION .....	200
FIGURE 9-43, BSC' DAMAGE DISTRIBUTION WITHIN IDEAL CITY FOR NORTHRIDGE SCENARIO .....	200
FIGURE 9-44, BSC STATE AFTER NORTHRIDGE SCENARIO .....	201
FIGURE 9-45, DAMAGE STATE FOR THE RAW LAND TOWERS FOR FOURTH SCENARIO .....	201
FIGURE 9-46, DAMAGE STATE FOR THE ROOF TOP TOWERS FOR FOURTH SCENARIO .....	202
FIGURE 9-47, BTS OUT OF ORDER FOR THE MNO1 FOR FOURTH SCENARIO.....	202
FIGURE 9-48, BTS OUT OF ORDER FOR THE MNO2 FOR FOURTH SCENARIO.....	203
FIGURE 9-49, BTS OUT OF ORDER FOR THE MNO3 FOR FOURTH SCENARIO.....	203
FIGURE 9-50, ABSTRACT OF THE DAMAGED BTS VALUES FOR EACH CONDITION FOR THE FOURTH SCENARIO .....	204
FIGURE 9-51, THR VALUE FOR USER CLUSTER GIVEN BY THE FIRST MNO FOR A PORTION OF IDEAL CITY <sup>1</sup> DOWNTOWN AFTER FOURTH CASE SCENARIO.....	204
FIGURE 10-1, SUMMARY DIAGRAM OF THE ANALYSIS FLOW .....	208

## List of Tables

TABLE 2-1, NUMBER OF BUILDINGS PER CATEGORY .....	14
TABLE 3-1, FEAUTERS OF BAND FOR MOBILE NETWORK .....	40
TABLE 3-2, VARIATION OF PARAMETER K AS A FUNCTION OF THE NUMBER OF CELLS PER ROW I AND THE NUMBER OF CELLS PER COLUMN J .....	46
TABLE 4-1, TOTAL BTS SELECTED BASED ON LOCATION FOR IDEAL CITY PROJECT .....	59
TABLE 4-2, ROOF TOP AND RAW LAND BTS BY EACH MNO.....	61
TABLE 4-3, BTS SUBDIVIDED BASED ON THE TYPE OF COVERAGE FOR EACH MNO .....	62
TABLE 4-4, SUBDIVISION BASED ON TYPE OF STRUCTURE FOR THE RAW LAND AND ROOF TOP TOWER.....	65
TABLE 4-5, SUBDIVISION OF THE TOWERS ON THE BASIS OF THE LOCATION AND THE TYPE OF STRUCTURE FOR EACH OPERATOR....	65
TABLE 4-6, TABLE 3.1 EN 1993-1-1: 2005 STRUCTURAL STEELS MECHANICAL CHARACTERISTICS.....	67
TABLE 4-7, TYPICAL SECTIONS USED FOR MUSTS AND TOWERS FORM EN 1993-3-1.....	69
TABLE 4-8, , TYPICAL HORIZONTAL BRACING SYSTEMS FOR TOWERS FROM EN 1993-3-1 .....	70
TABLE 4-9, , TYPICAL BRACING SYSTEMS FOR TOWERS FROM EN 1993-3-1 .....	70
TABLE 4-10, RELIABILITY CLASS TO ESTIMATE THE PARTIAL FACTORS FOR THE LOAD FOR TELECOM TOWERS.....	74
TABLE 4-11, PARTIAL FACTORS FOR THE ACTIONS FOR THE TOWERS .....	74
TABLE 4-12, GEOMETRICAL PARAMETERS RANGE FOR EACH STRUCTURAL CONFIGURATION OF RAWLAND TOWERS.....	88
TABLE 4-13, GEOMETRICAL PARAMETERS RANGE FOR EACH STRUCTURAL CONFIGURATION OF ROOFTOP TOWERS.....	88
TABLE 4-14, MECHANICAL PARAMETERS' CLASSES OF THE RAWLAND TOWERS.....	88
TABLE 4-15, MECHANICAL PARAMETERS' CLASSES OF THE ROOFTOP TOWERS.....	88
TABLE 4-16, BOTTOM AND TOP DIAMETER BASED ON THE HEIGHT OF THE MONOPOLE TOWER .....	90
TABLE 4-17, PRIMARY SECTIONS USED FOR RAWLAND TOWERS .....	91
TABLE 4-18, SECONDARY AND TERTIARY SECTIONS USED FOR RAWLAND TOWERS .....	91

TABLE 4-19, PRIMARY SECTIONS USED FOR ROOFTOP TOWER .....	91
TABLE 4-20, SECONDARY AND TERTIARY SECTIONS USED FOR ROOFTOP TOWERS .....	92
TABLE 4-21, PRIMARY VERTICAL BRACING USED FOR RAWLAND TOWERS.....	92
TABLE 4-22, SECONDARY VERTICAL BRACING USED FOR RAWLAND TOWERS.....	93
TABLE 4-23, HORIZONTAL BRACING USED FOR RAWLAND TOWERS.....	93
TABLE 4-24, PRIMARY VERTICAL BRACING USED FOR ROOFTOP TOWERS .....	94
TABLE 4-25, SECONDARY VERTICAL BRACING USED FOR ROOFTOP TOWERS.....	94
TABLE 4-26, HORIZONTAL BRACING USED FOR ROOFTOP TOWERS.....	94
TABLE 4-27, TYPE OF FONDATIONS SELECTED FOR RAWLAND TOWERS .....	95
TABLE 4-28, TYPE OF ANCHOR SYSTEMSSELECTED FOR RAWLAND TOWERS .....	95
TABLE 4-29, CONNECTION TYPES USED TO DESCRIBE THE RWLAND AND ROOFTOP TOWERS.....	96
TABLE 4-30, PARTIAL FACTORS FOR LOADS .....	97
TABLE 4-31, NUMBER OF BTS MANAGE BY EACH BSC FOR EACH MNO .....	103
TABLE 4-32, HIERARCHICAL LEVEL FOR BSCs.....	104
TABLE 5-1, CLASSIFICATION OF SIGNAL STRENGTH BASED ON RSSI .....	122
TABLE 5-2, CLASSIFICATION OF THE SIGNAL STRENGTH BASED ON SINR .....	126
TABLE 5-3, CHANNEL CHARATERISTICS BASED ON BW .....	127
TABLE 5-4, FEATURES OF THE ALL BAND USED IN WIRELESS COMMUNICATION .....	128
TABLE 5-5, MODULATIONS AND CODE RATE BASED ON CQI VALUE .....	131
TABLE 5-6, MCS INDEX AND TBS INDEX VALUES .....	133
TABLE 8-1, THRESHOLD VALUES OF INTER-STORY DRIFT PROPOSED BY GHOBARAH (2004) (MARASCO AND CIMELLARO 2018).....	172
TABLE 8-2, DAMAGE CRITERIA FOR THE TOWERS.....	174
TABLE 9-1, CHARACTERISTICS OF THE FOUR SCENARIOS SELECTED .....	179
TABLE 9-2, RESULTS FOR THE $R_{TOW}$ RESILIENCE INDEX .....	205
TABLE 9-3, WEIGHTED MEAN THROUGHPUT IN NORMAL CONDITION FOR EACH MNO .....	206
TABLE 9-4, WEIGHTED MEAN THROUGHPUT FOR EACH SCENARIO AND FOR EACH MNO.....	206
TABLE 9-5, $R_{THR}$ VALUES .....	206
TABLE 9-6, USERS PER BTS FOR EACH MNO IN NORMAL CONDITION .....	207
TABLE 9-7, USERS PER BTS FOR EACH MNO AFTER EACH SCENARIO .....	207
TABLE 9-8, $R_{UE-BTS}$ VALUES .....	207
TABLE 9-9, AVERAGE THROUGHPUT AND NUMBER OF USERS PER BTS AFTER THE COMBINATION OF THE MNO'S NETWORKS...	207



# Contents

Abstract .....	I
List of Figures.....	II
List of Tables.....	VII
Contents.....	IX
1 Outline .....	1
1.1 Introduction .....	1
1.2 The Concept of Resilience.....	2
1.3 Concepts about the Resilience .....	3
1.3.1 Resilience Based Design (RBD).....	3
1.3.2 Dimensions of resilience.....	5
1.3.3 Assessment and measurement of resilience .....	5
1.4 Lifeline Infrastructure.....	6
1.5 Resilience and Telecom Network Infrastructure: State of Art .....	7
2 Virtual simulation models .....	10
2.1 Introduction .....	10
2.2 Literature review .....	11
2.3 Ideal City's Models .....	12
2.4 IDEal reSCUE's Platform.....	21
3 Telecommunication Network .....	23
3.1 Overview.....	23
3.2 Types of Telecom Networks .....	25
3.2.1 Landline Telephone Network.....	25
3.2.2 Wireless cellular Network .....	29
3.2.3 Satellite Network.....	50
3.3 Network' Vulnerability .....	52
4 Design of the Ideal City' Wireless Telecommunication Network.....	56
4.1 Introduction .....	56
4.2 Network's exposed components Database.....	57
4.2.1 Data collection for the Base Transceiver Stations (BTS): .....	57
4.2.2 Data collection for the Base Station Controller (BSC): .....	74
4.2.3 Data collection for the Building Environment:.....	81

4.2.4	Data collection for the Users:.....	81
4.3	Data Processing for the Parameters .....	84
4.3.1	Preparation and assessment for the Base Transceiver Stations' data.....	84
4.3.2	Preparation and assessment for the Base Stations Controller' data:.....	100
4.3.3	Preparation and assessment for the data about the Building Environmental and User Cluster:.....	105
4.4	Network's Topology .....	105
4.4.1	Types of topologies chosen for the network' components.....	105
4.4.2	Data Input to build the network's Topology .....	107
4.4.3	Construction of Network's Topology.....	107
4.5	Assessment of the Frequency Reuse Factor (FRF) for the network .....	111
4.6	Data Output for the Ideal City's wireless network: .....	112
5	Estimate of normal operation of the Wireless Telecom Network .....	113
5.1	Introduction .....	113
5.1.1	Path Loss (PL) .....	113
5.1.2	Free Space Model.....	114
5.1.3	Hata and COST-231 Model.....	114
5.1.4	ITU model .....	116
5.2	Received signal strength indicator (RSSI) .....	121
5.3	Interference (I) and Noise (N) .....	122
5.4	Signal-to-Interference-and-Noise Ratio (SINR).....	124
5.5	Throughput (THR).....	126
6	Physical models to assess the seismic capacity of wireless network's components .....	138
6.1	Introduction .....	138
6.2	Base Stations Controller (BSC)' Modelling: .....	140
6.2.1	Defining the physical properties:.....	141
6.2.2	Managing of the uncertainties: .....	146
6.2.3	Physical modeling of the BSC: .....	146
6.3	Base Transceiver Stations (BTS)' Modelling:.....	147
6.3.1	Defining the physical properties:.....	148
6.3.2	Physical modeling of the BSC: .....	155
6.3.3	Validation of the model:.....	156
6.4	Ideal City Buildings' Modelling:.....	161
7	Seismic Scenario's Features.....	162
7.1	Introduction .....	162

7.2	Definition of a Seismic scenario .....	162
8	Damage assessment .....	163
8.1	Introduction .....	163
8.2	Nonlinear time history analysis .....	164
8.3	Damage Level for the Buildings.....	172
8.4	Damage Level for the BTS.....	173
9	Resilience Indices and Case Studies .....	175
9.1	Introduction .....	175
9.2	Resilience Indices.....	175
9.2.1	BTS Towers Resilience Index ( $R_{TOW}$ ) .....	175
9.2.2	Throughput Resilience Index ( $R_{THR}$ ) .....	177
9.2.3	Serviced Clusters Resilience Index ( $R_{UE-BTS}$ ) .....	178
9.3	Application to the Study Cases and Validation of Resilient Indices .....	179
9.3.1	Characteristics of the four scenarios of the study cases.....	179
9.3.2	Results for the First Scenario: El Centro .....	180
9.3.3	Results for the Second Scenario: Kobe .....	187
9.3.4	Results for the Third Scenario: Hachinohe .....	193
9.3.5	Results for the Fourth Scenario: Northridge.....	199
9.4	Assessment of the Resilience Indices for each scenario .....	205
10	Analysis implementation .....	208
	Conclusion .....	209
	Bibliography .....	I



# I Outline

## I.1 Introduction

The main objective of this research is to define resilience indices on an urban scale for the wireless telecommunication network of the virtual city called Ideal City under some reference seismic scenarios. The choice of analyzing the wireless network in detail and introducing only some concepts for other communication networks is since the wireless network offers greater study interest. For example, the fixed network hardly suffers extensive damage except in extremely disastrous events. Conversely, the vulnerability of the wireless network can be considerable even for disasters with shorter payback times, because the wireless network is closely linked to the built environment in an urban environment such as a city. Chapter 1 introduces the concept of resilience, what is meant by strategic infrastructure and the state of the art concerning the study of the vulnerability of wireless communication networks. Subsequently, what is and what is the project called IDEAL CITY, and the progress of its development are exposed in chapter 2. Several layers concerning other strategic infrastructures have already been developed. This is also to carry out future studies on the interdependence between the various infrastructures and urban environment. After that, chapter 3 is introduced which aims to provide a general overview of the types of telecommunication networks that affect an urban environment and illustrate in detail the main concepts for the wireless network. Once this is done, we move on to the central phase of the work (chapter 4), that of building a database for the wireless network of the virtual city based on the real data available to the wireless network of the city of Turin as the entire Ideal City project is based on the city of Turin, while for the missing information some hypotheses and simplifications proposed by the available literature have been assumed. All the steps of data collection and manipulation take place with codes written in the Python environment. Once the database was finished, each element making up the network was described by a series of parameters of various categories. Chapter 5 explains through a simple model that exploits the Throughput the practical operation of a wireless network and how it is possible to evaluate the connection between the user and the network. The model itself is developed in a Python environment. The next step presents the simplified physical models defined in the literature and used to simulate the global seismic capacity of each single component of the network within urban areas (chapter 6). To test the proposed simulation model, two different simplified seismic scenarios are defined (Chapter 7). Once the seismic input parameters have been defined, Nonlinear time history

analyses are performed through the CSI SAP2000 software. Once the results of the various simulations on the network components were known in Chapter 8, the damage levels were estimated using different methods for the various components. For example, the damage to the buildings was assessed through fragility curves already developed for the Ideal City project, while the other components more expeditious methods based on the comparison of displacements were applied. Finally, in chapter 9 simple resilience indices are presented to evaluate the response of the network to the various scenarios administered.

## 1.2 The Concept of Resilience

The concept of resilience into construction field, was introduced by Thomas Tredgold, in 1818 in England, as a mechanical parameter for a material. The term was used to describe a property in the strength of timber, as beams were bent and deformed to support heavy load (Baho, Allen et al. 2017). The concept of resilience is multi-dimensional, for this involves multiple subjects of various disciplines. In the fields of engineering and construction, the definition of resilience is the ability to absorb or avoid damage without suffering complete failure and is an objective of design, maintenance and restoration for buildings and infrastructure, as well as communities (Heinrichs, Jennings et al. 2013). Though there is a more comprehensive definition is that it is the ability to respond, absorb, and adapt to, as well as recover in a disruptive event, such as earthquake, wildfire, flood, tsunami, hurricane, etc.



Figure 1-1, A home in Gilchrist, Texas, designed to resist flood waters survived Hurricane Ike in

2008

For all these, recently disaster events, we wondered how communities, infrastructures and structures could recover itself from the damage caused by these episodes, and how we can assess their resilience. One of the most consolidated approach is to study the resilience of infrastructural system and the interdependence between different networks like, transports, power, telecommunication, water, etc.



Figure 1-2, City's Infrastructures

In fact, a resilient structure/system/community is expected to be able to resist to an extreme event with minimal damages and functionality disruptions during the event; after the event, it should be able to rapidly recovery its functionality similar to or even better than the pre-event level. The concept of resilience originated from engineering and then gradually applied to other fields. It is related to that of vulnerability. Both terms are specific to the event perturbation, meaning that a system/infrastructure/community may be more vulnerable or less resilient to one event than another one. However, they are not the same. One obvious difference is that vulnerability focuses on the evaluation of system susceptibility in the pre-event phase; resilience emphasizes the dynamic features in the pre-event, during-event, and post-event phases (Sun, Bocchini et al. 2020). So, all of this because the resilience of civil structures, resources and services is the first line of defense for today's modern societies and, resilient societies also have a greater propensity to bounce back after crises: they tend to recover more rapidly and can return to pre-crisis functional levels with greater ease than less resilient societies.

## 1.3 Concepts about the Resilience

### 1.3.1 Resilience Based Design (RBD)

A fast introduction on what resilience is and how to quantify it can be given in accordance with (Cimellaro, Reinhorn et al. 2010) and (Bruneau, Chang et al.

2003), Resilience (R) is defined as a function that indicates the ability to sustain an established level of functionality or performance for a given facility, rescue network or community, for a period defined as the TLC control time. Analytically, *resilience performance index* is defined as:

$$R(\vec{r}) = \int_{t_{OE}}^{t_{OE}+T_{LC}} Q_{TOT}(t)/T_{LC} dt \quad (1-1)$$

where  $Q_{TOT}(t)$  is the global performance function of the considered region;  $T_{LC}$  is the control time of the period of interest that is usually decided by owners, or society (usually is the life cycle, life span of the system etc.);  $t_{OE}$  is the time instant when the event happens;  $\vec{r}$  is the vector defining the geospatial coordinate of the system within the selected region where the resilience index is evaluated (Cimellaro, Reinhorn et al. 2010). The time  $T_{LC}$  includes the building recovery time,  $T_{RE}$  and the business interruption time that is usually smaller compared to the other one. The performance function is the combination of all functionalities related to different facilities, lifelines, etc. for the case when physical infrastructures, resources and services are considered. Schematic representation of disaster resilience is shown in .

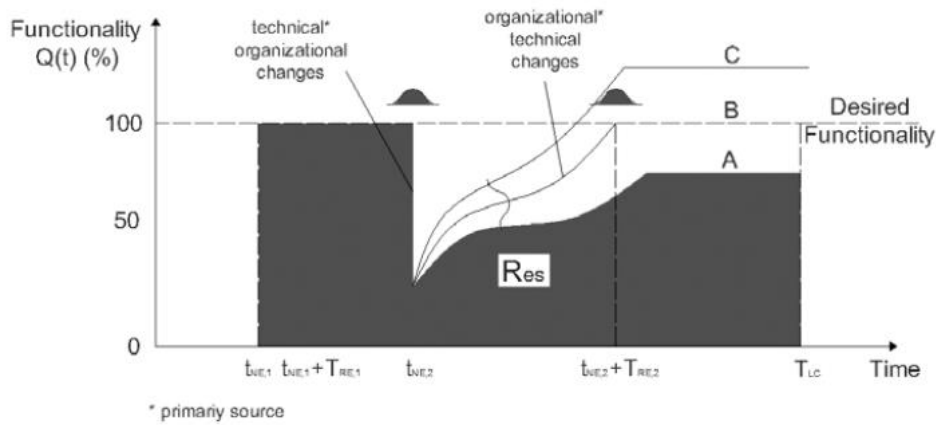


Figure 1-3, Schematic representation of disaster resilience (Cimellaro, Reinhorn et al. 2010).

More information on the concept of resilience and its formulation is illustrated in the study by (Cimellaro, Reinhorn et al. 2010).

Resilience is a dynamic quantity that changes over time and space. It can be applied to engineering, economic, social and institutional infrastructures and can use various geographic scales. The first thing to define resilience is always the spatial scale for which to evaluate it e.g. building, structure, community, city, region, etc.). The second step is to define the temporal scale (short term, etc.).



### 1.3.2 Dimensions of resilience

The Researchers at the MCEER have identified four dimensions along which resilience can be improved. These are robustness, resourcefulness, redundancy, and rapidity (Cimellaro, Reinhorn et al. 2010).

Robustness referring to engineering systems is, “the ability of elements, systems or other units of analysis to withstand a given level of stress, or demand without suffering degradation or loss of function”. Rapidity is the “capacity to meet priorities and achieve goals in a timely manner in order to contain losses and avoid future disruption”. Redundancy is “the quality of having alternative paths in the structure by which the lateral forces can be transferred, which allows the structure to remain stable following the failure of any single element”. Finally, Resourcefulness is “the capacity to identify problems, establish priorities, and mobilize resources when conditions exist that threaten to disrupt some element, system, or other unit of analysis; resourcefulness can be further conceptualized as consisting of the ability to apply material (i.e., monetary, physical, technological, and informational) and human resources to meet established priorities and achieve goals” (Bruneau, Chang et al. 2003). More details about these dimensions that set the concept of resilience and how to define them, they can be find in (Bruneau, Chang et al. 2003).

### 1.3.3 Assessment and measurement of resilience

The measurement of resilience can be defined according to various different types of approaches (Marasco and Cimellaro 2018). The best-known approach is the one that defines resilience through indices that evaluate a characteristic of the system under analysis. Score cards that are used to evaluate the progress of a system with respect to a goal. An example of a score card is a set of questions that, based on the answer, provide a resilience score. Use of models to represent the processes of the system for which resilience is to be assessed. They use mathematical expressions to describe interactions. Finally, the last approach is to use tools that provide a guide to assess resilience with sample procedures and survey tools, or data to be used in the compilation of indexes or score-cards (Marasco and Cimellaro 2018).

Each approach has its own appropriate scale of application. A conceptual framework is needed to understand community-level resilience at any scale. Scale, unit of analysis and temporal variability are essential issues in a resilience framework. The scale refers to the size of the domain in which the processes are investigated. The processes can then be evaluated on a different scale from that of the study community. In addition to the scale, it is important to define the unit of analysis, i.e. the assessment can vary from individual to continental. Finally, the other important aspect in the study of community level resilience is temporal variability (Marasco and Cimellaro 2018).

## 1.4 Lifeline Infrastructure

In engineering, infrastructure is defined as the element or set of components that structures a territory according to human needs. Depending on its location on the territory, we find network infrastructures and punctual infrastructures. The former makes up a network of systems and services interconnected with each other by specific nodal points. By its nature, this type of infrastructure needs to reach large areas of the territory or in any case many citizens to be efficient. Among these we find the transport networks, both of energy and of vehicles and people, consisting of roads, railways, canals, gas pipelines, oil pipelines, etc.

Then we find the telecommunication networks (telephone network, television broadcaster, radio broadcaster but also the computer network as a whole), vital (aqueducts), drainage (sewers) and soil defense (waste disposal plants, as well as networks hydro-geological risk prevention). The second type, on the other hand, has value as such. Examples are hospitals, schools but also the set of basic infrastructures made up of prisons, police and army stations, courts etc.

One way by which to classify types of infrastructure is to view them as two distinct kinds: hard infrastructure and soft infrastructure (Hamutuk). Hard infrastructure refers to the physical networks necessary for the functioning of a modern industry. This includes roads, bridges, railways, telecommunication systems etc., and, are also known as tangible or built infrastructures. On the other hand, soft infrastructure refers to all the institutions that maintain the economic, health, social, environmental, and cultural standards of a country, so represent the intangible infrastructure. This includes educational programs, official statistics, parks and recreational facilities, law enforcement agencies, and emergency services.

The term critical infrastructure means a system, a resource, a process, a whole, whose destruction, interruption or even partial or temporary unavailability has the effect of significantly weakening the efficiency and normal functioning of a country, but also security and the economic, financial and social system, including the central and local public administration systems.

In general, these infrastructures are related to the following resources:

- Heating (e.g. natural gas, fuel oil, district heating, etc...);
- Agriculture, food production and distribution
- Water supply (drinking water, waste water/sewage, etc...)
- Public health (hospitals)
- Transportation systems (fuel supply, railway network, airports, harbours, inland shipping)
- Security services (police, military, firefighters, etc...).

- Electricity generation, transmission and distribution; (e.g. natural gas, fuel oil, coal, nuclear power, etc...)
- Renewable energy, which are naturally replenished on a human timescale, such as sunlight, wind, rain, tides, waves, and geothermal heat.
- Telecommunication (cable network, wireless system, satellite network, etc...)
- Economic sector (banking, clearing, etc...);
- Strategic Facilities (chemical, critical manufacturing, etc...)

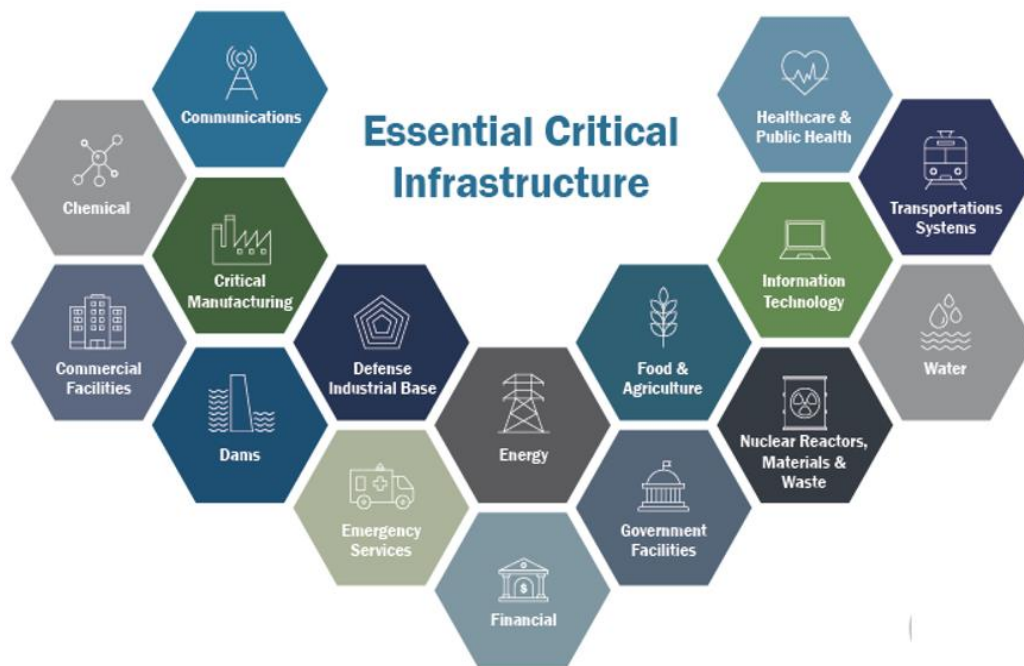


Figure 1-4, Critical Infrastructures for a city and a community

Therefore, as it has been understood from what has been introduced in this paragraph, the telecommunication network can be defined as a strategic infrastructure.

## 1.5 Resilience and Telecom Network Infrastructure: State of Art

The main network services are landline, wireless (also known as cellular) and the Internet. Telecommunication networks and especially cellular networks nowadays play an important role for a society under normal conditions, while they represent a fundamental role immediately after disastrous events in general (Kwasinski and Tang 2011). Damage to the telecommunication network, in addition to causing human losses, can also cause significant socio-economic losses

(Smith, Hutchison et al. 2011). They immediately after disastrous events allow to people to communicate with the emergency services. While they allow the emergency units to manage and plan rescue interventions. In the literature there are cases of serious damage suffered by communication networks. For example, landline telephone lines went down during Hurricane Katrina, while wireless lines were not reliable due to damage to some cell towers and a lack of electricity. Furthermore, the connection systems between the backbone stations have also failed, rendering the still functioning towers unusable (Booker, Torres et al. 2010). An example of how important the cellular network can be in warning during a disaster is that of Japan. Japan has implemented a seismic warning system connected to the cellular network that provides people with a few lifesaving seconds. It is therefore extremely important to maintain a functional telecommunications network to alert people of an impending earthquake. The few seconds allow people to be prepared before the strong shaking comes. While after an earthquake, keeping communication networks operational is important for many obvious reasons already mentioned. Another important reason is to be able to alert people to subsequent aftershocks (Kwasinski and Tang 2011). During the 2010 Haiti earthquake, the wireless communication network suffered damage on more than 70% of the network components, also losing connections with external countries (Abu-Al-Saud 2019). Immediately after the 2011 earthquake-tsunami, the authorities of the management of the Japanese networks NTT, found a peak in demand for service immediately after the first strong earthquake that caused an overload to the network (Sakano, Fadlullah et al. 2013). Also, during the 2011 earthquake in Japan, more than 29,000 BTS of the mobile network stopped working in the Tohoku region, the main causes were the destruction of the BTS, the destruction or extensive damage of the BSC control stations, the damage to wiring between the BTS and the BSC, or the power failure. The problem encountered in the case of the Tohoku region was the extreme vulnerability of the network of connections between BTS-BSC and between BSCs themselves, in most cases they were unique connections, without any redundancy in the network (Owada, Byonpyo et al. 2018). For all these reasons, estimating the reliability of communication networks during disastrous events is an important problem to be addressed. In the literature, at the urban level there are not many methods that estimate the vulnerability of a communication network after disastrous events. An example of a method for estimating the resilience of a network is the one proposed by Alves, Rodrigues et al. (2017) where the resilience is estimated through the ideal path that a signal must take and the emergency path for the same user. Another more complete method is the one proposed by Booker, Torres et al. (2010) where the reliability of a wireless network is analyzed during a hurricane. In this proposed method it is first necessary to model the various components of the network to evaluate the reliability of the individual

components, then using create traffic models for the network to estimate the number of users for each cell tower. Finally, it is necessary to define models to estimate the performance of the network under the external action (Booker, Torres et al. 2010). Broadly speaking, this was the path followed to study the vulnerability of the communication network of the virtual city called Ideal City. On the contrary, in the literature there is a lot of information that studies the behavior of the individual components of a wireless network as a result of various actions. For example, Galvez and McClure (1995) proposed a simplified method to describe the behavior of self-supporting cell towers under earthquake action using an equivalent SDOF model. Other studies such as I propose the creation of fragility curves for each component of the network. To study the resilience of these networks at an urban level, it is essential to create a database of the characteristics of the various components as broad as possible as proposed by Giovinazzi, Austin et al. (2017) for the study of the communications networks of New Zealand. A definition of resilience for a telecom network is given by (Mauthe, Hutchison et al. 2016) and it says: *"The resilience of a communication network is its ability to maintain the same level of functionality in the face of internal changes and external disturbances as a result of large-scale natural disasters and corresponding failures, weather outages, technology-related disasters and malicious activities."*

## 2 Virtual simulation models

### 2.1 Introduction

Virtual simulation models to study the effects of both natural and man-made disastrous events in an urban area are becoming increasingly popular in the scientific community (Cimellaro, Domaneschi et al. 2017). They are excellent tools for modeling different types of infrastructures and events according to well-defined methodologies. Recent natural and man-made disaster events have demonstrated the high vulnerability and unpreparedness of most communities. The importance of strategic infrastructures and their interdependence for modern societies is demonstrated by the fact that they provide essential services and contribute significantly to social and economic development (Marasco, Cardoni et al. 2020). These events cause a crisis in an urban community. The crisis is something natural which, however, can become a catastrophe when the ability to respond to this crisis is not adequate and human error gets into play. Simulating the damage caused by these events at an urban scale can potentially provide valuable information that can facilitate decision making, improve planning for disaster mitigation and reduce human and economic losses (Cimellaro, Renschler et al. 2016). Until now, within the civil sector we have focused on the modeling of the single element, or of the single infrastructure. Now, the modeling of several infrastructures to assess their interdependence as well as their vulnerability within the same virtual model is spreading more and more even if still limited by the high computational and knowledge cost (Cimellaro, Domaneschi et al. 2017). The next step is to build a hybrid model. In addition to the modeling of physical infrastructures (buildings, electricity networks, water networks, etc.), non-physical networks are also modeled (i.e., networks of people who manage the emergency, police, firefighters, etc.) as shown in the illustration in *Figure 2-1*. This for example, it is what the “IDEal reSCUE” project at the Polytechnic of Turin is trying to develop (Marasco, Cardoni et al. 2020). In these projects, it is difficult to find a virtual city modeled identically to a real city for many reasons, one of these, can be the difficult to have the data for security reasons (Brumbelow, Torres et al. 2007).

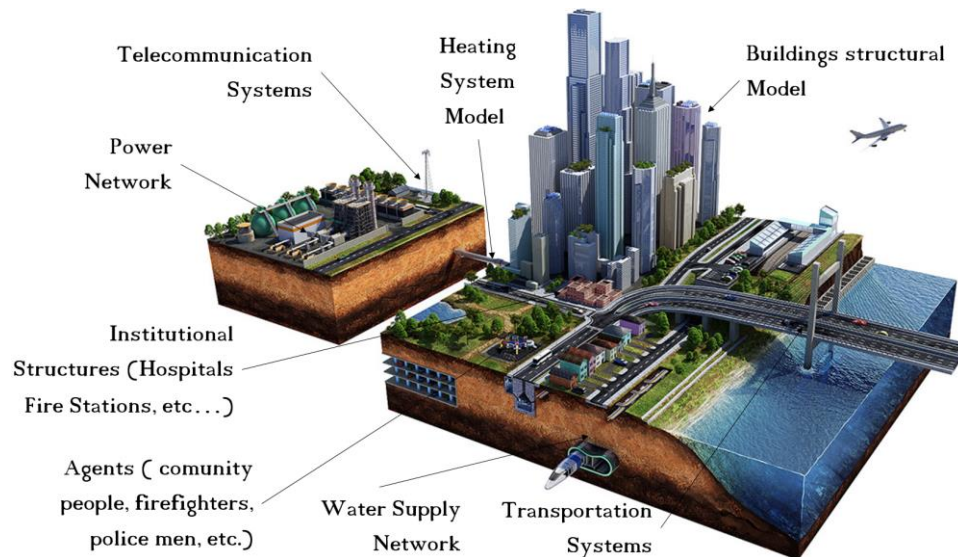


Figure 2-1, Idealization of a virtual city model

Having more accurate information on the behavior of these critical infrastructures at the urban scale and not at the single element level could provide a more complete view of the vulnerability of a community to disastrous events (Cash, Adger et al. 2006). Studying the vulnerability of strategic infrastructures (roads, buildings, electricity grid, etc.) is of fundamental importance as it allows to correctly assess the resilience of the community and of the city as well as disasters, which is defined as the capacity of a system to respond and recover from a harmful event (Cimellaro, Renschler et al. 2016).

## 2.2 Literature review

Different applications can be found for different scenarios and hazards. Into the literature there are various examples of virtual city' projects, all with the common feature of studying the vulnerability of infrastructures and therefore of the community to natural and man-made hazard (Marasco, Cardoni et al. 2020). The Center of Excellence for Risk-Based Community Resilience Planning developed and designed a virtual city to test its algorithms to understand what makes a community resilient. This city is called Centerville, it is imagined as a typical average city located in a Midwestern state. The city is made up of seven residential districts, an industrial district, various services such as schools, town hall, etc. are inserted. and a viability with roads and railways has also been defined. The city is geographically located 200 miles from the New Madrid seismic zone and is therefore susceptible to moderate to severe seismic risks. It is also close to the "tornado alley". Therefore, both earthquake and tornado risks are considered in assessing the resilience of the Centerville community. In this project, four distinct infrastructures are studied such as, buildings, transportation systems, electricity,



and water / wastewater systems. This is because, the fragility modeling process for their components is more mature and they represent distinct civil infrastructure topologies, which will respond to the demands of earthquake or tornado risks in different ways. The development of the Centerville project involved not only engineers but many different figures such as sociologists, computer scientists (McAllister 2015).

In addition to this project for assessing the resilience of strategic infrastructures and their interdependence, The Center of Excellence for Risk-Based Community Resilience Planning has developed other projects for assessing the effects on a community of combined events. Four distinct cities have been defined. Seaside community that takes its cue from the cities located on the west coast of the USA subject to a combination of earthquake and tsunami, Shelby County, a reality created for the study of the effects of floods and climate change, Joplin and Galveston projects that are inspired by cities of the coast southeast of the USA and made for the study of the effects of tornadoes and hurricanes (McAllister 2015).

An example of a specific study of the importance of an infrastructure for a community can be the one developed by Brumbelow, Torres et al. (2007). This study analyzes the importance of the water system. A virtual city called Micropolis is created from scratch, developing it also considering a time span, starting from a small settlement, and gradually expanding. This means that the infrastructure is also characterized by elements from different periods with different characteristics. The infrastructure is then analyzed through studies using the EPANET software, simulating various breaks on the network.

While the study conducted by Domaneschi, Cimellaro et al. (2019) using the Ideal City project focused on the interdependence between the damage caused by an earthquake on buildings and the roads closed due to rubble.

In the case of the study of the response of infrastructures and their interdependence to flood events, we can mention the work done by (Dudenhoeffer, Permann et al. 2006).

A final example of the use of a community for the study of resilience on an urban scale can be the one developed by Campanella (2006). This study evaluates the resilience of a real city that of New Orleans before and after the Katrina events that brought more than 80% of the city underwater.

These examples demonstrate that many platforms have developed in recent years to quantify the resilience of strategic infrastructures to disastrous events.

## 2.3 Ideal City's Models

The resilience laboratory at the Politecnico di Torino is developing a project called *Ideal reSCUE*. The goal of this project is to integrate all the IT resources developed



for the study of the resilience of a community to disastrous events within a single platform. An integrated platform can give a better and useful problem-solving approach to assist decision-making bodies during an emergency (Marasco, Cardoni et al. 2020).

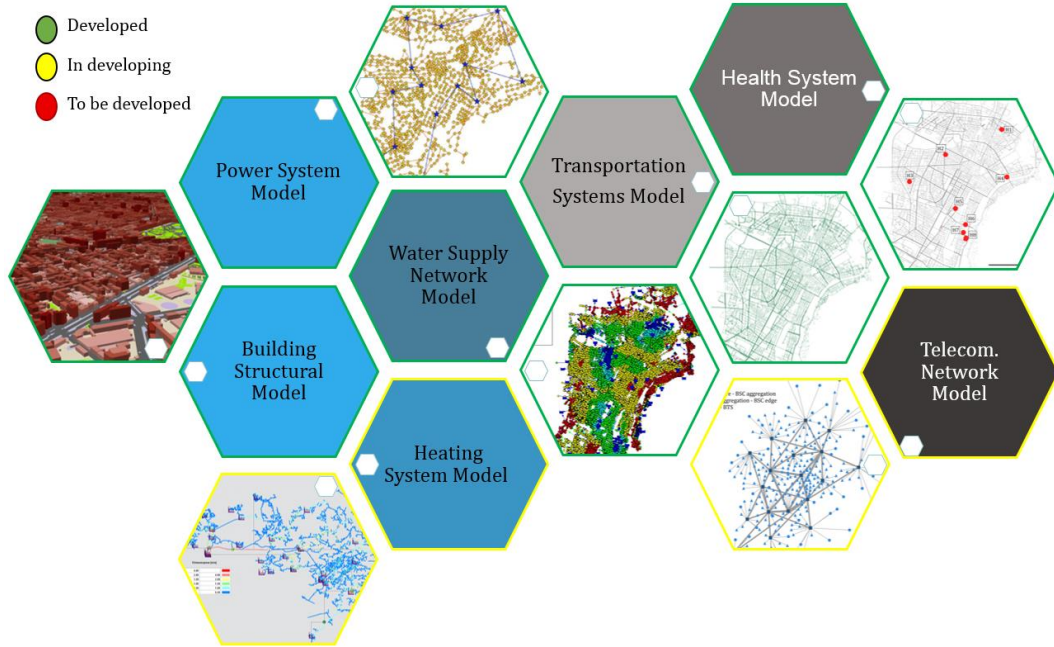


Figure 2-2, Ideal City' Models developed

Until now, the single infrastructure has always been modeled within the civil sector. While, the main objective of this work is to develop a hybrid model that includes the modeling of all physical networks, therefore the built environment, electricity network, water network, etc. and the non-physical networks, i.e. all those networks of people who deal with management of an emergency for example, firemen, police, etc. For this purpose, a virtual city called Ideal City is developed (Marasco, Cardoni et al. 2020).

To date, the models developed for the virtual city have been: the built environment, the electricity network, the water network, the transport infrastructure and the hospital network. The work carried out in this paper will focus on the development of the telecommunication network (also known as ITC network) for the virtual city. Finally, also the gas network is also under development. An overview is shown in the *Figure 2-2*.

The virtual city is conceived as representative of a typical European urban area and is inspired by the city of Turin in Italy. The development is started from the built environment and subsequently the various critical infrastructures were individually implemented which are combined in a single integrated platform with the agent models called ABM (agent based model) which represent the various networks of people. The entire analysis is controlled in a Python-based environment.

The software developed includes several algorithms necessary to assess the damage to the urban environment as well as to the different components of the various infrastructures. (Marasco, Cardoni et al. 2020). With this project, the resilience of individual infrastructures to extreme events is evaluated, then, the project also evaluates the interdependence between different network (for instance the telecom network it depend by power network), as well as studies the behavior of the so-called social networks in the various infrastructures and in the global context before and after a disastrous event. In this project, the effects of seismic events are studied principally (Marasco, Cardoni et al. 2020).

Physical Infrastructure			Social Infrastructure		Economic Infrastructure		
Building	Residential	21279	Hotel	31	Industrial Building	Light	321
	Mobile Homes	62	Historical Building	951		Heavy	108
Hospital	Hospital	8	Castel and Palace	18	Commercial	Retail Store	25
	Nursing Homes	9	Church	176		Malls	12
Fire Station	Stations	3	Sport	265			
Police Station	Carabinieri	18	Cinema	48			
	Polizia Municipale	11	Museum	156			
	Questura	31	Theater	38			
	Caserma	13	Library	15			
	Others	3	Public Administration	271			
Educational	Elementary School	157					
	Middle School	105					
	High School	97					
	University	70					
Transport	Stations	8					
	Building	11					

Table 2-1, Number of buildings per category

The virtual city designed consists into three main categories of buildings (physical infrastructure, social infrastructure and economic infrastructure) as *Table 2-1* shows (Noori, Marasco et al. 2017).

Each main category groups more sub-categories as can be seen in *Figure 2-3*, Ideal City's layer of built environment (Marasco, Cardoni et al. 2020). For example, the category of physical infrastructure groups residential buildings, school buildings, order buildings, etc.

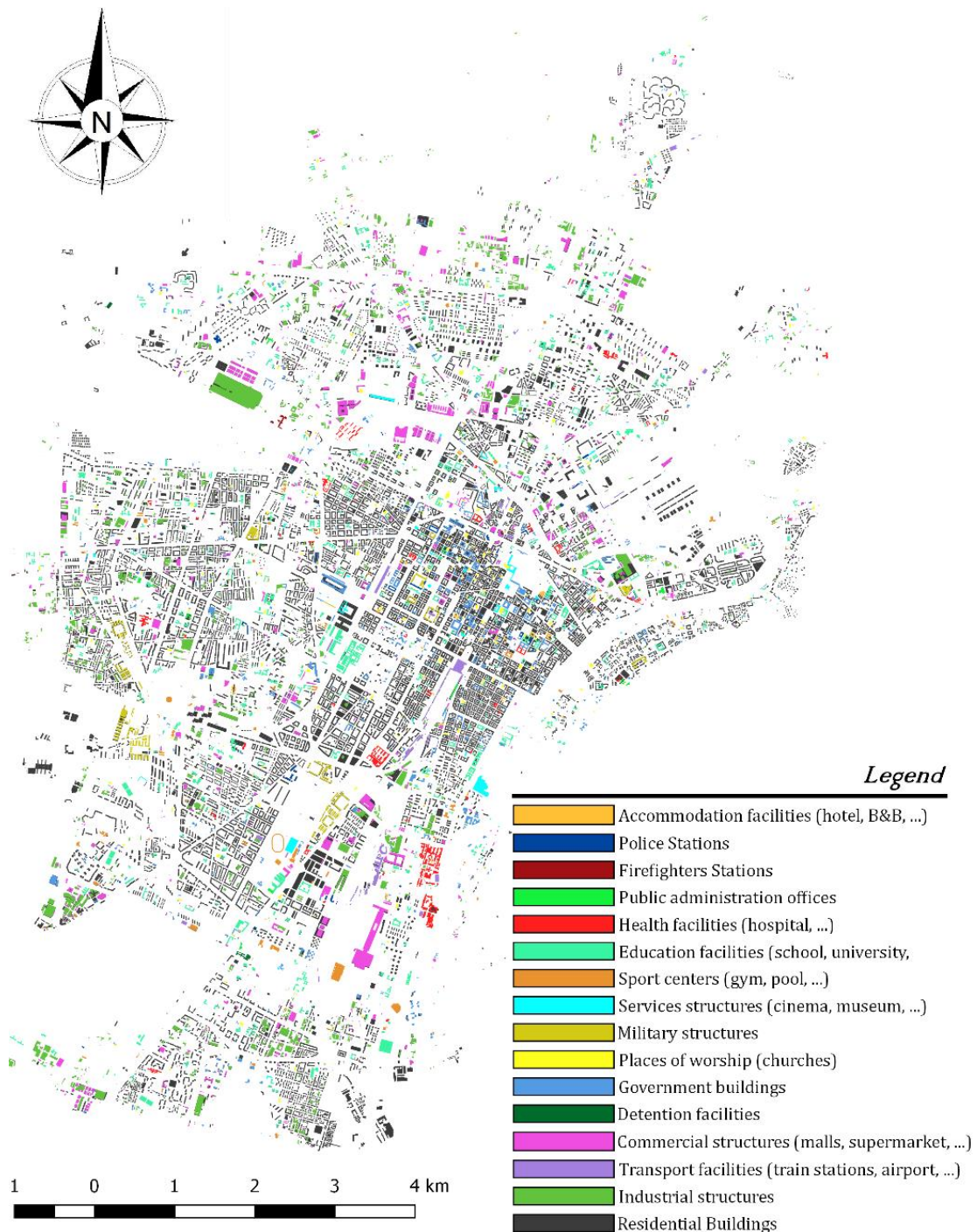


Figure 2-3, Ideal City's layer of built environment (Marasco, Cardoni et al. 2020)

The overall area of the city is about 120 km<sup>2</sup> with a population of over 900,000 inhabitants. The building heritage of the virtual city is the typical building heritage of a European city with a historic center mainly composed of masonry buildings, while in the areas around the center there are prevalenced housing in reinforced concrete of different years starting from the second post-war period onwards . Finally, steel structures being very rare are not taken into consideration in the construction of the model. In the last decade, residential areas were expanded in the disused industrial areas located on the outskirts. The residential building

heritage of the model is mainly composed of buildings with a limited number of plans (1-15 floors) with a significant percentage of historical and monumental structures. The geospatial distribution of buildings and the administrative division of the virtual city is based on the data collected by the city of Turin. The built environment model is then updated whenever you study and develop a critical infrastructure network that requires service buildings.

Each structure has been characterized through a series of basic parameters such as the year of construction, the type of floor, the percentage of reinforcement, and other parameters depending on the basic parameters such as the load combination is defined based on the 'year of construction. To address the uncertainty of the nature of the parameters, they were then considered as normally distributed random variables. Given the simulations to be carried out on a large scale, the limited availability of data and the high computational level required. The single building is modeled as a Multi degree of Freedom (MDOF) subject to an increasing monotonous force proportional to its fundamental mode of vibrating. The elastic parameters are obtained through the shear value at the base and displacement at the top which cause the first element to yield. While the post-elastic parameters are evaluated on the basis of the upper limit theorem of the limit analysis and the equal energy rule. These parameters allow you to define a backbone curve representative of an equivalent Single-Degree-Of-Freedom (SDOF) model. The backbone curve is computed for each single building by varying its parameter through Monte Carlo Simulation (MCS). A non-linear time history analysis is then performed to determine the maximum displacement at the top suffered by the building. This displacement is used to determine the damage status of the structure using the previously defined capacity curve (Noori, Marasco et al. 2017).

Other details about the model of the built environment can be introduced into subsequent chapters 4, 6 and 8 This because, it will be used in this work to study the vulnerability of the ITC network. For example, the telecommunication network uses service buildings whose vulnerability is studied by applying the same method proposed by Noori, Marasco et al. (2017). While as regards other layers that represent other physical and non-physical infrastructures will not use to study the ITC network directly, but concepts formulated in them can be used. For this reason, they are generally explained below. For example, the concept of the component vulnerability hierarchy applied to the electrical network can also be introduced in the study of the communication network. So, the second layer developed for the virtual city project is the one concerning the road transport network (RTN) shown in *Figure 2-4*, 'Transport network' layer (RTN). This is because within a community it is essential for the growth of the same and it is essential during a crisis. For example, it is essential to always have roads free of rubble to get to the rescue centers. Therefore, the interdependence between



buildings and the NTG following an earthquake is caused by the amount of debris generated by damage to buildings (Marasco, Cardoni et al. 2020).

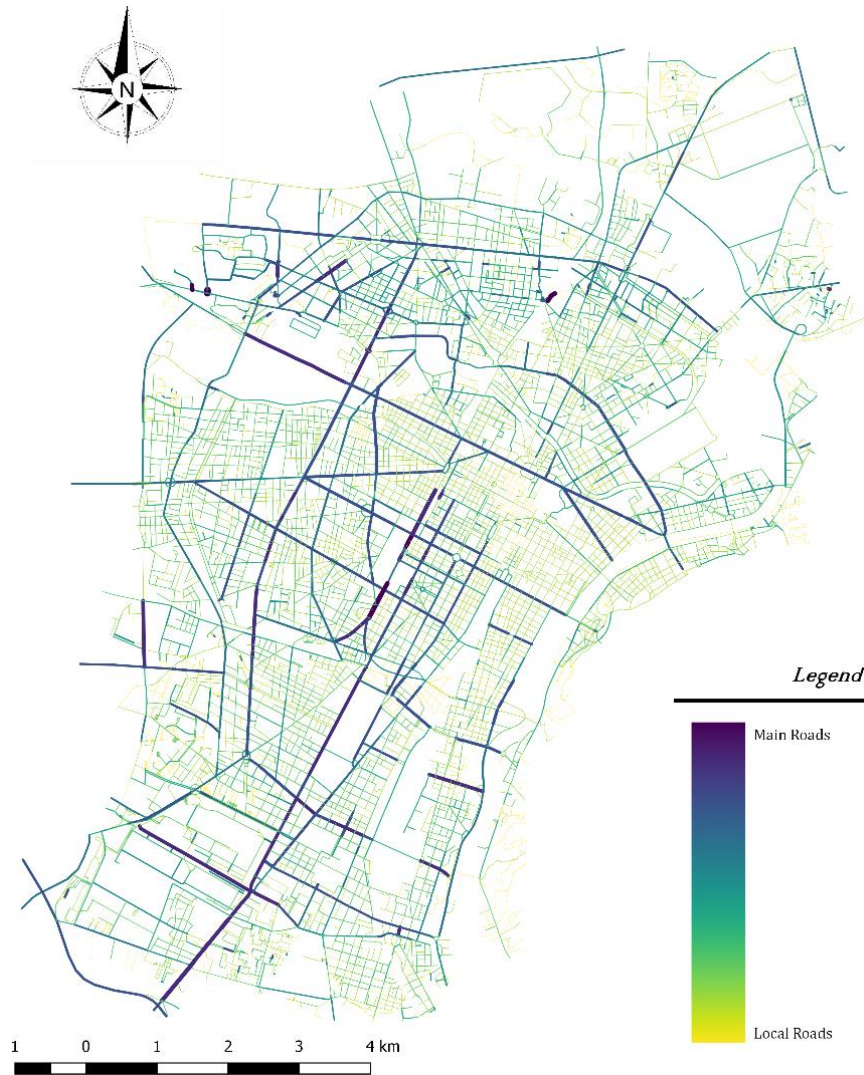


Figure 2-4, Transport network' layer (RTN) (Marasco, Cardoni et al. 2020)

The road network (RTN) of the city has been modeled as an undirected graph  $G$  (each path can be traveled in both directions because, in emergency conditions, the directionality that exists in the ordinary condition may not be respected to give priority to rescue operations.) which is composed of 14,239 nodes ( $N$ ), which represent the intersections of the road, and 18,798 edges ( $E$ ), or the connections (Marasco, Cardoni et al. 2020).

The third model developed concerns the electrical infrastructure. At the urban level, it generally consists of a transmission system, which runs long distances at high voltage, and a distribution system, which supplies medium and low voltage electricity. The Ideal City distribution network is made up of 15 primary substations and 1274 distribution substations (Marasco, Cardoni et al. 2020).

Primary substations operate at high and medium voltage and in most cases, they are in robust structures so that they can continue to operate even after extremely

disastrous events. While the distribution substations are buildings with structural characteristics of a normal building and therefore subject to even serious damage. Finally, the electrical components resist well to a seismic excitation. However, the debris generated by partial or total collapses of buildings can cause damage to the electrical components inside them, compromising the functionality of the entire network. Therefore, the weakest element of the network is often the building of the distribution substations. So, the vulnerability of the infrastructure is related to the damage to the buildings where the substations are located. This means that if the building in which a substation is installed collapses, the components in that substation will fail. As a result, when a substation fails, the electrical load drops to zero and all buildings connected to that substation are without energy. To assess the vulnerability of the network, the fragility of the substations is therefore assessed. It is evaluated through the fragility curves developed by HAZUS. The fragility of a substation varies according to whether its components are anchored or not. Considering the HAZUS methodology, to have an extended damage level (i.e., repairs needed to restore functionality), the median peak mass acceleration (PGA) should reach 0.34 g for low voltage substations with unconnected components and 0.45 g in the case of anchored components. These PGA values are more likely to cause severe damage to buildings, given the typical built environment of European cities. The fragility of the distribution lines was not considered since at the urban level the distribution lines are more robust than the distribution substations. In addition, distribution lines can operate both overhead and underground. In Ideal City, they are mainly meant to be underground, this is also reflected in the modernization of cities as underground lines are safer. This is demonstrated by the fact that a failure of the underground lines occurs only in the event of strong tremors with significant deformations of the ground, which would still cause serious damage to the buildings and therefore to the substations which are the elements that manage the distribution of energy to the community. Therefore, they represent the connecting element between users and infrastructure. Overhead distribution lines, in addition to their progressive disuse in urban environments, are instead generally affected by strong winds, while their vulnerability to earthquakes is limited due to the small size and slenderness of urban service poles (Cardoni, Cimellaro et al. 2020). More details about the power network can be found in (Cardoni, Cimellaro et al. 2020).

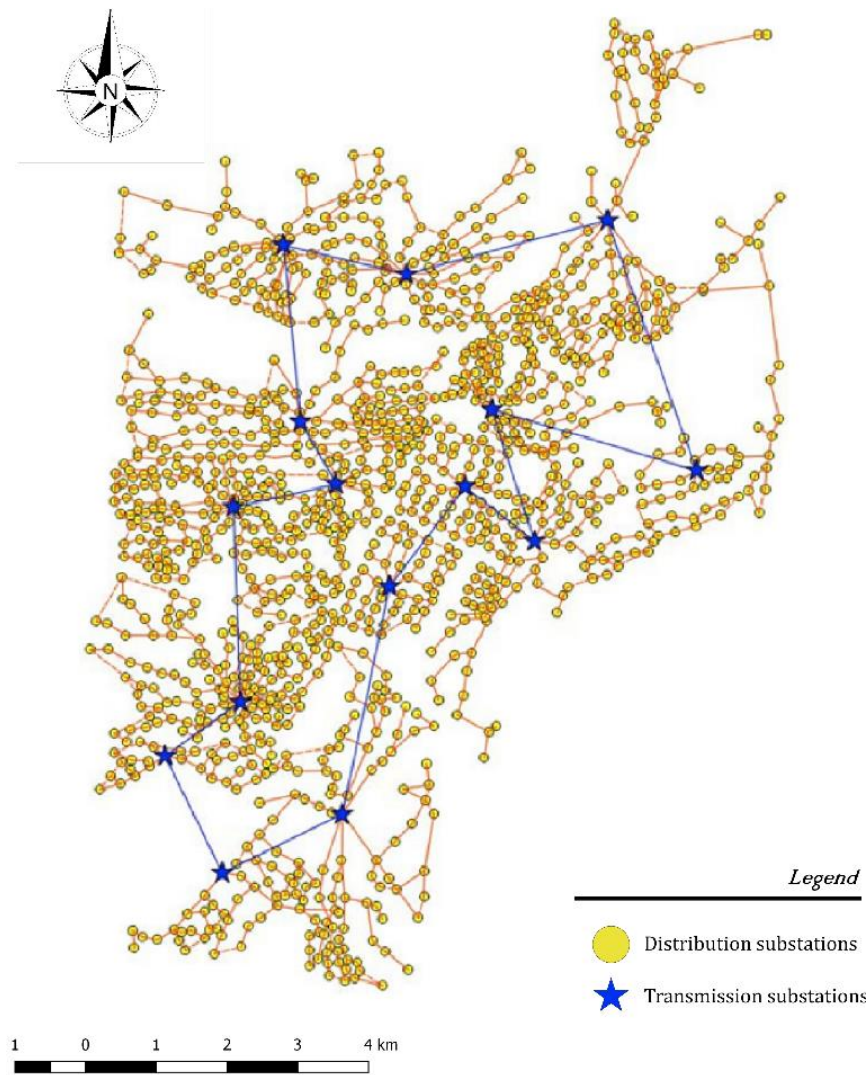


Figure 2-5, Electrical infrastructure' layer (PG) (Marasco, Cardoni et al. 2020)

The fourth model developed concerns the water distribution infrastructure. It is showed in Figure 2-6.

It is an essential service and damage caused by seismic events can cause a drop in water pressure and consequently a limited water supply. To build the model of the water network it was necessary to make several hypotheses. In fact, the network of a real city is not known for security reasons. The geometry of the water network is assumed to overlap the transport network of the city. The model is developed using various software including EPANET, Matlab, Python and Google Maps. The EPANET model includes 19654 ductile iron pipes with a Darcy-Weisbach roughness coefficient of 0.26 mm, 14996 knots, 9 valves, 38 pumps, 19 reservoirs and 26 tanks. The nodes are located 1.2 m below the ground surface. The elevation of the ground varies between 207.76 m and 340.68 m above sea level. The water sources are aquifers (82%) and other sources such as rivers and surface waters (18%) with a total average daily requirement of 353.38 Ml / day.

The diameters of the pipes and the positions of the valves, pumps, tanks, and reservoirs have been determined to ensure the following constraints:

$$0.5 \text{ m/s} \leq \text{Speed} \leq 2 \text{ m/s}$$

$$40 \text{ m} \leq \text{Pressure} \leq 80 \text{ m}$$

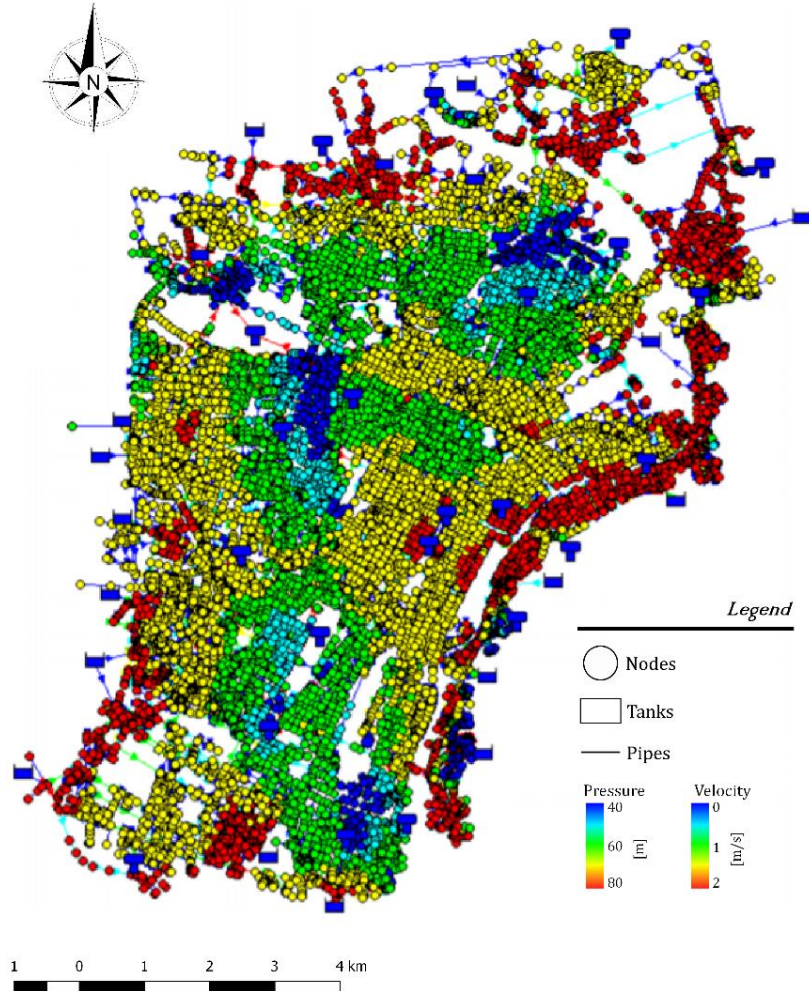


Figure 2-6, Water distribution network' layer (WDN) (Marasco, Cardoni et al. 2020)

The demand for water at each node depends on the number of people served by that node. This number does not depend on the population but on the number of families connected to the node, so it was necessary to find the population density for each unit of family volume. This density also varies with the district as the population density is not the same among all the districts (Taurino, Kammouh et al. 2018) .

More details about the water distribution network can be found in (Taurino, Kammouh et al. 2018).

The last developed layer consists of an agent based model (ABM), capable of managing the approximately 900,000 individual agents that interact dynamically with each other and with the urban scenario (Marasco, Cardoni et al. 2020). In particular, this model focused on the flow of patients in the eight main hospitals



(H1-H8) each with their own number of virtual city beds after a disaster such as an earthquake.

The model describes and simulates the flow of patients to the route to the nearest hospital. Once in the facility, the injured, according to the triage code based on the level of severity, must wait a certain time, compatibly with the resources and spaces available, before receiving all the drugs. The waiting time for each patient is then monitored by a discrete event model, so that when the hospital reaches its maximum capacity, patients can be transferred to another available facility. the ABM model considers two classes of agents, individuals, and ambulances; the latter collect seriously injured individuals and transport them to hospitals. While the lightly injured independently travel to the nearest hospital and eventually the healthy ones head to the nearest available emergency shelter. When the shelters are full, individuals are sent back to the nearest available city exit. In addition, the agent model interacts with the transportation network model to assess the fastest route after the earthquake. This is because after a seismic event, as seen with the transport infrastructure layer, some roads can be blocked by rubble (Marasco, Cardoni et al. 2020).

In addition to the layers presented so far, a layer concerning the gas network and a layer dealing with the telecommunications network are being developed. The latter is developed precisely in this work.

## 2.4 IDEal reSCUE's Platform

As introduced in the previous paragraph, the ultimate aim of the project is to create an integrated platform (as seen in *Figure 2-7*) that brings together all the layers that describe the urban environment, critical infrastructures and agents in a single work environment to assess the resilience of the community, of the infrastructures and their interdependence on seismic events. In fact, this project focuses in particular on the study of damage due to different earthquakes, the fact remains that the same methodology can be extended to all disastrous events (floods, fires, tsunami, etc.) that a city can suffer (Marasco, Cardoni et al. 2020).

The platform will allow users to upload the database concerning the urban environment of the city, i.e. the building stock represented by the simplified model and all the data to characterize the various strategic infrastructures available.

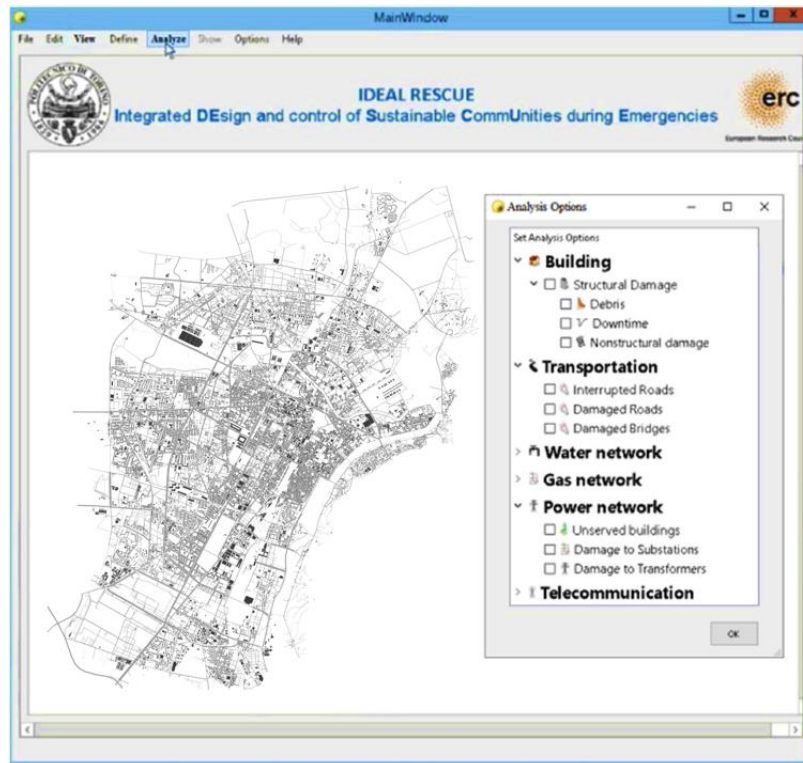


Figure 2-7, View of the main screen of the platform (Marasco, Cardoni et al. 2020)

As regards the selection of the damage states and the relative thresholds, they are set by default from the same integrated platform. Subsequently, the user can instead define the seismic scenario by selecting:

- Location of the epicenter,
- Magnitude of the earthquake,
- History recorded in the epicenter
- Ground motion prediction equation to evaluate geometric attenuation at any building location.

As for the attenuation model, it is set by default and is based on the Ambraseys' Ground Motion Prediction Equation (GMPE) (Ambraseys, Simpson et al. 1996), while the processing of the seismic recording is performed by the OpenSignal tool (Cimellaro and Marasco 2015). The developed platform can provide information on the damage associated with all layers of the analyzed area. Furthermore, the data flow can be completely managed by the user who can choose between different options. The starting point of the analyzes is the damage suffered by the buildings. The effects on infrastructures are then assessed on the basis of the damage suffered by the buildings. Several algorithms have been implemented to study the interdependence between the built environment, the agents and the various infrastructures. Finally, the emergency evacuation is also simulated as mentioned in the previous paragraph using ABM models (Marasco, Cardoni et al. 2020).

## 3 Telecommunication Network

### 3.1 Overview

Telecommunication is a complex system, but in simple terms it can be seen as a transmission of signals, signs, writings, words, messages, sounds and images, by radio, wire, optical, or other types of electromagnetic systems between people.

The telecommunication network (TLC network) has undergone a rapid evolution in the last 30 years (ISTAT 2018). It has now become an essential basic infrastructure in a community. In fact, it allows people to communicate immediately with the rest of the world. Thanks to the TLC network, the economy and capital move. After a disastrous event like an earthquake or wildfire, having a functioning Tlc network is essential for all aspects concerning the coordination of rescue activities.

So, for these reasons it is one of the most important lifelines infrastructures and its service has become an essential aspect for a country. This becomes even more evident when considering the demographic phenomena that are occurring. It is confirmed by estimates that around 2030, when the world population is expected to reach eight billion, it is estimated that 4.9 billion will reside in cities from the 3.3 billion of now (PRB.org 2020). This increase population generates the problem of having an increasing demand of services. Therefore, it is essential that in densely populated urban areas there is a much more resilient network that can be back in operation in a short time after catastrophic events.

A first definition of a telecommunications network can be: a set of nodes (users) connected to each other through a network represented by different elements (towers, service buildings), these connected to each other by means of links (cables, electromagnetic waves) which manages the connection between the nodes.

Looking in more detail, a Tlc network is a complex of technical means of telecommunications and structures like buildings, steel tower, cables, etc. and designed for routing, switching, transmitting and receiving the signals, in any form, between user's equipment via wired, wireless, radio, fiber optic or other electromagnetic systems (Adachi and Obata 1990).

There are several types of telecom network:

- Land line telephone and data networks
- Radio and television networks
- Wireless and data networks
- Satellite networks
- Aeronautical aircraft communications networks

Each of them characterized by different elements and different ways of data transmission. As regards the communication and transmission of data in the civil field, the typical ones are: the land line network, the wireless network and the satellite network all connected to each other as it can see in the *figure 3-1*.

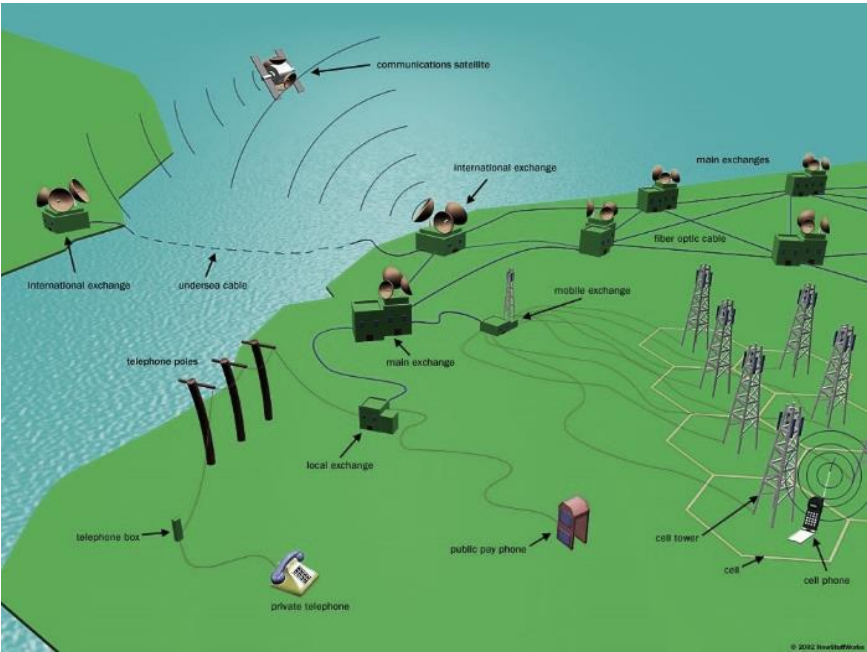


Figure 3-1, Different types of telecommunication networks connected to each other

In recent years, due to the increasing demand for voice and data traffic in urban areas, the mobile network is becoming increasingly important and widespread. During each of the next 5 years there will be about 350 million additional people on this earth who will be connected to the communications network or, in other words, 1 million new subscribers every day or 10 new subscribers every second. This is the mobile revolution (Mishra 2007).

On the contrary, the landline network with regard to the use of voice traffic in particular, is undergoing a progressive decline in its use (Opensignal 2017). As it can see from the data published by ITU the wireless network has helped make the world a global village with about 90 percent of the world under its network coverage (ITU 2020).

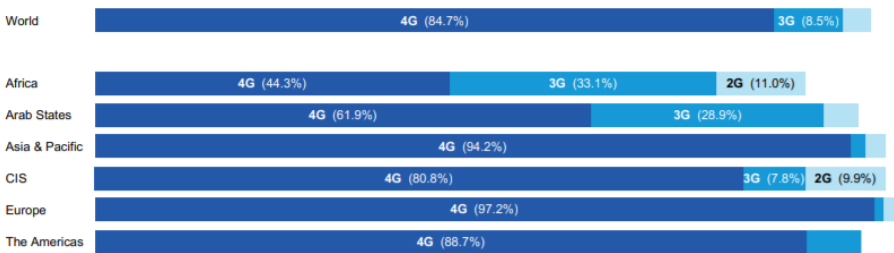


Figure 3-2, Population coverage by type of mobile network, 2020, ITU source

In the following paragraphs we will see the various types of telecommunication networks in the civil field. The wireless network will be analyzed in detail as it represents the network developed for the Ideal City project. This choice was made because, as we have seen in previous data, wireless networks in recent decades have seen a development especially in an enormous urban environment. While the fixed network is gradually losing its use. For these reasons and others related to the greater vulnerability of wireless networks, we have chosen to investigate precisely this type.

## 3.2 Types of Telecom Networks

As previously introduced, different communication networks can be found in urban areas (*figure 3-3*). All these networks are interconnected with each other in order to allow the users of the different networks to communicate with each other. In the following paragraphs they will be illustrated individually all networks by defining the various components that characterize them.

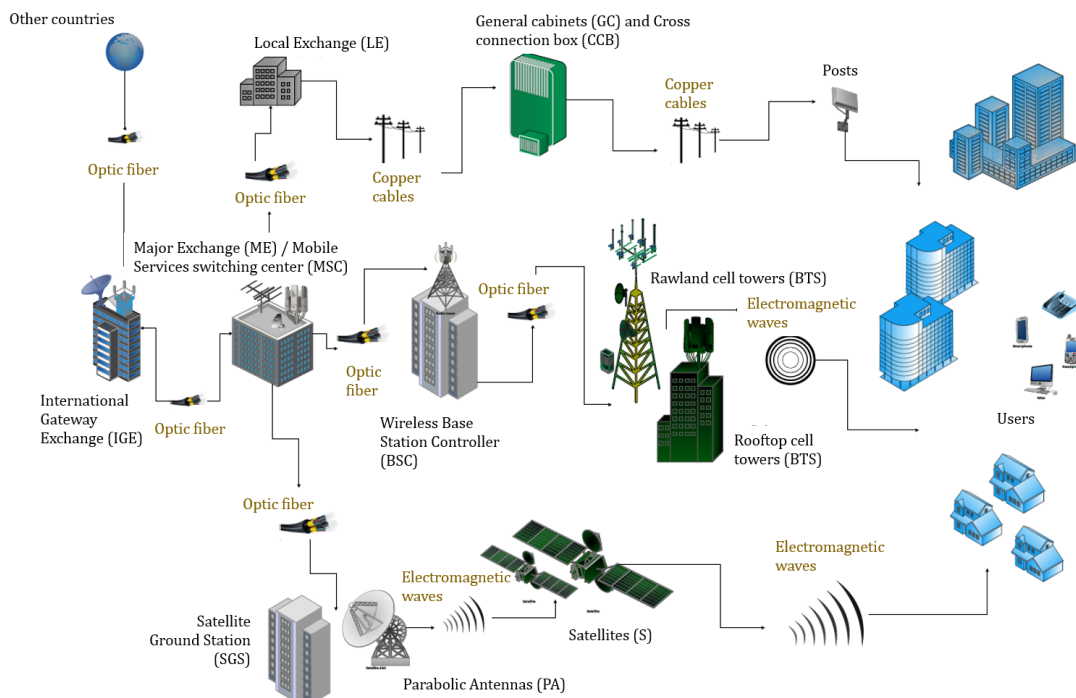


Figure 3-3, Principal component of principal types of Telecommunication Network

In particular, the wireless network will be seen in detail, while the other two types of networks for civil use will be introduced in a general manner.

### 3.2.1 Landline Telephone Network

A landline telephone network is a telecommunications network that connects telephones where they must be directly wired into a single telephone

exchange. This was the first communication system to be created and defined at a general level as PSTN Public Switched Telephone Network. It is the largest existing telephone network and users are required to pay a bill to use it. It is defined as the worldwide concatenation of circuit-switched telephone networks, in the same way that the Internet is the concatenation of public packet-switched computer networks based on the IP protocol. In this case, the connection is made by means of a cable made by intertwining copper wires with the task of transferring information (such as numbers, words, figures, electrical / mechanical / physical quantities, sounds, noises or images and videos) using electrical signals in electrical communications or light pulses in optical communications. The operation of laying and interlacing itself is called "wiring". Depending on the laying system, it is possible to have aerial, terrestrial or marine cables. Speaking about fixed telephony, the network is characterized by these elements:

- ***International gateway exchange (IGE)***: generally, it is a normal building which blends into the urban environment, it forms the gateway between a national telephone network and the other country international gateway exchanges. Thus, it provides cross-border connectivity. In Italy there are three of these buildings, they are situated in Milan, Rome, and Palermo.



Figure 3-4, 33 Thomas Street International gateway located in NYC,

- ***Major Exchange (ME)***: which is the central component of a telecom network has usually multi stories and would be designed as a traditional official building (Pakdel-Lahiji, Bastami et al. 2016). There are different facilities and operations on different stories, for instance, battery rooms are usually located on the ground floor and MDFs (main distribution frame) and switchers are located in the middle stories such as server components. The area of competence of these components in the case of the Italian network is the regional one. For the Italian network there are about two major exchanges for



each region. In total on the national territory there are 66. the connection between the general exchanges takes place via an optical fiber network.



Figure 3-5, The AT&T Madison Complex Tandem Office is a 17-story, building in Los Angeles, California



Figure 3-6, Harbour Centre is located at 555 West Hastings Street in Downtown Vancouver.

- **Local Exchange (LE):** They too are traditional buildings like the major exchanges, usually in multi-storey reinforced concrete, in which the service components are placed. They represent the connection between the access network and the backbone network. Each of them manages a series of roadside cabinets. These buildings are connected to major exchanges with a fiber optic network. While the connection to the general cabinets can be either with optical fiber or with copper slots, even if the latter are being gradually replaced.



Figure 3-7, example of the components within a local exchange

- **General cabinets (GC):** They represent the points of convergence of a limited number of cross connection boxes. They are connected to local exchanges through a fiber optic or copper network in most cases. They can be small single storey buildings or simple cabinets larger than cross connection boxes.
- **Cross connection box (CCB):** These are the road lockers, from where the so-called "last mile" that connects the final user to the network starts. Typically, the connection is made using a copper cable. Each locker manages a limited

number of end users and not a predetermined area. The connection between them, the general cabinets and the final user is called the access network.



Figure 3-8, example of cross connection box

- **Users (UE):** the final user in this case is represented by residential, industrial buildings, etc. and not by individuals.

The physical network of a landline telephone infrastructure when a large number of elements must be connected is hierarchical, the network is divided into: A access network that connects end users to the network through cross connection boxes. Typically, this network has a "star" type topology, that is, the user is connected to the network through a single connection. The access network is achieved by means of a cabling of copper wires. After that, there is the switching network that connects the local exchanges to the general substations, also in this case there is a univocal connection (star type). It is made by wiring copper or fiber optic cables. Finally, there is the backbone network, it serves to connect the various general exchanges to each other by means of a mesh structure, i.e. each general exchange is connected to different other general exchanges. The latter network is made entirely by optical fiber. (Giovinazzi, Austin et al. 2017) (Pakdel-Lahiji, Bastami et al. 2016).

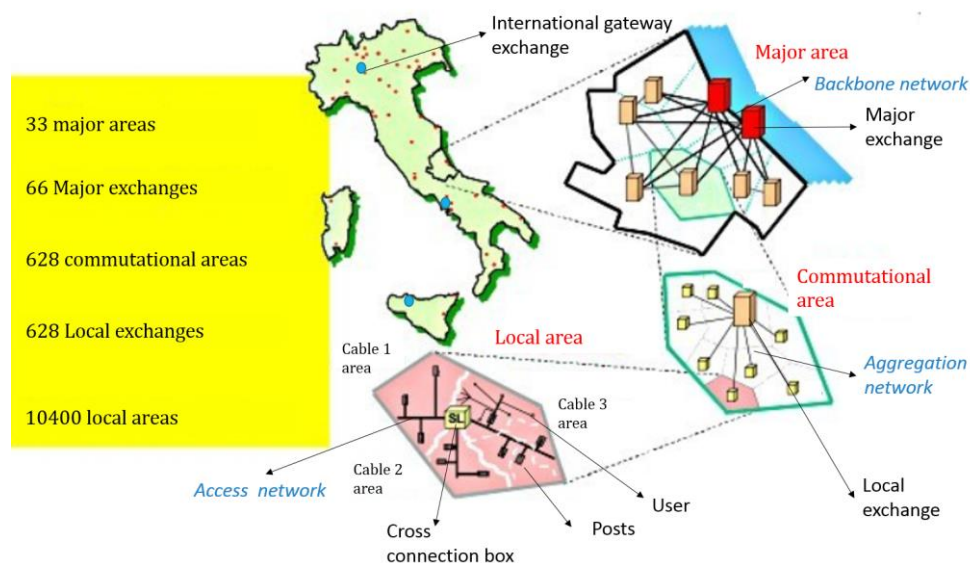


Figure 3-9, hierarchy in the fixed telecommunications network



## 3.2.2 Wireless cellular Network

### 3.2.2.1 Overview

The mobile network infrastructure runs over a combination of 2G, 3G and 4G technologies operated by different mobile network operator (MNO). In Italy the most popular are: TIM, Vodafone and Wind3. The first generation of cellular networks for mobile radio communications (1G) was born in the early 1980s. The main ones are: The Advanced Mobile Phone System (AMPS), born in the United States or The Total Access Communication System (TACS), born in England and used throughout Europe, including Italy, and also in Japan. Starting in the 1990s, second generation (2G) systems, based on digital technology. One of the main standards was: Global System for Mobile communications (GSM). Between the end of the 90s and the beginning of 2000, to meet the growing demand for services following the enormous success of second-generation systems, new standards were introduced through a new generation (3G) of systems. With the third generation (3G), an unsuccessful attempt has been made to achieve a single world standard. To date, there are at least two main standards: cdma2000, developed in the USA and the Universal Mobile telecommunication System (UMTS), used in Europe and Japan of 3G generation. Finally, in early 2008, the fourth generation (4G) standardization defined as LTE (long term evolution) was completed by 3GPP. It represents an extension of the third-generation standards. fourth generation (4G) (Mishra 2007).

From this we can see the impact of this type of infrastructure on the community. In a few decades, the wireless network has undergone enormous development. A communication system with mobile means (or even a mobile radio system) is a telecommunications system in which it is possible to maintain the connection or connection between two or more users even in situations of total or partial mobility of the users themselves. This is the principal difference with a landline network (Mishra 2007).

The main concept in wireless networks as we will see in detail in the following paragraphs is to divide the territory into uniform zones. These zones are called "cells". Each zone is then served by a specific radio station. These radio stations are defined as BTS (base transceiver station). Each group of radio stations are connected to the network through control stations that allow the user to connect to the cellular network of his provider and to all other cellular, satellite and landline networks. Over the years, with the improvement of the network access technology, the number of users who can connect to a radio station at the same time has gradually grown up to a few thousand users per slot. In addition to the number of users, the speed with which information can be exchanged has also increased.

### 3.2.2.2 Network Components

A network mobile system has two major components: the fixed installed infrastructure (network) and the mobile subscribers (users), who use the services of the network. The fixed installed network can be subdivided into three components: Base Transceiver Station, Base Station Controller, Mobile switching center (Mishra 2007).

**Mobile switching center (MSC):** A large building with multi store. It is a very robust building with a reinforced concrete structure, which generally covers a macro area of the order of thousands of square kilometers, for example for the national country there are about twenty of these management centers located throughout the territory. They are real switching centers, connected to each other via an internal network. Their main function is to connect control stations with other telecommunication networks. (other wireless network, internet network, etc.), but also performs the functions of a normal network's controller station. There are also some MSCs called GMSCs which are gateways, that they connect the wireless network with the public landline network.



Figure 3-10 An example of a MSC located in Grodzisk Mazowieck,



Figure 3-11 Example of MSC service room



Figure 3-12 Example of MSC server room

At urban level, these components are not considered in the study of the network, because they are included only on a larger scale. In addition, typically they are buildings with a high degree of robustness for this characterized by a low vulnerability to disasters like earthquake.

**Base Station Controller (BSC):** typically, it is composed by two main elements a multi-story building, with normal reinforced concrete frame structure and a BTS located on the roof or on the ground near to the building. About the BTS it is going to see in detail immediately after this element. Unlike the MSC, however, their structural characteristics are comparable to a normal reinforced concrete building, without any particular robustness solutions. This is due to the fact that in an urban environment they are very common, in fact, you can find a few dozen of them (Giovinazzi, Austin et al. 2017).

So, one of their main tasks is that to control the activities of the BTS. The BSC is referred to as a mediator and physical link between the BTS and the Mobile Switching Center (MSC). The databases for all the BTS sites, including information such as carrier frequencies, frequency hopping lists, power reduction levels,

receiving levels for cell border calculation, are stored in the BSC to which the BTS is connected. All this means that networks are often structured to have many BSCs distributed into regions near their BTSs which are then connected to large centralized MSC sites (Lyu, Hong et al. 1994).



Figure 3-13 An example of a BSC located in Turin city



Figure 3-14 An example of BSC located in Spain into the city of Barcelona

**Base Transceiver Station (BTS):** It represents the final element of the infrastructure. The element that connects the user to the network. BTS are elements composed of several sub-elements. These sub-components are:

**The sectoral antennas,** A sector antenna is a type of directional microwave antenna with a sector-shaped radiation pattern. The word "sector" is used in the geometric sense; some portion of the circumference of a circle measured in degrees of arc. 60°, 90° and 120° designs are typical, often with a few degrees 'extra' to ensure overlap and mounted in multiples when wider or full-circle coverage is required. The sectorial antennas are positioned in the upper part of the support structure called "tower", installing them as well as with a specific zenith angle (0°, 120° or 240°) to cover a certain area, even with an azimuth angle (7° - 15°) so that the base station can more effectively cover its immediate vicinity and not cause interference to distant cells. Their weight can vary a lot from a few kilograms (1-2) to almost 10 kg.

**Parables.** The parables are typically the cylindrical instrumentation placed immediately under the sectorial antennas. They are used to connect the BTS to the network when the latter is not connected to the network via the optical fiber. This mainly happens when the BTS is located extremely inaccessible and difficult to reach areas with cabling. The parabolas are directed with a specific azimuth angle defined with respect to the BSC that controls the BTS itself or with respect to another BTS if the BSC is too far away. Even for them we speak of a few kg (10 - 20) as a weight.

**Cables.** They are the fiber optic cables that run along the structure to connect the antennas to ground systems. In addition to these cables that run through the

tower, there are the cables that connect the BTS to the network, also in optical fiber.

**Tower.** It represents the structural element of the BTS. The tower can be placed on the roofs of buildings following a concession given to the MNO by the administration of the building and in this case, we will speak of Roof Top Tower (fig. 3-15). Or they can be installed on the ground again following a concession given by the landowner, in this case, we will talk about Raw Land Tower (fig. 3-16). The tower structure can be of the truss type, in this case we are talking about self-supported lattice tower (fig. 3-17) or guyed lattice tower if they have cables as anchorage, otherwise the structure can be as a prefabricated pole type, in this case we are talking about monopole tower (fig. 3-18). The lattice structure can have a square or triangular base. Generally, the vertical development of the structure towers starts with a wider section and then it gradually narrower at the top (in this case we speak of Pyramid tower (fig. 3-19)), sometimes it is common to find truss structures with the same section from the base to the top (in this case we speak of 4 sides, or 3 sides tower depending on the number of legs (fig. 3-20 and fig. 3.21)). While as regards the monopole towers, they are subdivided into two sub-categories based on the type of the connection between the section. If the sections are joined together by an overlapping area the tower is called monopole polygonal tower (fig. 3-22), while if the sections are joined with a flanged union the tower is called monopole flanged tower (fig. 3-23). The lattice towers are made by creating a reticular structure using bolted unions of simple profiles. While monopole towers are made by joining logs of predetermined length. Furthermore, for monopole towers, based on the type of union, two sub-categories of poles can be distinguished: those with trigger, that is, the trunks The sections typically used for lattice structures are hot rolled L or C profiles. While the poles are made using a polygonal section created by welding cold drawn steel lamellas. The steel used for the production of sections can also vary according to the size of the structure to be built and the loads it will have to carry, typically it can go from class S235 to S355. All this applies to both roof top towers and raw land towers. The towers on the roofs generally have a height that varies from 2 to 12 meters with a base that can go from 500 mm to 2500 mm. As for the towers on the ground, they can have a height that varies from 15 to 100 meters with a base that can go from 1 to 8 meters (Madugula 2001). Typically, the tallest lattice towers are installed using tie rods anchored to the ground to resist horizontal actions. The towers can then be characterized by other parameters as will be seen in the next chapter.





Figure 3-15, example of roof top BTS



Figure 3-16, example of raw land BTS



Figure 3-17, example of lattice tower



Figure 3-18, example of monopole tower



Figure 3-19, example of Pyramid lattice tower



Figure 3-20, example of 4 sides lattice tower



Figure 3-21, example of 3 sides lattice tower



Figure 3-22, example of polygonal monopole tower



Figure 3-23, example of flanged monopole tower

*Minor plants.* They concern all those secondary elements such as access stairs, connection cables between the antennas and the ground box, antenna holder, etc.

*Shelter or Locker.* At the base of the tower there is usually a shelter for all the instruments necessary for the regular operation of the BTS station such as the transmitter.

*Generator.* In addition to the shelter at the base there is usually always a diesel generator in case of emergency due to the lack of electricity from the normal electricity network. this can be seen as a point of interdependence between the two types of critical infrastructures.

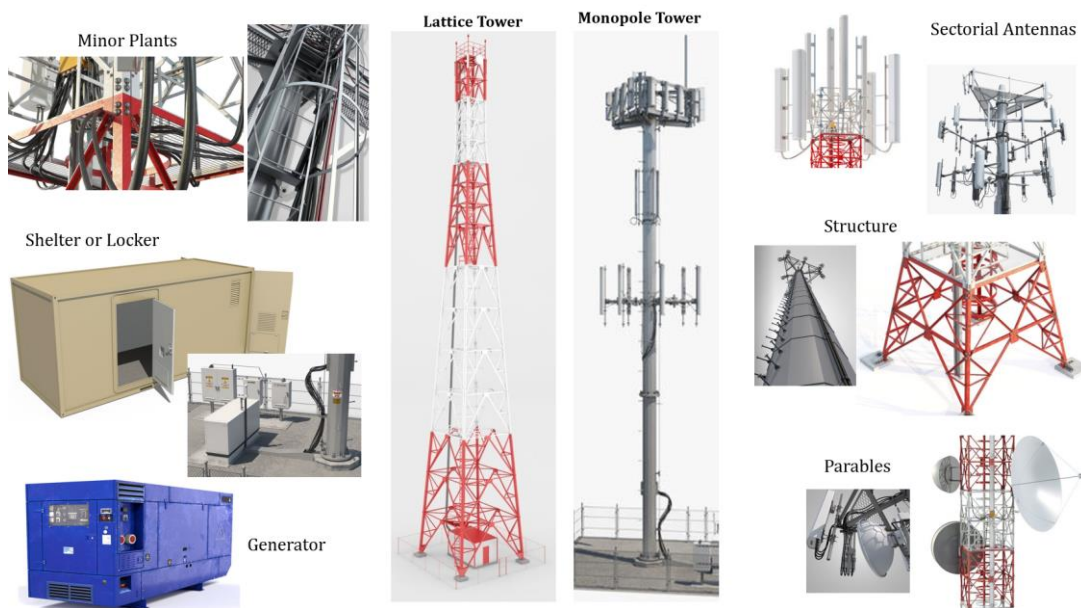


Figure 3-24, an overview of the elements of a BTS

*Users (UE):* People who uses and connects to the network via the personal device to connect with other network users. The connections that are established from an MS to the BTS are called uplink, while those in the opposite direction, that is from the BTS to the MS, are called downlink.

### 3.2.2.3 System Architecture

The purpose of a telecommunications network is to allow the exchange of information between two end users located in geographically distinct positions. The exchange is achieved through the conversion of information into a signal and the subsequent transport of this signal from one user to another using the network resources. The cellular network architecture can be seen basically as three sections. These sections are called subsystems, and each one is composed by the connection between some of the elements seen previously (Mishra 2007).

- Base Station Subsystems (BSS): This comprises the Base Station Controller (BSC) and the Base Transceiver Station (BTS).

- Mobile station subsystem (MSS): The MSS consists of the end user, more precisely the device with which it connects to the network identified by its subscriber identity module (SIM).
- Network and switching subsystem (NSS): It include the gateway centers (GMSC), all the other MSC exchanges and all the equipment contained within the MSCs necessary to route the signal through the network (eg the home location register (HLR), the equipment identity register (EIR), etc.) of which it is of little significance to deepen in the civil field.

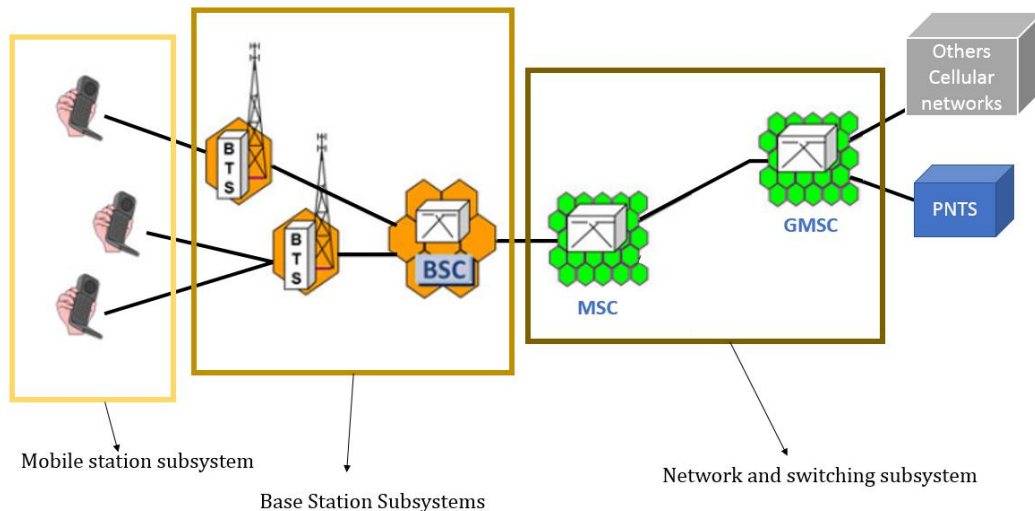


Figure 3-25, system architecture for a wireless network

Another way to see the network architecture is that which separates the system into two sub-networks defined as:

- the network access functionality which in turn identify the part of the network known as the access network (fig. 3-26).
- the transport functionality within the network which in turn identify the part of the network known as the transport network or core network (fig. 3-27).

The access functionality comprises the direct interaction between the end user with the first element of the network or the base station, which thus constitutes the terminal node or more simply the terminal; the conversion of the information into a signal, typically performed by the terminal.

The transport functionality is implemented through a particular mode of transfer and includes the routing of the signal between the internal nodes of the network and the maintenance of the integrity of the related information content along the entire path, in order to reach the destination terminal or terminals for return the information to the end user (s) through access functions (Jin, Li et al. 2013).

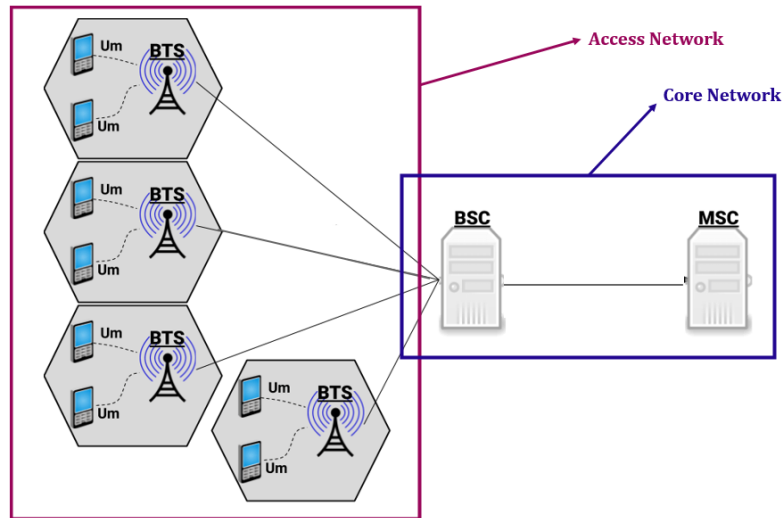


Figure 3-26, definition of what is a access network and a core network in a cellular network

#### 3.2.2.4 Network' Topology

The fundamental elements of the topology are the nodes and links. The node identifies an element of the network characterized by specific functions while the link highlights the connectivity relationship between the nodes. The topology is therefore represented in the form of a graph in which the nodes, capable of exchanging information directly, are connected to each other through one or more links (in fact the topology is an application of graph theory). This idea it can be applied for all types of telecom network. So, in this chapter, the fundamentals of cellular network's topology will discuss. Communicating devices are modeled as nodes and the connections between the devices are modeled as links or lines between the nodes (Alves, Rodrigues et al. 2017).

The connection between two nodes can be seen in two different ways:

As a physical connection, when between the two nodes there is a physical channel that connects them directly; in this case, the branch also represents a real physical entity (Stojcev 2005).

As a logical connection, when it is impossible to think of a physical connection for each pair of nodes or when one wants to consider the information distribution scheme according to a particular point of view. In this case, the branch represents only the logical relationship between the nodes, abstracting the physical meaning (Stojcev 2005).

The network topology is determined only by the configuration of the connections between the nodes. It does not concern: the distances between nodes, the technologies used for physical interconnections (optical fiber, copper cable, electromagnetic waves), transmission speeds, the type of signal (electrical, optical, electromagnetic, etc.).



A real network with a general arbitrary complexity can always be decomposed into a combination of elementary topologies which are in turn interconnected. Elementary topologies can be recognizing in seven basic topologies: point-to-point, bus, star, ring or circular, tree, mesh, or hybrid (fig. 3-27)(Sosinsky 2009).

*1.Point-to-point (P2P):* It is the simplest topology with a dedicated link between two nodes. A trivial example is the telephone with the jars and the cloth thread. A real example of the use of this network is in long distance wireless radio links and, therefore, the two stations are connected via a direct channel. In an open linear network consisting of N nodes, the number R of links necessary for the connection between all the nodes is given by the relation (Sosinsky 2009):

$$R = N - 1$$

*2.Bus:* In the bus topology, all nodes are connected to each other by means of a single shared branch. This topology is very efficient from the point of view of scalability (adding a node does not involve adding links or breaking existing links) and robustness, for these reasons it is widely used in data networks. However, in this type of topology, the presence of a single shared link between all nodes requires the use of access control mechanisms that avoid collisions or interference between nodes (Sosinsky 2009).

*3.Ring or circular:* A ring topology is a closed loop. Data travels around the ring in one direction. When one node sends data to another, the data passes through each intermediate node on the ring until it reaches its destination. The intermediate nodes repeat (re transmit) the data to keep the signal strong. There is no hierarchical relationship of clients and servers. The advantages are that when the load on the network increases, its performance is better than bus topology. There is no need of network server to control the connectivity between nodes. While the disadvantages are network capacity is bottlenecked by the weakest link between two nodes. In a ring network consisting of N nodes, the number of links (R) necessary for the connection between all the nodes is given by the relation (Sosinsky 2009):

$$R = N$$

*4.Star:* In star topology, every peripheral node is connected to a central node called a hub or switch. The hub is the server, and the peripherals are the clients. The network does not necessarily have to resemble a star to be classified as a star network, but all of the peripheral nodes on the network must be connected to one central hub. All traffic that traverses the network passes through the central hub, which acts as a signal repeater. The star topology is considered the easiest topology to design and implement. One advantage of the star topology is the simplicity of adding additional nodes. The primary disadvantage of the star topology is that the hub represents a single point of failure. Also, since all peripheral communication must flow through the central hub, the hub forms a network bottleneck for large network (Sosinsky 2009).

**5.Tree:** The tree topology is a more complex variant of a linear structure, characterized by the fact that several distinct and non-intersecting linear chains can branch off from each node, thus creating a multilevel structure. In this type of topology, for each pair of nodes there is only one connection path; each node is connected to a single upper-level node (parent node) through a single branch and to one or more lower level nodes (child nodes) through one or more dedicated branches (branch). The node from which the whole topology originates is also called the "root node" while the terminal nodes are called "leaves". Also, for this topology the relationship between nodes and links is given by:

$$R = N - 1$$

A feature of this network is that communication between two distinct nodes of the same level can only take place by going up the structure to the first common parent node, which must therefore be equipped with more sophisticated distribution functions in order to determine the correct branch to which to route the signal (Sosinsky 2009).

**6.Mesh:** The fully meshed or fully connected mesh topology is the one of the highest complexities as it requires each node to be directly connected to all the other nodes of the network with dedicated branches. The most important feature of this network is that, given any node, there is always at least one path that allows it to be connected to any other node on the network. The relationship between the number of nodes (N) and links (R) is quadratic and is given by:

$$R = N \cdot (N - 1)/2$$

**7.Hybrid:** Hybrid topology is also known as hybrid network. Hybrid networks combine two or more topologies in such a way that the resulting network does not exhibit one of the standard topologies (e.g., bus, star, ring, etc.). A hybrid topology is always produced when two different basic network topologies are connected.

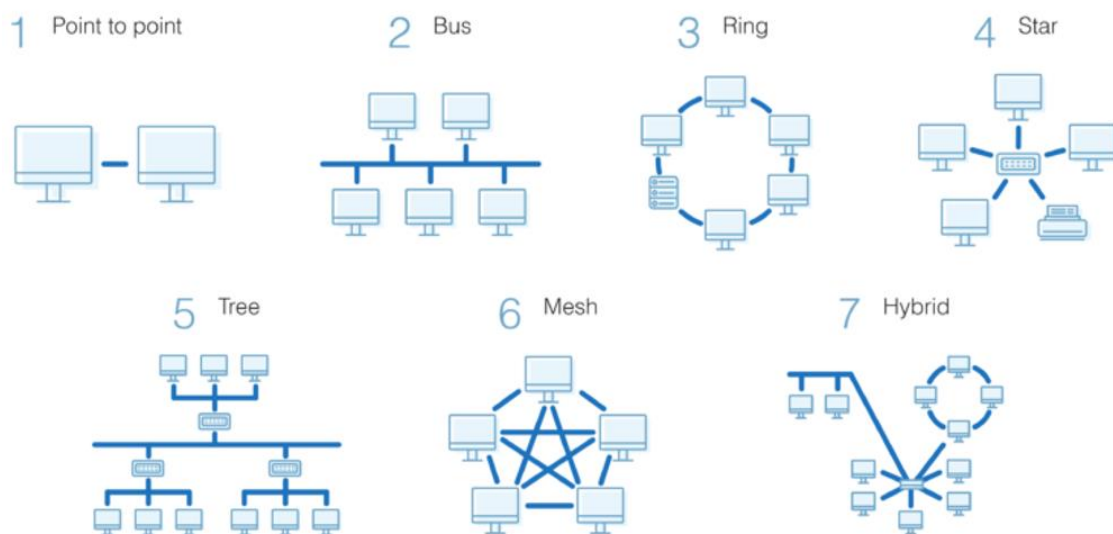


Figure 3-27, Network' Topology

For wireless networks it is impossible to think of using one of the basic topologies as a topology, since they are large and very complex networks. Generally, wireless networks use multiple topologies which can be complex. An example is the topology used between the BTS and the BSC, it is of the "star" type where the BSC is the hub, while the BTS associated with this BSC are the "clients" (fig. 3-28).

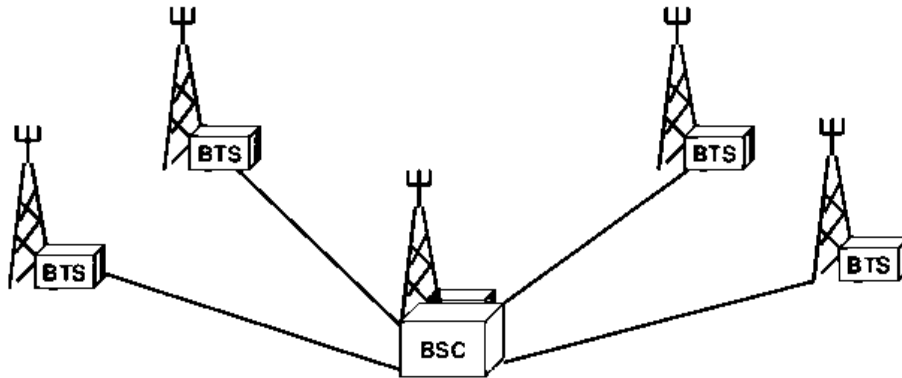


Figure 3-28, Star type for the link between BTS-BSC

**Nodes:** Nodes in graph theory are defined as the point where multiple links with other nodes converge or depart. In information technology and telecommunications, a node is any hardware device in the system capable of communicating with other devices that are part of the network. In a wireless communication network, they are associated with the components of the network seen previously.

**Links:** They are the means of data transmission in a network. They are often referred to as the physical medium that creates the link. This medium can basically be part of two categories:

The wired technologies are: *coaxial cable*, the cables consist of copper or aluminum wire surrounded by an insulating layer very popular technology in the past, it is now being progressively replaced by newer and more efficient technologies. *Ribbon cable* is a cable with many conducting wires running parallel to each other on the same flat plane. Twisted pair, cabling is a type of wiring in which two conductors of a single circuit are twisted together for the purposes of improving electromagnetic compatibility. And last type is optical fiber, is a flexible, transparent fiber made by drawing glass (silica) or plastic to a diameter slightly thicker than that of a human hair. They permit transmission over longer distances and at higher bandwidths (data transfer rates) than electrical cables. Fibers are used instead of metal wires because signals travel along them with less loss; in addition, fibers are immune to electromagnetic interference, a problem from which metal wires suffer.

The wireless technologies: These technologies do not use cables between nodes for data transmission. the main wireless technologies available are, radio waves, that is electromagnetic radiation with a frequency between 0 and 300 GHz.

Infrared light, which is also electromagnetic radiation but with a wavelength shorter than radio waves. The last method is that of laser systems which is a device that emits light through a process of optical amplification.

For wireless network, not all links are wireless. The connection between UE and BTS is wireless and always radio wave technology is used. While the remaining links between the other nodes in the network (BTS-BSC, or BSC-MSC) are typically wired types using fiber optic cables. Only in some cases of isolated BTS, they are connected to the BSC through radio wave link.

### 3.2.2.5 Band and Frequency

A frequency band is a range in the frequency domain, bounded by a lower frequency and a higher frequency. The frequency range of a system is the range within which the system is expected to perform satisfactorily, such as a useful signal level with an acceptable level of interference. Hence, each band corresponds to a frequency range assigned by government agencies through frequency allocation. *Table 3-1* shows all the bands available for mobile communication with their relative characteristics. It is an extrapolation from Tables 5.5-1 "E-UTRA Operating Bands" and 5.6.1-1 "E-UTRA Channel Bandwidth" of the latest published version of the 3GPP TS 36.101 (3GPP 2014).

Band	Duplex mode	f [MHz]	Common name	Subset of band	Uplink [MHz]	Downlink [MHz]	Duplex spacing [MHz]	Channel bandwidths [MHz]
1	FDD	2100	IMT	65	1920 – 1980	2110 – 2170	190	5, 10, 15, 20
2	FDD	1900	PCS	25	1850 – 1910	1930 – 1990	80	1.4, 3, 5, 10, 15, 20
3	FDD	1800	DCS		1710 – 1785	1805 – 1880	95	1.4, 3, 5, 10, 15, 20
4	FDD	1700	AWS-1	66	1710 – 1755	2110 – 2155	400	1.4, 3, 5, 10, 15, 20
5	FDD	850	Cellular (CLR)	26	824 – 849	869 – 894	45	1.4, 3, 5, 10
7	FDD	2600	IMT-E		2500 – 2570	2620 – 2690	120	5, 10, 15, 20
8	FDD	900	Extended GSM		880 – 915	925 – 960	45	1.4, 3, 5, 10
11	FDD	1500	Lower PDC	74	1427.9 – 1447.9	1475.9 – 1495.9	48	5, 10
12	FDD	700	Lower SMH	85	699 – 716	729 – 746	30	1.4, 3, 5, 10
13	FDD	700	Upper SMH		777 – 787	746 – 756	–31	5, 10
14	FDD	700	Upper SMH		788 – 798	758 – 768	–30	5, 10
17	FDD	700	Lower SMH	12, 85	704 – 716	734 – 746	30	5, 10
18	FDD	850	Lower 800 (Japan)	26	815 – 830	860 – 875	45	5, 10, 15
19	FDD	850	Upper 800 (Japan)	26	830 – 845	875 – 890	45	5, 10, 15
20	FDD	800	Digital Dividend (EU)		832 – 862	791 – 821	–41	5, 10, 15, 20
21	FDD	1500	Upper PDC	74	1447.9 – 1462.9	1495.9 – 1510.9	48	5, 10, 15
24	FDD	1600	Upper L-Band (US)		1626.5 – 1660.5	1525 – 1559	–101.5	5, 10
...								

Table 3-1, Features of band for mobile network

The various mobile telephony services (3G, 4G) use different radio frequencies of the electromagnetic spectrum depending on the services made available to users. Typically, the most common bands in an urban environment are bands 1, 3, 7, 8 and 20. The bands 8 and 20 having a lower frequency are those that can cover greater distances and at the same time are able to better penetrate buildings and walls. For this reason, these frequency ranges are mainly used in two contexts: in the countryside and in rural areas and in places with high population density and therefore many walls to penetrate. The downside of these bands is that they are

able to generate transfer rates lower than bands 1, 3 and 7. Therefore, depending on the frequency of use of the BTS, it is also possible to know whether it is a BTS that covers a large or small area. Generally, the BTS that use band 8 or 20 are called "umbrella stations", ie those stations that cover the entire territory to be served with minimal service. Then, to improve the service, stations with antennas using band 1, 3 or 7 are installed, which allow a higher connection speed and less interference problems, but with limited coverage of the territory. Generally, 2G and 3G services are handled by bands 8 and / or 20, while 4G, LTE and beyond are handled by bands with higher frequency.

Each MNO is then assigned a number of 5 MHz blocks of the different band on the basis of auctions. *Figure 3-29* shows the example of subdivision of the blocks assigned to the MNOs of the band 1.

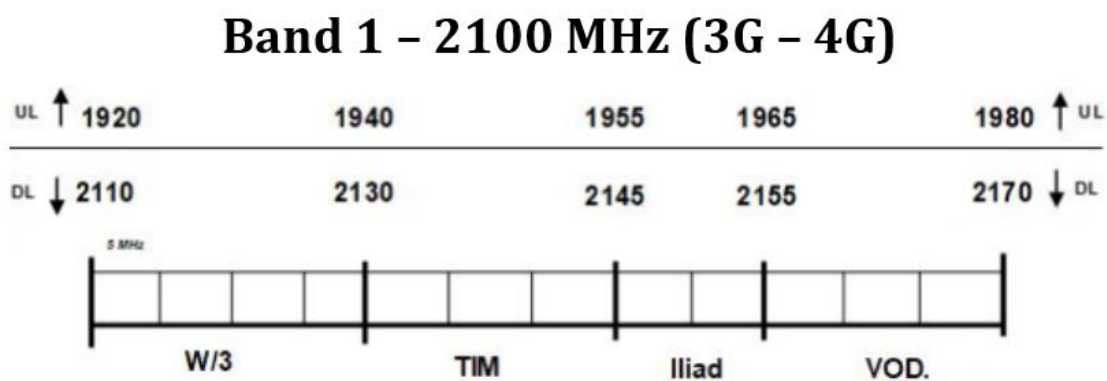


Figure 3-29, assignment of the portions of band 1 for the different MNOs

### 3.2.2.6 Concept of working for Wireless Cellular Network

In wireless networks, the connection is made using electromagnetic waves. This means that if you wanted to cover the entire area with only one or a few transmission devices, this would require an enormous amount of energy to power the necessary power that the transmitters should have, and this would be unthinkable. In addition to the energy problems, there are problems concerning the non-ideal conditions for the propagation of the signal due to the orography of the territory and the rapid saturation of the radio band dedicated to this service as the number of users served increases. What characterizes cellular networks is precisely the division of the territory to be served in small areas called "cells" in a pattern dependent on terrain and reception characteristics. This technique is called "cell splitting".

Although the antennas of the base stations have typically omnidirectional radiation patterns on the horizontal plane, so in reality the coverage of the antennas is circular, the reference shape of the cell is taken hexagonal.





Figure 3-30, example of a coverage area of a real cell

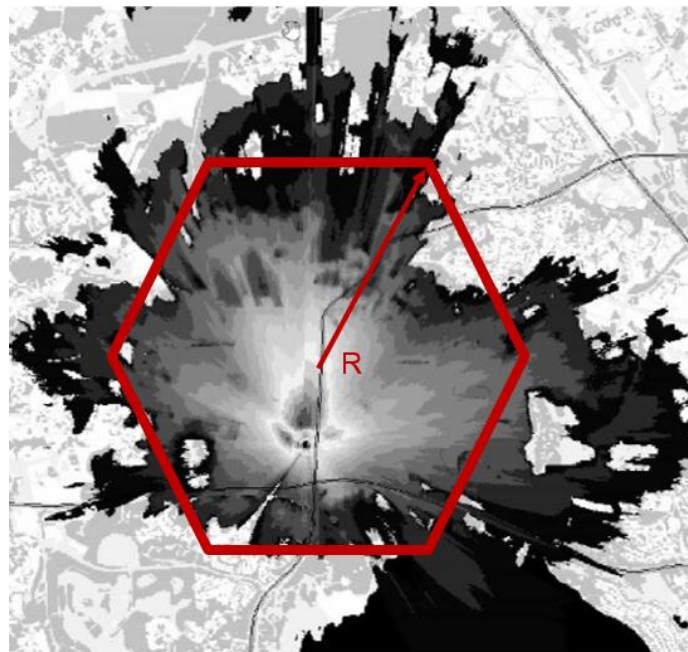


Figure 3-31, schematization of the coverage of a cell

This is since with hexagonal cells the entire territory can be covered without holes or overlaps. Furthermore, the hexagon is a good compromise between simplicity of shape and approximation of a circumference.

The subdivision into cells therefore allows to reduce the transmission power. While the implementation of frequency reuse has allowed to increase the capacity of the system. The basic principle of frequency reuse is to reuse the radio band

(the frequency range) (fig. 3-32), assigned to the system for the provision of services to the user. What is done is to divide the available frequency range into sub-ranges and assign a different sub-range to adjacent cells to reduce the interference that would be generated if adjacent cells had the same frequency range. The division into cells means that the same frequency range can be reused in cells that are not adjacent to each other to minimize co-channel interference. This is extremely useful because the radio band has a limited frequency range while the territory to be covered is of considerable extension.

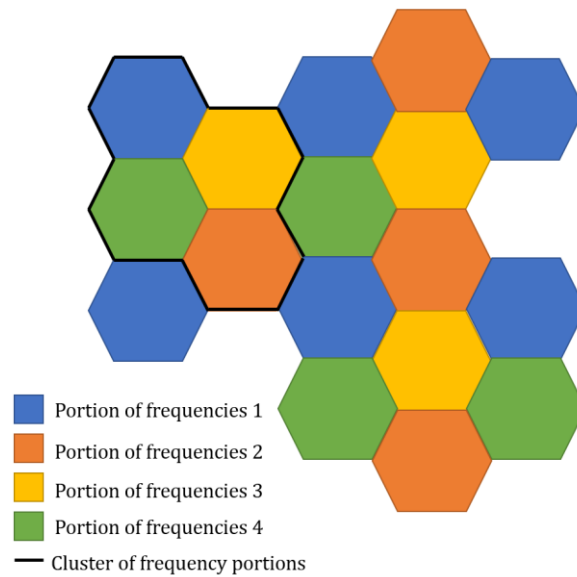


Figure 3-32, example of the reuse frequency

The next step to further increase the frequency reuse is usually resorted to the cell sectorization technique or the use of directional antennas which, by operating a spatial filtering, each cover a certain angular sector of the cell and to which the entire assigned band is assigned to the cell.



Figure 3-33, cell sectoring example with 120° sectorial antennas

There are no BTS in the center of the cells for real urban network. The BTS are always positioned on the corners of the hexagons. In this way, each BTS has a set of sector antennas with a certain azimuth angle so that each set of antennas covers

a certain cell. This provides a minimum of three channels and three towers for each cell and greatly increases the chances of receiving a usable signal from at least one direction for the user.

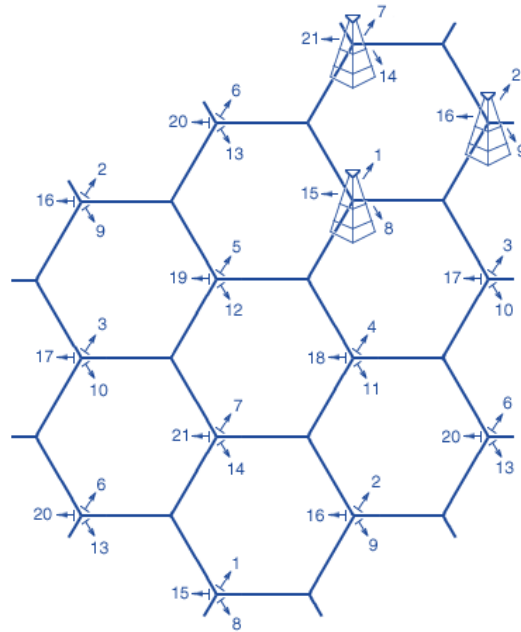


Figure 3-34, tri-cellular sectoring example

After that, the size of the cell depends on the traffic volume and the morphology of the territory. There is a nomenclature to indicate cells with different coverage. In fact, the large cells can be always subdivided into smaller cells.

Macrocell:  $R > 2 \text{ km}$

Microcell:  $200 \text{ m} < R < 2 \text{ km}$

Picocell:  $10 \text{ m} < R < 200 \text{ m}$  (also find into the buildings)

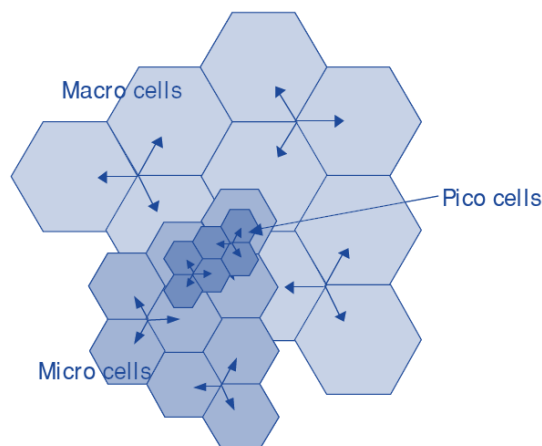


Figure 3-35, scaling the cell from Macro cell to Pico cell

The definition of the cell radius depends on case to case, but generally for from the second generation onwards it does not exceed 30 km (Mishra 2007).



In general, the techniques aimed at frequency reuse, i.e. cell sectorization and cell splitting, are commonly adopted in urban centers according to the population density where, since the need for traffic to be disposed of is significantly greater, the number of cells (and therefore the number of radio base stations) and the number of sectors per cell (and therefore the number of antennas per BTS) is greater and with a lower coverage area than in sparsely populated rural areas or with fewer users to serve.

The cell size is established starting from the geographical density of users for a cell ( $u_{cell}$ ) expressed in number of users per square kilometer and defined as the ratio between the number of channels available for each frequency ( $M$ ) and the cell area ( $A_{cell}$ ) (Mishra 2007).

$$u_{cell} = \frac{M}{A_{cell}} \quad (3-1)$$

The reason why the geographical density of users must be kept as high as possible is that it represents a common interest on the part of both network operators and users. In fact, on the MNO side, as  $u$  increases the number of potential customers increases, while, on the UE side, the likelihood of using the service when requested increases.

The number of channels for a cell ( $M_{cell}$ ) is defined as:

$$M_{cell} = \frac{M}{K} \quad (3-2)$$

where  $K$  is the number of cells that make up a cluster. As a result, the geographic density of the users in the cell ( $u_{cell}$ ) becomes:

$$u_{cell} = \frac{M_{cell}}{A_{cell}} = \frac{2M_{cell}}{3\sqrt{3}R^2} = \frac{2}{3\sqrt{3}R^2} \cdot \frac{M}{K} \quad (3-3)$$

Where  $R$  is the radius of the cell (Mishra 2007).

Obviously, as the radius of the cell  $R$  increases, the geographic density decreases. This explains why in areas with low user density, such as rural areas, it is better to take very large  $R$ , to have the same user density as a populated area, where, instead, there will be small cells, with a radius of few hundreds of meters. At the same time, it is possible to note that  $u$  decreases as  $K$  increases, and therefore it would seem appropriate to keep  $K$  small. On the other hand, small  $K$  involves a level of interference between adjacent clusters that is sometimes intolerable, as we discuss in the following paragraphs. For this reason, a good compromise must be found between these two conflicting needs (Mishra 2007).

It is necessary to understand that it is important to define the so-called reuse distance ( $D$ ) (figure 3-36) which in turn will define the frequency reuse factor (FRF). The reuse distance with the same cell radius  $R$ , it depends on the number of cells per cluster  $K$ . By increasing  $K$ , the reuse distance ( $D$ ) increases and

consequently the ratio C/I between the power (C) of the useful signal and that (I) of the interference. However, it should be remembered that the geographic density of users is decreasing (Mishra 2007).

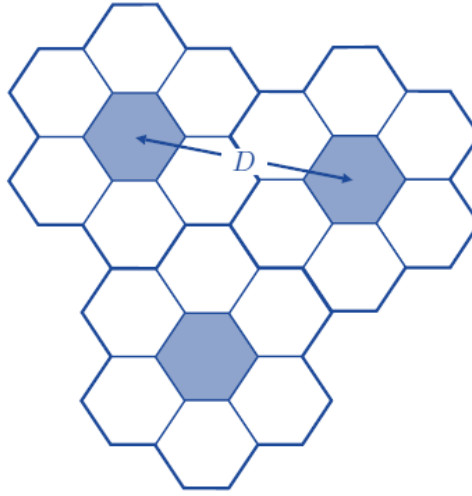


Figure 3-36, illustration about what it is D

Experimentally, it is found that K cannot be arbitrarily fixed (Mishra 2007), but must meet the following condition:

$$K = i^2 + j^2 + i \cdot j \quad i, j \in \mathbb{N} \quad i + j \neq 0 \quad (3-4)$$

<i>i</i>	0	0	0	1	1	1	1	2	2	2	3
<i>j</i>	1	2	3	1	2	3	4	2	3	2	3
<i>K</i>	1	4	9	3	7	13	21	12	19	28	27

Table 3-2, variation of parameter K as a function of the number of cells per row i and the number of cells per column j

Where i and j indicate a natural number chosen by the designer

The capacity of the system (C) will be given by:

$$C = M \cdot S \quad \text{with} \quad S = K \cdot M_{cell}$$

where M is the number of channels available to the network and S is the number of cell clusters. S is given by the product of K and  $M_{cell}$ .

Particular cases are: K = 1, there is a universal reuse typical of CDMA systems (Code division multiple access) and therefore of the third-generation network. K = 7 or 9, are typical values for the second-generation network.

Thanks to the properties of the hexagonal cells, it is possible to identify the homologous cells closest to a given cell, simply (fig. 3-37):

1. moving the cells perpendicular to one of the sides of the hexagon;
2. turning by  $\pm 120^\circ$  clockwise or counterclockwise;

### 3. moving of j cells.

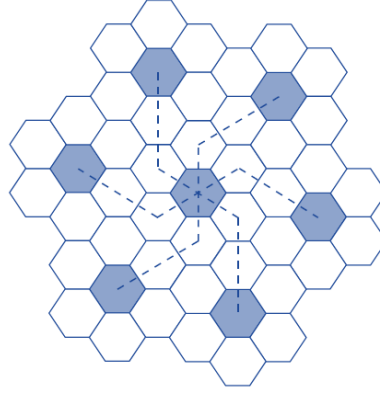


Figure 3-37, cell with the same frequencies

Once the K has been chosen for the network, the FRF can simply be defined as:

$$FRF = \frac{1}{K} \quad (3-5)$$

So, the FRF says the rate at which the same frequency can be used in the network (Mishra 2007).

At this point, it is possible to determine the distance D between two homologous cells (Fig. ...), using Carnot's theorem:

$$D = \sqrt{(i\sqrt{3}R)^2 + (j\sqrt{3}R)^2 - 2(i\sqrt{3}R) \cdot (j\sqrt{3}R) \cdot \cos \alpha} = \sqrt{3KR} \quad (3-6)$$

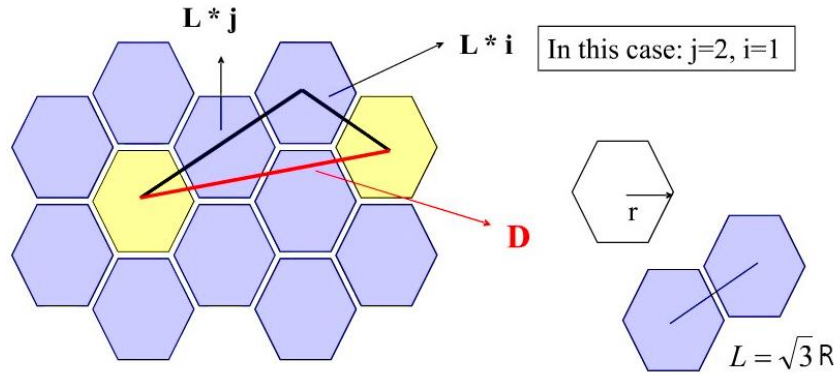


Figure 3-38, visualization about the calculation of the critical distance

Note D can also be defined as a parameter to evaluate the effect of the interference, it is called the interference reduction factor (q) given by:

$$q = \frac{D}{R} \quad (3-7)$$

If the total available bandwidth is B, each cell can only use a number of frequency channels corresponding to a bandwidth of B/K, and each sector can use a bandwidth

of  $B/(KN)$ . Where  $N$  is the number of sectorial antennas for each cell, typically  $N = 3$  (figure 3-39) (Mishra 2007).

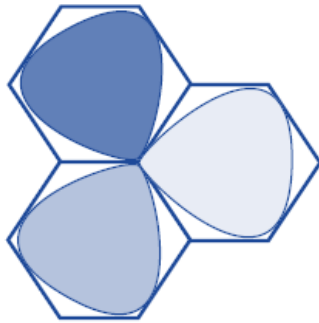


Figure 3-39, A sector BTS can cover three cells

In this subsection, we have seen what the parameters at play are in planning a cellular network. At this point, let us try to outline some conclusions. The main coefficient to study a cellular network are:

- Frequency reuse factor (FRF)
- Cell radius ( $R$ )

Those coefficients affect other network' parameters including:

- Power transmission ( $P_t$ )
- Ratio between  $P_t$  and interference ( $I$ )
- Density of users per cell ( $u_{\text{cell}}$ )

Bandwidth is nothing more than the signal spectrum width available to transmit information. It varies according to the band that the BTS uses. A BTS can use different bands, i.e., the same tower can be mounted antennas that work with a certain band and antennas that work with another one, in order to define different coverage areas (Mishra 2007). This is done in order to have a certain flexibility on the number of users that can be served, for example if an antenna goes out of service or there is a temporary increase in user density in a specific area. So, the cells can be divided into categories as well as with the coverage range also based on the band they use:

Macrocell = band 20 and other

Microcell = band 1 or 3 and other

Picocell = other bands

This is because if the frequency of the signal is lower it can cover an area further away from the receiver, on the contrary if the frequency is high the signal will have a lower coverage range.

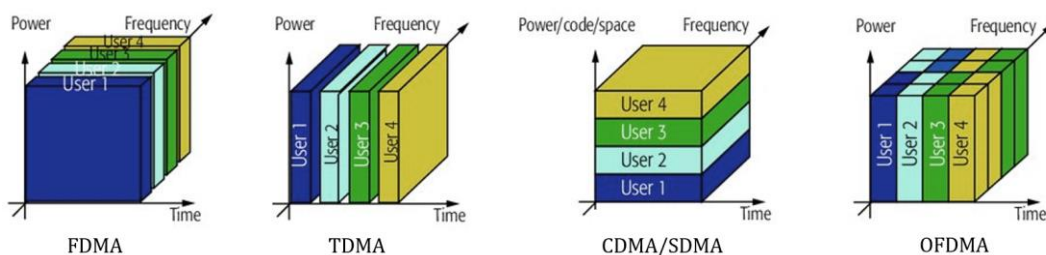
For each type of band, a lower frequency and a higher frequency are defined which in turn define the bandwidth for that band. The frequency table is detailed in the chapter on defining the transmission capacity of the network (chapter 5).

The basic techniques for accessing to the network, that is to the portion of the band of frequency allocated to the sector of cell are various (fig. 3-40) (Mishra 2007). The first method is called frequency division multiple access (FDMA). The FDMA

technique provides for the subdivision of the available band into a certain number of equal sub-bands, each centered around a frequency that identifies the channel. Each sub-band is granted to a single user who has control over it for the entire duration of the connection. The second method is called time division multiple access (TDMA). In the TDMA protocol, the time axis is divided into frames of fixed duration and in turn divided into a fixed number of smaller intervals called slots. Each slot in a particular position within the frame is assigned to a user. Each user can therefore transmit for a period equal to a slot at intervals equal to the duration of a frame, in this time, it has all the bandwidth of the system available.

The third method introduced with the third generation of the network, is called code or space division multiple access (CDMA/SDMA). CDMA/SDMA is a multiple access method, where many transmitters can send information simultaneously over a single communication channel. This allows several users to share a band of frequencies. To get this without a huge interference between the users, CDMA/SDMA uses a special coding scheme where each transmitter is assigned a code. The last method used for the fourth generation of the network is called orthogonal frequency division multiplexing access (OFDMA). The OFDMA is a multi-carrier modulation system in which data is transmitted as a combination of narrow-band orthogonal signals known as sub-carriers. OFDMA is a special form of multicarrier modulation (MCM) scheme, where a single data stream is transmitted over several lower data rate subcarriers. OFDMA is a combination of both modulation and multiplexing. In OFDMA method the signal itself is first split into independent channels, modulated by data and then re-multiplexed to create the OFDMA carrier. This can be understood by making an analogy with a shipment by truck. There are two options: one is to hire one truck and the other is take four smaller trucks. Both methods carry the same amount of data. However, in the case of an accident for the second option, only a quarter of the data will suffer or lost. Here the four smaller trucks when seen as signals are called the subcarriers in an OFDMA system and they must be orthogonal for this idea to work. The independent subchannels can be multiplexed by using frequency division multiplexing (FDM), or time division multiplexing (TDM), called multicarrier transmission, or can be based on code division multiplexing (CDM), called multi code transmission (Mishra 2007).

Nowadays the first method is no longer applied being a method used in the second generation of the network. While the minimum network available in developed areas is now that of the third generation.



From these basic techniques' others have developed more and more efficient from the point of view of the capacity and speed of data transmission.

All the features of the network introduced in this chapter, i.e. the bands and frequencies that the network uses, the bandwidth, the type of access used, the loss of signal and other parameters will be discussed in detail in the chapter 5.

### 3.2.3 Satellite Network

The last type of telecommunication network in the civil field is the satellite type. Satellite telecommunications are a form of radio frequency wireless telecommunications for the remote communication of information through satellite radio links between ground-based transceiver stations and artificial satellites in orbit in the form of satellite radio links.

These systems, made possible by the birth and development of launch technologies, often represent the only solution applicable in the absence of terrestrial infrastructures or difficult to locate and with a lower overall cost than the implementation of equivalent terrestrial communication systems.

These networks can be seen as radio communication systems to support terrestrial networks in the form of integration into coverage services (e.g. intercontinental radio links) or transmission redundancy in the transport network useful in case of need (greater transmission capacity required, malfunctions, failures) for example as a result of events such as natural disasters that may occur on the earth's surface, undermining the respective terrestrial communications infrastructures. Furthermore, the satellite remains unbeatable in all broadcast applications, that is, all those applications for which the same data must be sent to many receivers, much more than the broadcast of terrestrial systems. Its scalability, compared to the terrestrial network, is simply not comparable. The main disadvantage is certainly the cost, higher than terrestrial networks even if in recent years the launch technology has undergone a significant cut in the cost of building a satellite network. In addition to this, it must be said that the lower the orbit altitude is, the more the satellite coverage efficiency decreases and therefore the number of satellites needed increases. The main element (as can be the BTS in cellular networks) of these networks is certainly the satellite. Specifically, the components that make up the network are the following:

**Satellite Ground Stations (SGS):** All satellite systems must be somehow interfaced and interlaced with ground stations for the reception of upload data from the earth's surface and the retransmission in download to users on the earth's surface. In general, the ground stations can be transceiver stations or more simply receiving stations. In any case, they are characterized by directional antennas such as parabolic antennas aimed directly at the satellite, following it as

much as possible along its orbit and capable of possibly tuning in to different satellites of the same constellation as they pass within their range of coverage thanks to specific procedures. In particular during loading, that is, during the sending of data to the satellite before their retransmission on the earth's surface, complex satellite stations on the ground are often required, i.e. real dedicated satellite transmission and control centers. The ground stations can in turn be interlaced to terrestrial telecommunication networks such as for example cellular mobile telephone networks to make up for any coverage gaps or interlaced directly to wired transport networks.



Figure 3-41, example of satellite ground station, Centro Spaziale del Fucino

***Parabolic antenna (PA):*** A parabolic antenna is an antenna that uses a parabolic reflector, a curved surface with the cross-sectional shape of a parabola, to direct the radio waves. The most common form is shaped like a dish. The main characteristics of this category of antennas are the high directivity and consequently the "gain": these quantities depend on the ratio between its effective diameter and the wavelength used in the reception-transmission: the higher this ratio, the greater the ratio the "gain" and directivity. They are used for communications between satellites and their ground control stations.



Figure 3-42, example of parabolic antenna

***Satellite (S):*** The term artificial satellite refers to a device made by man and placed in orbit around the Earth. The set of several artificial satellites used for the same purpose forms a constellation. The main components of a satellite are: the main core that contains the tools necessary to perform the functions for which the



satellite was built, the photovoltaic panels to produce electricity, motors to move the satellites and finally the parabolas to transmit and receive the signals.



Figure 3-43, example of telecommunication satellite

### 3.3 Network' Vulnerability

Like all other infrastructures, telecommunications infrastructures are also subject to both natural and man-made disasters. Such as earthquake, tsunami, etc. (fig. 3-44). In this study it will see the vulnerability to the earthquakes for wireless telecom network.

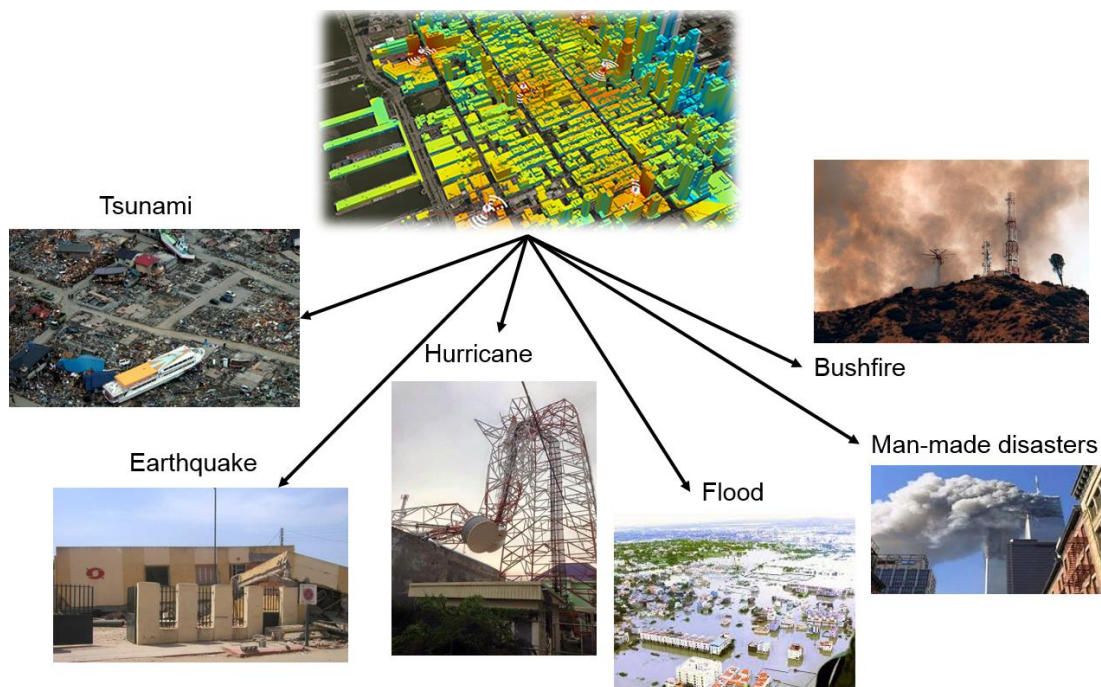


Figure 3-44, Disasters that can damage the network

The performance of telecommunication networks is of high priority as they have a substantial impact on our lifestyle during normal times. Their operation becomes even more important after a disaster scenario. This is because, such networks are used in civil protection and emergency plans, as well as for



coordination in the restoration of all other critical infrastructures (Mauthe, Hutchison et al. 2016).

Therefore, it is very important that such networks have the lowest possible vulnerability or least try to have it. Based on the specific types of networks, it can be said that in an urban environment the greatest vulnerability to the disaster scenario seen before is to be attributed to wireless networks (Sterbenz, Cetinkaya et al. 2011). This is because, typically, the ground control stations of satellite networks are located in less densely populated areas and designed with particular constructive measures to have a good level of robustness of the structure. While as regards the landline network it undoubtedly has a vulnerability to events such as earthquakes, floods, etc. However, this vulnerability particularly concerns cable lines, while is limited for the service building. In this study the effects on the cabling lines (snatch) for any network are not considered. So, for all these reasons just outlined and for the reasons previously introduced about the gradual inactivity of the landline network and the strong expansion of the wireless network instead, the study focused on assessing the vulnerability of the wireless network.

The wireless network can suffer direct damage to one or more elements that compose it, for example the collapse of a service building or the shearing of a cable due to ground movements during an earthquake. In an urban environment such as in the case of the Ideal City project, a telecommunication network in addition to direct damage can suffer to indirect damage. For example, the BTS are often installed on the roofs of residential buildings so that their possible collapse would cause irreparable damage to the BTS placed on the roof as well. This can lead to signal loss in a given area or overloading of users on other BTSs. However, efforts such as redundancy of elements, increase the network' resilience, and emergency response planning do provide lots of benefits during and after the extremely large events such as earthquakes (Kwasinski and Tang 2011).

In addition to the vulnerability of the individual elements that make up the network, the vulnerability to disasters of the network itself must be considered. An example of this, it is the case in which a member of a higher hierarchical level goes out of service. This will have a cascading effect of damage on the components connected to it if there is no alternate path.

Therefore, it is also important to evaluate the resilience of the network topology itself. It is impossible to have a fully meshed network due to cost and physical reasons. However, a topology can be studied to reduce as much as possible the effects of a possible disaster on the network (Alves, Rodrigues et al. 2017).

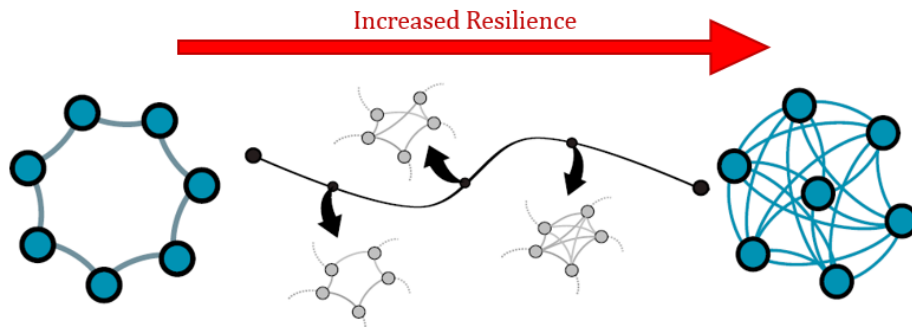


Figure 3-45, increasing the resilience for the network topology (Alves, Rodrigues et al. 2017)

An example of the different vulnerability for the various types of the network is represented by the case that occurred during the 2016 Kaikōura earthquake in New Zealand where, the substantial damage to the landline network mainly concerned cable tears in the underground due to the movements of these last or collapses of poles carrying copper cables. While the service buildings did not suffer structural damage but service components inside them were damaged. In the case of the mobile network, however, some BTS collapsed due to the collapse of the building on which they were installed. While two local control stations suffered severe structural damage and others suffered minor damage (Giovinazzi, Austin et al. 2017).

Instead, due to the earthquake and subsequent Tsunami, many elements of the ICT network have suffered damage or have been destroyed such as: offices, switching complexes and base stations as the figure 3-46, 3-47 below show.



Figure 3-46, base station control in Onagawa destroyed by earthquake-tsunami, Japan 2011



Figure 3-47, BSC components damage located in Iwate prefecture after Japan 2011 earthquake

It has been seen that immediately after the earthquake there was an explosion of requests for the telecommunications network both from citizens and from institutions and companies to organize relief, so much so that the traffic soon after congested both the fixed and mobile network.

About 1.5 million users were excluded from using the network and the traffic load on the network increased from 2 times the normal traffic as show in *figure 3-48* Nippon Telegraph and Telephone took just 6 weeks to recover the network, while it took 11 months to fully recover, but this is too long a time frame to deal with the emergencies generated by a disaster (Sakano, Fadlullah et al. 2013).

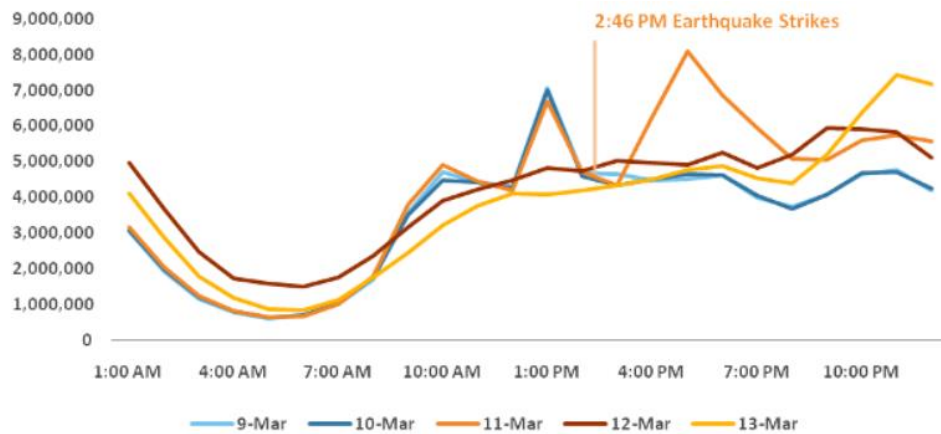


Figure 3-48, traffic network increase after the earthquake Japan 2011

During the 2011 Japan earthquake-tsunami, an appreciable number of base stations controller were destroyed by the tsunami, a few by the earthquake, and power outages were the causes of other base stations failures. Majority of BTSs went out of service due to the collapse of the buildings on which they were placed or did not have power generators to last a long time.

In addition to the damage to both service and residential buildings, it was also possible to find damage to the BTS on the ground in some cases some support towers have completely collapsed as the figures 3-49, 3-50 show (Kwasinski and Tang 2011).



Figure 3-49, Cell site destroyed by the tsunami in Rikuzentakata



Figure 3-50, A collapsed tower of a base station located in the Karakuwa Peninsula.

## 4 Design of the Ideal City' Wireless Telecommunication Network

### 4.1 Introduction

The concept of the virtual city is attracting the interest of many researchers due to the advantage in testing algorithms and methodologies, at a poorly studied scale. Virtual cities (as Ideal City) are capable to model different types of critical infrastructures and hazards (earthquakes, floods, etc.) according to pre-determined design approaches which may be representative of a risk area.

Modeling an urban telecom network requires a large quantity of data and information which may not be all available or accessible especially because, it represents a strategic infrastructure for the community (Hassan and Mahmoud 2020).

A built environment made up of physical systems such as buildings and lifeline considered as a complex system. Therefore, identifying all the different entities and attributes of this system may result in large economic and management efforts. In this work, as previously said we will focus on the telecom network. In particular, the wireless telecom network will be analyzed, which represents the largest, the most vulnerable and the fastest growing physical communication system within an urban area.

A complete characterization of the entire network at urban scale is the most accurate and consistent process to be addressed. However, some issues exist such as lack of detailed information (i.e. structural data), inaccessibility of the data (i.e. the location of base controller station), as well as limitation in data sharing (permission request to access to the data) lead to a time consuming and long data collection process, as well as the inevitable use of certain assumptions for the construction of the network. The sources of uncertainty are different and mostly related to the lack of knowledge on the mechanical, and geometric parameters, that can characterize a structural model.

So, this chapter will cover the process of creating the network for the case study. It will illustrate the type of data collected to characterize the different elements that are part of the network, where the data were found, and any hypotheses made on the information that were absent or not available.

## 4.2 Network's exposed components Database

Data collection is the process of gathering and measuring information on targeted variables in an established system, which then enables one to answer relevant questions and evaluate outcomes. It is a basic procedure required to get the essential features of a complex system how it can be a telecommunications network.

The whole project of the Ideal City developed by the Resilience Laboratory of the Polytechnic of Turin is based on the city of Turin. For this reason, the collection of data to design the communication infrastructure takes place getting as a reference the data available from the real city network. As defined in the chapter 3, a wireless network is composed of several elements: radio towers, minor control stations, general control stations, wiring networks, users, etc. In this study, the vulnerability of the wiring network due to ground movement caused by the earthquake is not assessed (Giovinazzi, Austin et al. 2017), therefore information regarding these elements is not taken into account.

The categories of data necessary to characterize each physical element of the network are:

- *Geographical*
- *Geometrical*
- *Telecommunicational*
- *Structural and Non-Structural*

### 4.2.1 Data collection for the Base Transceiver Stations (BTS):

As introduced in the chapter 3, the Base transceiver stations are elements composed of several parts (support tower, antennas, servers, etc.) and connect the user to the network, so they are fundamental element to study. The data collection for the BTS started obtaining information about their location in the urban environment (as seen previously in the chapter ..., generally they can be found on buildings, on steel tower or poles, or on tank). To do this, two opensource platforms were used. The first is called "CellMapper" (*figure 4-1*) and the second was the Geoportale Regione Piemonte (*figure 4-3*). The final data used were those provided by CellMapper. While the geoportal was used as a tool for verifying the correctness of the data provided by the first platform.



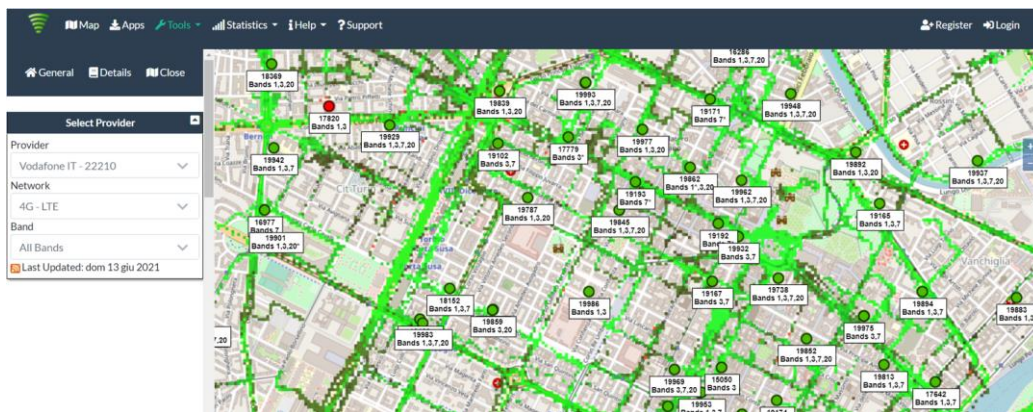


Figure 4-1, An overview on the CellMapper.com site



Figure 4-2, A zoom on the CellMapper.com site' map

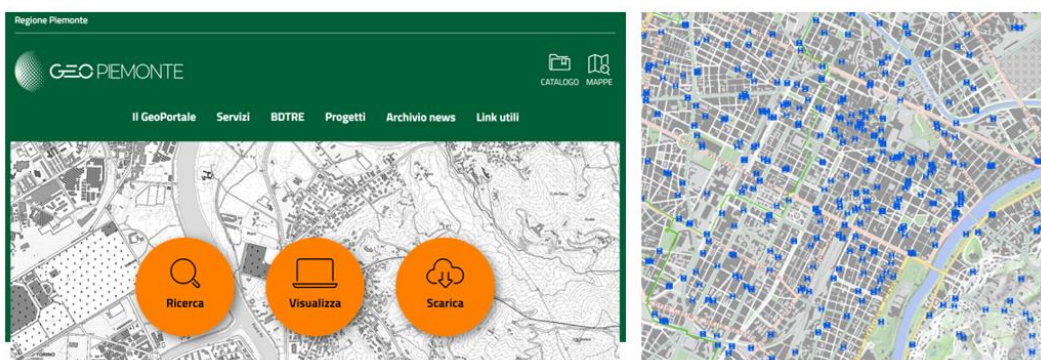


Figure 4-3, Map form Geoportale Site

#### 4.2.1.1 Geographical parameters:

The first data extracted from the CellMapper platform about the BTS were the geographic coordinates through a csv file format. Once the position of the BTS is available through the shape file, the file is loaded on a GIS software (QGIS) to overlap it on the shape file of the buildings (as seen in the *figure 4-5*). In this way we define the second geographical parameter, the location of the BTS (if the BTS is located above a building or on the ground). To do this, however, it was early necessary to verify that the output file provided by CellMapper was set with the same reference system as the built environment file. The reference system selected was UTM zone 32N (EPSG: 32632). So, the defined geographic parameters were:

- Geographic Coordinates (x[m] and y[m]) (GC)
- Location (Roof Top, or Raw Land) (L)

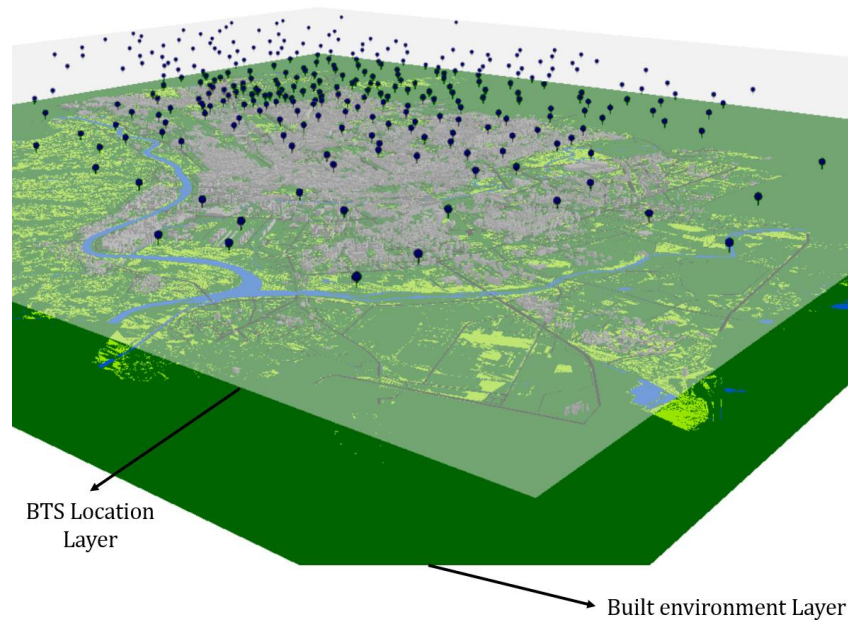


Figure 4-4, example of location knowledge about BTS

Two types of location are defined. The first one is Roof Top type when BTS is on the building roof and the second one is Raw Land type when BTS is on the ground. Based on the location parameter, it was possible to make a first subdivision of the BTSs positioned in the study area. This subdivision is show in the *table 4-1* below.

Type of tower	Total	%
Raw Land BTS	148	17,4
Roof Top BTS	702	82,6
BTSs	850	100

Table 4-1, Total BTS selected based on location for Ideal City project



As can be seen from the *table 4-1* in total 850 BTSs are found in the urban context studied, the most of the 850 BTSs found are positioned on building' roofs and this is normal for a city. This is clearly correct for a city. To check the correctness of the assigned location for the BTS, some verifications of the accuracy of the location assigned to the BTS were made through satellite images and live inspections. These values concern the physical number of BTS (some BTS can be shared by various MNOs) present in the reference area to build the network for the Ideal City project considering all the MNOs together. This is specified because, other subdivisions according to other parameters will be introduced and discussed later.

#### *4.2.1.2 Telecommunication parameters:*

The second category of data got from the CellMapper platform, was about the telecommunication characteristics introduced at a general level in the chapter 3. The information obtained concerned: which MNO (mobile network operator) own the BTS. In this work three MNO are considered. TIM, Vodafone and Wind3. As said in the chapter before they are the most popular in Italy and also, they have been selected because they were the only MNO with complete information on CellMapper. The second parameter selected was the type of band and therefore consequently the type of frequency that the BTS uses, then the method of connection with the BSC was defined, and the last characteristic got, was the type of coverage of the BTS (e.g. Macro cell), and that it is used to approximate the tower' coverage radius (i.e. the towers classified as Macro cell have 3 km as coverage radius). For the Ideal City's network, two working bands have been selected, band 3 and 20, consequently knowing the band two frequency ranges one for each band, 800 MHz. for band 20 and 1800 MHz for band 3 have been identified. Finally, two types of coverage based on the band have been identified, namely Macro cells or Micro cells. So, the BTSs with a low frequency have been included in the Macro cell subcategory, while the BTS with high frequency have been inserted in the Micro cell subcategory. Should be also say that some BTS can have many levels of antennas that work with different frequencies as *figure 4-6* shows. So, it could be that one level works with a band and another level that work with a different band. In these cases, the same BTS in signal evaluation provides two different values based on which level of antennas the user connects. For this reason, a BTS can be counted several times. That is, the physical BTS are 850, but if they are counted according to the type of coverage, they are greater because, a single BTS can carry out coverage with two levels instead of one.

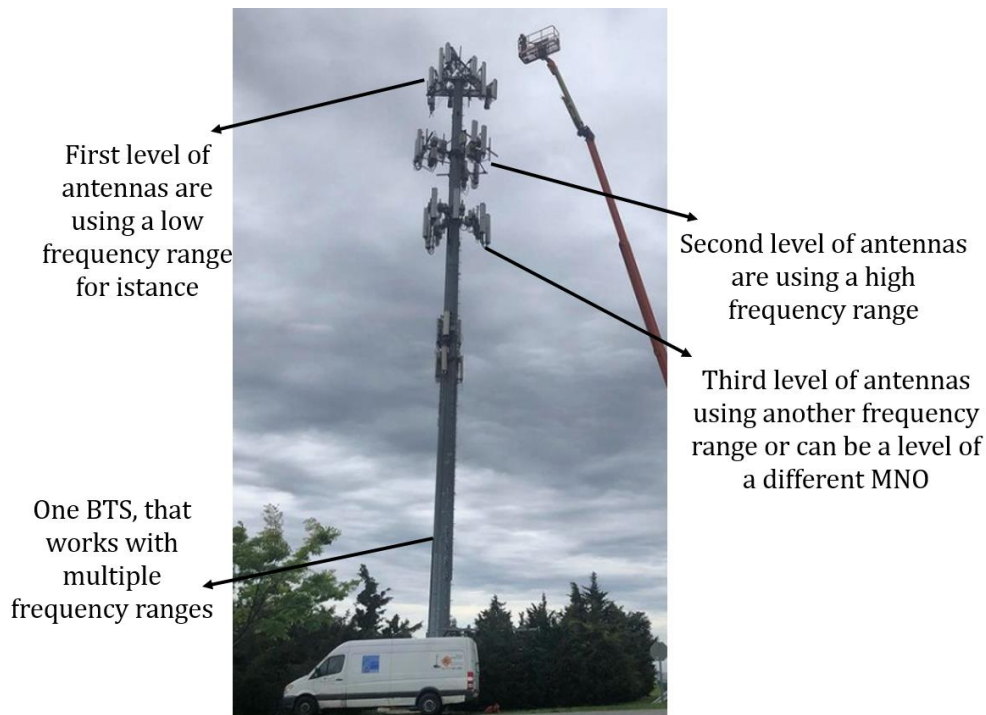


Figure 4-5, BTS with many level of work frequency range

- Type of MNO (e.g. MNO1, MNO2, or MNO3) (MNO)
- Bands used by each BTS (3 or 20) (Bd)
- Frequencies used by each Band (f)
- Type of connection with the BSC (wired, wireless) (W)
- Type of Coverage (e.g. Macro cell or Micro cell) (MA or MI)

Once the telecommunication parameters have been defined, various subdivisions of the BTS can be extrapolated. The first subdivision concerns which MNO the BTS belongs to. Then the BTS assigned to the various MNOs can be divided according to their location introduced previously. Finally, the BTS of each MNO are divided according to the coverage radius, that is macro cells or micro cells and therefore according to the frequency that the BTS uses. It must be said that a single BTS can be counted multiple times as it can work with multiple frequencies.

<i>MNO</i>	<i>Total Physical BTS</i>	Raw Land BTS	Roof Top BTS
MNO 1 (TIM)	304	57	247
MNO 2 (Vodafone)	286	53	233
MNO 3 (Wind3)	260	38	222
Ideal city network	850	148	702

Table 4-2, Roof top and Raw land BTS by each MNO

<i>MNO</i>	<i>Total BTS</i>	Macro Cell BTS	Micro Cell BTS
MNO 1 (TIM)	387	103	284
MNO 2 (Vodafone)	359	108	251
MNO 3 (Wind3)	359	117	242
Ideal city network	1105	328	777

Table 4-3, BTS subdivided based on the type of coverage for each MNO

#### 4.2.1.3 *Geometric parameters:*

The work to complete the BTS's database has continued with the geometrical category. This category concerns the geometrical characteristics of the BTS tower. The support towers' geometrical data (i.e., height) have been collected from the GeoPortale Piemonte site and verified through the MNO' sites when they were available (for example TIM provides a website where are publish some data about the BTS of the network). GeoPortale Piemonte tool allows the free visualization of the general information about the whole telecommunication systems (2G, 3G, etc.) for the whole administrative territory of Piedmont Region, so even for the city of Turin. All the data are organized in csv-file format (readable by QGIS). For the towers for which the Piedmont Geoportal platform does not provide any data, the geometric parameters were estimated through in situ investigations, or by satellite photos investigations or also comparing with the data available of similar BTS. The geometric information extracted was:

- Height ( $h$ )
- Bottom base width ( $B_{\text{bott}}$ )
- Top base width ( $B_{\text{top}}$ )
- Type of tower (i.e., Monopole)
- Base variation in height (pyramid, 4 sides, 3 sides, pole)
- BTS-BSC distance ( $D_{\text{BTS},i}$ )

Where  $h$  indicates the height of the tower,  $B_{\text{bottom}}$  is the width of the tower at the base, while  $B_{\text{top}}$  is the width of the tower at the top, then, being symmetrical elements, the dimensions are identical in both directions. Going on, some types of towers may vary the size of the base according to the height. Finally, a first structural distinction is made, it based on the type of support tower structure. If fact, as it saw in the previous chapter 3, there are mainly two major distinctions for support towers, that is valid for both on the ground tower (called Raw Land Towers) and for the tower on the roof of buildings (called Roof Top Towers), that is, monopole towers, or lattice towers. It will be seen that these two categories fall into sub-categories. Once, the information about BTS and their subdivisions based on type had been collected, this was verified using the satellite images provided by googlemaps.com and in some cases in person (same example in the *figure 4-6* below). Base variation and type of tower will determine together the structural

configuration that it will be introduced in the next category for the tower. Finally, the last geometric parameter to be introduced is represented by the distance that each BTS has with respect to each BSC. It will be necessary to define a telecommunication parameter for the BSCs and to implement the network topology.



Lattice Raw land tower



Monopole Raw land tower



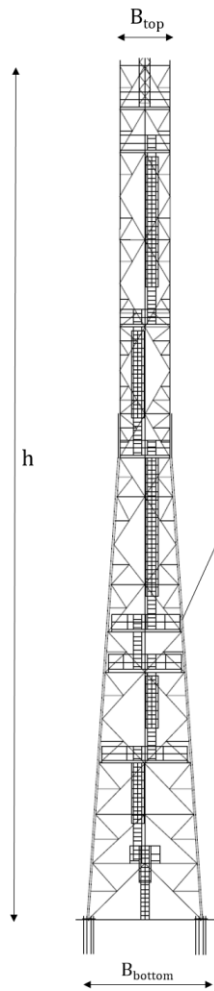
Lattice pyramid Raw land tower



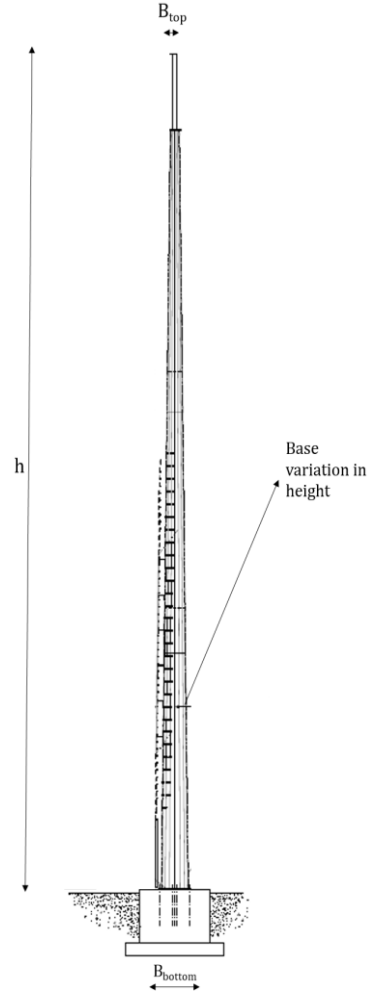
Monopole Roof top tower

Figure 4-6, grouping of BTS, which have been verified in person

The *figures 4-7 and 4-8* below show an example of the meaning of geometric data.



Example of lattice tower



Example of monopole tower

Figure 4-7, prospect example of raw land tower

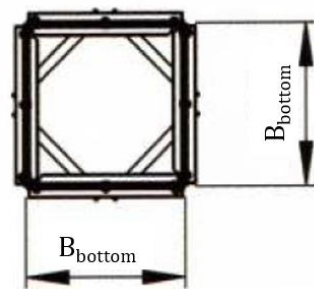


Figure 4-8, section example of lattice raw land tower

Based on type of tower the division into the two categories is:

Type of tower	Lattice tower BTS	Monopole tower BTS	Total by each Type
Raw Land BTS	62 (42%)	86 (58%)	148

Roof Top BTS	189 (27%)	513 (73%)	702
Ideal city network	251 (29,5%)	599 (70,5%)	850

Table 4-4, subdivision based on type of structure for the raw land and roof top tower

As you can see into the *table 4-4*, most of the support structures on the roofs are poles. While for the ground support towers, there is an almost uniform distribution. In *table 4-5* below, the BTS are not only divided according to the type as before, but also according to the MNO that they belong to.

<i>MNO</i>	<i>BTS's location</i>	Lattice tower BTS	Monopole tower BTS	<i>Total BTS by location</i>	Total BTS by MNO
MNO 1	Raw Land BTS	23	34	57	304
	Roof Top BTS	61	186	247	
MNO 2	Raw Land BTS	22	31	53	286
	Roof Top BTS	63	170	233	
MNO 3	Raw Land BTS	17	21	38	260
	Roof Top BTS	65	157	222	

Table 4-5, subdivision of the towers on the basis of the location and the type of structure for each operator

#### 4.2.1.4 *Structural and Non-structural parameters:*

The last category to complete the characterization of the BTS, it was that about the structural and non-structural parameters to describe the support tower for the BTS. At the urban scale with these number of elements, finding these parameters may result complicated in terms data available. For this reason, these parameters have been defined based on previous studies defined in the literature, through the European Eurocodes legislation and with some in situ inspections where it was possible. The parameters chosen are the following:

- *Structural Configuration (SC)*
- *Mechanical Characteristics (MC)*
- *Primary sections (PS)*
- *Secondary sections (STS)*
- *Tertiary sections (STS)*
- *Tipical Primary Vartical Bracing Patterns (PV)*

- *Typical Secondary and Tertiary Vartical Bracing Patterns (SV)*
- *Typical Horizontal Bracing Patterns (H)*
- *Foundations (F) or anchoring system (A)*
- *Typical Connections for the tower (C)*
- *Typical Base Portal Frame Patterns (PF)*
- *Coating Process Types (CO)*
- *Loads definition (LC)*

It's important to note that not all cell towers are the same. There are three different general structural configuration of communication towers that can be used. Each type of cell tower can be installed depending on the specific purpose. The general structural configurations are, Monopole, Self-supporting and Guyed. Monopole towers work well when space is limited, zoning is difficult or harsh weather conditions need to be considered. Designed as a single-pole that can be a tubular section design or a formed, tapered pole, they are the least intrusive – making them the most popular tower types in the wireless communication industry. Because of the single-pole design, it advantageously reduces visual impact and results in a shorter construction time (and typically cost) compared to traditional lattice structures. Many monopoles can also be designed as stealth, camouflage towers. Their limit is in the maximum height that can be get. The range of height goes from 15 to 60 meters. Self-support towers offer the most possibilities compared to other types of telecom towers and are considered appropriate for nearly all wireless communication applications. Available in 3-legged triangular and 4-legged square lattice-type structures, their braces can accommodate the heaviest of loads and the strongest of winds. Their height's range goes from 20 to 140 mt. Guyed towers can be lightweight to heavyweight towers often seen as slender steel structures. Commonly seen in the tower industry, guyed towers are designed to provide maximum strength, efficiency, and versatility with easy installation. They are supported by one or more levels of braided or stranded steel guy cables that anchor to the ground. Their main advantage is the high height they can reach, over 200 meters. The disadvantage is that they occupy an overall area (therefore also considering the tie rods) greater than the previous configurations (Madugula 2001). *Figure 4-9* shows the main structural configurations. The second parameter introduced was to define the mechanical characteristics of the structure. The design requirements (e.i. mechanical and strength characteristics, resilience, etc.) have been collected in accordance with the EN 1993-1-1:2005 standard regarding steel structures, EN 1993-1-3:2006 supplementary rules for cold-formed members and sheeting and EN 1993-1-10:2006 Material toughness and through-thickness properties. *Table 4-6* gets that structural steel available into the market.



*Monopole*

*Self-Supporting*

*Guyed*

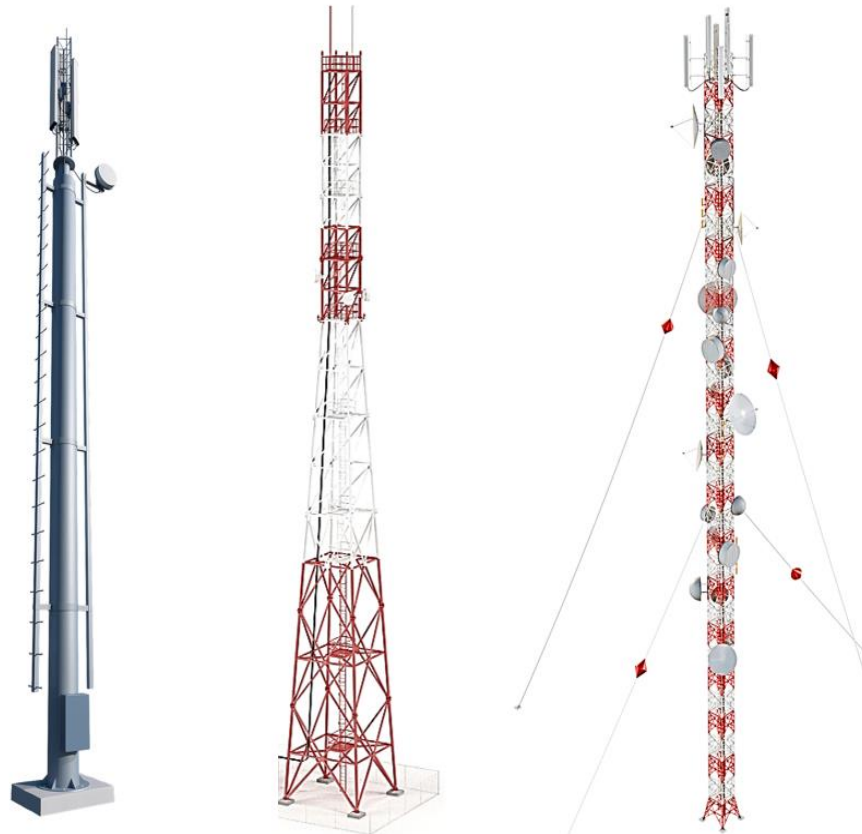


Figure 4-9, principal structural configuration for telecom towers

Standard and steel grade	Nominal thickness of the element $t$ [mm]			
	$t \leq 40$ mm		$40 \text{ mm} < t \leq 80$ mm	
	$f_y$ [N/mm <sup>2</sup> ]	$f_u$ [N/mm <sup>2</sup> ]	$f_y$ [N/mm <sup>2</sup> ]	$f_u$ [N/mm <sup>2</sup> ]
<b>EN 10025-2</b>				
S 235	235	360	215	360
S 275	275	430	255	410
S 355	355	$\text{AC}_2$ 490 $\text{AC}_2$	335	470
S 450	440	550	410	550
<b>EN 10025-3</b>				
S 275 N/NL	275	390	255	370
S 355 N/NL	355	490	335	470
S 420 N/NL	420	520	390	520
S 460 N/NL	460	540	430	540
<b>EN 10025-4</b>				
S 275 M/ML	275	370	255	360
S 355 M/ML	355	470	335	450
S 420 M/ML	420	520	390	500
S 460 M/ML	460	540	430	530
<b>EN 10025-5</b>				
S 235 W	235	360	215	340
S 355 W	355	$\text{AC}_2$ 490 $\text{AC}_2$	335	490
<b>EN 10025-6</b>				
S 460 Q/QL/QL1	460	570	440	550

Table 4-6, table 3.1 EN 1993-1-1: 2005 structural steels mechanical characteristics

The most used steel for single-pole towers is 235JR or J0, while steels with higher strength can also be used for lattice towers, such as 275 or 355.

The lattice towers whether their location is, on the roofs or on the ground are built according to a hierarchy of basic elements as shown in the *figure 4-10*. That is, the primary sections concern the legs of the tower, the secondary sections concern the primary bracing system and finally the stiffeners of the bracing are defined by the third level sections. In contrast, monopole towers have a single class of basic elements.

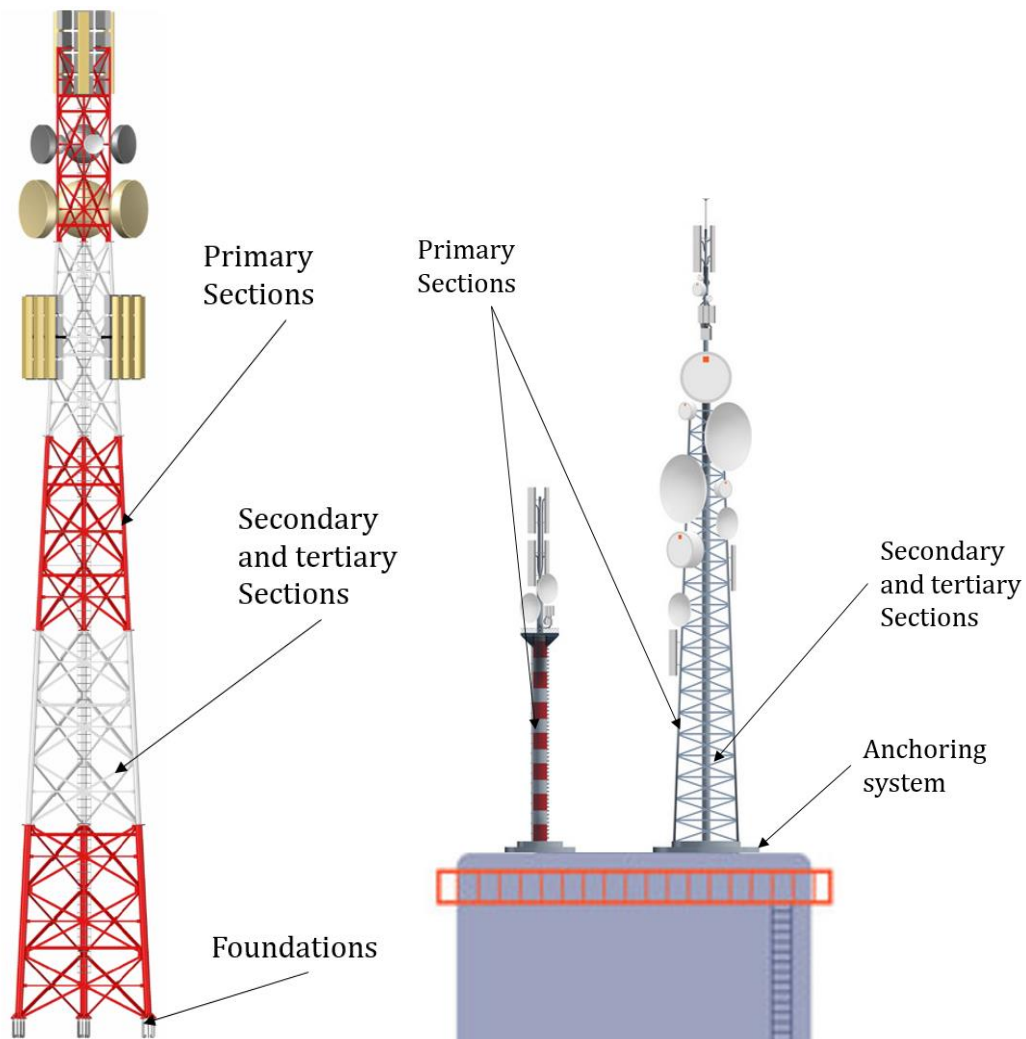


Figure 4-10, elements hierarchy for the towers

In accordance with the EN 1993 3-1 standard relating to the design of poles and trusses, the primary sections (PS), i.e., those that make up the legs of the tower most used in the construction of lattice towers, are the L-shaped corner profiles with equal sides. and an angle of  $90^\circ$  or  $60^\circ$  the latter case when having a three-legged structure. While for pole towers the only sections used are those of hot rolled circular hollow sections for towers that are located on buildings or cold formed polygonal hollow sections. Also, for the secondary and tertiary sections (STS) for the construction of the bracing and stiffeners of the lattice towers the

most used sections are the L-shaped profiles with equal wings. There are lattice structures which are made using other sections, such as tubular or c-shaped sections for the bracing. However, they are not very widespread. Therefore, in accordance with the work presented by Madugula (2001) where the most common lattice towers are analyzed, only angular sections have been chosen. The sections chosen and the method used to assign the appropriate section to each tower will also be illustrated in the next paragraph. *Table 4-7* shows an extract from the figure 1.1 in the EN 1993-3-1 standard which concerns the common sections used in the design of lattice towers.

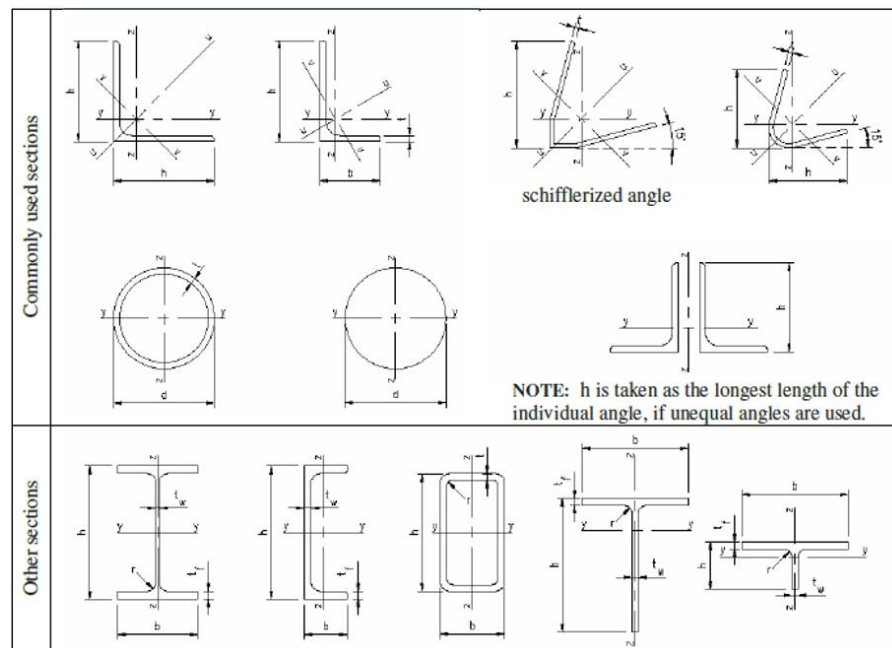


Table 4-7, Typical sections used for masts and towers from EN 1993-3-1

The next step concerns the definition of the parameters that characterize the system of both vertical and horizontal bracing that are used in lattice towers. In accordance with the European standard EN 1993-3-1, three parameters have been defined to characterize the bracing systems of the tower. The first parameter concerns with which primary vertical bracing system the tower is built (PV), the second parameter defines which type of secondary vertical bracing (SV) has been used and finally the third parameter defines which floor bracing system (H) are used by the tower. The EN 1993-3-1 standard specifically defines the most common systems for lattice towers. The following paragraph illustrates the principle of choice between the various types of bracing system that the standard proposes. *Tables 4-8* and *4-9* immediately below show the most common vertical and horizontal bracing systems for lattice towers. The tables are taken from figures H.1 and H.3 of the EN 1993-3-1 standard.

Triangulated	
<p>* If there are two diagonals, they may be designed as tension members.</p>	
Not fully triangulated (not recommended for design, unless careful attention is given to bending effects)	

Table 4-8, , typical horizontal bracing systems for towers from EN 1993-3-1

Typical primary spacing patterns					
parallel or tapering			usually tapering		usually parallel
I Single lattice $L_{d1} = L_d$	II Cross bracing $L_{d1} = L_{d2}$	III K-bracing $L_{d1} = L_{d2}$	IV Discontinuous bracing with continuous horizontal intersections $L_{d1} = L_{d2}$	V Multiple lattice bracing	VI Tension bracing
Typical secondary bracing patterns (see also Figure H.2)				<p>NOTE: The tension members in pattern VI are designed to carry the total shear in tension, e.g.</p>	
IA Single lattice $L_{d1}$	IIA Cross bracing $L_{d1}$	IIIA K-bracing $L_{d1} = L_{d1}$ $L_{d1} = L_{d2}$ on rectangular axis	IVA Cross bracing with secondary members $L_{d1} = L_{d1}$		

Table 4-9, , typical bracing systems for towers from EN 1993-3-1

Subsequently, a parameter was defined to describe the type of foundation for the towers on the ground (F) and a parameter to describe the type of anchoring of the towers on the roofs (A). According to EN 206-1, there are various types of foundations and anchors for telecommunication towers in accordance with the European Codes. While, in the *figure 4-11* extracted from the work done by Kyung and Lee (2015), the most common types of foundations for telecommunication towers are shown.

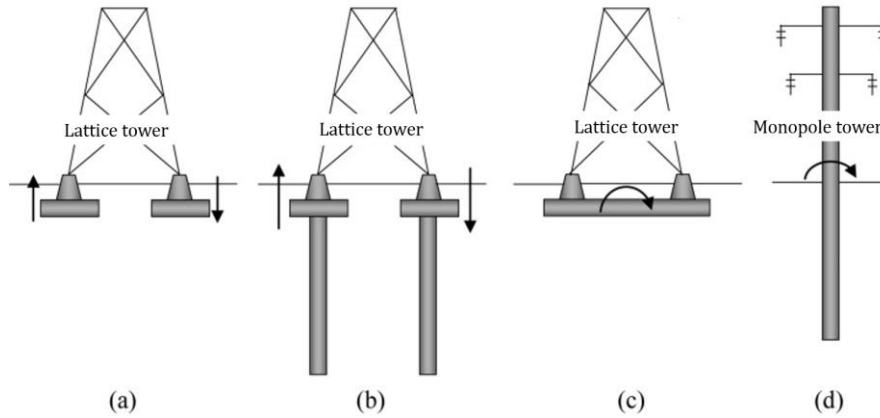


Figure 4-11, typical types of foundation used for telecom towers

While the *figure 4-12* represents the most common connection systems between antenna and building defined in the work done by Bhosale, Kumar et al. (2012).

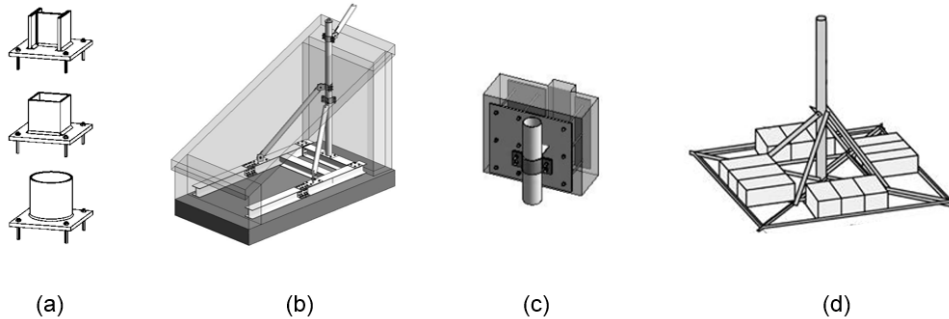


Figure 4-12, typical types of anchor system used for roof top telecom towers

These parameters are introduced with the sole purpose of fully describing the structure, and so that the hypothesis of considering the structure wedged at the base is consistent with the type of foundation or anchoring system that the tower uses. In the calculation model each tower is considered as embedded at the base without any study of the interaction between soil and foundation.

The next parameter introduced in the database to characterize the structure of the BTS was the one that defines the main types of connections that are used in the construction of the tower (C). This is due to the fact of knowing the type of constraint that occurs in the nodes of the structure in order to create a detailed model of verification of the methodology followed that is as consistent as possible

with reality. As regards the connections, reference is made to the EN 1993-1-8 standard of 2005. This standard defines the most common types of connections for steel structures and therefore also for both pole and lattice towers. As for the other parameters, also for the parameter that describes the tower connections, the approach followed for its assignment is explained in the next paragraph.

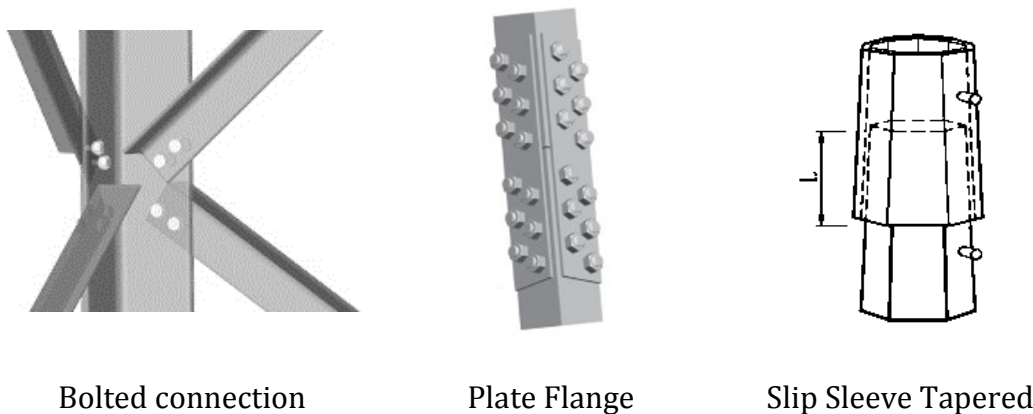


Figure 4-13, examples of typical connections for telecom towers

For the ground lattice towers, a further parameter has been introduced to describe the type of portal at the base (PF). In accordance with the EN 1993-3-1 standard there are different types of base portals depending on the type of bracing used for the tower and on the height of the tower itself. *Figure 4-14* shows an extract of the most common portals defined by the notice.

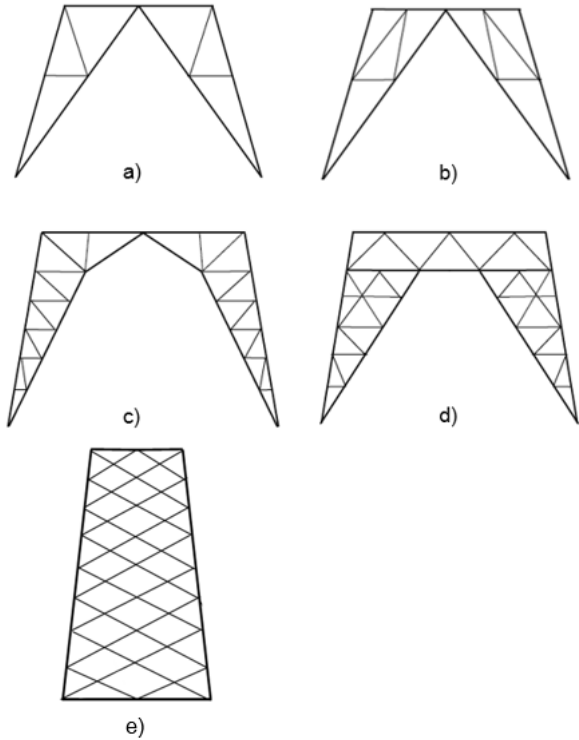


Figure 4-14, different types of portal base for lattice towers

One of the last parameters introduced is the one that defines the type of coating of the structure itself (CO). It is a purely descriptive parameter. In accordance with the EN 1993-3-1 standard, both pole and lattice towers can undergo two coating methods. The first is a galvanizing as shown in *figure 1-15* the second is a painting. In some cases, the tower can be treated with both methods. Galvanization or galvanizing is the process of applying a protective zinc coating to steel, to prevent rusting. The most common method is hot-dip galvanizing, in which the parts are submerged in a bath of molten hot zinc. The zinc coating, when intact, prevents corrosive substances from reaching the underlying steel or iron. Additional electroplating such as a chromate conversion coating may be applied to provide further surface passivation to the substrate material. In the event the underlying metal becomes exposed, protection can continue if there is zinc close enough to be electrically coupled. After all the zinc in the immediate area is consumed, localized corrosion of the base metal can occur.

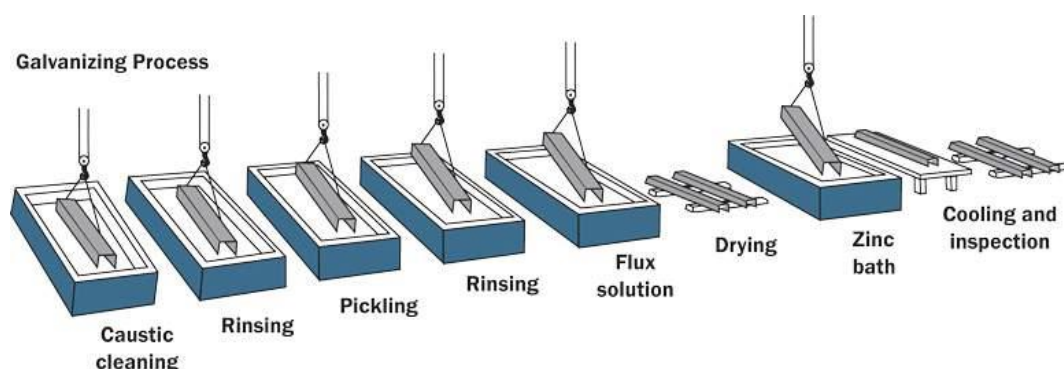


Figure 4-15, galvanization process that the elements that compose a tower have to need to do

Typically, painting can be a further process that is performed after galvanization. The metal painting process is a process of coating metal surfaces with an organic film, this treatment is carried out for decorative purposes and / or for the purpose of protection from corrosion and aggressive agents.

The last parameter introduced concerns the load combination (LC) used to subsequently define the mass of the structure to be assigned to the simplified model for future simulations. In accordance with the EN 1993-3-1 standard, the loads to be considered and the relative multiplicative coefficients are defined.

The last parameter introduced concerns the load combination (LC) used to subsequently define the mass of the structure to be assigned to the simplified model for future simulations. In accordance with the EN 1993-3-1 standard, the loads to be considered and the relative multiplicative coefficients are defined. The legislation defines two categories of actions: permanent and variable actions. In the permanent actions, the weight of the communication system and the weight of the lower system are considered. While as variable actions are considered, an accidental load defined by legislation (which considers any maintenance actions), the load due to ice and the seismic action. The snow load is neglected for



telecommunication towers as there are no relevant walking surfaces. As regards the horizontal wind load, which in a detailed analysis is certainly the most burdensome for this type of structure, it is not considered in this work. This is because, the study focuses on assessing the response of the network to seismic events and therefore assessing the seismic vulnerability of the network on an urban scale. Therefore, seismic action was chosen as the main variable action. The multiplicative coefficients are summarized in the *table 4-11*, it is obtained from table A.2 of the EN 1993-3-1 standard. The coefficients are established based on the reliability class to which the tower belongs. The reliability classes are reported in the *table 4-10* that have been taken from table A.1 of EN 1993-3-1 legislation. The study concerns the network in an urban environment; therefore class 3 was chosen as the reliability class.

Reliability Class	
3	towers and masts erected in urban locations, or where their failure is likely to cause injury or loss of life; towers and masts used for vital telecommunication facilities; other major structures where the consequences of failure would be likely to be very high
2	all towers and masts that cannot be defined as class 1 or 3
1	towers and masts built on unmanned sites in open countryside; towers and masts, the failure of which would not be likely to cause injury to people

Table 4-10, reliability class to estimate the partial factors for the load for telecom towers

Type of Effect	Reliability Class, see NOTE to 2.1.2	Permanent Actions	Variable Actions ( $Q_s$ )
unfavourable	3	1,2	1,6
	2	1,1	1,4
	1	1,0	1,2
favourable	All Classes	1,0	0,0
Accidental situations		1,0	1,0

Table 4-11, partial factors for the actions for the towers

#### 4.2.2 Data collection for the Base Station Controller (BSC):

Being a strategic infrastructure, the telecommunication network is almost impossible to obtain detailed data on the network configuration. It is impossible to know precisely from the MNOs the number and location of all the BSCs present in the area. This is because by providing an essential service, the dissemination of relevant data could lead to terrorist attacks on the network itself. For this reason, the data collected regarding the BSCs are only partial and not updated data. In this context, it will be necessary to introduce reasoned hypotheses for the construction of the network and therefore also to determine the data.

##### 4.2.2.1 Geographical parameters:

Thanks to the CellMapper platform, it was possible to start from a good starting point. In that, the platform provided the location of some of the most used and

therefore still active BSCs in the area. *Figure 4-16* shows an extract of the visualization map provided by cellmapper where it is observed how the BSCs are marked with a logo and a numbering different from that for the BTS.



Figure 4-16 visualization of the window from CellMapper.com

Further research was done using data provided by the region's Geoportal and through satellite photos. Therefore, just like for the BTS, also for base control stations (BSCs), the search for data started by defining the geographic parameters. Once all the available resources had been used, it was observed that the number of localized BSCs was not sufficient to respect the telecommunication parameters hypothesized by Giovinazzi, Austin et al. (2017) and illustrated in more detail when discussing the telecommunication parameters. For this reason, a position coherent with the built environment layer of two BSCs in the districts of the city that had no coverage by any BSC was assumed. At the end of these steps, the total number of BSCs considered was 18. This number will allow us to be in line with the hypotheses made in the study presented by Giovinazzi, Austin et al. (2017) regarding the number of BTS of each MNO that each BSC must check. As can be seen from *Figure 4-17*, it is observed that each district of the city has at least one BSC that covers the territory of the same.

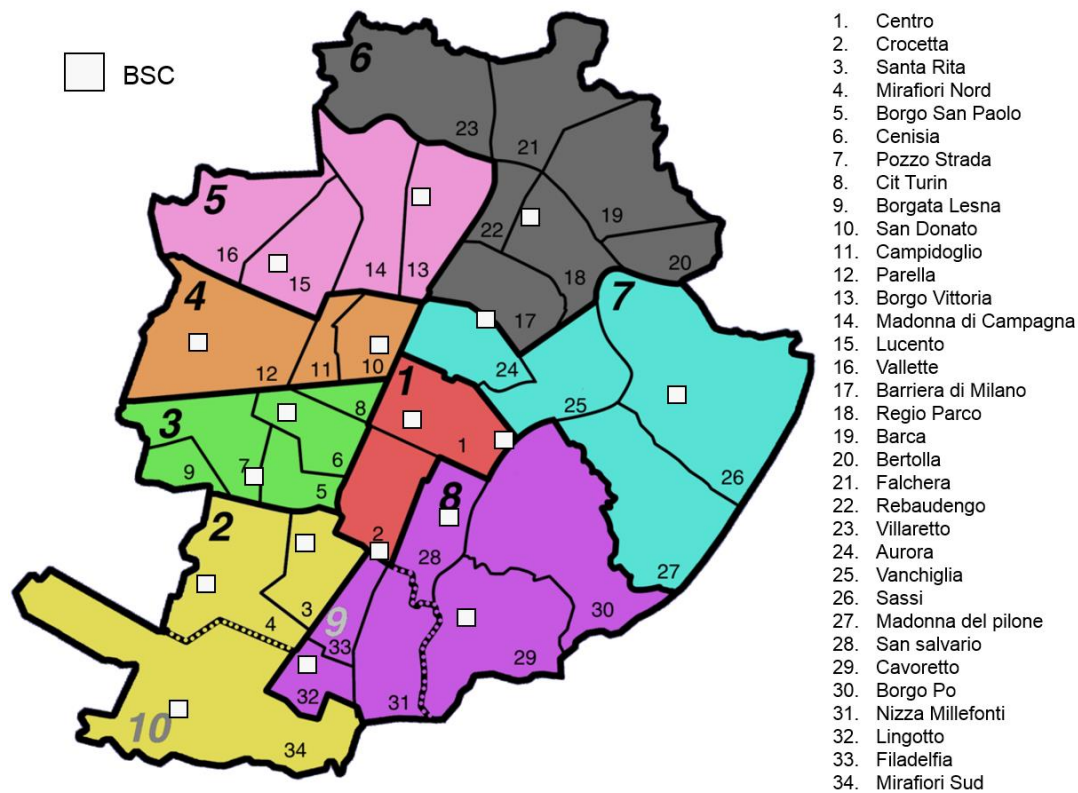


Figure 4-17, Administrative districts and neighborhoods of *IDEAL CITY* (based on the city of Turin).

Once the geographic coordinates of all the base control stations (BSC) in the appropriate reference system were obtained, they were converted into geometric coordinates. Then, through the .csv file, a shapefile layer dedicated to the localization of the BSCs was created, used later to determine the geometric parameters. Therefore, as regards the category of geographic parameters, the only parameter introduced concerns the coordinates of each BSC. In addition to what has been said so far, another hypothesis made regarding the BSCs is that each station is shared with all the operators, this is consistent with reality%. However, it must also be said that in real networks the idea of a proprietary network is becoming more and more frequent and therefore of having their own BSCs by each operator%. As will be seen later in the part where the telecommunication parameters are illustrated, as stated before, the final number of BSCs considered was 18. This number allows to respect all the limits imposed for a real wireless network.

In *Figure 4-18*, a photo taken from outside the BSC that is located in the point that the *Figure 4-16* shows.



Figure 4-18, photo taken from the outside and from satellite for the BSC located in the figure 4-16

- Geographic Coordinates (x[m] and y[m])

#### 4.2.2.2 *Geometric parameters:*

As regards the geometric and structural parameters, the same parameters used to describe the buildings of the built environment layer developed by Marasco for the Ideal City project were adopted (Noori, Marasco et al. 2017).

Once the position of the base control stations was known by interpolating the BSC position layer with the building layer provided by the Piemonte geoportal, it was possible to identify the BSC buildings (*Figure 4-19*). In this way it was possible to define the parameters concerning the category of geometric data.

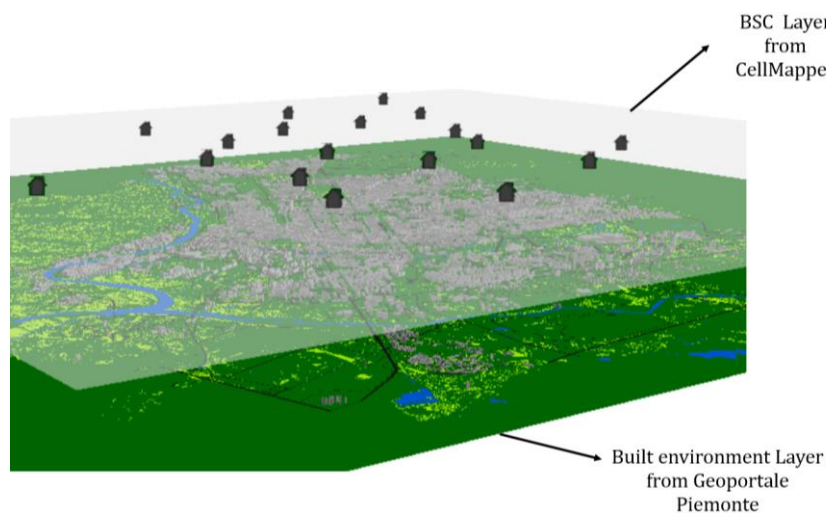


Figure 4-19, example of location knowledge about BSC

The geometric parameters obtained for each BSC were the following:

- Building perimeter (P)
- Building area (A)
- Number of floors for the building (nF)



- Building height (H)
- Type of Building (Masonry or Reinforced concrete)
- Year of construction (Y)

The geometric parameters are obtained from the table of attributes linked to the shapefile that describes the buildings of the city of Turin provided by the Geoportale Piemonte website. The year of construction defines a time frame that describes a distinct construction methodology for that era. The type of building, on the other hand, indicates whether the building structure is in masonry or in reinforced concrete.

#### 4.2.2.3 *Structural and Non-structural parameters:*

The next category of parameters introduced for the BSCs was that concerning structural and non-structural parameters. As for the previous category, here too, the same parameters introduced by Noori, Marasco et al. (2017) were used for the buildings of the built environment layer. Since the BSC buildings are only in reinforced concrete (RC), the structural and non-structural parameters that are introduced are only those that characterize the RC buildings. The parameters used to describe the stations were the following:

- Floor type (F)
- External Wall Type (EW)
- Reinforced element type (RF)
- Mechanical parameters (MP)
- Load combination (LC)
- Structural configuration (SC)

For the dynamic characterization and therefore to define the physical properties of the single control station, the same parameters introduced by Noori, Marasco et al. (2017) for the construction of the porphyry of the buildings were used. In this way it was possible to apply the same method developed by Noori, Marasco et al. (2017) to the BSCs to define the damage that the BSC structure undergoes during a seismic event. The approach used is the one that defines the concept of building typology. It has become commonly accepted in many European countries at national and regional level which is based on the classification of the building stock according to some common properties. This classification approach leads to easy characterization of large-scale buildings.

To determine the characteristics of many buildings, the TABULA project (Typology Approach for Building Stock Energy Assessment) was therefore used, which aimed to characterize the types of buildings to assess their energy consumption. Through the contribution of Italian research, in this project tables have been created that describe the construction types of the various elements that are part of a building based on the year of construction of the building itself. Therefore, once the construction period of the BSC was known, the construction

types of the floors, external walls, etc. were assigned to it. An extract of the classification of the elements according to the year of construction by Corrado, Ballarini et al. (2012) used to describe the porphyry of the buildings of the Ideal City and therefore also applied to the BSCs is shown in *figures 4-20* and *4-21* below. The types chosen to characterize the elements of the base station control buildings will be introduced in the next paragraph.

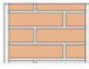
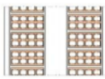

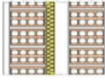

Walls		
Example	Description	Period
	Solid brick masonry (38 cm)	1900 - 1950
	Hollow wall brick masonry (40 cm)	1930 - 1975
	Concrete masonry (30 cm)	1955 - 1970
	Hollow wall brick masonry(40 cm), low insulation	1976 - 1990
	Honeycomb brick masonry (high thermal resistance), high insulation	> 2006

Figure 4-20, , External wall type by Corrado et. al. (2012)




Floors		
Example	Description	Period
	Floor with reinforced concrete	1901 - 1930
	Floor with reinforced brick-concrete slab	> 1930
	Floor with reinforced brick-concrete slab, medium insulation	> 1991

Figure 4-21, floor types by Corrado et. al. (2012)

As for the definition of the mechanical characteristics and the load combination to be assigned to each BSC, it is based on the construction period assigned to the structure itself. While the average span of the floors was used as a parameter to define the various types of different structural configurations. Finally, the percentage of reinforcement in structural elements is unknown in most buildings on an urban scale. For this reason, the assignment of the percentage of reinforcement of the structural elements takes place in a statistical way using a

random variable (RV). This RV is normally distributed with maximum and minimum limits defined by the seismic guidelines which vary according to the construction period (Noori, Marasco et al. 2017). In the next paragraph all the different types of parameters chosen and their values for the various categories will be explained.

#### 4.2.2.4 Telecommunication parameters:

The last parameters' category introduced to characterize the BSCs is the one concerning the parameters of the telecommunication sector. The parameters that are used in this category are the following:

- Number of BTS managed and what BTS it manages
- Hierarchical level in the network topology

Each BSC is called upon to manage a certain number of BTSs of each mobile network operator (MNO) present in the area. For the security reasons introduced at the beginning of the paragraph, it is not known by which BSC each BTS is controlled. According to the criteria in the literature, each BSC checks from a minimum of 10 to a maximum of 20 BTS of each MNO (Giovinazzi, Austin et al. 2017). To assign the BTS to the control station, the parameter of the maximum distance between BTS and BSC was then used. That is, each BSC has been assigned the BTS of a certain area. According to (Yu and Kim 2013), this area can be defined through the Voronoi's subdivision (*Figure 4-22*).

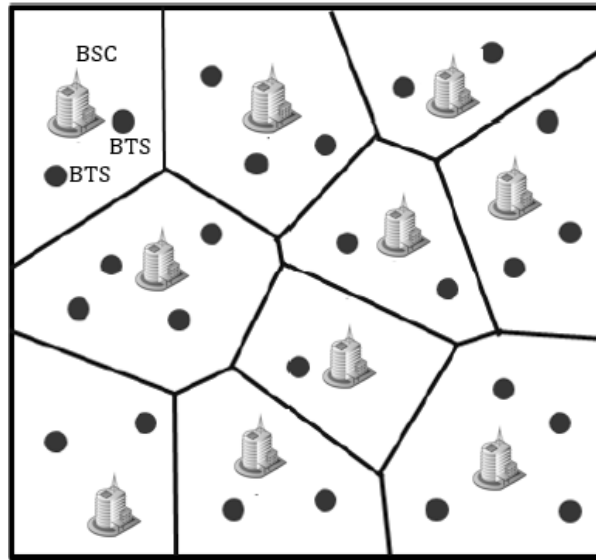


Figure 4-22, Voronoi's Area subdivision illustration (Yu and Kim 2013)

Once the areas of competence of each BSC were obtained, it was possible to know the BTS controlled by each BSC, always checking to respect the BTS range set by Giovinazzi, Austin et al. (2017) for the base stations control. If a BSC exceeds the 20 BTS of a single operator to manage, then the surplus BTS are connected to the second closest BSC and so on.



Finally, each BSC is assigned a layer in the topological network. This was necessary, since as seen in the general part of wireless networks, the connections through the links of the network nodes take place following a hierarchical order. Having no information on the hierarchy of the BSCs of the real network, again for the safety reasons already mentioned, it was decided to use the dimensions of the BSC itself as parameters to determine the level of each BSC in the network topology, also in accordance with what has been done by Ellingwood, Cutler et al. (2016) for the design of the virtual city telecom network of Centerville project. Typically, the largest BSCs are the ones that handle the most data traffic. So, they are the central stations of the network.

#### 4.2.3 Data collection for the Building Environment:

During the installation of a wireless network in an urban environment, the space for ground support towers is almost always not enough. To overcome this problem, the MNOs use licenses to install their BTSs on the roof of private buildings. For the project of the Ideal City's telecommunication network, it was not necessary to build the portfolio of the buildings of the city. This because, for the Ideal City project, the built environment layer has already been developed by Noori, Marasco et al. (2017) as *figure 4-23* shows. So, it already defines all the characteristics of the buildings.

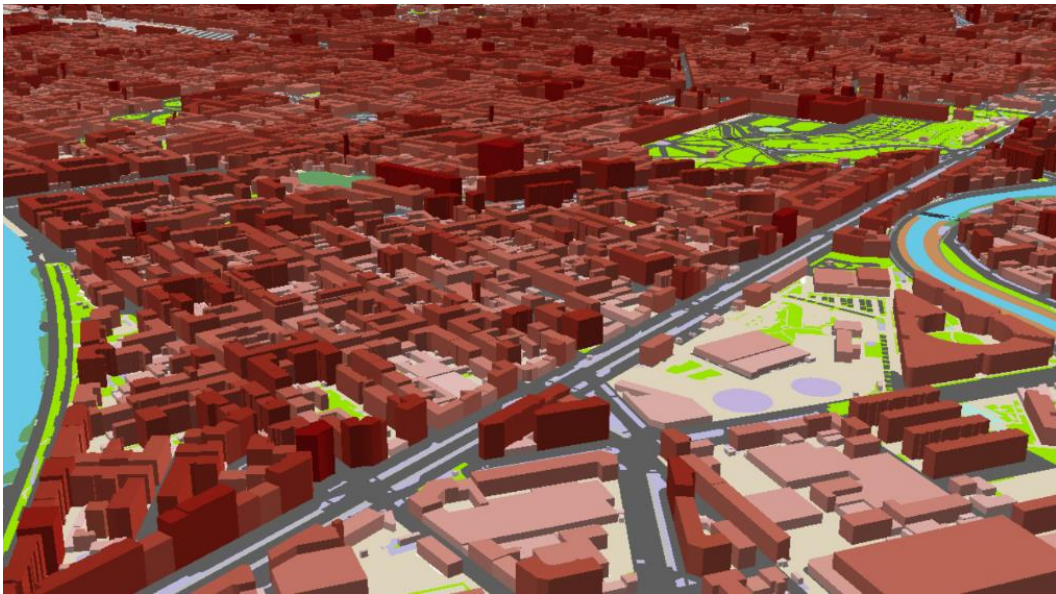


Figure 4-23, Building portfolio developed by Noori, Marasco et. al. (2017)

#### 4.2.4 Data collection for the Users:

The last element to be introduced for the creation of the wireless network of the virtual city is the users who use the infrastructure. As mentioned for the Ideal City project, the population is around 900,000 units. The population is known through the census provided by the city of Turin. Each person is located in their own

residential building. In this way, user clusters are created that group people belonging to the same building (*figure 4-24*).



Figure 4-24, User cluster defined for Ideal City

The clustering of users is since after a seismic event, generally, the population is concentrated in identifiable groups in the residential buildings and located right near the buildings themselves.

In addition to the above, information on users was available only in this form of grouping. In fact, it is not possible for MNOs to know data or information regarding real data traffic and therefore a real position of the various users in the territory considered. Having said that, the hypothesis of user clusters is more than widespread in the literature for the study of communication networks (Di

Francesco, Malandrino et al. 2017). So, as categories of parameters regarding users, the category of geographic parameters has been defined.

#### 4.2.4.1 *Geographical parameters*

The geographical parameters defined for each user cluster were:

- Geographic coordinates (x [m], y [m])

As with the network components, user clusters are also located through geometric coordinates. The coordinates indicate the residence building of the users belonging to the considered cluster.

#### 4.2.4.2 *Telecommunication parameters*

The second category considered for user cluster is that of telecommunication parameters. The telecommunication parameters considered were:

- Number of users in the cluster
- Connection height
- Market share of each MNO

As for the number of users per cluster, it is defined based on the number of people residing in each building and as seen it is limited in a range.

The connection height is fixed for all clusters. It is assumed to be 1.5 meters according to Malandrino et. al. work (Malandrino, Chiasserini et al. 2017) and will be used specifically for the calculation of the signal between the BTS and the cluster as will be seen in the next chapter.

The height is assumed to be 1.5 meters because in most cases the people who call for help are on the street.

Finally, the percentage of users that each MNO manages is defined through the data released by AGCOM (2020). This is because, each MNO manages a certain number of users.

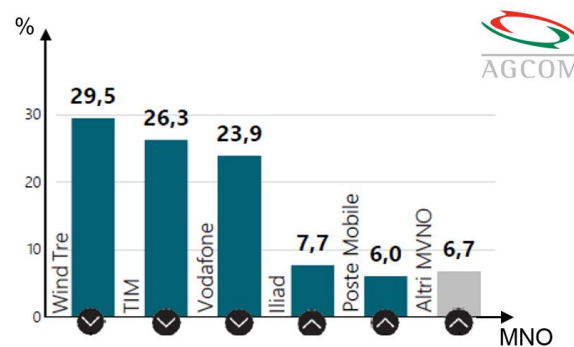


Figure 4-25, market share by MNO AGCOM (2020)

## 4.3 Data Processing for the Parameters

Once the various parameters were introduced to characterize the different components of the network, it was necessary to introduce some methodologies for estimating some of them. This is since not all previously defined information about the individual elements is available, it is always due to the security reasons mentioned above. It was necessary to process and elaborate the data defined in the previous paragraph through the studies, the hypotheses and the principles proposed in the literature until now. Data processing and manipulation can be seen as the center of the work cycle for the construction of the wireless network for Ideal City. They consist in the application of specific methodologies aimed to estimate and assigning the most correct values based on the information available to the individual parameters. The procedures used to assign the different parameter values previously illustrated to characterize the individual components of the network are illustrated below.

### 4.3.1 Preparation and assessment for the Base Transceiver Stations' data

After the data collection and definition phase to describe the network components, they often need to be manipulated to be suitable for further analysis. We therefore speak of data preparation. Data preparation can be done by organizing and rearranging the raw data. Or in the case of lack of some information for some parameters, hypotheses or simplifications for their definition can be introduced. The accuracy of the data must be carefully checked at this stage. Inaccurate or inconsistent data will affect further phases of the calculation cycle. The manipulated data is then used in a code-readable format to be processed by a computer to obtain results on the virtual network.

#### 4.3.1.1 *Geographical Parameters:*

The only manipulation of the geographic data carried out was the conversion of the geographic coordinates obtained from the CellMapper CSV file into geometrical coordinates and assigning them the same reference system as the shape file of the buildings. While to define the location of the BTS the hypothesis used was based on whether the coordinates of the BTS obtained before would indicate a point on the ground or on a building. Some localization checks were performed using live images as can be seen from *Figure 4-27*.





Figure 4-26, illustration showing some checks with pictures taken in person of some BTS and BSC

#### 4.3.1.2 Telecommunication Parameters:

The information obtained by CellMapper was also exhaustive for the telecommunication parameters. The only information obtained from the hypothesis introduced was that to define the type of coverage (MA or MI) of the BTS. In fact, the coverage was defined according to the band that the BTS itself uses. However, this hypothesis is widely used in the literature (Malandrino, Chiasserini et al. 2017).

#### 4.3.1.3 Geometric Parameters:

The basic geometric parameters, i.e. height, type of tower and base, were obtained directly from the databases provided by CellMapper and some MNO sites. Based on this information, it was possible to establish for lattice towers whether they were characterized by a variable or constant height development. This last data was then fundamental to subsequently understand the structural configuration of the tower. In fact, according to (Tah, Alsilevanai et al. 2017) if the width at the top and at the base were different, then this meant that the tower had a variable development. The only parameter that needs an evaluation is that relating to the distance between BTS and BSC. For each BTS the distance to all the base control stations was calculated. This is done through *the equation 4-1*.

$$D_{BTS,i} = \min \left( d_{i-j} = \sqrt{(x_{BTS} - x_{BSC})^2 + (y_{BTS} - y_{BSC})^2} \right) \quad (4-4-1)$$

$$\forall j = BSC, BTS = i$$

#### 4.3.1.4 *Structural and Non-structural parameters:*

Some of the geometrical parameters may affect the assignment of the structural and nonstructural properties of a building. Let's suppose to identify the building typology of a ten-story building. The geometrical parameter is identified by the number of stories, while the structural property is represented by the building typology. Since the maximum number of stories for a masonry building may be limited to 5, it is suitable to assume a RC typology for the building selected. This example highlights how certain "reasonable" considerations and/or well-known design rules can be adopted to assess the missing structural parameters. In the case of structural and non-structural parameters, the information available was very scarce. The hypotheses and simplifications introduced thanks to the existing literature have been many. It must be said that the hypotheses and simplifications assumed by studies in the literature have concerned single structures or groups of a few units. No work involved an entire network. For this reason, this database can certainly be improved by having more detailed information available for each BTS. It started by defining the structural configuration (SC) of each tower. It is obtained through the geometric information and images collected about each tower. For instance, a self-supporting tower with a top base different from the bottom base is surely a pyramid-type tower. It has been observed that the main configurations present are two, the monopole and the self-supporting. According to Madugula (2001), each main structural configuration has sub-categories. As for self-supporting towers, pyramid-type self-supporting towers can be found, i.e., towers with a cross section that varies in height, self-supporting towers with a constant cross section with 4 legs or self-supporting towers with a constant cross section with 3 legs. This applies to both ground and roof towers. While the monopoles on the ground are divided into two sub-categories, there are the slip-type monopole, i.e., pole towers in which the trunks are grafted into each other, or you can find the flange-type monopole, i.e., pole towers in which the logs are connected to each other by means of bolted flanges. For monopole on roofs there are no sub-categories as towers with a single midsection are installed on the roofs. *Figure 4-27* shows a summary diagram regarding the structural configurations for the towers on the ground. While *figure 4-28* shows a summary diagram of the structural configurations defined for the towers on the buildings. Therefore, five structural configurations were identified for the towers on the ground (SC1, SC2, SC3, SC4, SC5), while for the towers on the roofs, four configurations were identified (SC1, SC2, SC3, SC4). Once the structural configurations present were defined, it was possible to define intervals of the main geometric characteristics (height, base, etc.) for each structural configuration. This is based on the information collected for each tower that make up the sub-category itself. *Tables 4-12* and *4-13* show the ranges of geometric parameters for each structural



configuration adopted, for the towers on the ground and for the towers on the roofs, respectively.

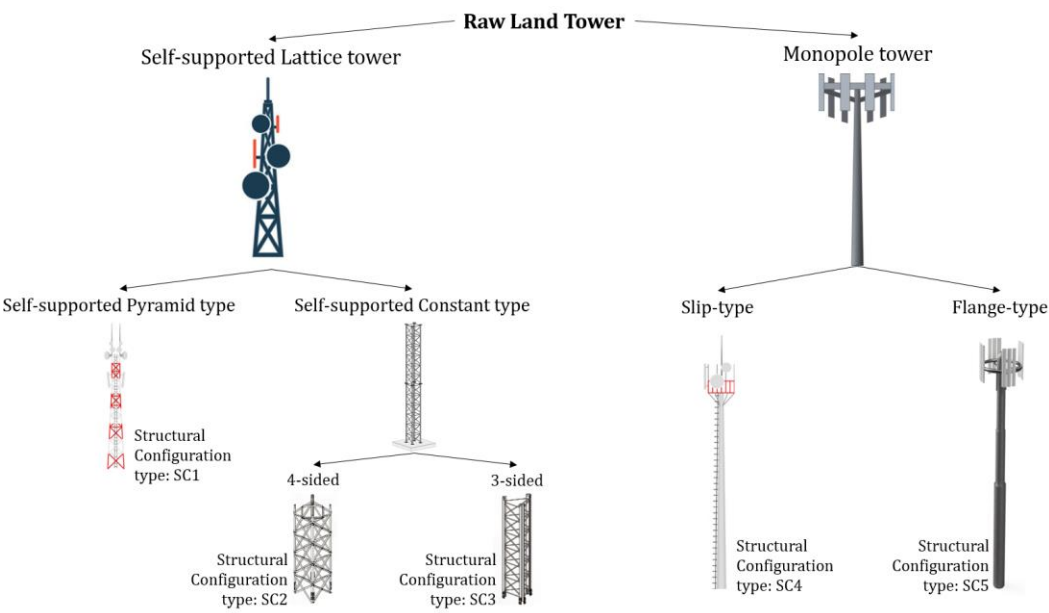


Figure 4-27, summary diagram for the structural configurations of the rawland towers

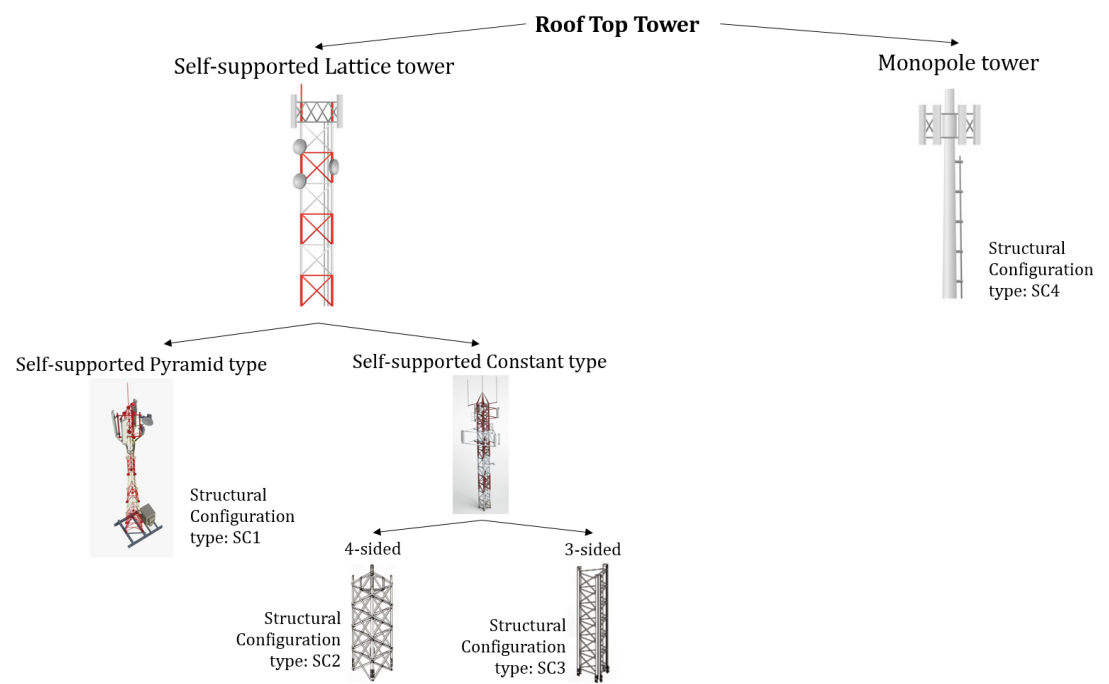


Figure 4-28, summary diagram for the structural configurations of the rooftop towers

<i>ID type</i>	<i>Range of Heigh [m]</i>	<i>Range of bottom Base [m]</i>	<i>Range of Top Base [mm]</i>
SC1	25 – 45	4000 - 7000	1000 - 2000
SC2	25 – 35	2000 – 4000	2000 – 4000

SC3	20 – 30	1000 - 2000	1000 - 2000
SC4	18 - 36	800 - 1100	400 - 500
SC5	18 – 36	800 - 1100	400 - 500

Table 4-12, Geometrical parameters range for each structural configuration of rawland towers

<i>ID type</i>	<i>Range of Heigh [m]</i>	<i>Range of bottom Base [m]</i>	<i>Range of Top Base [mm]</i>
SC1	6 - 8	1000 - 1500	250 - 500
SC2	4 - 6	500 - 1000	500 - 1500
SC3	3 - 5	500	500
SC4	2 – 5	50 - 250	50 - 250

Table 4-13, Geometrical parameters range for each structural configuration of rooftop towers

Having no information regarding the mechanical parameters, it was decided to assign them according to the structural configuration previously defined, following the works presented in the literature. Three categories to describe the mechanical parameters were used for the ground towers in accordance with the proposed work by Madugula (2001). While, for the roof towers two categories were defined for the mechanical parameters in accordance with the work done by Assi (2006). *Table 4-14* shows the three classes defined (MC1, MC2, MC3) for the mechanical parameters for the towers on the ground, while *Table 4-15* summarizes the mechanical parameters of the two chosen classes (MC1, MC2) for the towers on the ground. roofs.

<i>ID type</i>	<i>SC</i>	<i>f<sub>y</sub> [MPa]</i>	<i>f<sub>u</sub> [MPa]</i>	<i>E [Gpa]</i>	<i>R</i>	<i>G [Gpa]</i>	<i>ν</i>
MC1	SC4, SC5	235	360	210	J0	81	0,3
MC2	SC2, SC3	275	430	210	J0	81	0,3
MC3	SC1	355	490	210	J0	81	0,3

Table 4-14, Mechanical parameters' classes of the rawland towers

<i>ID type</i>	<i>SC</i>	<i>f<sub>y</sub> [MPa]</i>	<i>f<sub>u</sub> [MPa]</i>	<i>E [Gpa]</i>	<i>R</i>	<i>G [Gpa]</i>	<i>ν</i>
MC1	SC4	235	360	210	J0	81	0,3
MC2	SC1, SC2, SC3	275	430	210	J0	81	0,3

Table 4-15, Mechanical parameters' classes of the rooftop towers

Where:

SC = structural configuration type

$f_y$  = the nominal values of the yield strength

$f_u$  = the nominal values of the ultimate strength

E = modulus of elasticity

R = resilience grade

G = shear modulus

$\nu$  = Poisson's ratio

Surely, the choice of a single class for the mechanical properties to be assigned to each tower is a simplification in the study as in reality, especially for self-supporting towers, more classes are used for the mechanical properties for various levels of sections that make up the structure. For example, in self-supporting towers the legs are made with a certain class, while the braces are usually made with a different class (Dias 2007). Due to the lack of knowledge, even the choice of the sections used by each tower takes place through some simplifications proposed in the literature. In accordance with Madugula (2001) proposes, the choice of the section for each level of the structural elements of each tower takes place according to the height of the tower itself (Madugula 2001). The process by which the sections of the elements for the towers are assigned is by means of a logarithmic function of the height of the structure itself. The process by which the sections of the various elements (PS and STS) for the towers are assigned takes place through a function of the height of the structure itself, providing the minimum necessary size of the L section. The *equations 4.2* and *4.3* report the empirical formulations proposed by Madugula (2001) to determine the minimum sections to be assigned to the lattice towers according to the height of the tower.

$$PS_{min} = \alpha \ln h - \beta^\varepsilon + \delta \quad (4-2)$$

$$STS_{min} = \alpha \ln h - \beta \quad (4-3)$$

Where:

h = height of the tower

$\alpha$  = cost. = 82,61

$\beta$  = cost. = 161,07

$\varepsilon$  = cost. = 1,05

$\delta$  = a/h ratio of the length of the main leg member at the base to the total height of the tower

The height is known on the basis of the data collected. Once it known the minimum section, the section to assign to the tower is taken from the tables provided by the European legislation. The L-shaped profiles with equal sides are obtained from the EN 10056-1: 2017 standard. While the hollow profiles for the single-pole

towers have been obtained from the EN 10219-2: 2019 and EN 10210-2: 2019 standards. For both ground towers and roof towers, based on the height range of each structural configuration, sections have been defined for the primary elements, for the secondary elements and for the tertiary elements. As for the monopole towers, being prefabricated elements, they have standard sections according to the height. Based on the data collected, four different heights were found in this study. Therefore, according to the database provided by the work proposed by (Lanier, Schnersch et al. 2009), each height has its primary base and primary top section. *Table 4-16* summarizes the base and top diameter values proposed by (Lanier, Schnersch et al. 2009) for single-post towers as a function of height.

h [mt]	D <sub>bott</sub> [mm]	D <sub>top</sub> [mm]
2,5	50	50
3	100	100
4	150	150
5	200	200
6	250	250
18	800	400
24	900	400
30	1000	500
36	1100	500

Table 4-16, Bottom and Top diameter based on the height of the monopole tower

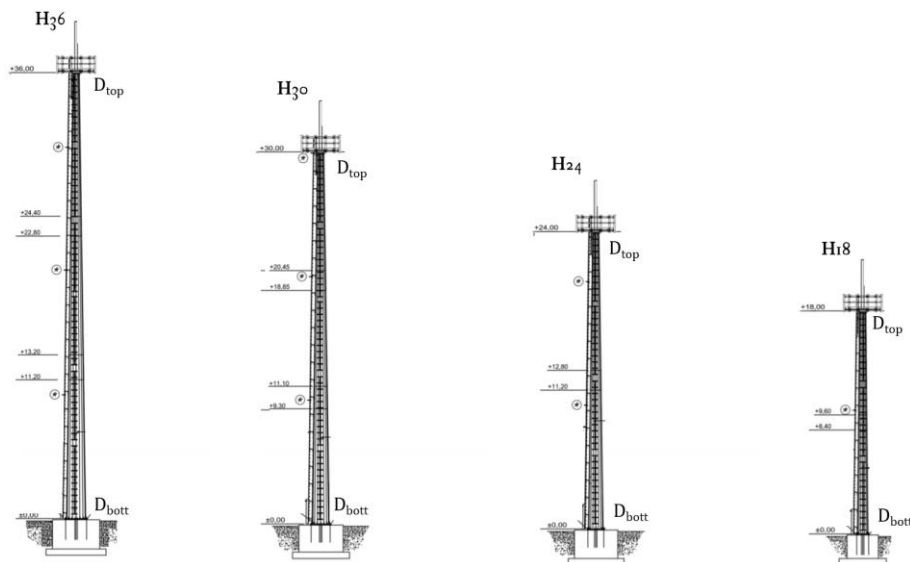


Figure 4-29, schematization of rawland monopole Tower

Based on the height of the tower, a section is attributed for the primary, secondary, and tertiary elements. *Tables 4-17* and *4-18* show the sections defined

for the rawland lattice towers for primary, secondary and tertiary sections. While *tables 4-19* and *4-20* show the sections defined for the rooftop lattice towers for primary, secondary and tertiary sections.

<i>ID type</i>	<i>Section type</i>	<i>Mass [Kg/m]</i>	<i>Area [mm<sup>2</sup>]</i>	<i>J<sub>x</sub> = J<sub>y</sub> [mm<sup>4</sup>]</i>	<i>C<sub>x</sub>=C<sub>y</sub> [mm]</i>	<i>l [mm]</i>	<i>t [mm]</i>	<i>d [mm]</i>	<i>α [g]</i>
PS1	L 150x150x15	33,8	4300	8980000	42,5	150	15	-	90
PS2	L 140x140x13	33,8	3750	6390000	39,2	140	13	-	90
PS3	L 130x130x12	23,6	3000	4720000	36,4	130	12	-	90
PS4	L 120x120x12	21,6	2750	3680000	34	120	12	-	90
PS5	L 120x120x10	18,2	2320	3130000	33,1	120	10	-	90
PS6	V 100x100x10	15	1920	1770000	28,2	100	10	-	60
PS7	V 90x90x9	12,2	1550	1160000	25,4	90	9	-	60
PS8-PS11	Polygonal	36,3 – 188,6	~4630 - 24030	~ 97555 - 3589518	-	-	4 – 7	400 - 1100	-

Table 4-17, Primary sections used for rawland towers

<i>ID type</i>	<i>Section type</i>	<i>Mass [Kg/m]</i>	<i>Area [mm<sup>2</sup>]</i>	<i>J<sub>x</sub> [mm<sup>4</sup>]</i>	<i>J<sub>y</sub> [mm<sup>4</sup>]</i>	<i>C<sub>x</sub>=C<sub>y</sub> [mm]</i>	<i>l [mm]</i>	<i>t [mm]</i>	<i>α [g]</i>
STS1	L 100x100x10	15	1920	1770000	28,2	100	10	-	90
STS2	L 90x90x9	12,2	1550	1160000	1160000	25,4	90	9	90
STS3	L 80x80x8	9,63	1230	722000	722000	22,6	80	8	90
STS4	L 75x75x7	7,93	1010	526000	526000	21	75	7	90
STS5	L 70x70x6	6,38	813	369000	369000	19,3	70	6	90
STS6	L 65x65x6	5,91	753	292000	292000	18	65	6	90

Table 4-18, Secondary and tertiary sections used for rawland towers

<i>ID type</i>	<i>Section type</i>	<i>Mass [Kg/m]</i>	<i>Area [mm<sup>2</sup>]</i>	<i>J<sub>y</sub> [mm<sup>4</sup>]</i>	<i>J<sub>x</sub> [mm<sup>4</sup>]</i>	<i>C<sub>x</sub>=C<sub>y</sub> [mm]</i>	<i>l [mm]</i>	<i>t [mm]</i>	<i>d [mm]</i>	<i>α [g]</i>
PS1	L 100x100x10	15	1920	1770000	1770000	28,2	100	10	-	90
PS2	L 90x90x9	12,2	1550	1160000	1160000	25,4	90	9	-	90
PS3	L 75x75x7	7,93	1010	526000	526000	21	75	7		90
PS4	V 65x65x5	4,98	634	247000	247000	17,2	65	5		60
PS5- PS8	Circular	3,45 – 24,26	~440 - 3090	~ 67265,37- 11980451,0 2	~ 67265,37- 11980451,02	-	-	3 - 4	50 - 250	-

Table 4-19, Primary sections used for rooftop tower

ID type	Section type	Mass [Kg/m]	Area [mm <sup>2</sup> ]	Jy [mm <sup>4</sup> ]	Jx [mm <sup>4</sup> ]	Cx=Cy [mm]	$\frac{l}{J}$ [mm]	t [mm]	d [mm]	$\alpha$ [g]
STS1	L 75x75x7	7,93	1010	526000	526000	21	75	7	-	90
STS2	L 60x60x5	4,57	582	194000	194000	16,4	60	5	-	90
STS3	L 50x50x5	3,77	480	110000	110000	14	80	5	-	90
STS4	L 40x40x4	2,42	308	44700	44700	11,2	40	4	-	90

Table 4-20, Secondary and tertiary sections used for rooftop towers

As seen into the paragraph before for the data collection about the BTS, the European legislation defines a series of main typologies for the configurations of the primary and secondary vertical braces and horizontal for the self-supporting towers. Given the lack of information regarding the type of bracing used by each tower, it was decided to use the method proposed by Tah, Alsilevanai et al. (2017). This method defines the type of bracing as a function of the mass of the tower itself. Based on the height and the sections of the elements defined previously, an approximate mass of the tower was obtained to define the type of bracing to be assigned to each tower. According to the method introduced by Tah, Alsilevanai et al. (2017), not all the bracing models illustrated by the legislation are taken into consideration. *Tables 4-21, 4-22 and 4-23* show the types of primary vertical bracing, secondary vertical bracing, and horizontal bracing for ground towers.

ID type	Category	Type on EN 1993-3-1	Description	$L_d$	Base range [mm]	Height range [m]
PV1	Parallel or Tapering	I	A single lattice may be used where the loads are light and the lengths relatively short, as for instance near the top of towers.	$L_d = L_{di}$	500 - 800	20 - 30
PV2	Parallel or Tapering	II	It is applied in cases where the load that the tower must carry is such as not to allow the use of model I. the critical length becomes half the length of the bracing provided that the bracing are joined at the crossing point.	$L_d = L_{di}/2$	500 - 2500	20 - 40
PV3	Parallel or Tapering	III	Widely used scheme for pyramid communication towers. this scheme is also used in limited portions of the structure such as the first or last levels. in the absence of secondary elements, the critical length is equal to the length of the diagonal.	$L_d = L_{d2}$	2500 - 6000	25 - 45
PV4	Usually Tapering	IV	The horizontal member should be sufficiently stiff in the transverse direction to provide restraints for the load cases where the compression in one member exceeds the tension in the other or where both members are in compression.	$L_d = L_{d2}$	3500 - 7000	35 - 45

Table 4-21, primary vertical bracing used for rawland towers



<i>ID type</i>	<i>Type on EN 1993-3-1</i>	<i>Description</i>	<i>L<sub>d</sub></i>	<i>Base range [mm]</i>	<i>Height range [m]</i>
SV1	IA	Horizontal single lattice as secondary bracings. This method is used when the loads are relatively low. Generally it used for lattice tower with a constat vertical development.	$L_d = L_{di}$	500 - 2500	20 - 40
SV2	IIIA	Very common scheme for telecom towers. It is used for towers with considerable loads and heights. Generally used for pyramid lattice towers.	$L_d = L_{di}/2$	2500 - 6000	25 - 45
SV3	IVA	Scheme in which horizontal secondary membranes are inserted to stabilize the legs. The diagonals are stabilized with others diagonals.	$L_d = L_{d1}$	3500 - 7000	35 - 45

Table 4-22, secondary vertical bracing used for rawland towers

<i>ID type</i>	<i>Category</i>	<i>Type on EN 1993-3-1</i>	<i>Description</i>	<i>Base range [mm]</i>
H1	Triangulated	I	Scheme generally used for the top part of pyramid lattice towers.	500 - 1000
H2	Triangulated	II	Scheme generally used for the top part of pyramid lattice towers, or for towers with a square base.	1000 - 3500
H3	Triangulated	III	Scheme used only in lattice towers with a constant triangular base.	500 - 800
H4	Triangulated	IV	Scheme used in the lower part of the pyramid lattice towers with a medium-high height.	3500 - 7000
H5	Not fully triangulated	VI	Scheme used in the central part of the pyramid towers. It is widely used throughout the development in lattice towers with a constant square base.	1500 - 3000
H6	Not fully triangulated	VII	Scheme used in the lower part of pyramid lattice towers with medium height.	3000 - 6000

Table 4-23, horizontal bracing used for rawland towers

While *tables 4-24, 4-25 and 4-26* show the types of primary vertical bracing, secondary vertical bracing, and horizontal bracing for rooftop tower that have been considered for this study.

<i>ID type</i>	<i>Category</i>	<i>Type on EN 1993-3-1</i>	<i>Description</i>	$L_d$	<i>Base range [mm]</i>	<i>Height range [m]</i>
PV1	Parallel or Tapering	I	A single lattice may be used where the loads are light and the lengths relatively short, as for instance near the top of towers.	$L_d = L_{di}$	400 - 800	3 - 5
PV2	Parallel or Tapering	II	It is applied in cases where the load that the tower must carry is such as not to allow the use of model I. the critical length becomes half the length of the bracing provided that the bracing are joined at the crossing point.	$L_d = L_{di}/2$	400 - 1800	3 - 6
PV3	Parallel or Tapering	III	Widely used scheme for pyramid communication towers. this scheme is also used in limited portions of the structure such as the first or last levels. in the absence of secondary elements, the critical length is equal to the length of the diagonal.	$L_d = L_{d2}$	1000 - 2500	4 - 8

Table 4-24, primary vertical bracing used for rooftop towers

<i>ID type</i>	<i>Type on EN 1993-3-1</i>	<i>Description</i>	$L_d$	<i>Base range [mm]</i>	<i>Height range [m]</i>
SV1	IA	Horizontal single lattice as secondary bracings. This method is used really often for roof top lattice tower even in both cases: with pyramid type that with constant type.	$L_d = L_{di}$	400 - 1800	3 - 6
SV2	IIIA	Very common scheme for telecom towers. It is used for towers with considerable loads and heights. Generally used for pyramid lattice towers.	$L_d = L_{di}/2$	1000 - 2500	4 - 8

Table 4-25, secondary vertical bracing used for rooftop towers

<i>ID type</i>	<i>Category</i>	<i>Type on EN 1993-3-1</i>	<i>Description</i>	<i>Base range [mm]</i>
H1	Triangulated	I	Scheme generally used for the top part of pyramid lattice towers.	800 - 1800
H2	Triangulated	II	Scheme generally used for the top part of pyramid lattice towers, or for towers with a square base.	1000 - 2500
H3	Triangulated	III	Scheme used only in lattice towers with a constant triangular base.	400 - 800
H4	Not fully triangulated	VI	Scheme used in the central part of the pyramid towers. It is widely used throughout the development in lattice towers with a constant square base.	800 - 1800

Table 4-26, horizontal bracing used for rooftop towers

The assignment of the type of foundation to each tower on the ground occurs in a deterministic way, as there is no information about it. The assignment of the type of foundation is not relevant from the point of view of analysis but has the sole purpose of describing the structure in an exhaustive manner. Therefore, following what was proposed by Kyung and Lee (2015), insulated plinths and bolted connections were assigned to the self-supporting towers as a foundation, while for the monopole towers, the foundation is made using a bored pile and anchors. In this way both foundations can be described as interlocking as a constraint. *Table 4-27* shows the foundation types used to describe the towers.

<i>ID type</i>	<i>Type</i>	<i>Type's Name</i>	<i>Tower Tipology</i>	<i>Bolts Class</i>	<i>Type of Restraints</i>
F1	d	Anchor bolts	Monopole	8.8	Fixed
F2	a	Base joint	Lattice	8.8	Fixed

Table 4-27, type of foundations selected for rawland towers

On the contrary, the connection to the base for the towers on the roofs is not done by the type of foundation, but by the type of anchor. For them the information was even less, for this reason anchors were chosen that could represent an interlocking constraint among those proposed by Assi (2006) in her work. The anchorage is assigned according to the structural configuration and the height of the tower itself. It is a totally subjective and deterministic assignment that does not follow any method proposed in the literature. *Table 4-28* shows the anchors used.

<i>ID type</i>	<i>Description</i>	<i>SC</i>	<i>Bolts Class</i>	<i>Type of Restraints</i>
a	Simple flange bolted to a beam of the last floor of the building.	SC1/SC2/SC3/SC4	8.8	Fixed
c	Pole fixed to a wall or pillar of the building or to the wall of the stairwell leading to the roof of the building itself.	SC4	8.8	Fixed
b	System of steel beams as a base (usually IPE beams) anchored to the last floor of the building by means of a series of bolted joints. The tower in turn is anchored to the base beam system with bolting (flange, L-profiles, et.). It used for both, lattice towers and single poles.	SC1/SC2/SC3/SC4	8.8	Fixed

Table 4-28, type of anchor systems selected for rawland towers

Continuing with the evaluation of the data, the classic connections used for the construction of the towers were defined. Here too the information was minimal. To assign the types of connections used for their construction to each tower, it was based on the previously defined structural configuration. The most common connections for telecommunications towers are five types according to the EN

1993-3-1 standard, some are applied only to self-supporting towers and others are applied only to single-pole towers. *Table 4-29* summarizes the connections used to describe communication towers.

<i>ID type</i>	<i>Type's Name</i>	<i>SC</i>	<i>Bolts Class</i>	<i>Type of Restraints</i>
C1	Bolted connection	SC1, SC2, SC3	8.8	Rolled
C2	Gusset joint	SC1, SC2, SC3	8.8	Rolled
C3	Plate Flange	SC1, SC2, SC3	8.8	Fixed
C4	Flanged Pipe Pole	SC4, SC5	8.8	Fixed
C5	Slip Sleeve Tapered	SC4, SC5	8.8	Fixed

Table 4-29, connection types used to describe the rmland and rooftop towers

Finally, it is established which loads must be considered for the calculation of the mass of the tower.

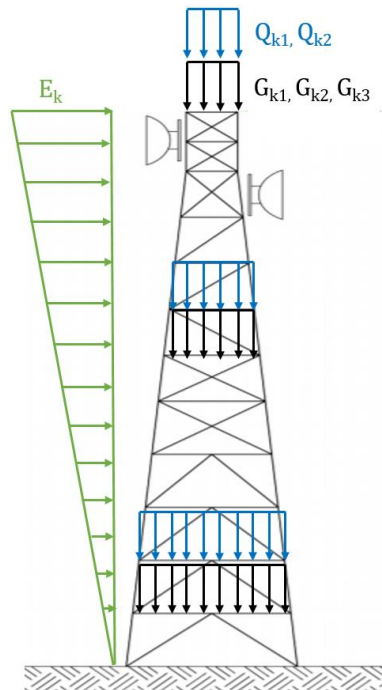


Figure 4-30, illustration of the loads concerned the tower

Permanent loads are represented by:

$G_{k1}$  = self-weight

$G_{k2}$  = weight of the main plant (antennas, etc.)

$G_{k3}$  = weight of the lower systems (ladders, cables, etc)

As a horizontal action, the only action due to seismic events was considered. The action of the wind has been neglected even if for this type of structures, it is more burdensome because the main focus of the study is to study the seismic vulnerability of the network.

$E_k$  = earthquake load

While as regards the variable loads, only an accidental load defined by the legislation and the load due to ice that can cover the structure were considered.

$Q_{k1}$  = accidental load

$Q_{k2}$  = ice load

As far as the snow load is concerned, it is neglected since for telecommunication towers there are generally no horizontal planes (Madugula 2001). The self-weight is given by the L-shaped or hollow profiles that make up the steel structure, and is a weight distributed along the height of the structure itself. The weight of the main plant is given by the antennas for connection to the network and is considered as a concentrated load. The weight of the minor plant is a load defined by the EN 1993-3-1 standard. For each truss there is a uniformly distributed average load of 1.5 kN/m, for the height of the structure, including small systems, ladders, cables etc. The EN 1993-3-1 standard also defines an average accidental load distributed along the height equal to 1.0 kN/m. Finally, the additional load produced by the layer of ice that can be created around the steel profiles (*figure 4-30*) is taken into account as a second variable load. The legislation requires that a uniform layer be considered for all the elements that make up the structure. The thickness is established by the altitude at which the tower is built. In the case of the Ideal City, an average altitude of 300 meters above sea level has been assumed. Appendix B of the EN 1993-3-1 standard provides for a thickness of 7.5mm for altitude between 300 mt and 800 mt.

The loads were then combined with the partial factors proposed by the EN 1993-3-1 standard regarding towers. To define which coefficients to use it was necessary to establish the Reliability Class for the towers. Being in an urban environment, the Reliability Class is equal to 3. The partial factors used are shown in *table 4-30*.

<i>Type of effect</i>	<i>Reliability Class</i>	<i>Permanent Actions</i>	<i>Variable Actions</i>
unfavourable	3	1,2	1,6
favourable	All classes	1,0	1,0

Table 4-30, partial factors for loads

*Figures 4-31 and 4-32* show a graphic schematization of the structural and non-structural parameters used.

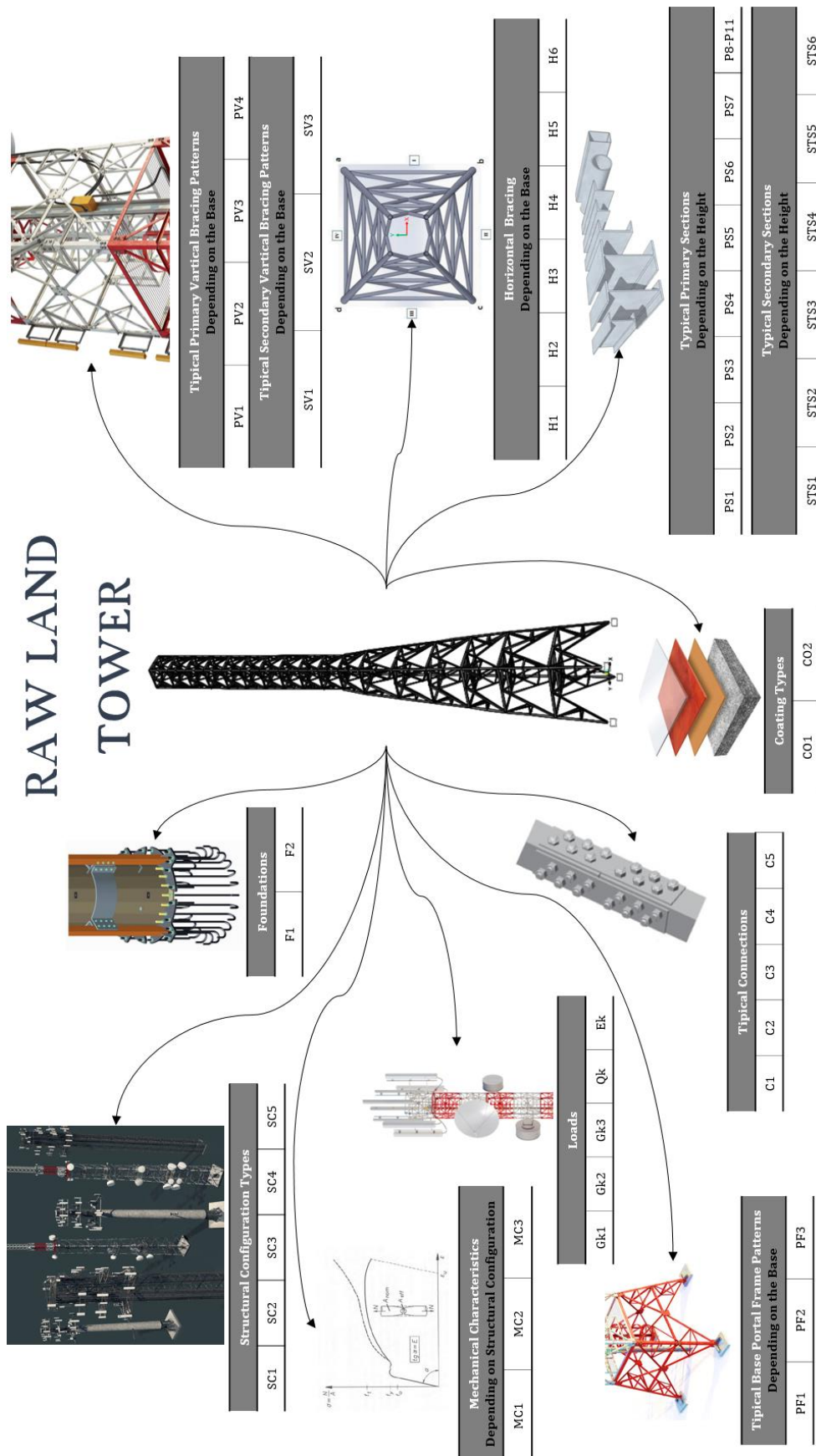


Figure 4-31, Summary diagram of the structural and non-structural parameters that characterize the rawland towers



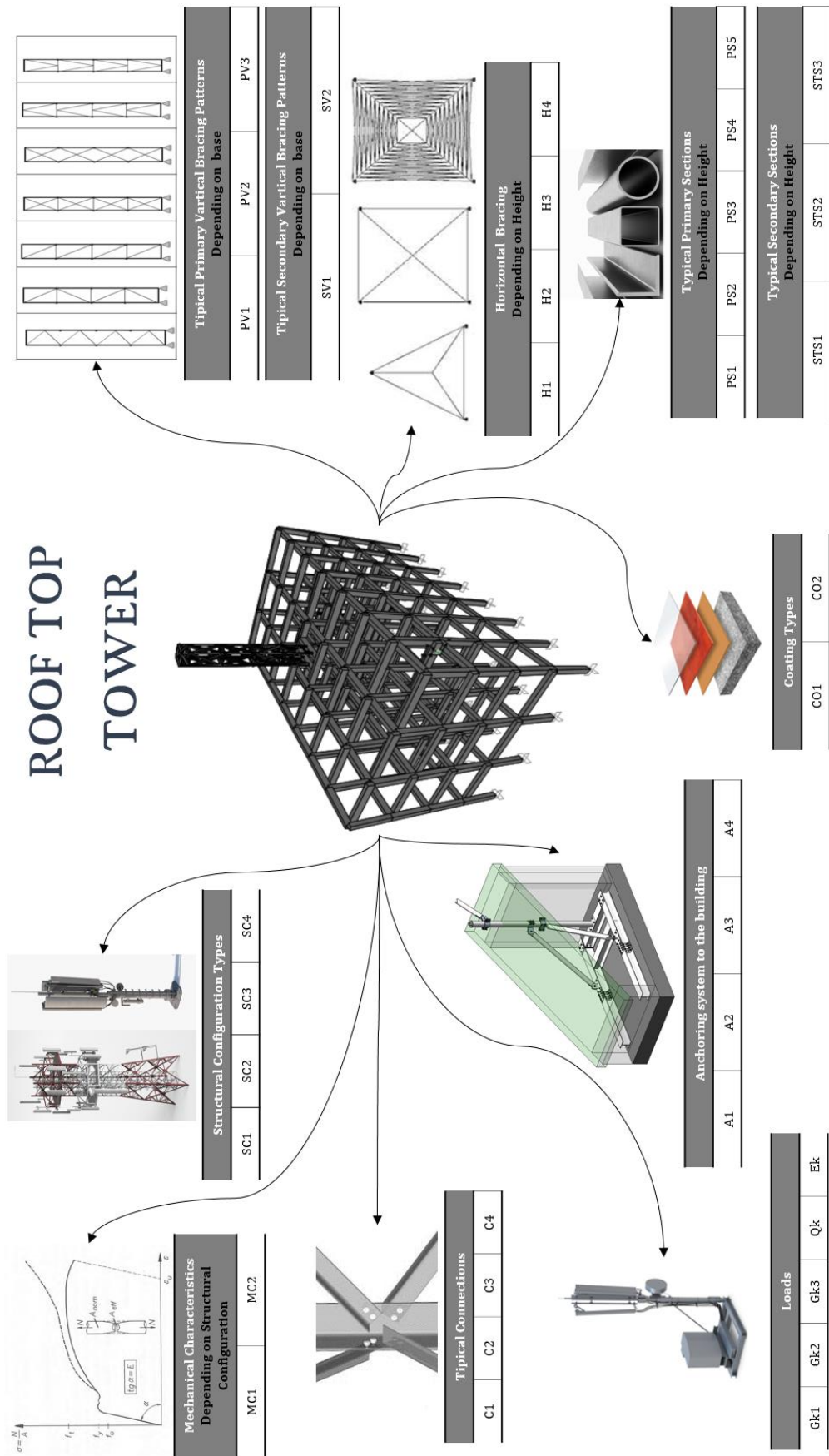


Figure 4-32, Summary diagram of the structural and non-structural parameters that characterize the rooftop towers

#### 4.3.2 Preparation and assessment for the Base Stations Controller' data:

After the data collection and definition phase to describe the network components, they often need to be manipulated to be suitable for further analysis. We therefore speak of data preparation. Data preparation can be done by organizing and rearranging the raw data. Or in the case of lack of some information for some parameters, hypotheses or simplifications for their definition can be introduced. The accuracy of the data must be carefully checked at this stage. Inaccurate or inconsistent data will affect further phases of the calculation cycle. The manipulated data is then used in a code-readable format to be processed by a computer to obtain results on the virtual network.

##### 4.3.2.1 Geographical Parameters:

No manipulation or assumptions were required for the geographic data. The only process performed as done for the BTS was to convert and report the coordinates to the same reference system of the building layer developed in past works for the Ideal City.

##### 4.3.2.2 Geometric Parameters:

Geometric parameters also did not require large manipulations. Known the file of the position of the control stations through the geographical coordinates from CellMapper, it was crossed with the shape file of the city of Turin provided by the Geoportale of Turin (*figure 4-33*) to obtain which building represented a BSC and obtain the geometric parameters of the same through the tables associated attributes.

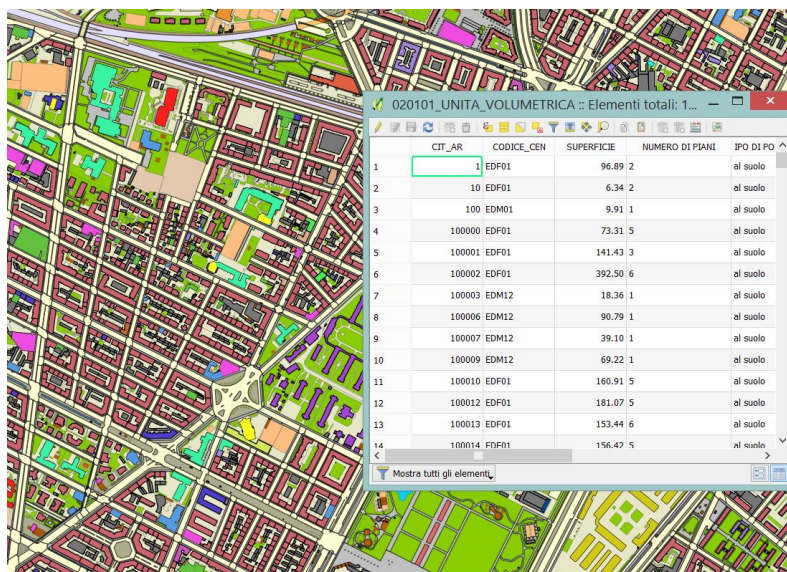


Figure 4-33, extrapolation of the shapefile with attribute table of Turin buildings

### 4.3.2.3 Structural and Non-structural Parameters:

Being the BSCs to all effects of the buildings with average characteristics. Since a layer of the built environment has already been developed for the Ideal City project, it was not necessary to define the values or characteristics for the structural and non-structural parameters defined in the previous paragraph regarding the BSCs through methods and simplifications. This is because the work carried out by the resilience center of the Polytechnic University of Turin of DISEG for the virtual city project called Ideal City was used. Therefore, the work carried out by Marasco and Cimellaro (2018) for the Ideal City project was used to define these parameters. Therefore, in accordance with the work of (Marasco and Cimellaro 2018), seven types of floor slabs, seven types of structural configurations, three types of perimeter masonry, four types of reinforcement for the columns, six types for the mechanical properties and the same for the combination of loads. *Figure 4-34* summarizes the newly introduced parameters by Marasco and Cimellaro (2018).

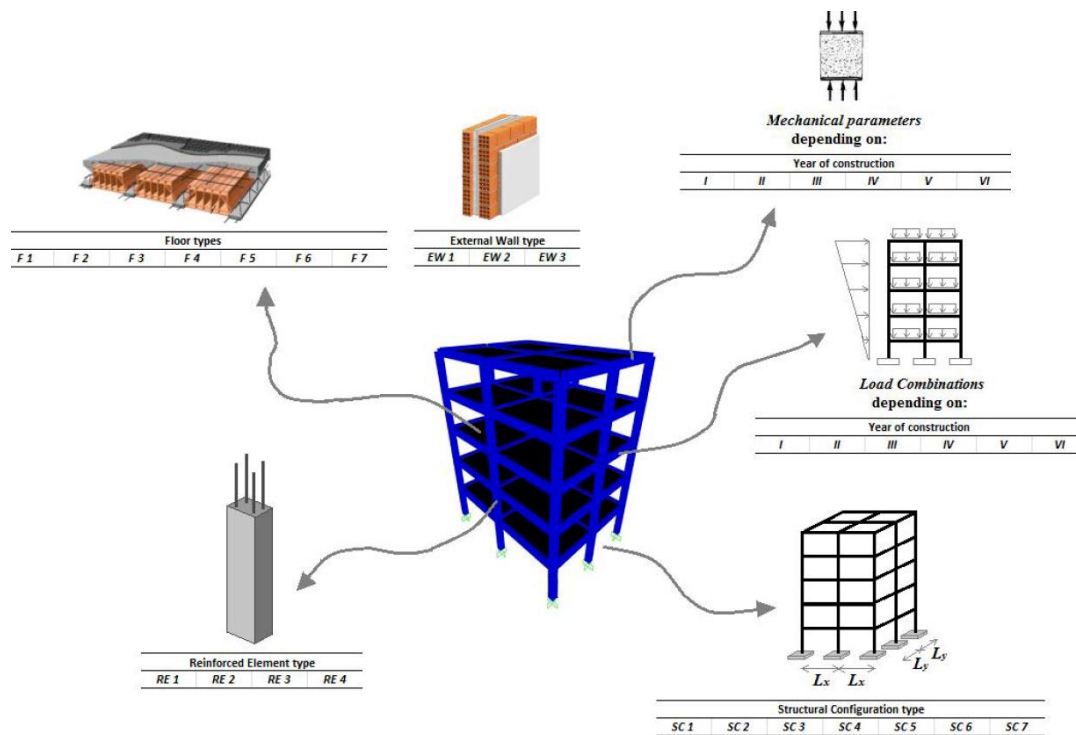


Figure 4-34, summary of the various values of the parameters to characterize the reinforced concrete buildings defined by Marasco et. to the. (2018)

Therefore, in this study the method developed by Marasco and Cimellaro (2018) to define and assign the values for the different parameters for the buildings will not be illustrated in detail as it is already explained in detail in the work carried out by Marasco and Cimellaro (2018) for the Ideal City buildings. It can be mentioned that the assignment takes place by means of an algorithm in MATLAB, that some values of certain parameters are assigned based on the construction

period and that others are determined in a deterministic way based on the collected data. It should also be mentioned that the uncertainties present in the choice of some parameters are managed by means of statistical inference processes. In this way, as for the BTS, each BSC was characterized with mechanical parameters such as to allow the subsequent dynamic analysis to be carried out.

#### 4.3.2.4 Telecommunication Parameters:

Using the Voronoi division to define the areas of competence of the various BSCs (figures 1-35) it was possible to make a first estimate of the number of BTSs that each BSC must manage for each MNO (Yu and Kim 2013).

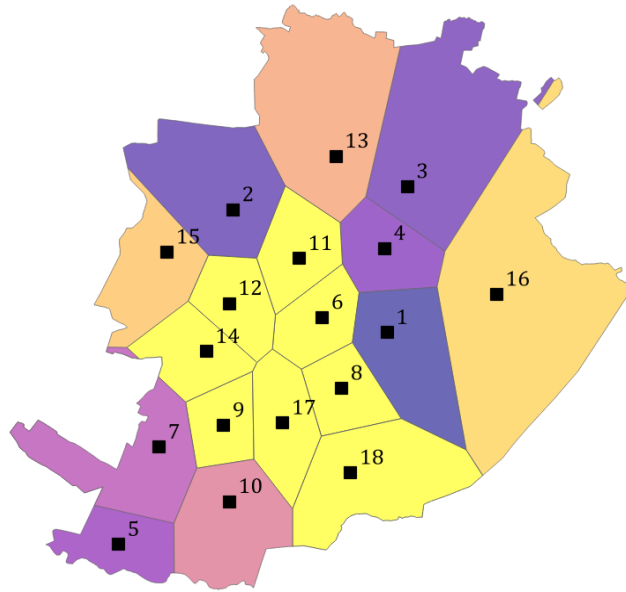


Figure 4-35, Voronoi's subdivision for BSC

Once this was done, it was observed that some BSCs were assigned an excessive number of BTS per MNO to be checked based on what Giovinazzi, Austin et al. (2017) stated in their study where each BSC manages around 20 BTS per MNO. For this reason, a second parameter was introduced to distribute the BTS more homogeneously. The distance between BTS and BSC as proposed by Yu and Kim (2013) was used as a discriminative parameter. In this way, if a BSC were initially assigned more than twenty BTS to be managed for each MNO, by means of the second discriminatory parameter, the distance calculated with *equation 1-1*, the excess BTS (i.e. the most distant), are reassigned to the second closest BSC, if it has fewer BTSs to manage. Otherwise the BTS is reassigned to the third closest BSC and so on. In this way, which and how many BTSs each BSC must manage, and control have been defined. Therefore, for each MNO the single control station will manage a maximum of twenty BTS. *Table 4-31* reports the number of BTSs to each MNO that each BSC manages.

<i>BSC</i>	MNO 1	<i>MNO 2</i>	MNO 3
1	20	19	17
2	20	19	17
3	18	14	17
4	18	15	16
5	12	11	10
6	20	19	17
7	13	13	11
8	20	18	13
9	13	13	15
10	14	13	14
11	19	18	16
12	18	18	16
13	19	17	16
14	13	17	12
15	19	17	15
16	17	14	14
17	16	16	13
18	15	15	11
Total BTS by MNO	304	286	260

Table 4-31, number of BTS manage by each BSC for each MNO

Also as regards the definition of the hierarchical position in the network of each BSC, the initial information available was null. It is important to define as the data that is transmitted follows a certain path to reach the end user. For example, it could happen that the BTS is able to transmit data to the BSC to which it is connected, after which even if the BSC has not suffered damage but if the control stations of the higher hierarchy level to which the first BSC was connected have suffered damage then the communication fails to take place. For this reason, it is essential to define the hierarchy of the network control stations. However, even in this case some simplifications and hypotheses had to be made for the reasons already mentioned at the beginning of the chapter. To define the hierarchy among the control stations as discriminatory parameters, the surface of the control stations and their location in the city (Weatherspoon 2014) were chosen. *Figure 4-36* shows an extract of the attribute table from QGis for the BSCs. *Table 4-32* summarizes the hierarchical level that each BSC has.

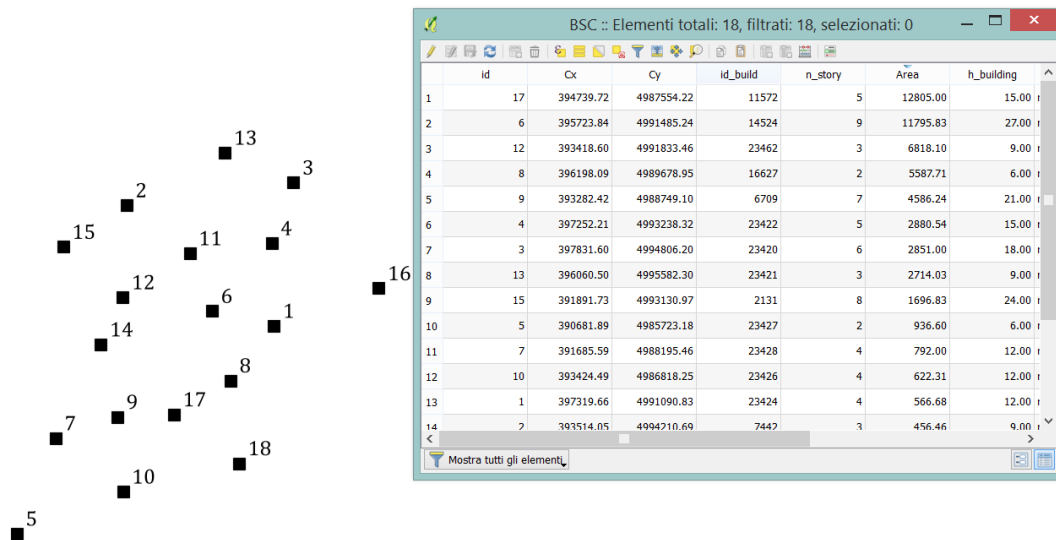


Figure 4-36, raw data about the BSC from QGIS

<i>BSC</i>	Hierarchical level in the network
1	3
2	3
3	3
4	2
5	3
6	1
7	3
8	2
9	2
10	3
11	3
12	2
13	3
14	3
15	3
16	3
17	1
18	3

Table 4-32, hierarchical level for BSCs

As can be seen from *table 4-32*, two BSCs were chosen for the first level, four for the second and the rest were classified in the third. This is due to what Weatherspoon (2014) illustrated to define a topology similar to the Fat-Tree theory, which allows the BSCs to be connected in a reasonable way. The Fat-Tree topology will be explained in more detail in the section on topology.



Both telecommunication parameters as will be seen in the next paragraph will be fundamental to build the topology for the wireless network of the virtual city.

#### 4.3.3 Preparation and assessment for the data about the Building Environmental and User Cluster:

As mentioned for the raw data collection phase, no work was required for the manipulation phase as well. This is since the built environment layer had already been developed for the Ideal City project (Marasco and Cimellaro 2018).

Also, for the data collected about users it was not necessary to perform any manipulation or assume any assumptions. In fact, during the collection phase they have already been grouped in clusters according to the residence building.

### 4.4 Network's Topology

#### 4.4.1 Types of topologies chosen for the network' components

In the wireless network topology for the Ideal City, the nodes are represented by the BTS and BSCs, while the links represent the physical connection (a cable or an electromagnetic wave) between the node elements. The topology of a real wireless network is typically a hybrid topology that uses multiple base topologies seen for wireless networks at the same time. It is not possible to obtain the real topology for the Turin network as this information is considered confidential by the MNOs. Therefore, the concepts defined in the literature have been relied upon for the construction of the topology.

In accordance with what defined by de Souza Couto, Secci et al. (2016), the most used topology in real networks to connect the BTS to the BSC is the star one. It is widely used in densely populated areas, such as cities. In the star topology, each site (represented by the BTS) is directly connected just to one BSC. This type of connection has advantages but also disadvantages. The advantages are:

- If for example a node or its connection is broken, this break does not affect the remaining part of the network.
- Further nodes can be added without interrupting the normal operation of the other nodes connected to the control station.
- It is very suitable for working with heavy data loads.

However, there are also disadvantages:

- Expensive due to the number and length of cables needed to wire each BS to the BSC, in fact when the distance is too much between the two nodes or a node it is in a remote location it is used a wireless connection.
- If the link between BS and BSC fails, the BS will be excluded from the network and therefore also the area it covers

- If a BSC fails, the BTS connected to it will also be automatically excluded from the network

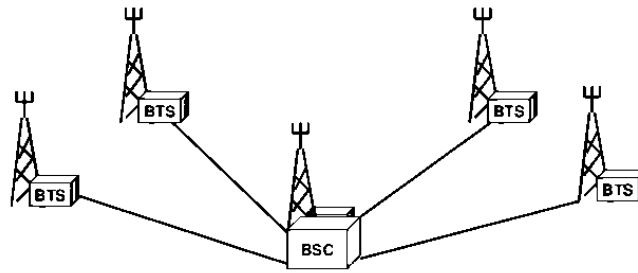


Figure 4-37, Illustration of the Star topology between BTS and BSC

Instead, as concerns the part of the network that provides for the connection between the Base Stations Controller (BSC), the information on the real topology of the network was not known for security reasons.

So, for the connection between the BSCs, the topology called Fat-Tree was adopted. It was introduced by Leiserson (1985). The Fat-tree model represents a topology very similar to the models of real wireless networks, which is why its use in the literature is widely accepted and widespread. This type of topology provides the network with a certain level of redundancy in connections. In this way, even if a link is damaged, the signal has alternative ways to proceed along its path. In addition to this, the Fat-Tree system allows to maintain the same connection speed as each link uses the same bandwidth to transmit or receive the signal. The Fat-Tree network foresees that there are three levels of switches. The highest level is formed by the Core Switches, that is, they are the elements that manage the network at the urban level. Then at the lowest level are the Aggregation Switches. Each aggregation is connected to all cores. Finally, at the lowest level are the Edge Switches. Each Edge is controlled by two Aggregations. Naturally, each Switch controls a series of BTSs through the star topology. Typically, Aggregations and Edges form so-called Pods. *Figure 4-38* illustrates the hierarchy. (de Souza Couto, Secci et al. 2016).

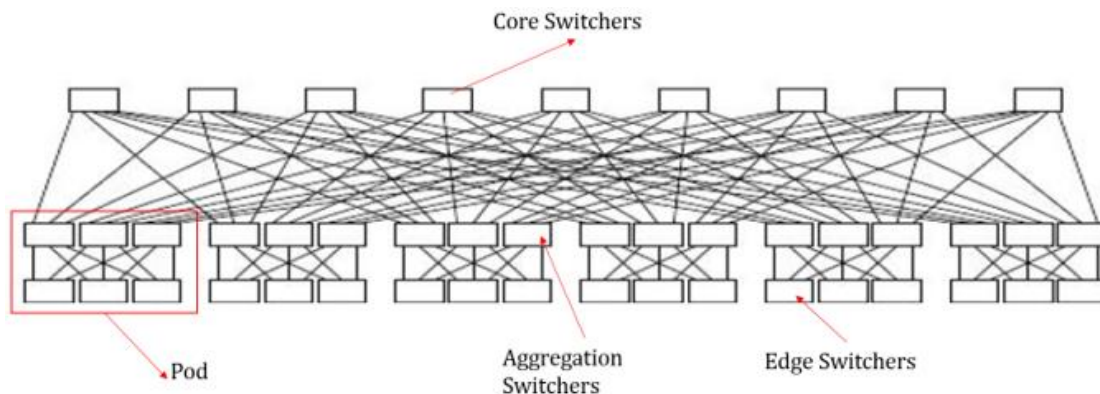


Figure 4-38, scheme of Fat-Tree topology

A Fat-tree employs a more redundant core than the classic Tree-layer topology, so, that can be useful to have a less vulnerability network from same breaks. Also, in the Fat-tree topology there are no links between elements of the same level.

#### 4.4.2 Data Input to build the network's Topology

The telecommunication parameters related to the BSCs, and the distances calculated between BSC and BTS were used as starting input data for the construction of the wireless network topology of the virtual city.

#### 4.4.3 Construction of Network's Topology

Therefore, based on the telecommunication parameters previously introduced for BSC, the star links between BTS and BSC can be defined. This is because it is known which BTSs are linked to which BSCs through the subdivision into areas of competence with the forms of Voronoi and through the BTS-BSC distance as an additional discriminatory parameter. *Figure 4-39* is an example of the star links between the BTSs of the first MNO of the network and the BSCs, while *Figure 4-40* shows the star links between all the BTSs (i.e. all three MNOs) and the BSCs.

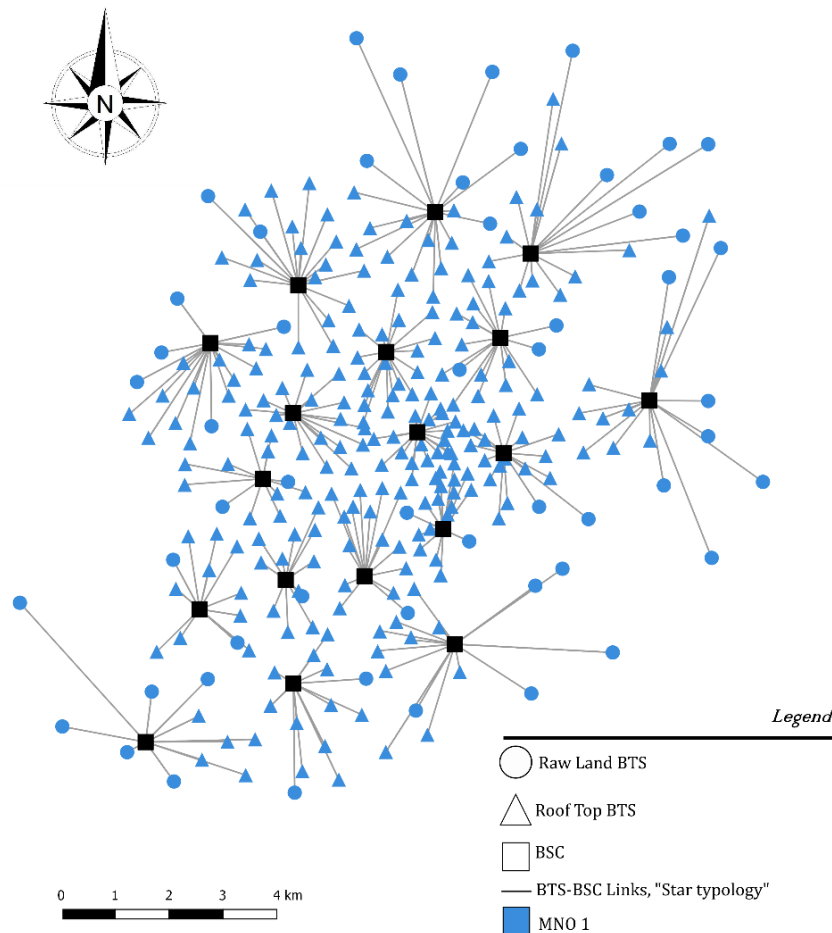


Figure 4-39, star links between the first MNO's BTS and the BSC

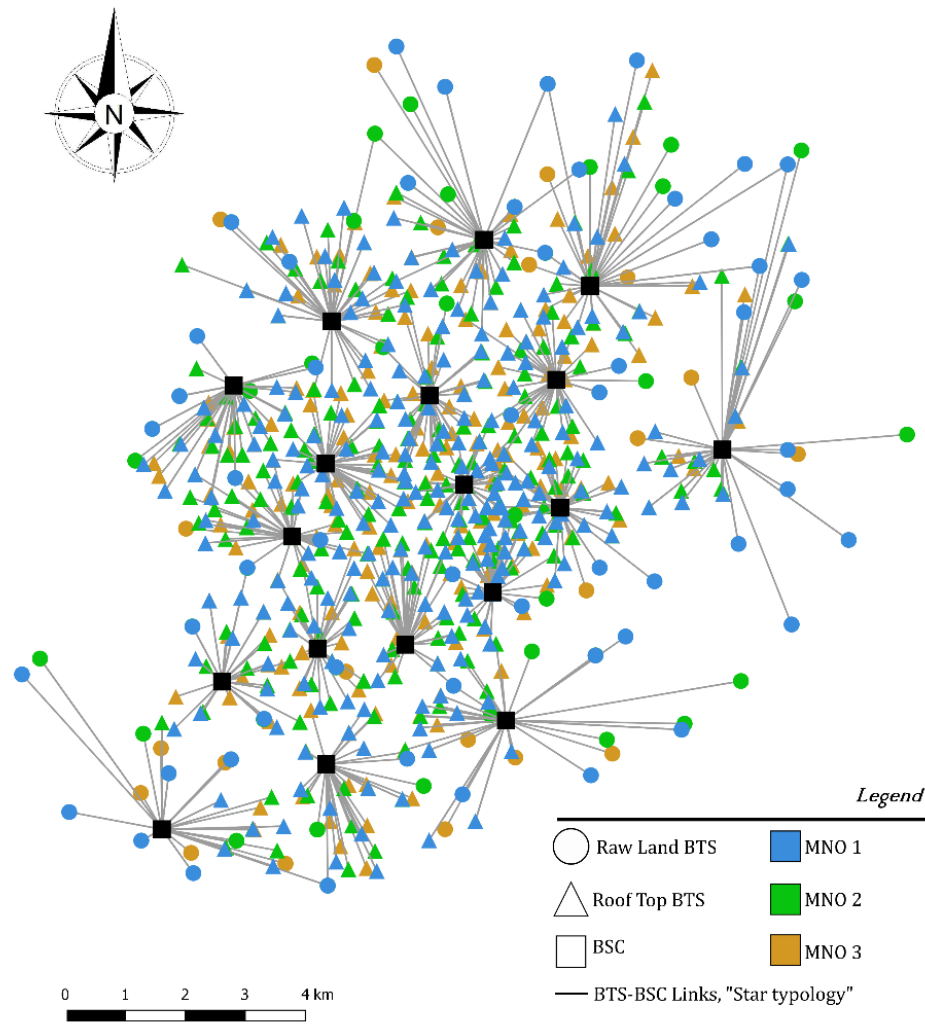


Figure 4-40, star links between all the BTS and the BSC

In accordance with the hierarchy defined for the BSCs, it was possible to build the network of links based on the Fat-Tree topology between the various BSCs. So the stations with a hierarchical level of 1 were classified as Core, the second level ones as Aggregation and the rest as Edge. Having said that, according to the principles used for classification, stations 6 and 17 are the Core nodes, stations 4, 8, 9, and 12 are the Aggregation nodes, while the rest are classified as Edge nodes. *Figure 4-41* shows the classification for the BSCs to use to build the part of network topology of themselves. As for the connections between elements, each Aggregation is connected to each Core, while each Edge is connected to only two Aggregations, based on the hypotheses defined by de Souza Couto, Secci et al. (2016) in their work. To define which Aggregation nodes each Edge node was connected to, the same condition of the minimum distance proposed by (Weatherspoon 2014) in his principles of Fat-Tree topology was always used. Therefore, each Edge node is connected to the two Aggregation nodes closest to its position (Weatherspoon 2014). This creates the final link network for the BSCs. It is shown in *figure 4-42*.

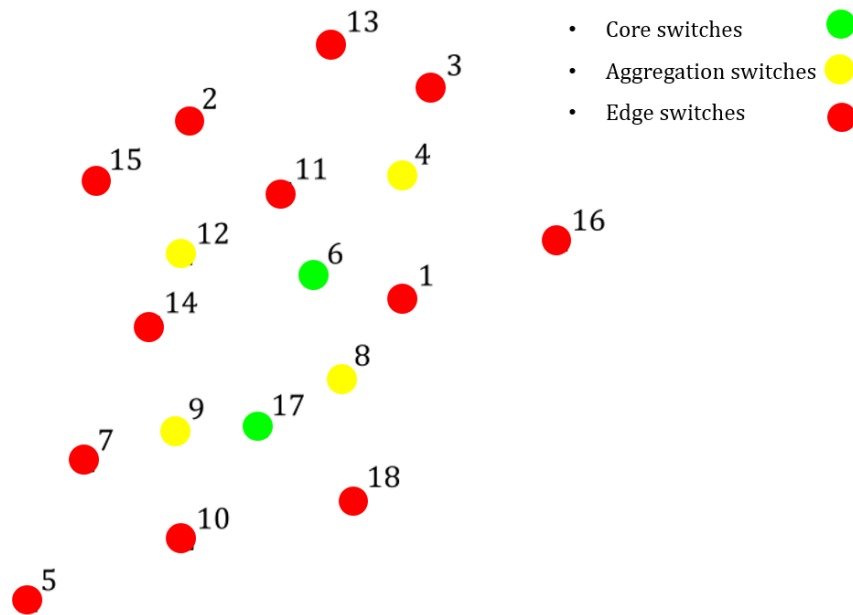


Figure 4-41, hierarchical levels for the BSCs for the construction of the topology between them

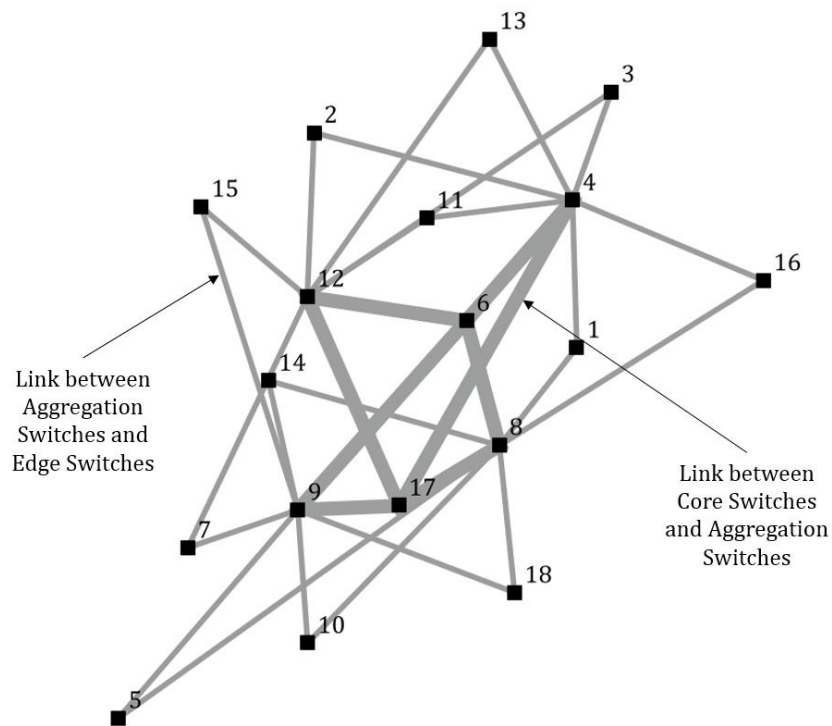


Figure 4-42, link obtain between the BSCs using the Fat-Tree topology

As seen in the previous chapter, the link between two elements is physically represented by a connection through an optical fiber cable, or through parabolas to transmit signals with electromagnetic waves. A summary scheme of the hierarchy among the BSCs is proposed in *figure 4-43*.

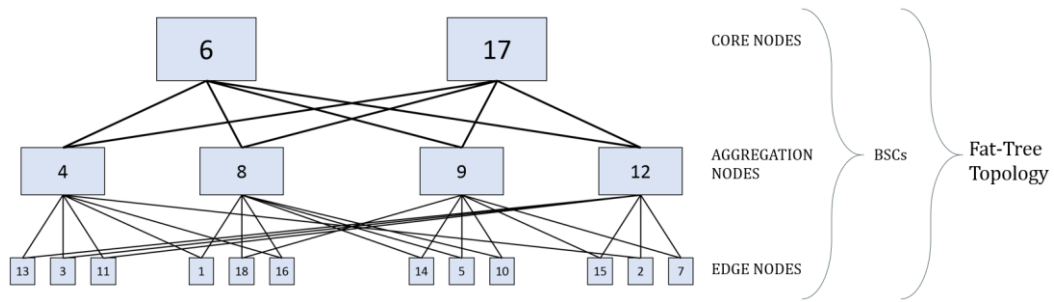


Figure 4-43, summary diagram of the network topology

The result is the topology for the entire wireless network for the virtual city. *Figure 4-44* shows the general scheme of the topology with all the MNOs considered. We observe the star links between BTS and BSC and the Fat-Tree topology for the connection between the BSCs.

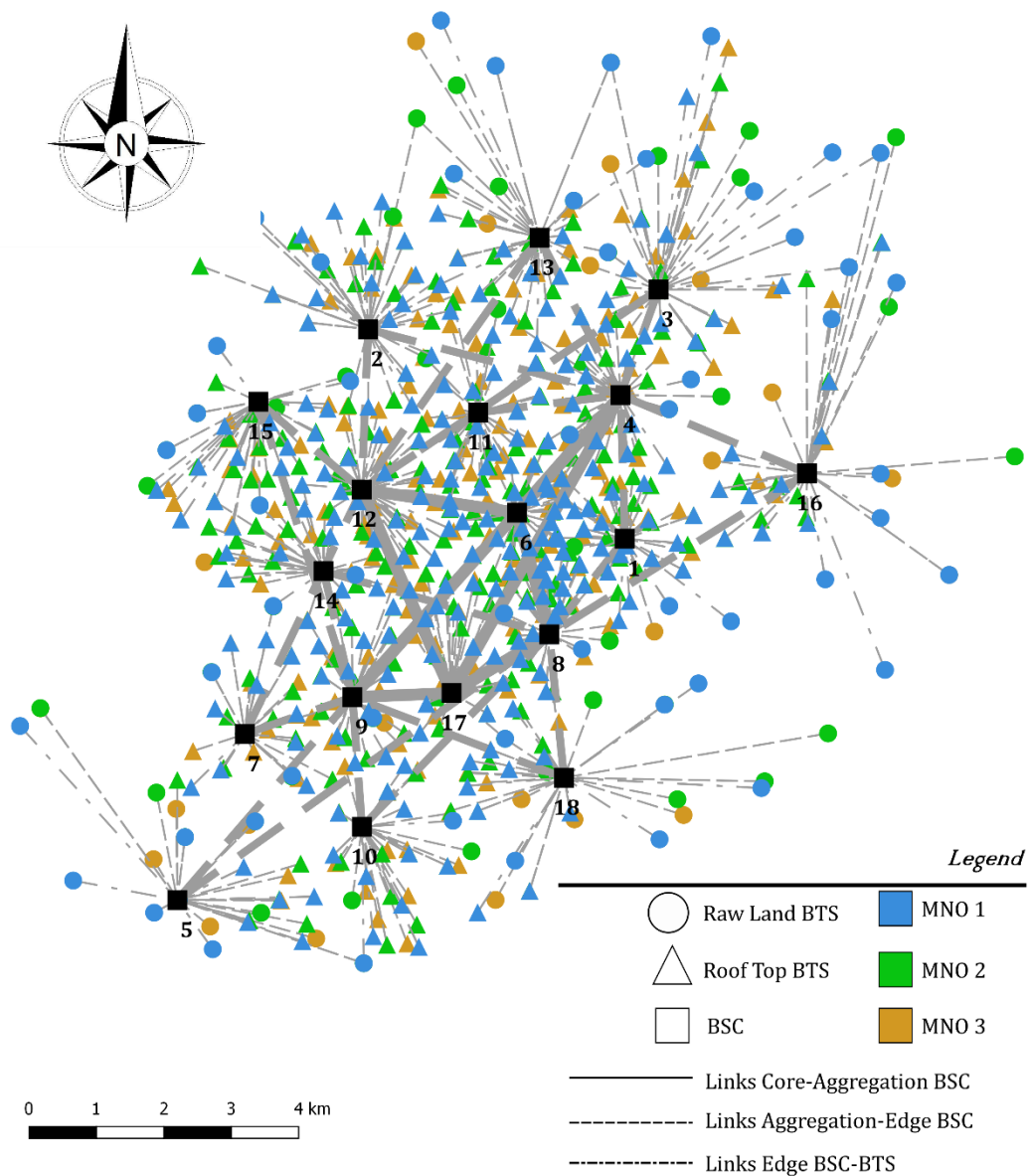


Figure 4-44, summary map of network's topology



## 4.5 Assessment of the Frequency Reuse Factor (FRF) for the network

In the previous chapter, which explains the general structure of a wireless network. It defines the concept of subdivision into cells of the territory to be covered by the network. Such division is advantageous for the reuse of the same frequencies, to have little loss in the quality of data transmission, as the interference would be generated only by the antennas that use the same frequency. While if this division into cells was not taken into consideration, each antenna would create interference to the others, causing a worse quality in data transmission (Abu-Al-Saud 2019). For the development of the wireless network for the virtual city it was not possible to obtain any information on the division into cells of the city of Turin. No information was also found regarding the reuse of frequencies. Not being able to make any hypothesis of detailed modeling of the subdivision into cells of the territory, the only feasible way was to consider an interference given by all the other BTS in the calculation of the signal between user and BTS. In other words, it was decided to use a frequency reuse factor (FRF) equal to one as also proposed by Malandrino, Chiasserini et al. (2017) in the study of the San Francisco Bay network.

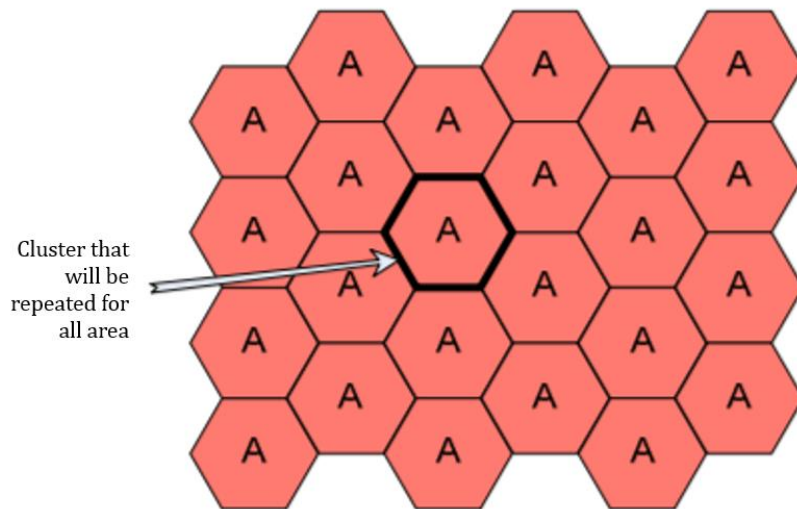


Figure 4-45, scheme for a FRF equal to one

As will be seen in the chapter concerning the calculation of the quality of the connection between the User and the BTS, the average value for the virtual city will not be so low compared to the real average value of the city of Turin for each MNO.

#### 4.6 Data Output for the Ideal City's wireless network:

The goal of the data collection and processing was to create a complete database about each component that is part of an urban wireless network, to be used by each user. All data processed must be kept for future purposes and uses, and therefore must be stored in databases that allow rapid access and retrieval of information. In this research, all generic information about network components has been structured into text files that allow for a faster import process into programming environments such as python. The files are organized into rows representing towers and into columns, where each column represents a specific parameter.

All generated text files containing the information of the wireless network components and their design properties will be stored in the IDEAL\_SERVER database which is the main server of the Disaster Simulation Resilience Center (DSRC) located in the Department of Structural and Geotechnics (DISEG) of the Polytechnic University of Turin and used for the Ideal City project.

Through this catherization process it is therefore possible to fully describe the elements of the network in such a way as to allow the creation of a simplified physical model to analyze the behavior during disastrous events.

# 5 Estimate of normal operation of the Wireless Telecom Network

## 5.1 Introduction

Having defined the infrastructural network and its components, the next step was to evaluate it under ordinary conditions of working. So, this paragraph aims to determinate a method to evaluate the capacity of cellular network during normal operating conditions using simply indicators focusing on downlink data transfers (Malandrino, Chiasserini et al. 2017).

To this purpose, the methodology described in (Malandrino, Chiasserini et al. 2017) and (Di Francesco, Malandrino et al. 2017) was followed. This method is to follow this procedure:

- Compute the attenuation of the signal between BTS and UC.
- Define the power of signal from BTS
- Define the interference of signal and the background noise
- Compute the *signal-to-interference-and-noise ratio (SINR)*
- Determinate the *Throughput* according to SINR values

## 5.2 Path Loss (PL)

The first step was to compute the attenuation of the signal as known into scientific field as Path Loss (PL). The PL is the reduction in power density (attenuation) of an electromagnetic wave emitted by a BTS as it propagates through space. It usually measured in Decibels (dB). That, because, in system planning for mobile telephone service or service quality evaluation, it is essential to estimate the propagation characteristics of the signal (Hata 1980). In fact, the path loss may be due to many effects, such as free-space loss, refraction, diffraction, and reflection of the signal.

In general, this loss is greater in an urban environment where there are many more buildings than in a rural one. That is also an explanation of the fact that many BTS are present in a highly man-made environment. To understand the importance of correctly evaluating the path loss of the signal and how it can be strongly influenced by the surrounding environment, it was decided to evaluate it starting from a simpler model, than up to a more detailed model.

### 5.2.1 Free Space Model

The first model tested it was the *Free Space Model*, this, is the simplest way to model the path loss. It always considers for each pair of points (User-BTS) the hypothesis called *line of sight*, that is, all obstacles that might affect the propagation are neglected. The path loss is given by:

$$PL_{[dB]} = 32,45 + 20 \log_{10}(d) + 20 \log_{10}(f) \quad (5-1)$$

proposed by Balanis and Polycarpou (2003) and it can be used with no limits on distance or frequency.

Where:

- $d$  = distance between Bs and User in [Km];
- $f$  = frequency of the signal in [MHz];

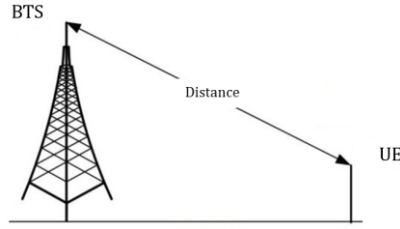


Figure 5-1, Path loss's Free Space Model

This model is useful to understand the order of magnitude of the signal loss, as can be seen in *graph 1*, where the calculation of the path loss for different frequencies is reported, however in an urban environment such as in the case of the Ideal City it is too approximate compared to reality.

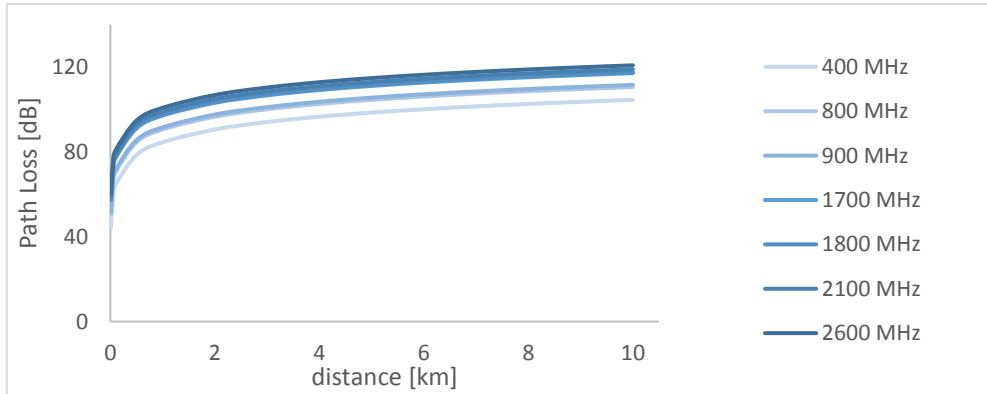


Figure 5-2, path loss as distance and frequency change

### 5.2.2 Hata and COST-231 Model

The second way followed was, to use the model proposed by Hata (1980). It is an empirical model used to predict the path loss in both open land and in built up areas, and, it based on data collected in Tokyo, Japan by Okomura. Since the ideal city is an urban environment, only the formulation of this model for that type of

environment is reported. The Hata model is valid for frequencies between 150–1500 MHz, base station antenna heights,  $h_b$ , up to 200 m, mobile antenna heights,  $h_m$ , up to 10 m and distances up to 20 km. The general expression is given by (Hata 1980):

$$PL_{[dB]} = 69,55 + 26,16 \log_{10}(f) + \\ - 13,82 \log_{10} h_{BTS} + A \log_{10} d - a(h_{FU}) + B \quad (5-2)$$

Where:

- $d$  = distance between Bs and User in [Km];
- $f$  = frequency of the signal in [MHz];
- $h_{BTS}$  = heigh of BTS in [m];
- $h_{FU}$  = heigh of users by default equal to 1,5 m;
- $A$  = constant depending from heigh of BTS;

$$A = 44,90 - 6,55 \log_{10} h_{BTS} \quad (5-3)$$

- $a$  and  $B$  are defined according to the type of area studied (rural, medium city, etc..). For a large city are equal to:

$$B = 0 \quad (5-4)$$

$$a = \begin{cases} 8,29 * (\log_{10}(1,54h_{FU}))^2 - 1,10 & f \leq 200 \text{ MHz} \\ 3,20 * (\log_{10}(1,54h_{FU}))^2 - 4,97 & f > 200 \text{ MHz} \end{cases} \quad (5-5)$$

Into the Ideal City's infrastructural network, there are also antennas that work with a frequency higher than 1500 MHz, for this reason the second method has been integrated with an extension of the HATA model developed by the European Co-operative for Science and Technical research (COST) and called COST 231-HATA specifically designed for BTS that work with a frequency higher than 1500 MHz. This model is given by (COST 1996):

$$PL_{[dB]} = 46,30 + 33,90 \log_{10}(f) + \\ - 13,82 \log_{10} h_{BTS} + A \log_{10} d - a(h_{FU}, f) \\ + (44,90 - 6,55 \log_{10} h_{FU}) \log_{10} d + C \quad (5-6)$$

Where:

- $d$  = distance between Bs and User in [Km];
- $f$  = frequency of the signal in [MHz];

- $h_{BTS}$  = heigh of BTS in [m];
- $h_{FU}$  = heigh of users by default equal to 1,5 m;
- $A$  = constant depending from heigh of BTS;

$$A = 44,90 - 6,55 \log_{10} h_{BTS} \quad (5-7)$$

- $a$  and  $C$  are defined according to the type of area studied (rural, medium city, etc..). For a large city are equal to:

$$C = \begin{cases} 0 \text{ dB} & \text{for medium cities and suburban areas} \\ 3 \text{ dB} & \text{for large cities} \end{cases} \quad (5-8)$$

$$a = 3,20 * (\log_{10}(1,54h_{FU}))^2 - 4,97 \quad (5-9)$$

### 5.2.3 ITU model

The last model considered to evaluate the path loss was, the one built by the International Telecom Union and presented in the report (ITU 2009). This model have been developed based on measurement results carried out in references (Dong, Zhang et al. 2007), (Fujii 2003), (Xu, Zhang et al. 2007), (Zhang, Dong et al. 2008).

Like the Hata model, the ITU model considers in the evaluation of the path loss the influence of type of scenario, for example whether rural or urban. But, in addition to this, the model proposed by the ITU introduces two new ideas. The first one, is that to regard the type of antenna (whether the BTS is a Micro cell, or a Macro cell as reported in Chapter ...) to perform the calculation.

The second one, is that if the distance between the BTS and the FU is small enough, then the BTS-FU pair can be considered in line of sight (LoS), otherwise it is considered not in line of sight (NLoS). Line-of-sight propagation is a characteristic of electromagnetic radiation or acoustic wave propagation which means waves travel in a direct path from the source to the receiver without diffracted, refracted, reflected, or absorbed by the atmosphere and obstructions like buildings, as shown in *figure 5-3*.

In general, to be in line of sight is always desirable but not a critical requirement to establishing good performance because, nowadays, the radio link used by the phones is a digital link with extensive error correction and detection in the digital protocol.



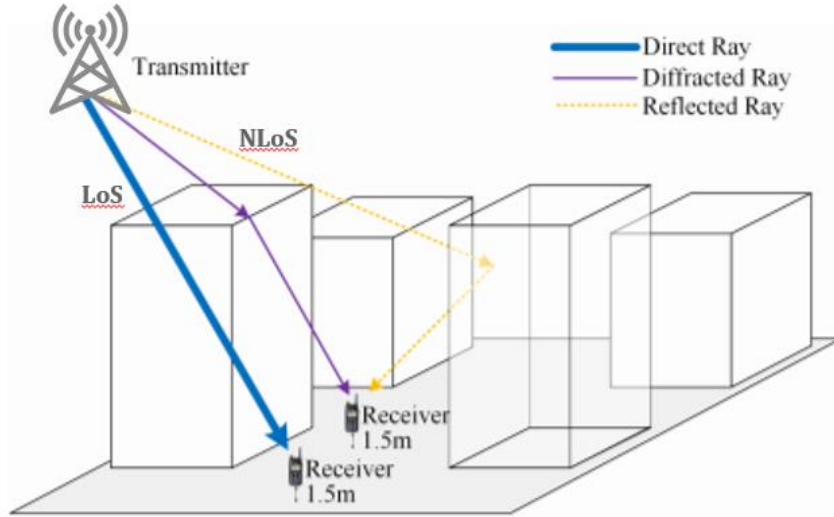


Figure 5-3, examples of LoS and NLoS paths

There have been many good models to capture the LoS probability specific to certain applications (or scenarios). The most known of which, are the models recommended by the International Telecommunication Union (ITU 2009) as a function of distance and focusing on common cellular scenarios such as Macro and Micro cellular sites. For a Urban Macro cell and Micro cell the LoS probability (which means the probability that a given user is in line-of sight of the serving BTS) given by ITU are:

$$P_{LoS,UMa} = \min\left(1, \frac{18}{d}\right) \left(1 - \exp\left(-\frac{d}{63}\right)\right) + \exp\left(-\frac{d}{63}\right) \quad (5-10)$$

$$P_{LoS,UMi} = \min\left(1, \frac{18}{d}\right) \left(1 - \exp\left(-\frac{d}{36}\right)\right) + \exp\left(-\frac{d}{36}\right) \quad (5-11)$$

Where:

- $d$  = distance between Bs and User in meters

In Urban Macro cell if the  $P_{LoS}$  is greater than 0,20 then the user is in line of sight with the serving BTS. While in Urban Micro cell if the  $P_{LoS}$  is greater than 0,23 then the user is in line of sight with the serving BTS (ITU 2009) .

So, the ITU model provides the equations for calculating the Path Loss based on:

- *Line of sight or no Line of sight (LoS or NLoS)*
- *Macro cell or Micro cell (Ma or Mi)*
- *Indoor, Urban, Sub-Urban or Rural environmental (I, U, S or R)*

The Figure 5-4 summarized the possible cases defined by the ITU model to define the Path Loss in a cellular network.

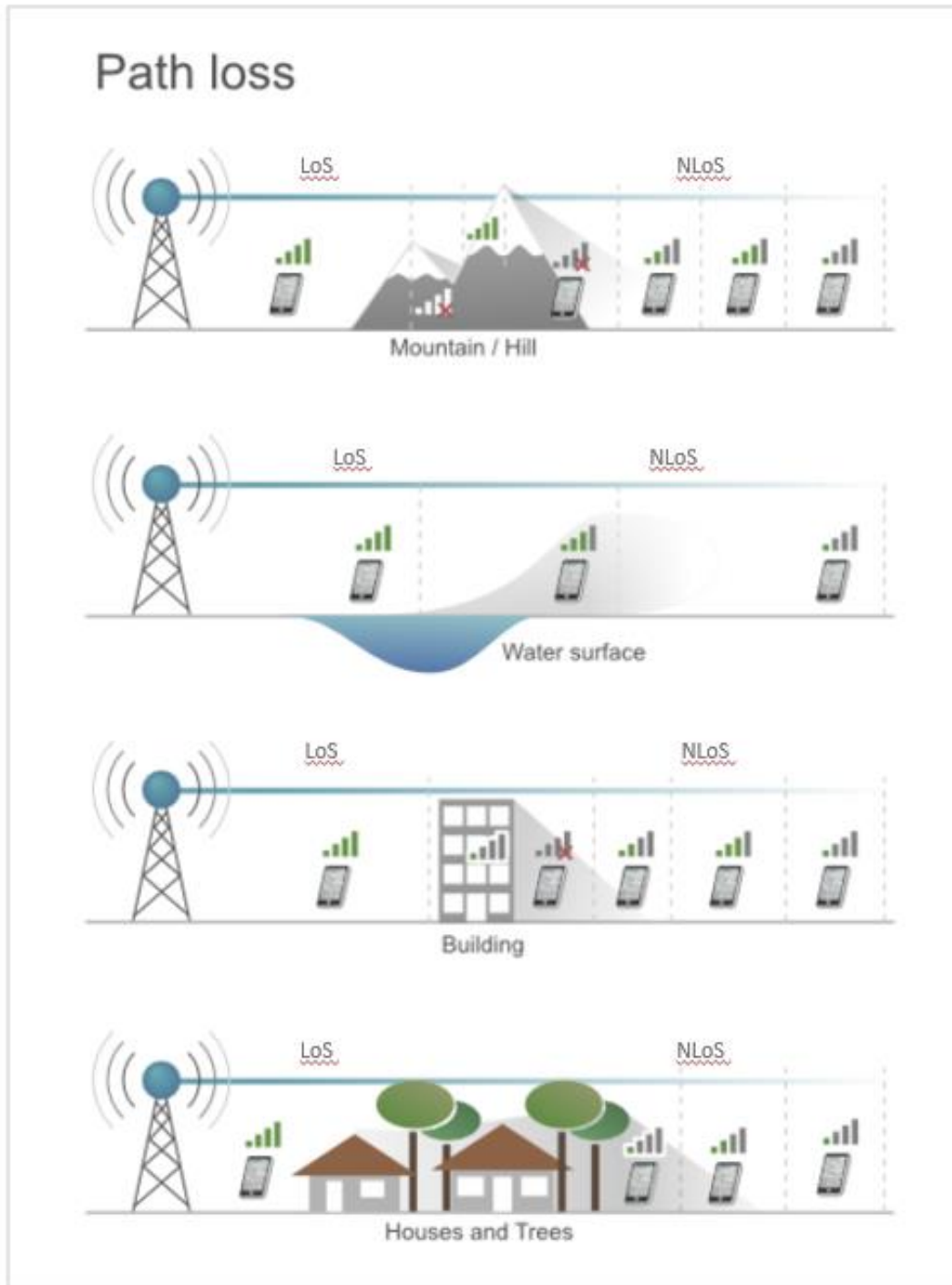


Figure 5-4, Cases by ITU model

Being the case study an urban environment, only the formulations for urban environment were used, distinguishing however, the BTS on the basis of their type of coverage (defined in the chapter 4) and whether or not the user was in line of sight with the BTS considered.

The equations of the ITU model used were:

$$PL_{UMi-LoS,dB} = 22 \log d + 28.0 + 20 \log f \quad (5-12)$$

$$PL_{UMi-NLoS,dB} = 36,7 \log d + 22,7 + 26 \log f \quad (5-13)$$

$$PL_{UMa-LoS,dB} = 22 \log d + 28.0 + 20 \log f \quad (5-14)$$

$$PL_{UMa-NLoS,dB} = 161,04 - 7,1 \log_{10} W_m + 7,5 \log_{10} \frac{h_m}{h_{BTS}} - \\ + \left( 24,37 - 3,7 \left( \frac{h_m}{h_{BTS}} \right)^2 \right) \log_{10} h_{BTS} + (43,42 - \\ 3,1 \log_{10} h_{BTS})(\log_{10} d - 3) + 20 \log_{10} f - (3,2(\log_{10} 11,75 h_{UE})^2 - \\ 4,97) \quad (5-15)$$

Where :

- $d$  = distance between Bs and User in meters;
- $f$  = frequency of the signal in GHz;
- $h_{BTS}$  = heigh of Base station in meters;
- $h_{FU}$  = heigh of users by default equal to 1.5 meters;
- $W_m$  = average width of the roads in meters;
- $H_m$  = average high of buildings in meters;

To conclude, the choice of the model for the path loss calculation fell on the model developed by the ITU.

This because, it represents the most complete and detailed model, and in addition to always considering the distinction of the scenario (urban, rural or sub-urban) for which the calculation is performed as the HATA model, first, it considers the probability or otherwise that a user is in line of sight with the antenna to which it is connected. Second, the ITU model differentiates the calculation based on the type of BTS (i.e. Macro cell or Micro cell).

*Figure 5-5 and figure 5-6* below, shows an example of application of the model for calculating the path loss for a selected cluster user, respect to all the BTSs of provider 1, plotting the path loss for the different types of cell of the BTS. As you can see from the image, the path loss calculation is strongly influenced by the distance.

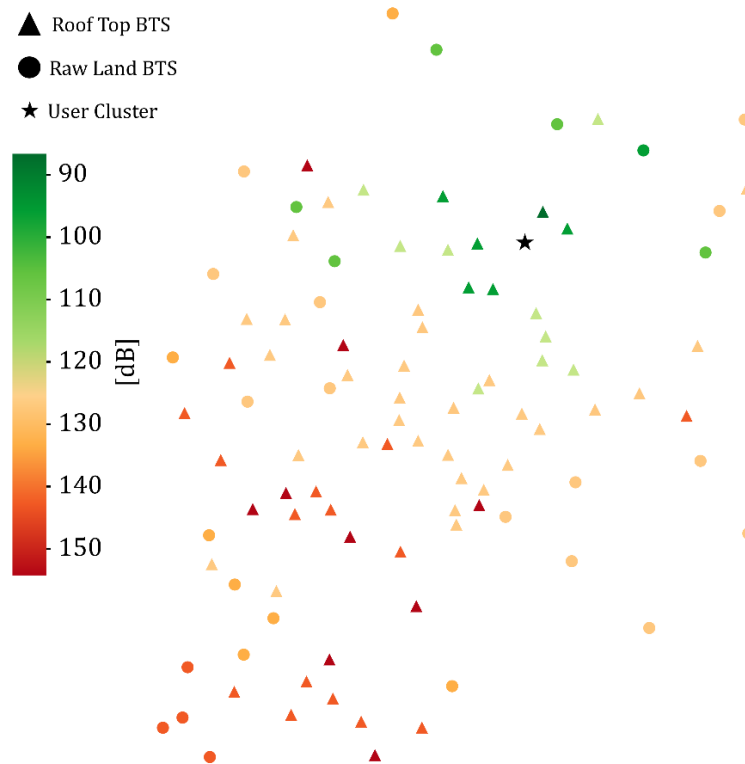


Figure 5-5, Path Loss for A cluster user relative to the BTS of the macro cell type of the first provider

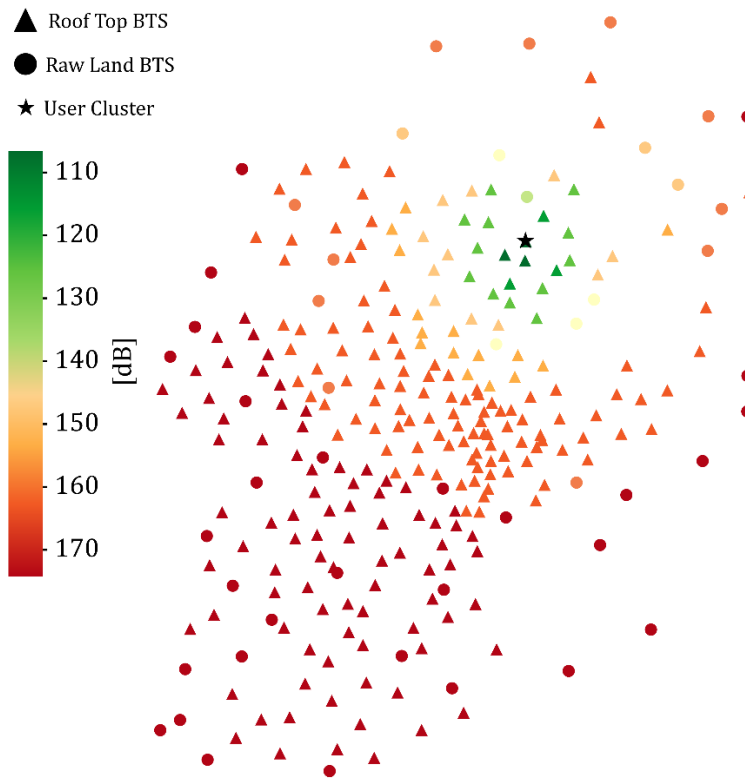


Figure 5-6, Path Loss for A cluster user relative to the BTS of the micro cell type of the first provider

### 5.3 Received signal strength indicator (RSSI)

The next step is to compute the received signal strength indicator (RSSI) by each subscriber cluster from each base station. In cellular network, RSSI is a measurement of the net power present in a received radio signal by an user and generally expressed as decibels per milliwatt (Sauter 2010).

This is simply the difference of the transmission power of the base station transceiver and the path loss between it and the subscriber cluster, computed as explained earlier (Shang, Su et al. 2014).

The transmission power (PT) at which base stations transmit is not always available in cellular datasets. If needed, we can simply fall back to the standard values of 43 dBm for macro-base stations transceiver and 30 dBm for micro-base stations transceiver in line with (Access 2010) and (Di Francesco, Malandrino et al. 2017).

$$RSSI = PT - PL \text{ [dBm]} \quad (5-16)$$

These calculations were made for all user clusters with respect to each BTS. *Figure 5-7* and *figure 5-8* shows an example plot of the RSSI of a subscriber cluster with respect to the BTS of provider 1 divided according to the type of antenna (Micro or Macro cell). While, into the *table5-1*, there is a classification of the signal strength based on the value of the RSSI.

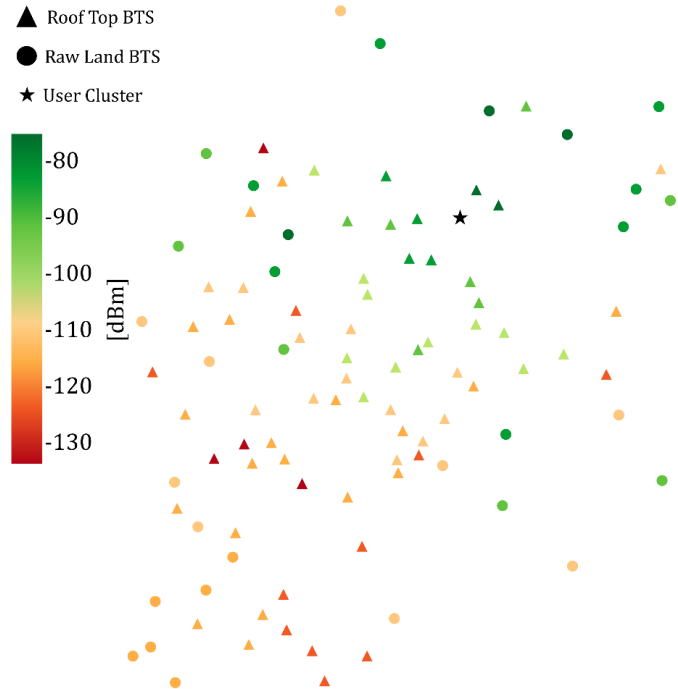


Figure 5-7, RSSI for A cluster user relative to the BTS of the macro cell type of the first provider

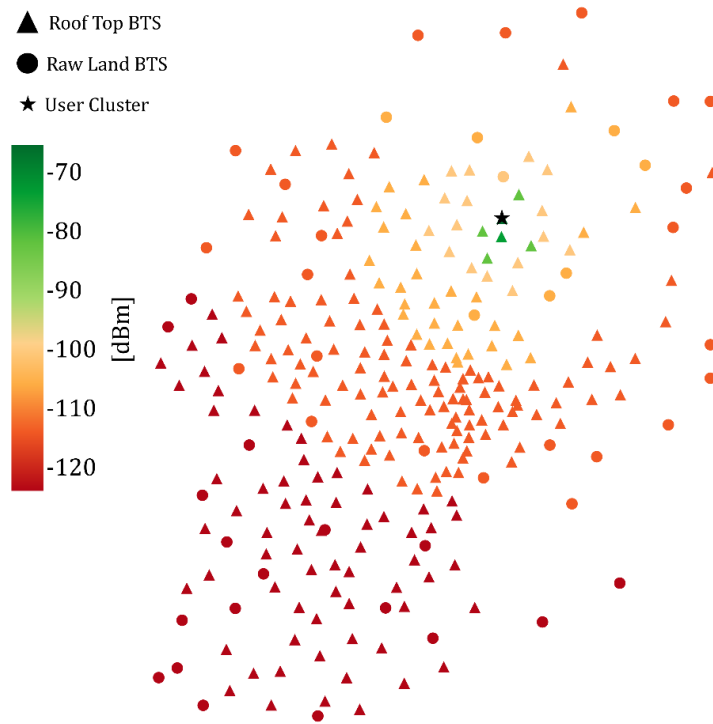


Figure 5-8, RSSI for A cluster user relative to the BTS of the micro cell type of the first provider

RSSI	Signal strength	Description
> -75 dBm	Excellent	Strong signal with max. data speeds
-75 dBm to -85 dBm	Good	Strong signal with good speeds
-85 dBm to -95 dBm	Fair	Fair but useful, fast and reliable data speeds may be attained, but marginal data with drop-outs is possible
-95 dBm to -110 dBm	Poor	Performance will drop drastically
≤ -110 dBm	No signal	Disconnection

Table 5-1, Classification of signal strength based on RSSI

## 5.4 Interference (I) and Noise (N)

The interference is a function of the network geometry. In the chapter ... the concept of subdivision into cells of the area covered by a cellular network and the concept of frequency reuse were defined. As already detailed in the chapter 3, the frequency reuse factor (FRF) has been set equal to one. Setting the FRF equal to one means evaluating the cellular network in the most difficult condition for the network itself.

Assuming an FRF equal to one, it means that all the BTS are able to transmit to the selected user cluster, generating a high level of interference. In fact, the interference is defined as the sum of the transmitted power (RSSI) of all the base stations except the one for which the SINR is being calculated for the desired cluster of users.

For instance, in the example illustrated in *figure 5-9*, the interference for user A when connected with the BTS 1 is given by the sum of all the signals (i.e. the RSSIs) sent by all the BTS except BTS 1 which is the one for the which signal quality is being calculated. So, the formulation in this case will be:

$$I_{A-1} = \left( \sum_{i=1}^j RSSI_i \right) - RSSI_1 \quad (5-17)$$

Where:

$I_{A-1}$  = is the interference for Cluster A when it is connected to BTS 1

A = User Cluster selected

1 = BTS selected

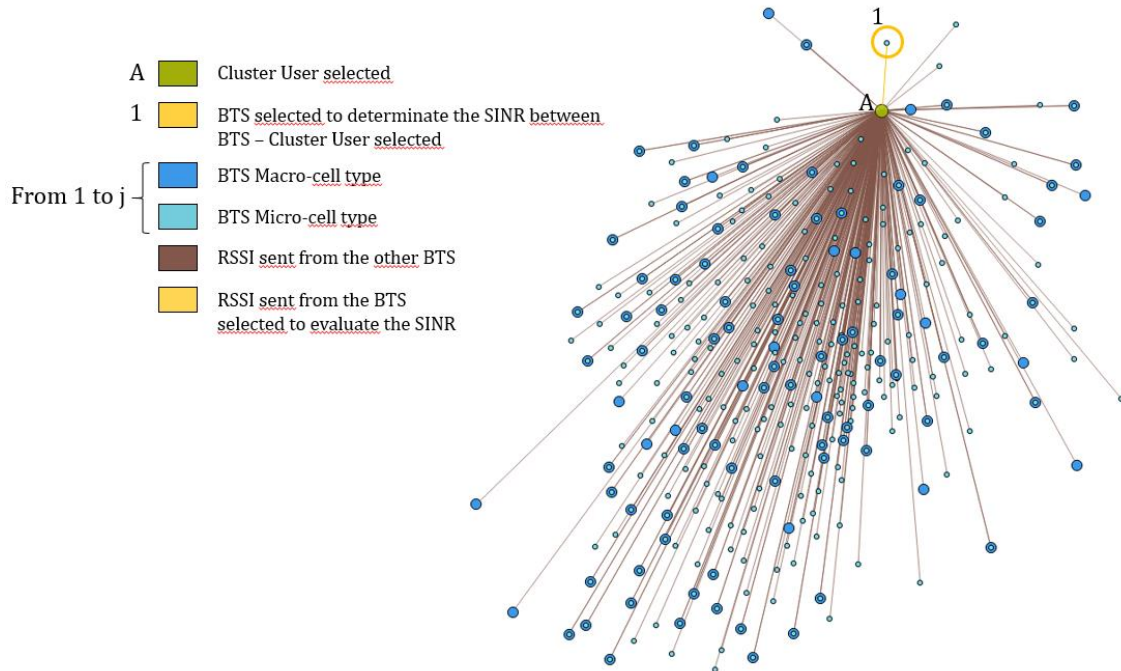


Figure 5-9, Example of interference for a User Cluster - BTS pair

While as regards the term of noise, when working with radio signals there is always a noise from the background environment. Then, this noise is generally added to the interference generated by signals from other sources previously



defined. However, a cellular network with a FRF equal to one has been assumed. Which represents an extremely conservative condition that takes an heigh level of interference and the latter dominates the noise. So, it was decided to neglect the noise.

## 5.5 Signal-to-Interference-and-Noise Ratio (SINR)

The SINR is widely used in wireless communication network as a way to measure the quality of wireless connections and it is often expressed in decibels. Once the signal attenuation has been evaluated, the interference defined and the signal strength calculated, the SINR can be calculated as (Haenggi, Andrews et al. 2009):

$$SINR = \frac{S}{I + N} [Watt] \rightarrow [dB] \quad (5-18)$$

where  $S$ ,  $N$  and  $I$  are the desired signal represented by the RSSI, noise, and interference powers, respectively.

$S$ ,  $N$  and  $I$  are given by:

- $S = \text{Net power} = \text{RSSI} = P_T - P_L [\text{Watt}]$
- $I = \text{Interference} = \sum(\text{RSSI}) - \text{RSSI}_{\text{BTS selected}} [\text{Watt}]$
- $N = \text{Noise} [\text{Watt}]$

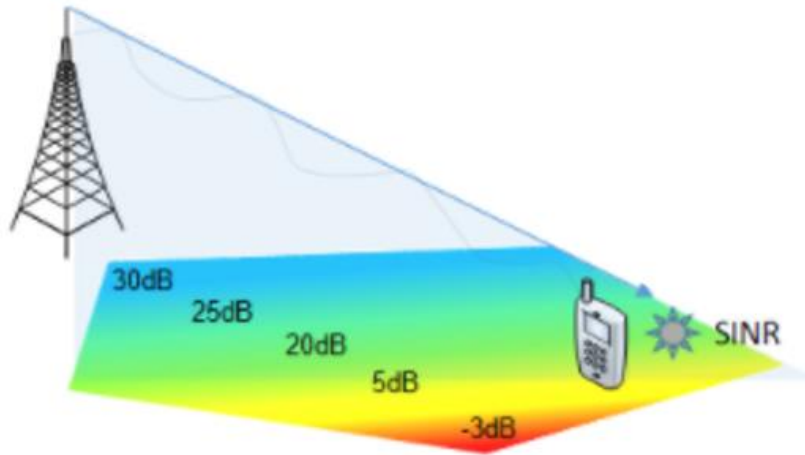


Figure 5-10, General illustration of the SINR's trend

To this end, into the *figure 5-11* and *figure 5-12*, it is mapped the SINR experienced by a user cluster at a given location onto the amount of data that can be carried by each BTS, always with the subdivision based on the type of BTS.

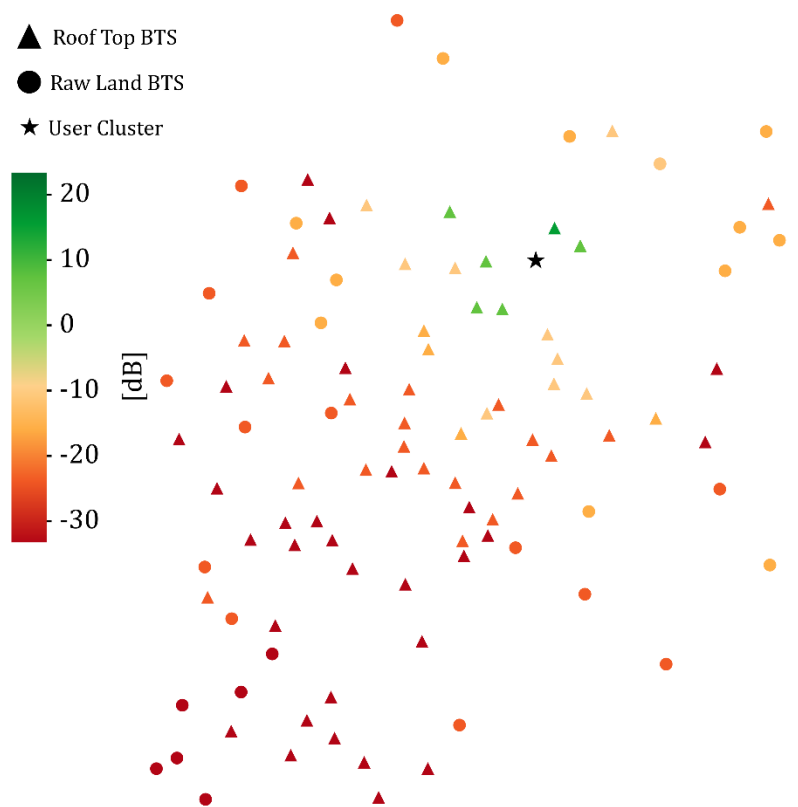


Figure 5-11, SINR for cluster user selected from BTS macro-cell

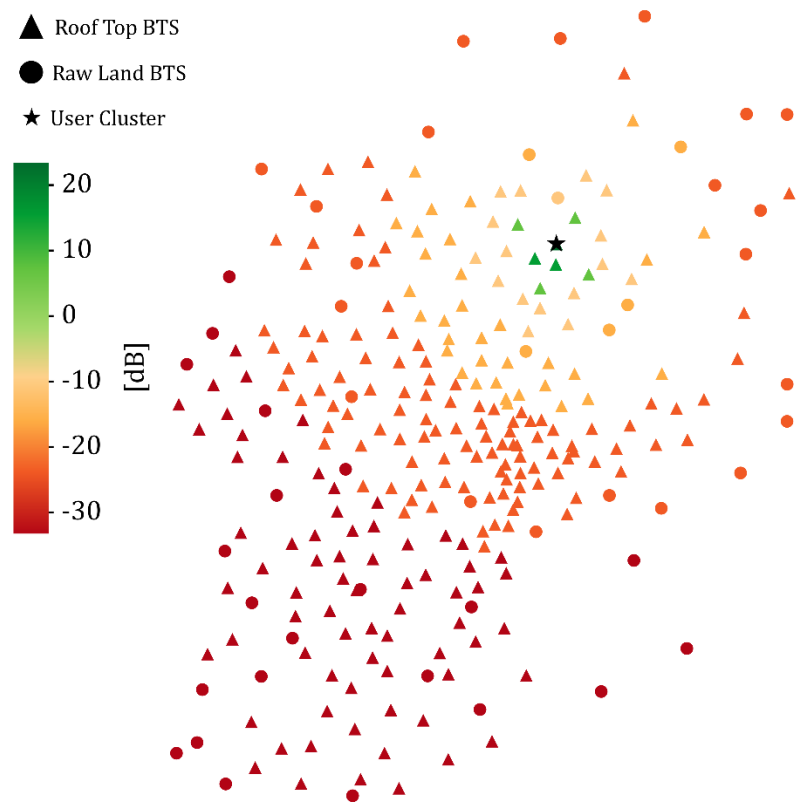


Figure 5-12, SINR for cluster user selected from BTS micro-cell

SINR	Signal strength	Description
$\geq 20$ dB	Excellent	Strong signal with maximum data speeds.
10 dB to 20 dB	Good	Strong signal with good speeds.
0 dB to 10 dB	Fair	Fair but useful, fast, and reliable data speeds may be attained, but marginal data with drop-outs is possible.
-15 dB to 0 dB	Poor	Performance will drop drastically.
$\leq -15$ dB	No signal	Disconnection.

Table 5-2, Classification of the signal strength based on SINR

## 5.6 Throughput (THR)

In general terms, throughput is the rate at which data is processed in the time unit in telecommunication systems. Typically, it measured in bit/s or Mbit/s.

An experimental curve based on SINR is typically used to evaluate the throughput. However, this curve represents only the final step of the throughput definition process. In fact, to get the THR-SINR curve it is necessary to evaluate several parameters of the network including:

- Channel Bandwidth (BW)
- Resource Block (RB)
- Type of transmission (OFDM/OFDMA)
- Duplex Mode (e.g. FDD, TDD)
- Channel Quality indicator (CQI)
- Modulation Coding Scheme (MCS)
- Transport block size (TBS)
- MIMO Antenna Configuration

Bandwidth (BW) defines how many radio resources are available to transmit data. So, bandwidth directly affects the throughput. Different BW means different number of Resource block (RB). A resource block (RB) is the smallest unit of resources that can be allocated to a user. As shown in *figure 5-13*, in 3G and 4G wireless connection a single RB consisting of 12 subcarriers in the frequency domain and 1 time slot (0.5 ms) in the time domain (Rathi, Malik et al. 2014). A single subcarrier matches to 15KHz of frequency. While a time slot corresponding to 7 OFDM (Orthogonal Frequency Division Multiplexing) symbols. The OFDM is a type of digital transmission and a method of encoding digital data on multiple carrier frequencies, it will be seen in detail later. So, 12 subcarriers x 7 symbols = 84 Resource Element (RE) makes a Resource Block. The RE is the smallest unit of transmission resource in wireless communication, in both uplink

and downlink. A RE consists of 1 subcarrier in the frequency domain for duration of 1 Orthogonal Frequency Division Multiplexing (OFDM) (Rathi, Malik et al. 2014).

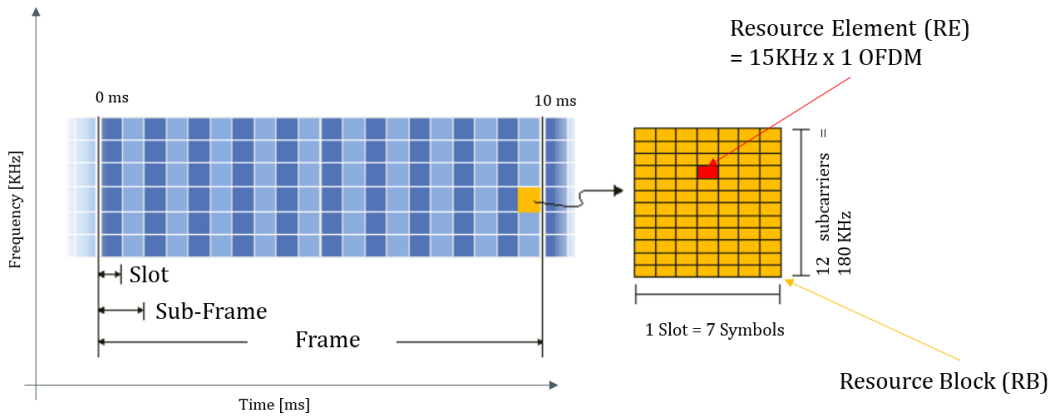


Figure 5-13, Structure of a resource block (RB)

According to (3GPP 2014) there are six possible bandwidth for 3G and 4G channel, and these are 1.4, 3, 5, 10, 15, 20 MHz. For each bandwidth the number of resource block available is defined by (3GPP 2014) and they are shown in *table 5-4* and in a schematize in *figure 5-14*.

Channel bandwidth [MHz]	1,4	3	5	10	15	20
Effective bandwidth allocated	1,08	2.7	4,5	9	13,5	18
Theoretical Subcarriers	93,3	200	333,3	666,6	1000	1333,3
Number of occupied Subcarriers	72	180	300	600	900	1200
Transmission bandwidth configuration (RB)	6	15	25	50	75	100

Table 5-3, Channel characteristics based on BW

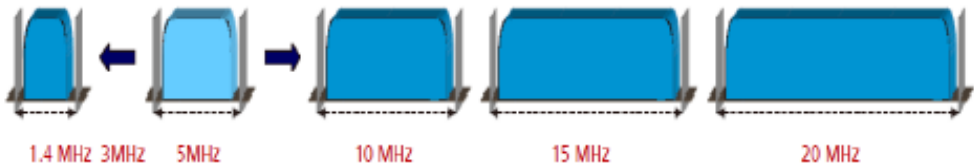


Figure 5-14, schematization of channel bandwidth

For this case study, the BTS work with Band 3 or Band 20, for these bands the available bandwidths were those shown in *table 5-5*. Table 55- is an extrapolation from Tables 5.5-1 "E-UTRA Operating Bands" and 5.6.1-1 "E-UTRA Channel Bandwidth" of the latest published version of the 3GPP TS 36.101 (3GPP 2014).

Band	Duplex mode	f [MHz]	Common name	Subset of band	Uplink [MHz]	Downlink [MHz]	Duplex spacing [MHz]	Channel bandwidths [MHz]
1	FDD	2100	IMT	65	1920 – 1980	2110 – 2170	190	5, 10, 15, 20
2	FDD	1900	PCS	25	1850 – 1910	1930 – 1990	80	1.4, 3, 5, 10, 15, 20
3	FDD	1800	DCS		1710 – 1785	1805 – 1880	95	1.4, 3, 5, 10, 15, 20
4	FDD	1700	AWS-1	66	1710 – 1755	2110 – 2155	400	1.4, 3, 5, 10, 15, 20
5	FDD	850	Cellular (CLR)	26	824 – 849	869 – 894	45	1.4, 3, 5, 10
7	FDD	2600	IMT-E		2500 – 2570	2620 – 2690	120	5, 10, 15, 20
8	FDD	900	Extended GSM		880 – 915	925 – 960	45	1.4, 3, 5, 10
11	FDD	1500	Lower PDC	74	1427.9 – 1447.9	1475.9 – 1495.9	48	5, 10
12	FDD	700	Lower SMH	85	699 – 716	729 – 746	30	1.4, 3, 5, 10
13	FDD	700	Upper SMH		777 – 787	746 – 756	–31	5, 10
14	FDD	700	Upper SMH		788 – 798	758 – 768	–30	5, 10
17	FDD	700	Lower SMH	12, 85	704 – 716	734 – 746	30	5, 10
18	FDD	850	Lower 800 (Japan)	26	815 – 830	860 – 875	45	5, 10, 15
19	FDD	850	Upper 800 (Japan)	26	830 – 845	875 – 890	45	5, 10, 15
20	FDD	800	Digital Dividend (EU)		832 – 862	791 – 821	–41	5, 10, 15, 20
21	FDD	1500	Upper PDC	74	1447.9 – 1462.9	1495.9 – 1510.9	48	5, 10, 15
24	FDD	1600	Upper L-Band (US)		1626.5 – 1660.5	1525 – 1559	–101.5	5, 10
...								

Table 5-4, Features of the all Band used in wireless communication

As you can see, for Band 3 and Band 20 (that are the bands used by BTS for Ideal City' telecom network) are available different channel bandwidth.

In the research of the data for the creation of the database to define the network for the case study of the ideal city, it was not possible to obtain any information on bandwidth. it was therefore decided to follow the same procedure proposed by (Malandrino, Chiasserini et al. 2017) and therefore assuming a bandwidth for each band of each provider equal to 10 MHz. This channel bandwidth is available for each band in this case study according to what say the 3GPP report. Having now the bandwidth, even the number of available resource blocks it is known which is equal to 50.

As seen before, the 3G and 4G network use the OFDM transmission technique. The basic idea of this technique is to divide the available spectrum into several sub-channel (subcarriers) (Edfors, Sandell et al. 1996). To obtain a high spectral efficiency the frequency response of the subchannels are overlapping and orthogonal, hence the name OFDM. The OFDM signal is made up of a sum of  $N$  complex orthogonal subcarriers (indexed with  $k = \{0, 1, 2, \dots, N - 1\}$ ), each one independently modulated. One OFDM symbol with duration  $T$  and starting at  $t = t_s$  has the following passband expression in the time domain:

$$(t) = \begin{cases} Re \left\{ \sum_{k=0}^{N-1} d_k \cdot e^{j2\pi \left( f_c + \frac{(N-1-2k)}{2T} \right) \cdot (t-t_s)} \right\} & ; \quad t \in (t_s, t_s + T) \\ 0 & ; \quad otherwise \end{cases} \quad (5-19)$$

Where  $d_k$  is the modulation and  $f_c$  is the carrier frequency (Edfors, Sandell et al. 1996).

Figure 5-15 shows a representation of a general OFDM system, where the modulation and demodulation are performed as block-oriented processes that can be efficiently implemented through the Fast Fourier Transform (FFT) algorithm (Edfors, Sandell et al. 1996).

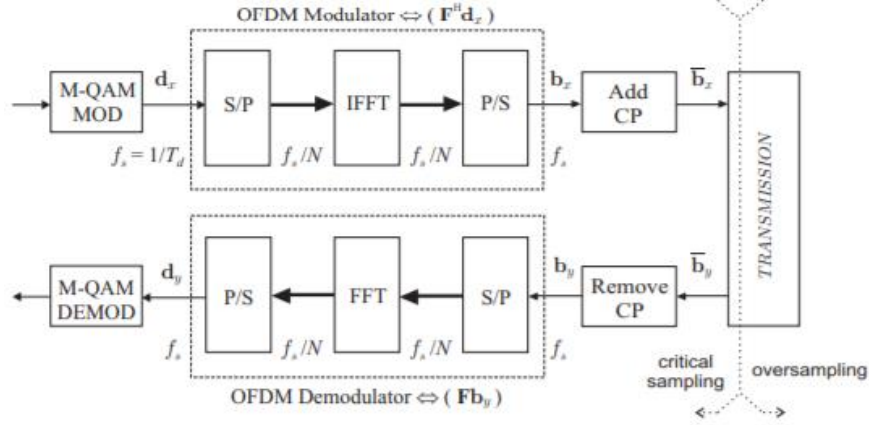


Figure 5-15, Block diagram of the OFDM modulation

In this system, the incoming symbols are critically sampled (one sample per information symbol/subcarrier) and grouped within the column vector:

$$d_x = [d_x[0], \dots, d_x[N-1]] \quad (5-20)$$

thus, forming the information signal blocks of length  $N$ .

The symbols  $d_x[n]$  are generated at a rate  $f_s = 1/T_d$  and modulate separately the  $N$  orthogonal subcarriers during the whole  $i$ -th time interval  $I_i = [iT, iT + T]$ , defined for one OFDM symbol with period  $T = NTd = N/f_s$ . Then, the continuous time complex envelope of the baseband OFDM signal ( $b_x(t)$ ) can be written for any instant  $t$  as:

$$b_x(t) = \frac{1}{\sqrt{N}} \sum_{k=0}^{N-1} d_x(k, i) e^{j2\pi f_k t} \quad \text{for } t \in I_i \quad (5-21)$$

Where:

$$f_k = \frac{k \cdot f_s}{N} = \frac{k}{T} \quad \text{is the } k - \text{th subcarrier frequency} \quad (5-22)$$

$d_x(k, i)$  is the symbol modulating the  $k$  – th carrier during the whole  $i$  – th OFDM symbol interval.

To manage the accesses of multiple users, it is used a multiple access technique based on the OFDM transmission technique introduced before, and this access technique is called OFDMA (Orthogonal frequency-division multiple access).

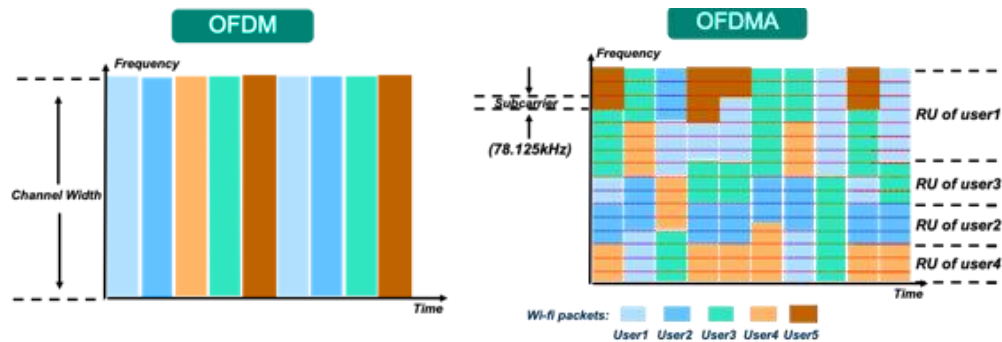


Figure 5-16,

Always, from *table 5-5* it is possible to see that each band 3 and 20 use a FDD (Frequency division duplex) duplex mode. Frequency division duplex means that the radio transmitter and receiver operate on different frequencies, and both use the design bandwidth. instead in the TDD (Time division duplex) means, uplink and downlink transmissions occupy the same frequency spectrum but are separated in time. FDD and TDD are mode of transmission and reception of information on a communication channel with typical characteristics of complete bidirectionality. They can be represented like in *figure 5-17*.

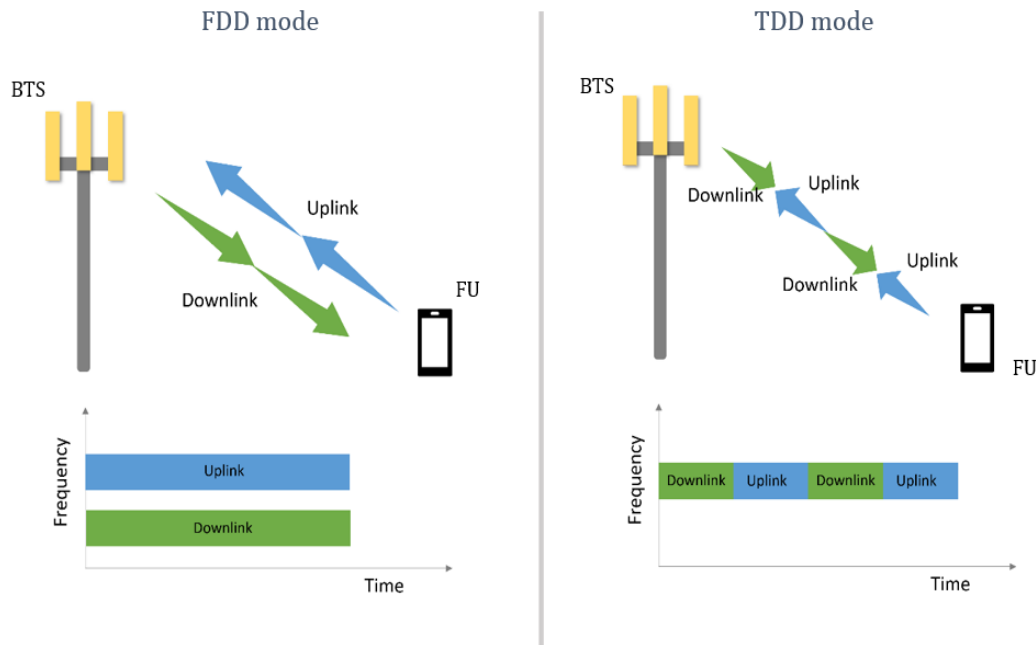


Figure 5-17, illustration of the difference between FDD and TDD mode

Next point, it is to define the Channel Quality Indicator (CQI). Generally, it is calculated from the SINR directly by the user's device that connects to the network and sends it to the BTS to which it is connected. The CQI indicates the maximum



modulation scheme (MCS) supported by the user in order to ensure traffic reception with a Block Error Rate (BLER) of less than 10%. BLER is a ratio of the number of erroneous blocks to the total number of blocks transmitted. According to (3GPP 2014) the CQI for LTE generation wireless technologies (3G and 4G) can assume 15 levels to which they correspond different modulations and codes rate that the user could operate. The *table 5-6* shows the different characteristics of the connection based on the CQI given by (Fan, Yin et al. 2011).

CQI	Modulation	Bits/RE	Code Rate	Bit per RE	MCS <sub>max</sub> Index
1	QPSK	2	0,0762	0,1524	0
2	QPSK	2	0,1172	0,2344	0
3	QPSK	2	0,1885	0,3770	2
4	QPSK	2	0,3008	0,6016	5
5	QPSK	2	0,4385	0,8770	7
6	QPSK	2	0,5879	1,1758	9
7	16QAM	4	0,3691	1,4764	12
8	16QAM	4	0,4785	1,9140	14
9	16QAM	4	0,6016	2,4064	16
10	64QAM	6	0,4551	2,7306	20
11	64QAM	6	0,5537	3,3222	23
12	64QAM	6	0,6504	3,9024	25
13	64QAM	6	0,7539	4,5234	27
14	64QAM	6	0,8525	5,1150	28
15	64QAM	6	0,9258	5,5548	28

Table 5-5, Modulations and Code rate based on CQI value

Once that, the user's device sends the CQI to the BTS, the BTS defines the modulation and code rate based on it. Note Modulation (M) and Code Rate (CR), the BTS always defines the MCS index for the selected user.

Modulation defines how many bits can be carried by a single RE or symbol. In LTE there are following modulations supported: QPSK, 16QAM, 64QAM and 256QAM the last one just for LTE-Advanced. With QPSK there are 2 bits can be transmitted per RE, with 16QAM - 4 bits, and with 64QAM - 6 bits. As it can see in the image reported in *Figure 5-18*.

Of course, that the higher the modulation a user can have, the faster the data transfer will be with the BTS.

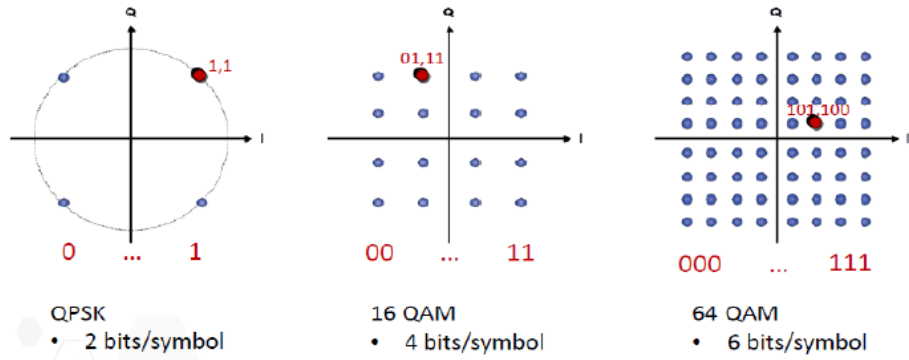


Figure 5-18, different modulations

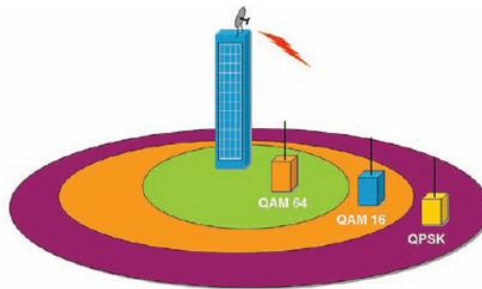


Figure 5-19, artistic representation of the Modulation with respect the distance that there is between BTS and User

Instead, the CR describes the efficiency of particular modulation scheme. For instance, with a modulation equal to 16 QAM and a code rate of  $0.4785 \approx 0,5$ , it means this modulation has 50% of efficiency; i.e. as 16QAM can carry 4 bits theoretically, but with coding rate of  $\sim 0.5$ , it can carry 2 information bits and rest of the 2 bits are for redundancy of information.

The combination of Modulation and Coding rate is called Modulation Coding Scheme (MCS). The MCS defines how many useful bits can be transmitted per Resource Element. MCS depends on radio link quality express with CQI. The better quality and so better M and CR, the higher MCS and the more useful data can be transmitted. In general, with a CQI it can have a range of values of MCS with a superior limit as reported in *table 6*. That, because it may have a good modulation but a bad coding rate like the example before. During the connection between BTS and user the BTS changes the MCS continuously and automatically in order to keep the BLER below the 10% threshold. In fact, in LTE the calculation of the MCS by the BTS is performed once every TTI (Transmission Time Interval) that is equal to 1ms. When the MCS is known, the BTS selects the TBS (transport block size) index associated. The below *table 7* shows MCS index, TBS index and Modulation. LTE supports 0 to 28 MCS in Downlink and 0 to 22 MCS in Uplink given by (Rathi, Malik et al. 2014) and taken from specification given by (3GPP 2014). This procedure is carried out automatically by the software of the single provider. The formulas of this software are not explicitly known.

MCS <sub>INDEX</sub>	Modulation	Bits/RE	TBS <sub>INDEX</sub>
0	QPSK	2	0
1	QPSK	2	1
2	QPSK	2	2
3	QPSK	2	3
4	QPSK	2	4
5	QPSK	2	5
6	QPSK	2	6
7	QPSK	2	7
8	QPSK	2	8
9	16QAM	4	9
10	16QAM	4	9
11	16QAM	4	10
12	16QAM	4	11
13	16QAM	4	12
14	16QAM	4	13
15	16QAM	4	14
16	16QAM	4	15
17	64QAM	6	15

18	64QAM	6	16
19	64QAM	6	17
20	64QAM	6	18
21	64QAM	6	19
22	64QAM	6	20
23	64QAM	6	21
24	64QAM	6	22
25	64QAM	6	23
26	64QAM	6	24
27	64QAM	6	25
28	64QAM	6	26
29	64QAM	6	Reserved
30	64QAM	6	Reserved
31	64QAM	6	Reserved

Table 5-6, MCS index and TBS index values

The TBS together with the RB says the number of bits ( $N_{PRB}$ ) which can be transmitted per 1 TTI (=1ms) and multiply it by 1000 to get the Bits can be transmitted in one second (bps).

The  $N_{PRB}$  for each pair of TBS-RB are defined in a series of tables reported in the reports provided by (3GPP 2014). Right below in *figure 5-20* there is an extrapolation of these tables provided by 3GPP specifications, useful for understanding how it is used.

$I_{TBS}$	$N_{PRB}$									
	41	42	43	44	45	46	47	48	49	50
0	1128	1160	1192	1224	1256	1288	1320	1352	1384	
1	1480	1544	1544	1608	1608	1672	1736	1736	1800	1800
2	1800	1864	1928	1992	2024	2088	2088	2152	2216	2216
3	2408	2472	2536	2536	2600	2664	2728	2792	2856	2856
4	2984	2984	3112	3112	3240	3240	3368	3496	3496	3624
5	3624	3752	3752	3880	4008	4008	4136	4264	4392	4392
6	4264	4392	4584	4584	4776	4776	4968	4968	5160	5160
7	4968	5160	5352	5352	5544	5736	5736	5992	5992	6200
8	5736	5992	5992	6200	6200	6456	6456	6712	6968	6968
9	6456	6712	6712	6968	6968	7224	7480	7480	7736	7992
10	7224	7480	7480	7736	7992	7992	8248	8504	8504	8760
11	8248	8504	8760	8760	9144	9144	9528	9528	9912	9912
12	9528	9528	9912	9912	10296	10680	10680	11064	11064	11448
13	10680	10680	11064	11448	11448	11832	12216	12216	12576	12960
14	11832	12216	12216	12576	12960	12960	13536	13536	14112	14112
15	12576	12960	12960	13536	13536	14112	14688	14688	15264	15264
16	13536	13536	14112	14112	14688	14688	15264	15840	15840	16416
17	14688	15264	15264	15840	16416	16416	16992	17568	17568	18336
18	16416	16416	16992	17568	17568	18336	18336	19080	19080	19848
19	17568	18336	18336	19080	19080	19848	20616	20616	21384	21384
20	19080	19848	19848	20616	20616	21384	22152	22152	22920	22920
21	20616	21384	21384	22152	22920	22920	23688	24496	24496	25456
22	22152	22920	22920	23688	24496	24496	25456	25456	26416	27376
23	23688	24496	24496	25456	25456	26416	27376	27376	28336	28336
24	25456	25456	26416	26416	27376	28336	28336	29296	29296	30576
25	26416	26416	27376	28336	28336	29296	29296	30576	31704	31704
26	27376	27376	28336	29296	29296	30576	31704	31704	32856	32856

Figure 5-20, An extrapolation of tables to define the  $N_{PRB}$

For example, with 50 RBs and MCS index of 28, the TBS is 26, so the  $N_{PRB}$  is equal to 32856.

Finally, in LTE communications it is common to have cases in which the receiver, the transmitter or both use multiple antennas to improve the performance of the communication channel. There are several techniques to increase performance as showed in *Figure 5-21*. One of these techniques is the one called MIMO (Multiple-input and multiple-output). There are different types of MIMO techniques, a very common type for LTE networks is that of 2x2 MIMO in agreement also with what is stated in (Malandrino, Chiasserini et al. 2017). A 2x2MIMO technique was therefore assumed for the network built for the case study.

the advantage of using multiple antennas is to increase the data transported in a communication and therefore also the available throughput. For example, a 2x2MIMO allows to almost double the transmitted bps.

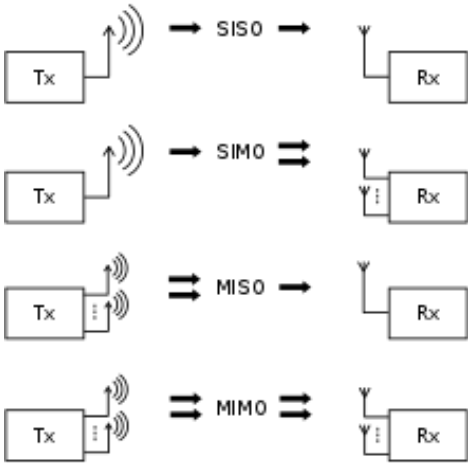


Figure 5-21, Different typologies of techniques to improve of the bits transmitted

the process between BTS and user can be summed into the following figure (*Figure 5-22*).

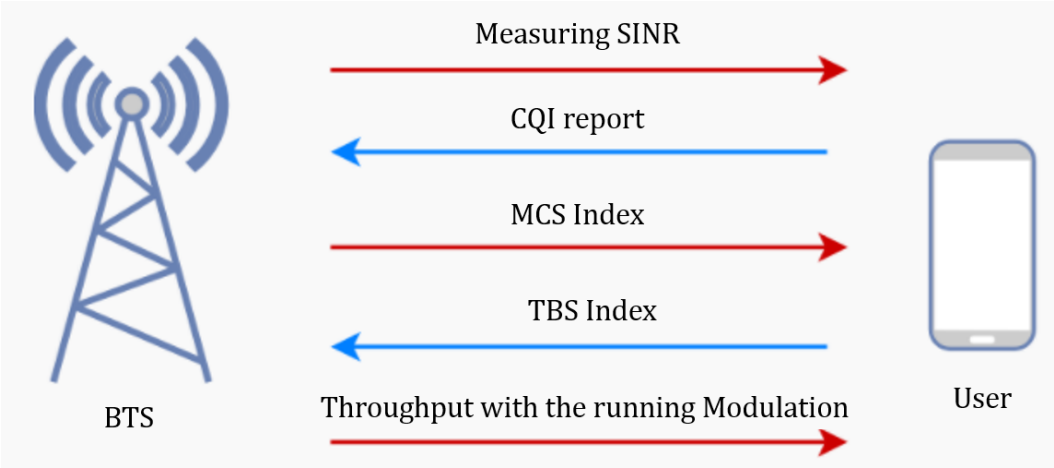


Figure 5-22, exchange of information between BTS and User

All these steps are carried out automatically and in a few seconds by the network as mentioned. The final result is to obtain a series of experimental curves for each type of modulation to determine the throughput (THR) based on the SINR

available between BTS and User. These curves are obtained from (Mühleisen, Bültmann et al. 2011) and (Ketonen, Juntti et al. 2010) and are reported into the *Figure 5-23*. Based on the SINR available to the user, the user himself does not always have the best modulation and therefore consequently the best THR. This is because, the modulation selected is influenced by many factors such as the distance between the BTS and the User or the number of users who are connected to the BTS itself.

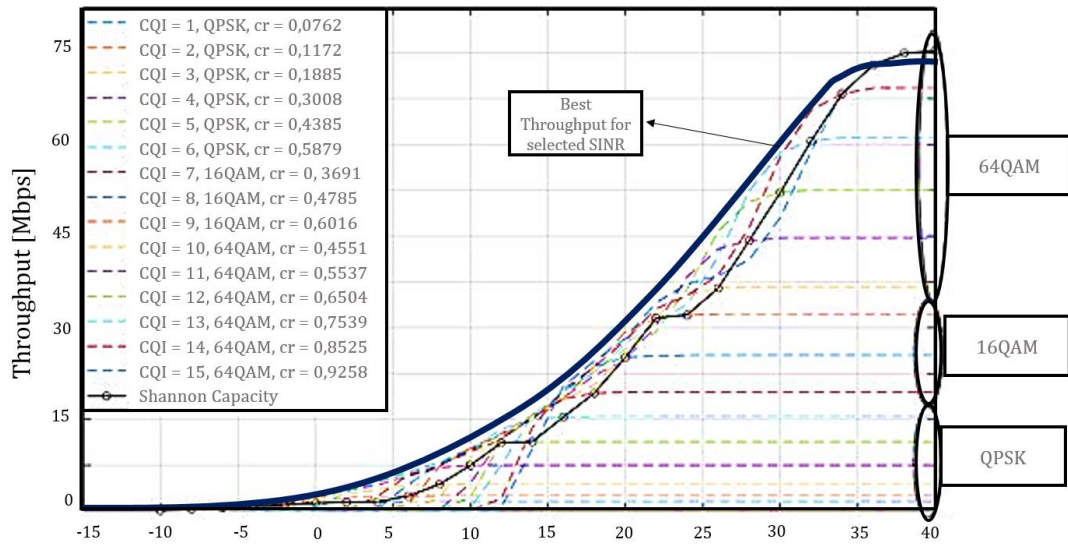


Figure 5-23, experimental curves for each modulation scheme

For this case study which does not deal in detail with specific telecommunication issues, it is assumed that the user's device that connects to the network always has the best modulation available and therefore the best THR with the SINR it has. This is a hypothesis assumed for the developed network. Also, because since no data was available on the data traffic of the network and considering having already limited the capacity of the network with the hypothesis made on the frequency reuse factor, it can be consistent with reality.

If the device always has the best modulation, the experimental curves converge in a single curve that is proposed in *Figure 5-24*.

So once the SINR for the user cluster is known, using the THR-SINR curve defined before, with a linear interpolation the throughput for that cluster can be obtained. If the THR is greater than zero, that means there is the possibility to connect to the network.

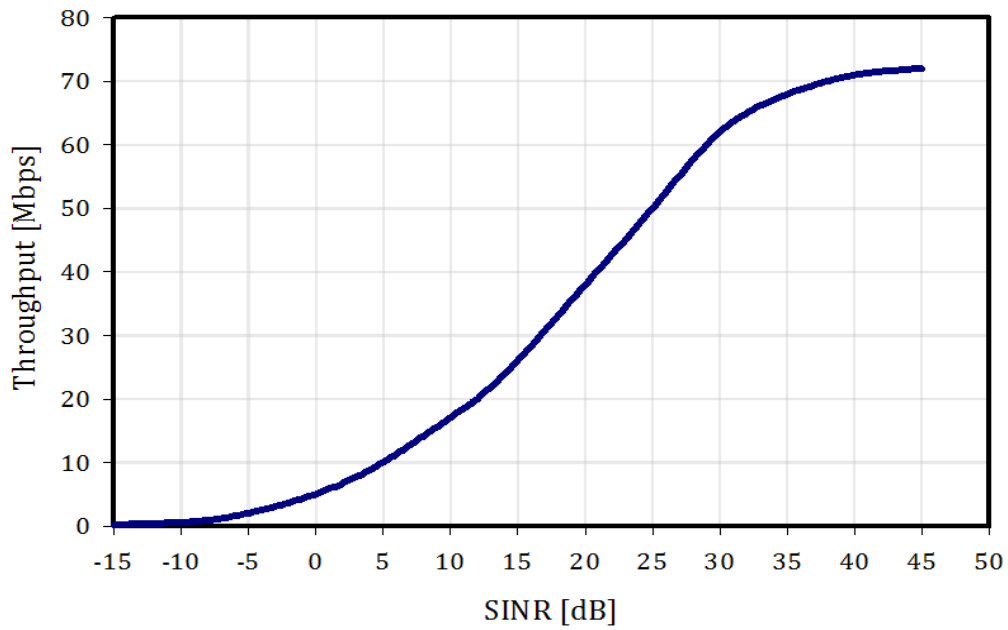


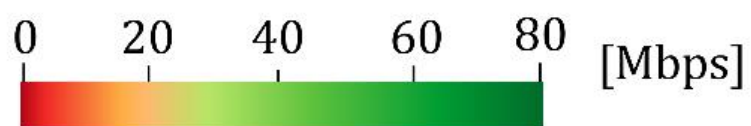
Figure 5-24, THR-SINR result curve

The *figures 5-26* shows the map of throughput for the whole user-cluster of the city, while the *figure 5-25* shows a detailed of the throughput trend for a portion of downtown of the Ideal City. These are the results during normal network operation.



Figure 5-25, THR value for user cluster given by the first MNO for a portion of Ideal City' downtown





○ Users of Cluster

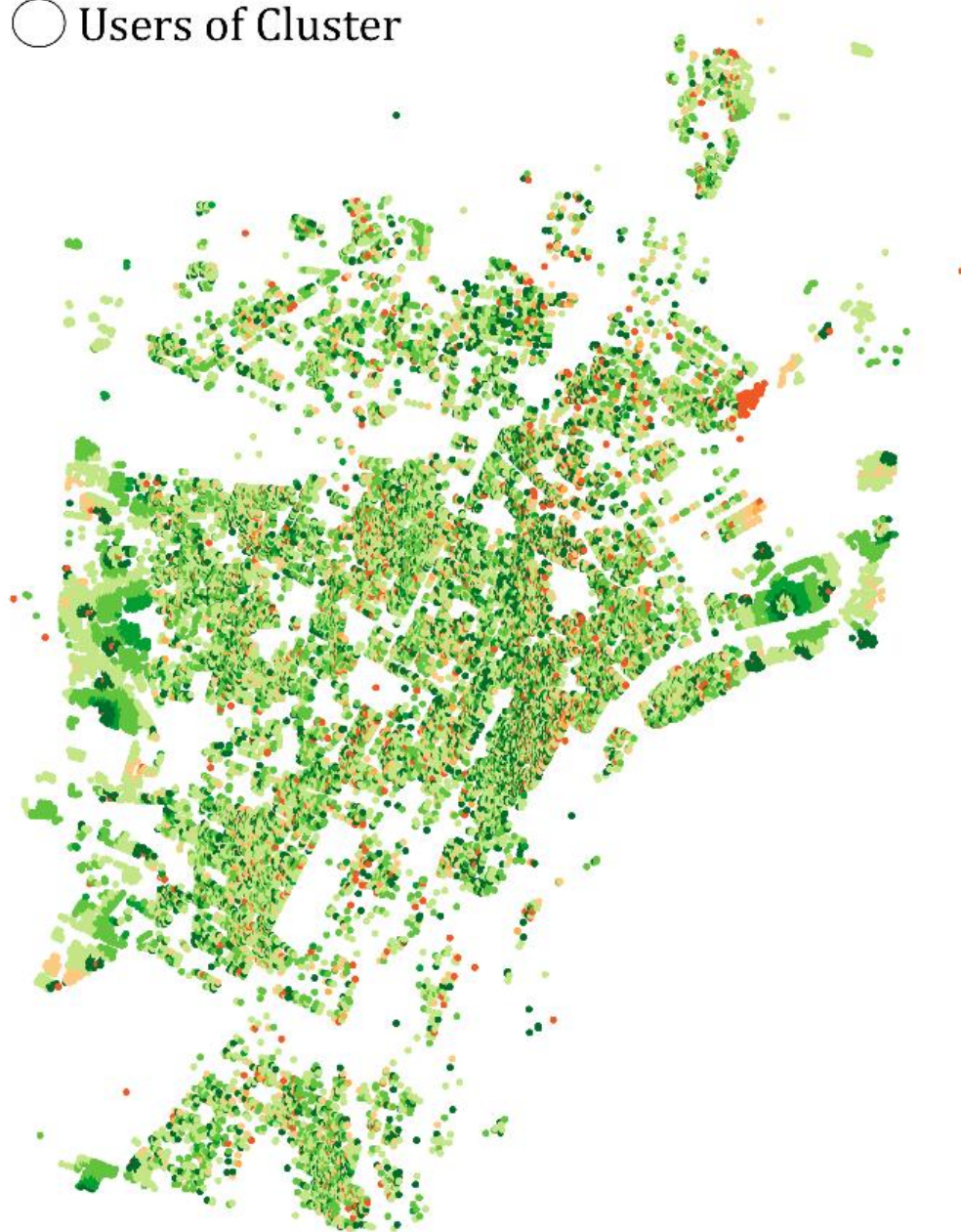


Figure 5-26, THR by MNO 1 for whole user cluster



# 6 Physical models to assess the seismic capacity of wireless network's components

## 6.1 Introduction

To improve the predictability of network structural damage for a given hazard scenario, it is essential to identify the factors that influence the structural response of the components that make up the wireless network and evaluate their contributions. This on an urban scale must be done using simplified models in order to reduce the computational burden required by the analysis (Noori, Marasco et al. 2017).

The aim of the chapter is therefore to define models using the parameters described above, which describe the physical behavior of the various elements of the network. For the control stations (BSC) being classic reinforced concrete buildings, to study their behavior to disastrous events and in particular to seismic events, there are many more or less complex approaches and models in the literature. This is since they are extremely widespread structures in the urban area, in the civil area more generally and for which the seismic vulnerability is assessed in detail due to the damage suffered by these structures in the past. Many existing research aim at the definition of standardized force-displacement ratios by simulating the structural behavior of a certain category of buildings (Ellingwood, Rosowsky et al. 2008, Steelman and Hajjar 2009). These searches were in most cases limited to SDOF systems with controlled mass distribution and stiffness characteristics. Since the BSCs are inserted in the building portfolio layer developed for the Ideal City in order to update it, the approach used to determine their response to disastrous events and therefore define their state of damage was the one developed by Marasco and Cimellaro (2018) for the buildings portfolio itself. This method was developed to determine the response of the virtual city buildings portfolio of the Ideal City project. The approach is an individual approach that consists in capturing the physical properties of the structure with precision through a non-linear multi-degree-of-freedom (MDOF) cutting model. Once the physical parameters to describe the structure are known, the displacement in the head of the building is evaluated through a simplified model with one degree of freedom (SDOF). The global seismic capacity of the building is then defined through a quadrilinear backbone curve and by comparing the

displacement obtained from the SDOF model with the curve, the level of damage suffered by the structure can be defined (Marasco and Cimellaro 2018).

For the base transceiver stations (BTS) the structural element is represented by the support tower. Unlike buildings, the literature offers not too much studies and models for this type of structures (Deidda, Pala et al. 2020). Many studies have focused on studying the best model to describe the joints or to understand the ultimate load for singular members (Rao and Kalyanaraman 2001). However, more and more works are facing the study of these towers due to the increasing importance of wireless communication networks (Deidda, Pala et al. 2020). It must also be said that often the studies of the behavior of the towers focus mainly on the study of the action of the wind on the towers themselves. Indeed, it must be said that up to now telecommunication towers are generally designed considering the effects of wind as the main or only source of lateral loads without paying too much attention to the effect of earthquakes (Khedr and McClure 2000). This is because historically the disastrous effects due to earthquakes on towers have been limited to few cases around the world in particular conditions. For example, the 2011 earthquake in Japan, where few towers were damaged by the effects of the earthquake, instead many of them were destroyed by the subsequent tsunami. Generally, the greatest damage is suffered by the service buildings or the towers that are installed on the residential buildings that collapse make the BTS itself out of service. The tower is a very tall structure with a uniformly distributed mass along the height, which can be traced back to a cantilever beam (Deidda, Pala et al. 2020). However, this does not mean that the effects of earthquakes must not be neglected. In fact, in a recent study conducted on three different lattice towers with variable height showed that for towers located in areas with high seismic risk, the forces induced by the earthquake could exceed the forces obtained from the wind load calculations (Lefort 1998). These results suggest that for towers located in high seismic risk areas, the effects of earthquakes on towers cannot be overlooked with respect to wind effects and at least a simplified design control should be considered (Lefort 1998). Previous studies on the seismic response of telecommunication towers were performed by Mikus (1994) and Galvez and McClure (1995), who demonstrated that modal superposition analysis including the three lowest bending modes can accurately predict their response to earthquake. In this work, the approach followed to describe BTS behavior was the one proposed by the work of (McClure, Gálvez et al. 1997) and taken up by Khedr and McClure (2000). This method involves considering the towers as single degree of freedom (SDOF) systems, subjecting them to an analysis with response spectra or through a time history analysis. Therefore, the first step was to determine the physical properties that characterize the SDOF, after which to determine a simplified trilinear capacity curve and finally to derive the displacement and rotations at the top of the tower to define the state of structural

damage and/or operation of the tower by comparing it with the capacity curve. The details of the models for the various components are illustrated in the following paragraphs of the chapter (Khedr and McClure 2000).

## 6.2 Base Stations Controller (BSC)' Modelling:

For the BSCs' modelling, the model developed by Marasco and Cimellaro (2018) for the Ideal City's RC buildings was used. It defines the RC buildings' physical features with a 3D MDOF model with some assumptions:

- Uniform frame distributions in both horizontal directions;
- inextensible frame elements;
- bending type system;
- lumped mass;
- regular planar layout;
- seismic global capacity simulated through a four-linear backbone curve



Figure 6-1, MDOF model for RC buildings used to define the Physical properties

The global capacity is expressed as a function between the shear at the base ( $V_b$ ) and the displacement at the top ( $u_{top}$ ). HAZUS (FEMA 2011) provides a standardized relationship between building performance for a given seismic intensity and associated damage status (DS). For buildings with high ductility and strength, approximating the capacitance curve with a trilinear function is not an accurate model (Marasco and Cimellaro 2018). For this reason, according to (Marasco and Cimellaro 2018), a quadrilinear backbone curve is a more adequate approximation of the seismic capacity of a RC building (*figure 6-2*).

The first point of the dorsal curve (1) refers to the performance condition associated with the formation of the first plastic hinge in the weakest column. After the yield point, the overall stiffness decreases to the next point (2). This point is representative of the moderate damage level at which the weakest column reaches its maximum capacity. The structure is subject to a massive distribution of internal actions as the rigidity decreases. When all the columns of the weakest

floor are plasticized, the maximum capacity is reached (point (3)). The structure is then subjected to a plastic mechanism until it collapses (point 4). Collapse occurs when the number and arrangement of plastic hinges generated are such as to identify an unstable pattern (collapse mechanism). The various points are identified through the elastic parameters and the post-elastic parameters (Marasco and Cimellaro 2018).

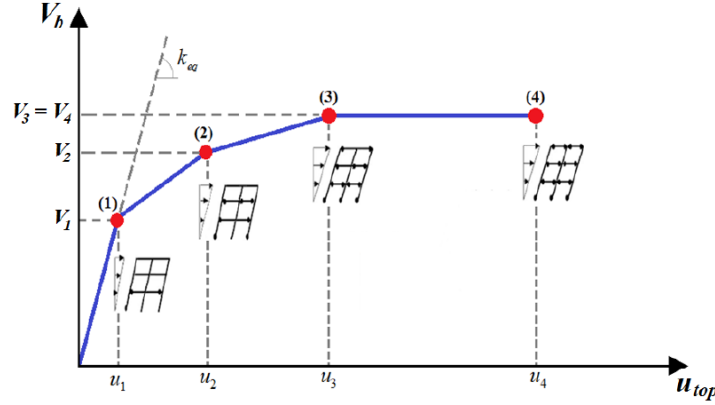


Figure 6-2, Proposed four-linear backbone curve, representative of the global capacity of RC buildings (Marasco and Cimellaro 2018)

### 6.2.1 Defining the physical properties:

Using a modal analysis, the elastic parameters of the structure are determined. These parameters are those that identify point (1) of the quadrilinear capacitance curve. A flexural model is used to determine the stiffness matrix. It is a model that requires more computational effort than a shear model. this burden can be reduced if the DOFs of the system are divided into slave DOFs (s) and master DOFs (m), i.e., the Guyan reduction is applied. The master DOFs are the lateral shifts of the roof, while the slave DOFs are the nodal rotations. So, the matrix form of the equation of motion is written as:

$$\begin{bmatrix} [M_{mm}] & [M_{ms}] \\ [M_{sm}] & [M_{ss}] \end{bmatrix} \begin{Bmatrix} \ddot{\delta}_m \\ \ddot{\delta}_s \end{Bmatrix} + \begin{bmatrix} [K_{mm}] & [K_{ms}] \\ [K_{sm}] & [K_{ss}] \end{bmatrix} \begin{Bmatrix} \delta_m \\ \delta_s \end{Bmatrix} = \begin{Bmatrix} F(t)_m \\ F(t)_s \end{Bmatrix} \quad (6-1)$$

This equation can be simplified by assuming that the inertial contributions associated with the slave DOFs are equal to zero and the external forces applied to the slave DOFs can be neglected. So, the *equation 6-1* can be simplified into:

$$\begin{bmatrix} [M_{mm}] & [0] \\ [0] & [0] \end{bmatrix} \begin{Bmatrix} \ddot{\delta}_m \\ \ddot{\delta}_s \end{Bmatrix} + \begin{bmatrix} [K_{mm}] & [K_{ms}] \\ [K_{sm}] & [K_{ss}] \end{bmatrix} \begin{Bmatrix} \delta_m \\ \delta_s \end{Bmatrix} = \begin{Bmatrix} F(t)_m \\ 0 \end{Bmatrix} \quad (6-2)$$

The reduced or condensed stiffness matrix([K<sub>R</sub>]) is then determined:

$$[K_R] = ([K_{mm}] - [K_{ms}][K_{ss}]^{-1}[K_{sm}]) \quad (6-3)$$

The dimension of this matrix is equal to the master DOFs. The reduced stiffness matrix of a bending type frame is a full matrix as reported in the *equation 6-4*:

$$[K_{BT_R}] = \begin{bmatrix} k_{11} & k_{12} & \cdots & \cdots & k_{1n} \\ k_{21} & k_{22} & \ddots & \ddots & \vdots \\ \vdots & \ddots & \ddots & \ddots & \vdots \\ \vdots & \ddots & \ddots & \ddots & k_{n-1\ n} \\ k_{n1} & \cdots & \cdots & k_{n\ n-1} & k_{nn} \end{bmatrix} \quad (6-4)$$

The stiffness matrix components are calculated based on the mean mechanical and geometrical properties collected into the database defined in the chapter before (Marasco and Cimellaro 2018).

As for the calculation of the building mass, it is based on the combination of the vertical load associated with the year of construction of the building. The permanent structural and non-structural loads are estimated considering the different types of parameters defined for the BTS by Marasco and Cimellaro (2018).

$$[M] = \frac{1}{g} \cdot \begin{bmatrix} (G_{k1} + G_{k2}) \cdot \gamma_G + \psi_G \cdot \gamma_Q \cdot Q_{k,int} & 0 & \cdots & \cdots & 0 \\ 0 & (G_{k1} + G_{k2}) \cdot \gamma_G + \psi_G \cdot \gamma_Q \cdot Q_{k,int} & \ddots & \ddots & \vdots \\ \vdots & \ddots & \ddots & \ddots & \vdots \\ \vdots & \ddots & \ddots & \ddots & 0 \\ 0 & \cdots & \cdots & 0 & (G_{k1} + G_{k2}) \cdot \gamma_G + \psi_G \cdot \gamma_Q \cdot Q_{k,top} \end{bmatrix} \quad (6-5)$$

In the methodology proposed by (Marasco and Cimellaro 2018), modal analysis is performed to evaluate the vibration modes in both horizontal directions of buildings. The seismic demand is assumed as an invariant lateral force distribution proportional to the calculated equivalent modal form (*equation 6-6*).

$$\{F\} = \alpha [K_{BT_R}] \{\Phi_{eq}\} \quad (6-6)$$

Pushover analysis is performed by increasing  $\alpha$  coefficient at each step of the analysis. The seismic resistance of a building is mainly provided by the columns which are subjected to a shear stress induced by the earthquake excitation. The global capacity of a building is then strictly dependent on the column's resistance. The global yielding of the building (point (1)) occurs when the most stressed column reaches the maximum allowable internal stress for the concrete or for the reinforcement in the considered direction. The pushover analysis is stopped at the step corresponding to the conditions and the yield base shear force ( $V_{bl} = V_{b,y}$ ) and the associated top displacement ( $u_l = u_y$ ) are identified (Marasco and Cimellaro 2018). For more details about the procedure for defining the elastic parameters of the model for RC structures used to define the behavior of the BSCs, please refer

to the work developed by (Marasco and Cimellaro 2018) for the Ideal City buildings portfolio.

The post-elastic parameters are associated with the basic shear-top displacement corresponding to points (2), (3) and (4) of the dorsal curve. Performing a pushover analysis to determine these parameters for each building would require a great deal of computational and time-consuming effort. For this reason (Marasco and Cimellaro 2018) proposed a simplified procedure to evaluate the post-elastic behavior of RC buildings. The maximum shear capacity ( $V_{b3}=V_{b4}$ ) is estimated based on the kinematic theorem of the limit analysis. After the global yield condition, the building is subject to an invariant distribution of horizontal forces with increasing monotonous intensity. When the total number of plastic hinges generated makes the structure unstable, collapse occurs. The value of the multiplier that identifies the collapse condition is called the collapse multiplier ( $\lambda$ ). Several in-plane collapse mechanisms can be identified for RC buildings. Two collapse mechanisms are considered, a global (figure 6-3 (a)) and a local mechanism (figure 6-3 (b)).

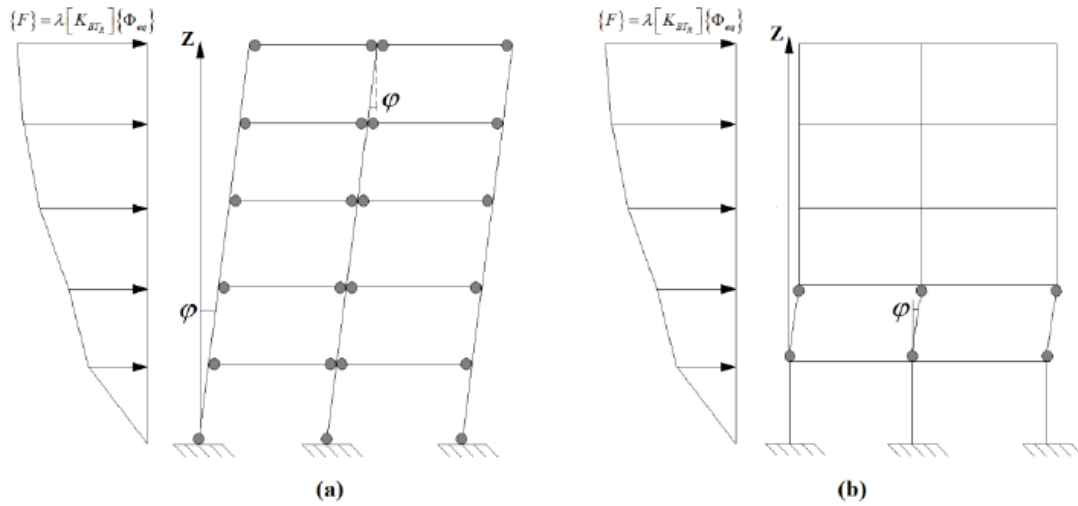


Figure 6-3, Global (a) and local (b) collapse mechanism of a RC building (Marasco and Cimellaro 2018).

The collapse multiplier for both mechanisms is then calculated (equation 6-7 and 6-8).

$$\lambda = \frac{n_c \cdot M_{c,y,j} + \sum_{i=1}^{dof} 2 \cdot n_{b,pl,i} \cdot M_{b,y,i}}{\sum_{i=1}^{dof} \{F_i\} \cdot \{z_i\}} \quad (6-7)$$

$$\lambda = \frac{2 \cdot n_c \cdot M_{c,y,j}}{\sum_{i=1}^{dof} \{F_i\} \cdot \{z_i\}} \quad (6-8)$$

where  $i$  represents the  $i$ th story level and  $j$  identifies the  $j$ th weakest story in which the plastic hinge forms.  $M_{c,y,i}$  and  $M_{b,y,i}$  are the yield bending moment of the  $i$ th columns and beams, respectively. The denominators refer to the external work due to the horizontal forces distributions, while  $n_c$  and  $n_{b,pl,i}$  represent the number of plasticized columns and the number of plasticized beams for the  $i$ th story level. By verifying the internal stresses of the beams and columns in order to know if a global or local collapse mechanism occurs. After having known the collision multiplier, the maximum shear capacity can be calculated (*Equation 6-9*).

$$V_3 = V_4 = \lambda \cdot V_{b,y} \quad (6-9)$$

One of the limitations of this procedure is the form of the loading diagram. The ultimate displacement associated with the previously calculated maximum shear is estimated using *equation 6-10* below.

$$u_4 = \theta_u \cdot h_j + H_e \cdot \left( \theta_u - \frac{F_j \cdot h_j^2}{3 \cdot E_j \cdot I_j} \right) \quad (6-10)$$

Where,  $\theta_u$  is the ultimate chord rotation,  $H_e$  is the building height measured from the weakest level to the top,  $F_j$  is the horizontal force applied at  $j$ th story for the collapse condition,  $h_j$  is the floor height, and  $I_j$  and  $E_j$  are moment of inertia and module of young of the columns of the  $j$ -th plane. These considerations are made for the two horizontal directions of the building. For more details, please refer to the work done by (Marasco and Cimellaro 2018). The base shear associated with the point (2) of the backbone curve is identified through the *equation 6-11*:

$$V_2 = c_2 \cdot \lambda \cdot V_{b,y} \quad (6-11)$$

The parameter  $c_2$  represents the rate of ultimate shear capacity which provides the base shear  $V_2$  and it assumes values lower than 1. The coefficient  $c_2$  is derived by performing a sensitivity analysis using the features of five RC buildings as data input and obtaining the *equation 6-12*.

$$c_2 = 0.928 - (1 - 0.968^{\rho_d}) - 0.0155 \cdot n_{st} - 0.0037 \cdot n_{sp} \quad (6-12)$$

where  $n_{st}$  and  $n_{sp}$  are the number of story and the number of spans of the building, respectively and,  $\rho_d$  is a dummy variable which assumes the value of 0 for low reinforced building and 1 for medium and high reinforced building (Marasco and Cimellaro 2018). Finally, the displacements associated with points (2) and (3) are obtained by considering two hypotheses, the first is that the equal energy rule is verified, the second is that the line of the capacity curve passing through the point (2) and (3) is parallel to the line passing through the yield point (point (1)) and the collapse point (point (4)).





(2018) for the portfolio of the buildings of the virtual city called Ideal City where the process is explained in an exhaustive manner.

### 6.2.2 Managing of the uncertainties:

Despite the data collected, in some cases it is not possible to know all the information for some facilities; in fact, large-scale simulations suffer from a lack of knowledge. For this reason, the approaches that can be followed in these cases can be, estimate the missing data as a function of the data available as was done for the BTS, we speak of the deterministic method, or use the procedure that was applied by Marasco and Cimellaro (2018) for the Ideal City building portfolio, which is a statistical method.

The building portfolio is treated as an uncertain system and its inherent uncertainties must be taken into account. All physical attributes of the building are considered as random variables (RV) which vary between a fixed maximum and minimum threshold based on a normal PDF. Considering some correlations between some variables, for example the mechanical characteristics depend on the construction period. Through a Monte Carlo simulation,  $n$  capacity curves are defined for each building by varying the sets of values of the parameters that describe them. Then the mean curve is taken as the capacity curve, this is done for both directions. *Figure 6-5* resume the process (Marasco and Cimellaro 2018).

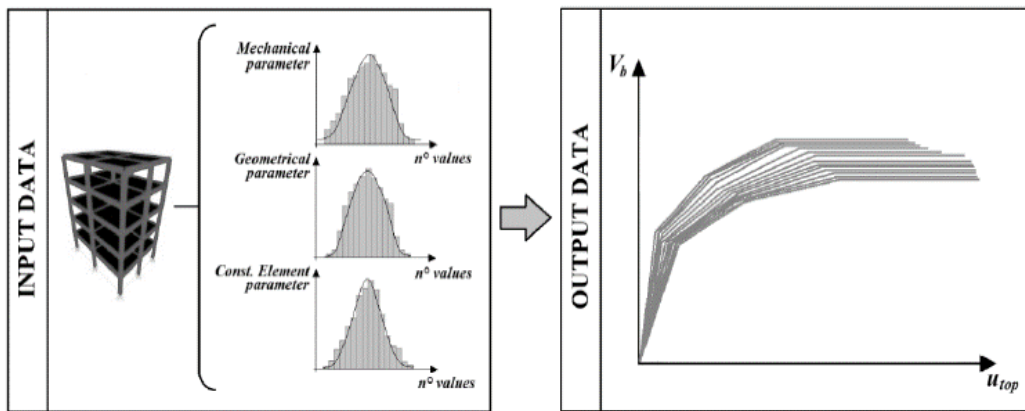


Figure 6-5, Input and Output data flow (Marasco and Cimellaro 2018)

### 6.2.3 Physical modeling of the BSC:

For the BSCs, the physical calculation model for carrying out the analysis is the one proposed for all the buildings of the Ideal City portfolio and developed by Marasco and Cimellaro (2018). It is schematized in *figure 6-6*. It is an equivalent SDOF model whose characteristics are determined by means of the MDOF calculation model of the physical parameters that characterize the behavior of the building.

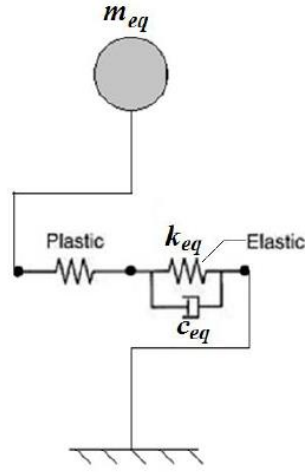


Figure 6-6, Proposed physical building model by (Marasco and Cimellaro 2018) for the buildings of the  
Ideal City

The equivalent mass  $m_{eq}$  of the SDOF model corresponds to the total mass of the building associated with the vibration modes considered in the analysis. The equivalent elastic stiffness  $k_{eq}$  of the SDOF is evaluated as the ratio between the shear at the base and the upper displacement corresponding to point (1) of the median dorsal curve (Marasco and Cimellaro 2018).

$$k_{eq} = \frac{V_{b,1}}{u_1} \quad (6-17)$$

Equivalent damping  $c_{eq}$  is evaluated according to the Rayleigh formulation by assuming the two predominant frequencies and damping ratio and is fixed to 5%. The dynamic strength degradation is modeled according to the Takeda model (Marasco and Cimellaro 2018). For more details about the Physical model used to do the analysis, always refer to the work done by Marasco and Cimellaro (2018).

### 6.3 Base Transceiver Stations (BTS)' Modelling:

Regarding BTS, the model used to evaluate the physical properties to describe the behavior is the one proposed by Madugula (2001) and Khedr and McClure (2000) which in turn is based on the work by Gálvez (1995). It describes the physical properties of the towers through an SDOF model with some assumptions:

- distributed mass;
- lumped mass for the antennas;
- linear distributed stiffness;
- shear deformation equal to zero;
- the first three mode of vibration are included;
- symmetrical and regular layout;

- seismic global capacity simulated through a bi-linear backbone curve

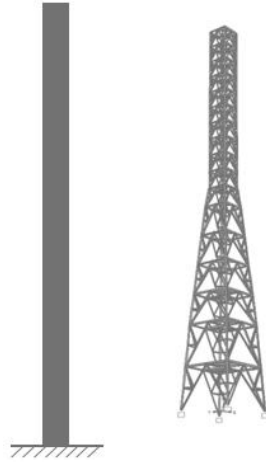


Figure 6-7, SDOF model for Support tower used to define the Physical properties

The global capacity is expressed as a function between the shear at the base ( $V_b$ ) and the displacement at the top ( $u_{top}$ ). In accordance with what proposed by Madugula (2001), the capacity curve for the support towers of BTS is approximated with a three-linear curve whose points are defined by means of a simplified approach based on the characteristics of the generalized system. Point (1) indicates the yield conditions and arrives when the first plastic hinge is formed in the weakest membrane. Point (2) indicates the point where the tower suffers extensive damage, until it reaches the last point (3) indicated by the ultimate displacement.

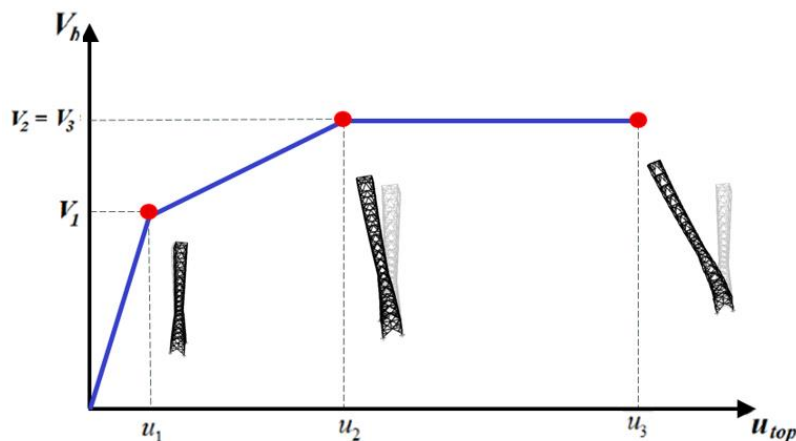


Figure 6-8, , Proposed tri-linear backbone curve, representative of the global capacity of the BTS towers

### 6.3.1 Defining the physical properties:

Unlike buildings, BTS cannot be described through a lumped mass model. This is because towers are structures with uniform mass and stiffness along the height.

When a structure has almost uniform distributed mass and stiffness the idealization of lumped masses cannot be used (Stokey 1988). In these cases, the problem becomes more complex because the DOFs are infinite (Cimellaro and Marasco 2018). The equation of motion of any generalized linear single-degree-of-freedom (SDOF) forced system can be expressed as *equation 6.18* shows (Khedr and McClure 2000).

$$M_i \cdot \ddot{q}_i(t) + C_i \cdot \dot{q}_i(t) + K_i \cdot q_i(t) = L_i \quad (6-18)$$

Where  $M_i$  is the generalized mass,  $C_i$  is the generalized viscous damping constant,  $K_i$  is the generalized stiffness,  $L_i$  is the generalized force. *Equation 6-19, 6-20, 6-21 and 6-22* defines their mathematical expressions (Khedr and McClure 2000).

$$M_i = \int_0^h m(x) \cdot (\phi_i(x))^2 dx \quad (6-19)$$

$$K_i = \int_0^h EJ(x) \cdot (\phi_i''(x))^2 dx \quad (6-20)$$

$$C_i = 2\omega_i \cdot \xi_i \cdot M_i \quad (6-21)$$

$$L_i = \int_0^h m(x) \cdot \phi_i(x) dx \quad (6-22)$$

where  $\Phi_i$  is the mode shape  $i$ ,  $m(x)$  is the distributed mass of the system as a function of position  $x$ ,  $E$  is the Young module,  $I(x)$  is the module of inertia as a function of position  $x$  and  $\xi_i$  is the viscous damping ratio equal to 3% and  $\omega_i$  (rad/s) is the undamped natural frequency of the SDOF system and it can be evaluated using *equation 6-23* (Khedr and McClure 2000).

$$\omega_i = \sqrt{\frac{K_i}{M_i}} \quad (6-23)$$

The mass of the main plants ( $M_{mp}$ ) is considered as a mass concentrated at the top of the tower. For this reason, it is excluded from the calculation of  $m(x)$  and considered as a constant. So, *equation 6-19* is rewritten as in *equation 6-24*.

$$M_i = \left( \int_0^h m(x) \cdot (\phi_i(x))^2 dx \right) + M_{mp} \quad (6-24)$$

The first step is to define the mass profile for each structural configuration of the towers. According to Sackmann (1996), the average mass profile for lattice towers with structural configuration SC1 can be defined through a polynomial function of the second degree height reported by *equation 6-25*, for lattice towers with structural configuration SC2 or SC3 it can be defined through a polynomial function of the second degree height reported by *equation 6-26*, and also for monopole towers the mean mass profile is defined by a polynomial function of the second degree height reported by *equation 6-27*.

$$m(x) = 1 - \alpha x + \beta x^2 \quad x \in (0, h) \quad (6-25)$$

$$\alpha = 1,24 \quad \beta = 0,37$$

$$m(x) = 1 - \alpha x + \beta x^2 \quad x \in (0, h) \quad (6-26)$$

$$\alpha = 1,54 \quad \beta = 0,87$$

$$m(x) = 1 - \alpha x + \beta x^2 \quad x \in (0, h) \quad (6-27)$$

$$\alpha = 0,94 \quad \beta = 0,24$$

To better describe the behavior of the towers, it would be necessary to obtain the three lowest flexural vibration modes of the tower. On an urban scale, however, this entails an excessive computation burden. For this reason, only the first way of vibrating is considered. To define the function that describes the first mode of vibration of the tower, the hypothesis is assumed to consider the tower as a cantilever beam as *figure 6-9* shows.

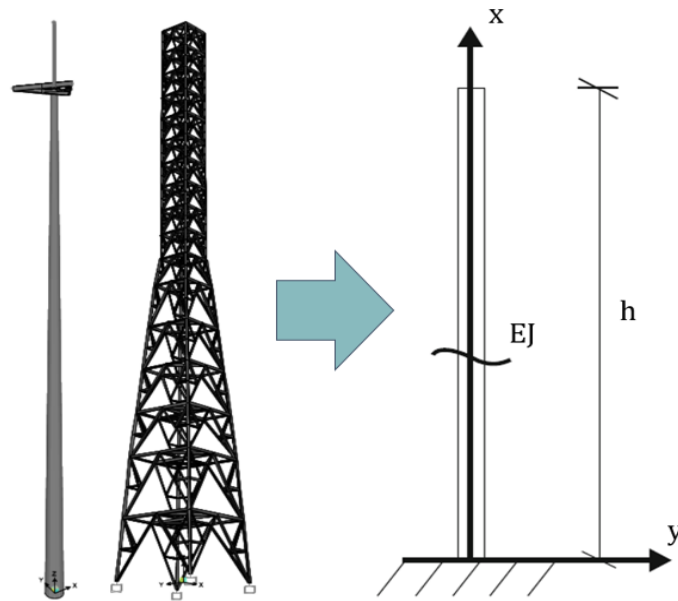


Figure 6-9, approximation of the behavior of the towers in a cantilever beam

In this case, the definition of a shape function is not exact, because it depends on an infinite number of modes. Since it is known that the first mode is always predominant cantilever beam, the shape function can be assumed equal to the first vibrational mode. For the cantilever beam, it was observed that the mathematical expression of the vibrational modes is complex and must be solved numerically. Generally, the shape function is chosen to respect the boundary conditions and the real elastic behavior. For this purpose, the shape function of the cantilever beam can be deduced as flexural deformed shape due to a unitary force applied to the free node (Eulero-Bernulli condition assumed). Therefore, the function that defines the main mode of vibration for the towers is that given by *equation 6.28* (Cimellaro and Marasco 2018).

$$\Phi(x) = \frac{x^2}{2h^2} \left( 3 - \frac{x}{L} \right) \quad (6.28)$$

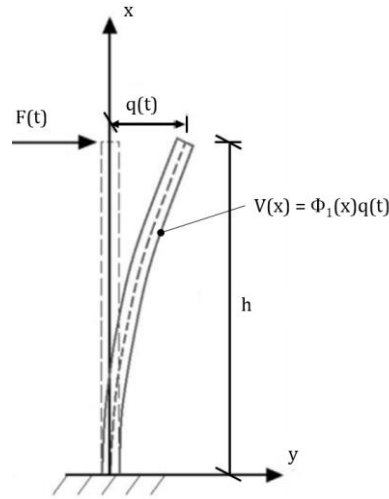


Figure 6-10, Generalized cantilever system equal to the tower (Cimellaro and Marasco 2018)

As for the resistance modulus  $E$ , it is constant along the entire height of the tower. This is because in this study the hypothesis was made to assign to the towers a single parameter that defines the mechanical properties for it. Therefore, the module is defined by the mechanical parameters assigned to the tower. In reality, the structure can be made with elements that have different properties. Finally, it is necessary to define the module of inertia ( $J$ ) of the tower. It is defined for each structural configuration assumed. This is because, for example, for the structural configuration SC1, it varies as the height varies, this is because the cross section of the tower varies. While for the SC2 and SC3 configurations, i.e. the lattice towers with a constant base, they remain constant along the height. For the towers with structural configuration SC1, three functions have been defined based on whether the variation of the cross section of the tower ends at  $1/3$  of the height, at half or



at 2/3 of the height. *Equation 6-29* defines the variation of inertia for the structural configurations SC4 and SC5.

$$J(x) = \eta - \delta x \quad \forall x \in [0; h] \quad (6-29)$$

*Equation 6-30* defines the variation of inertia for the structural configurations SC2 and SC3.

$$J(x) = cost \quad \forall x \in [0; h] \quad (6-30)$$

*Equation 6-31* establishes the trend of inertia for the structural configuration SC1 with variation of the cross section up to half of the height. While *equation 6-32* and *6-33* establish the inertia trend for the structural configuration SC1 but with variation of the cross section up to 1/3 of the height and up to 2/3 of the height respectively.

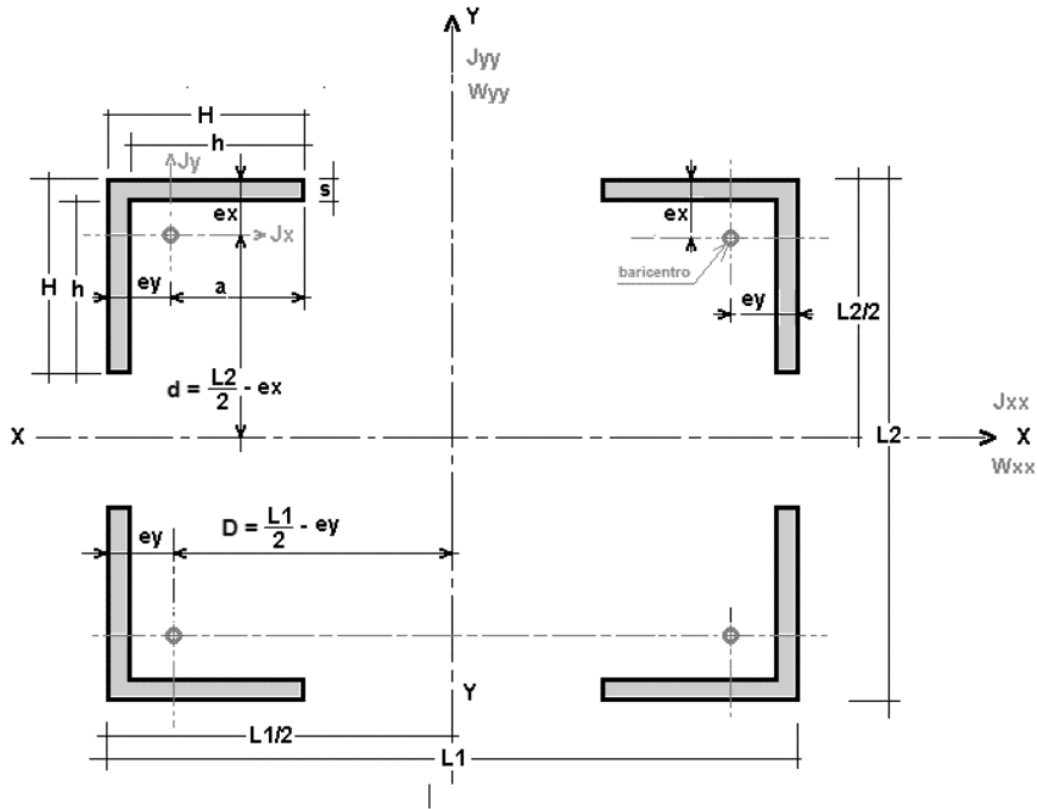


Figure 6-11, example of cross section of a lattice tower to calculate the Inertia of the section

$$J(x) = \eta - \delta x \quad \forall x \in \left[0; \frac{h}{2}\right] \quad (6-30)$$

$$J(x) = cost \quad \forall x \in \left[\frac{h}{2}; h\right]$$

$$J(x) = \eta - \delta x \quad \forall x \in \left[0; \frac{h}{3}\right] \quad (6-31)$$

$$J(x) = cost \quad \forall x \in \left[\frac{h}{3}; h\right]$$

$$J(x) = \eta - \delta x \quad \forall x \in \left[0; \frac{2h}{3}\right] \quad (6-32)$$

$$J(x) = cost \quad \forall x \in \left[\frac{2h}{3}; h\right]$$

$\eta$  and  $\delta$  are calculated as a function of the Inertia at the base and top as shown in *figure 6-11* for example for the lattice towers.

$$J = 4 \left( J_{sec} + A_{sec} \left( \frac{B(x)}{2} - e_{sec} \right)^2 \right) \quad (6-33)$$

Where  $J_{sec}$  and  $A_{sec}$  are the Inertia and the Area of a L section,  $B$  is the base of the tower that is a function of the height of the tower and  $e_{sec}$  is the eccentricity of the L section to respect its local center of gravity.

To conclude, the tower own period ( $T$ ) can be derived from the natural frequency defined in *equation 6-35*.

$$T_{TOW} = \frac{2\pi}{\omega} \quad (6-34)$$

Where  $\omega$  is the sum of  $\omega_i$  for each mode.

In accordance with the approach proposed by Madugula (2001) and Khedr and McClure (2000) it is possible to obtain the shear values at the base and displacement at the top of the tower that characterizes point (1) of the capacity curve for the towers. They are defined through the computed properties of the equivalent generalized system.

$$V_{b1} = V_{b,y} = \int_0^h m(x) \phi_i(x) \frac{L_i}{M_i} \alpha(\omega, T) \quad (6-35)$$

Where  $\alpha$  is a coefficient that depends on the period and the natural frequency of the tower itself calculated with the formulas of generalized systems (Madugula 2001).

$$u_1 = u_y = \kappa_h \cdot \ln h_{TOW} - \delta \quad (6-37)$$

Where,  $\kappa_h$  and  $\delta$  are constant estimated as a function of the set of towers studied in the work proposed by (Madugula 2001). For their values see the work proposed by (Madugula 2001).

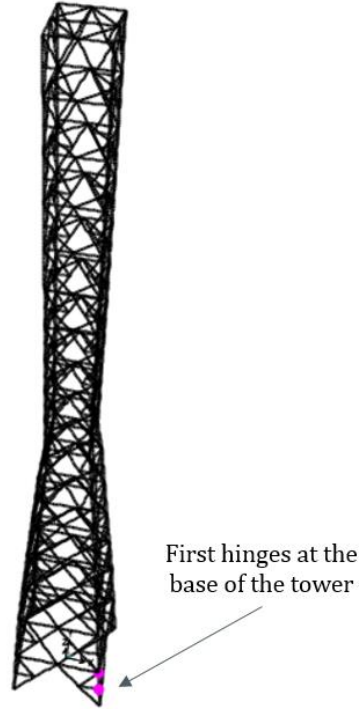


Figure 6-12, example of pushover analysis of lattice tower with the formation of the first hinges, that it corresponds to the first point of the capacity curve

The post-elastic parameters are associated with the basic shear-top displacement corresponding to points (2) and (3) of the dorsal curve. Even for the towers performing a pushover analysis to determine these parameters would require a great deal of computational and time-consuming effort. For this reason (Madugula 2001) and (Khedr and McClure 2000) proposed a simplified procedure to evaluate the

$$V_{b2} = V_{b3} = \alpha \cdot V_{b,y} \quad (6-36)$$

Where  $\lambda$  is a multiplier defined from (Sackmann 1996) work and its value it depend from the type of structural configuration of the tower and from the height of the tower itself.

$\alpha = 1,4 - 1,9$  for SC1 tower configuration.

$\alpha = 1,3 - 1,9$  for SC2 and SC3 tower configuration.

$\alpha = 1,1 - 1,8$  for SC4 and SC5 tower configuration.

$$u_3 = \beta \cdot u_1 \quad (6-37)$$

$$u_2 = 1,1 \cdot \left( \frac{u_1 + u_3}{2} \right)^\gamma \quad (6-40)$$

Where,  $\beta$  is a constant depend on type of tower and  $\gamma$  is defined as  $1/T_{TOW}$ .

$\beta = 7,55 - 8,25$  for SC1 configuration

$\beta = 5,65 - 5,90$  for SC2 and SC3 configuration

$\beta = 3,10 - 3,55$  for SC4 and SC5 configuration

### 6.3.2 Physical modeling of the BSC:

For the BTS support tower, the physical calculation model for carrying out the analysis is schematized in *figure 6-13*. It uses an equivalent degree of freedom (SDOF) system where its characteristics are defined through the physical properties defined in the previous paragraph.

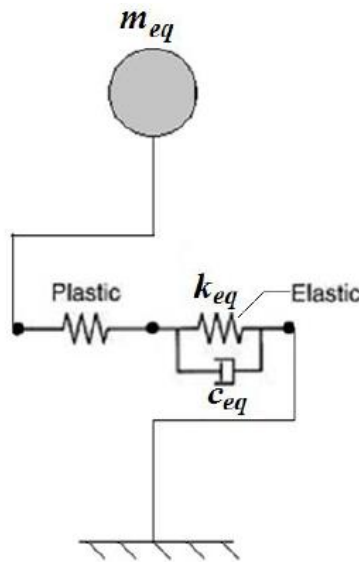


Figure 6-13, Proposed physical model for the support towers of the BTSs

Where, the equivalent mass  $m_{eq}$  of the SDOF model corresponds to the associated calculated generalized mass, while the equivalent elastic stiffness  $k_{eq}$  of the SDOF corresponds to that defined through the formulas of the generalized SDOF model calculated in the previous paragraph. Equivalent damping  $c_{eq}$  is evaluated according to the formulation by generalized systems seen before using a damping ratio fixed to 3%. The dynamic strength degradation is modeled according to the Kinematic model (Madugula 2001). Kinematic model is commonly used in nonlinear seismic response analysis.

### 6.3.3 Validation of the model:

The degree of accuracy associated with the proposed capacity model has been verified by comparison with two study case towers. Both case studies concern rawland towers. The first one is a pyramid-type lattice tower. The second concerns a monopole tower (*figure 6-15*).

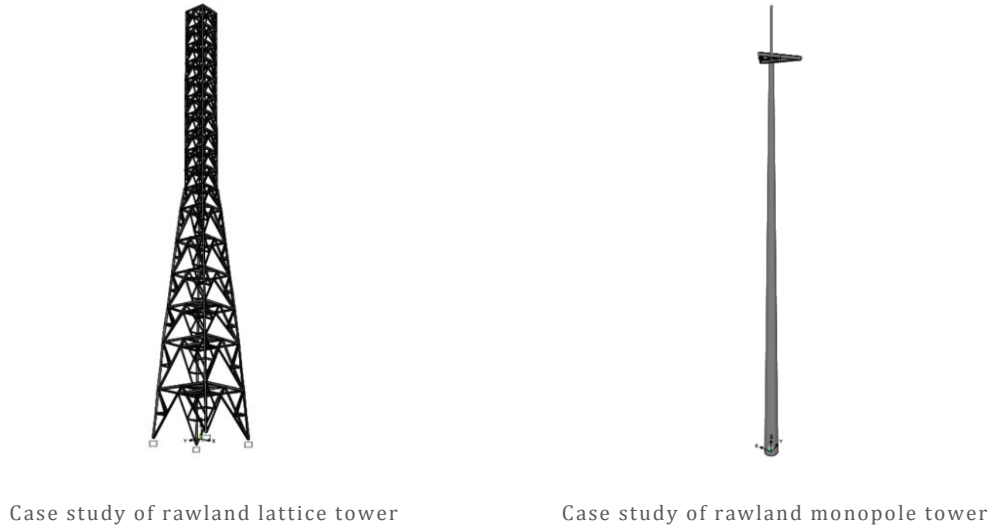
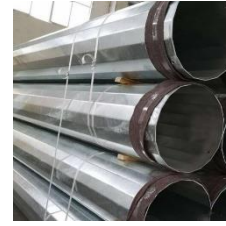


Figure 6-14, case studies

The structural elements have been designed according to the European legislation concerning steel structures (En 1993-1-1 and EN 1993-3-1). The seismic hazard was chosen to be representative of a high seismic hazard of the national territory. The single-post tower is 24 meters high and is built with prefabricated polygonal poles made with cold drawn sheets. The diameter at the base is 800 mm, while at the top it is 400 mm. All the weights defined in the previous chapter are considered. The tower is used by only one MNO. The structure is made with graft joints of 6 m long trunks each. The structural steel used to make the logs is S235J0. The support structures of the antennas are also made of the same steel. Finally, the thickness of the logs is 5 mm. While as regards the lattice tower, it has a height of 40 meters, it is made with L-shaped profiles with equal wings. The sections used for the tower legs are L 140x140x13, the primary vertical braces use 90x90x9 sections, the secondary and tertiary ones use 75x75x7 sections instead. Finally, the horizontal braces use 100x100x10 sections. The structural steel used for the legs and primary vertical and horizontal braces is S355J0, while for the secondary and tertiary vertical braces it is S235J0. The scheme of both primary and secondary bracing is K-bracing. The width of the lower base is 5.5 meters, while the upper one is 1 meter. The base varies up to  $h / 2$ , after which the base remains constant.



L section typically used to build lattice towers



Polygonal section typically used to build monopole towers

Figure 6-15, examples of the sections used to build the telecom towers of the case studies

Sap2000 software (CSI, 2018) was used to build the Finite Element Model (FEM) of the two towers studied. The concentrated plasticity model (FEMA 356 type P-M2-M3 for the legs, while type P for the bracing) was chosen to take into account the non-linearity in the structural components. The non-linear pushover analysis was performed in only one horizontal direction as the structure is perfectly symmetrical. The lateral force distribution considered was that with respect to the fundamental vibration mode of the structure in the direction considered.

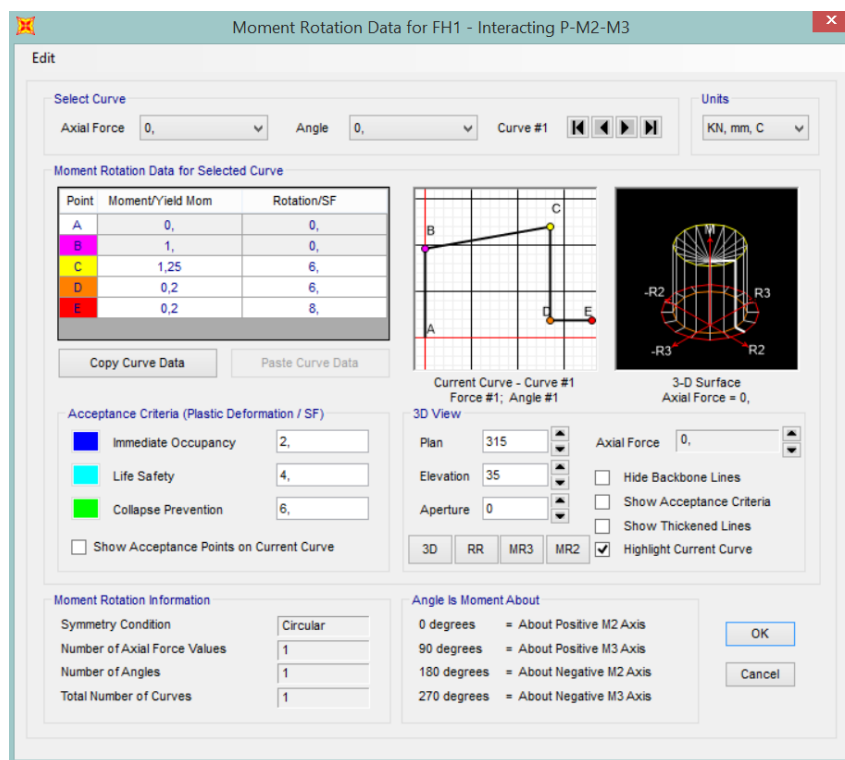


Figure 6-16, set up of the hinges for the legs of the tower

Once the parameters for the pushover analysis have been established, the capacity curve for each case study is obtained and compared with the capacity curve obtained from the proposed model. *Figure 6-18* and *figure 6-19* shows the capacity curve obtained from the simulation ran with SAP2000 for the lattice tower and for the monopole tower respectively. Where top displacement is in millimeter and the base reaction is in kilonewton.

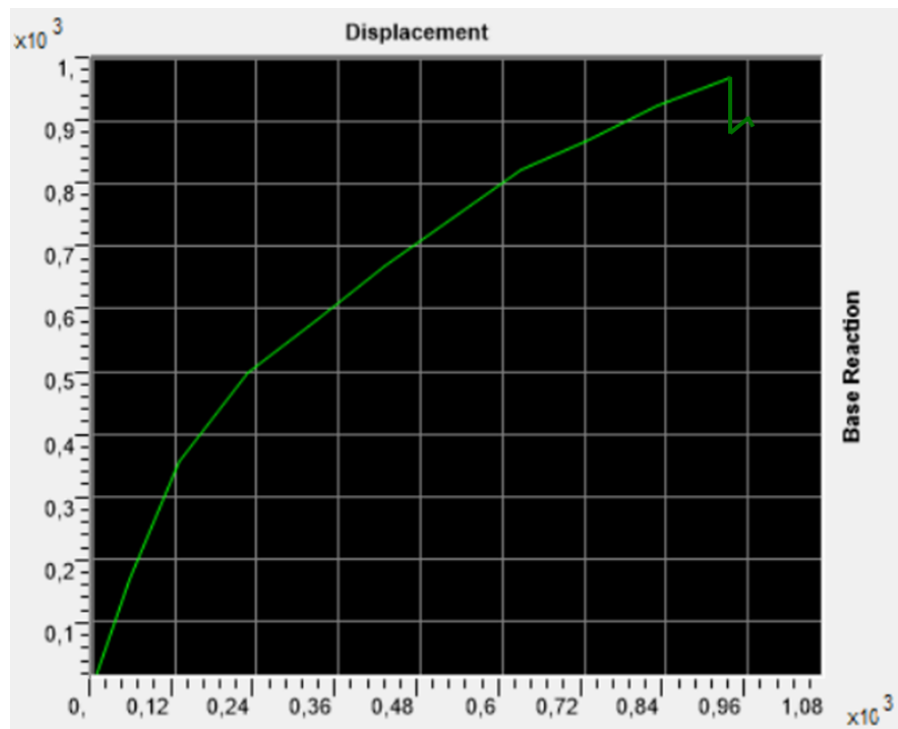


Figure 6-17, capacity curve obtained for rawland lattice tower case study

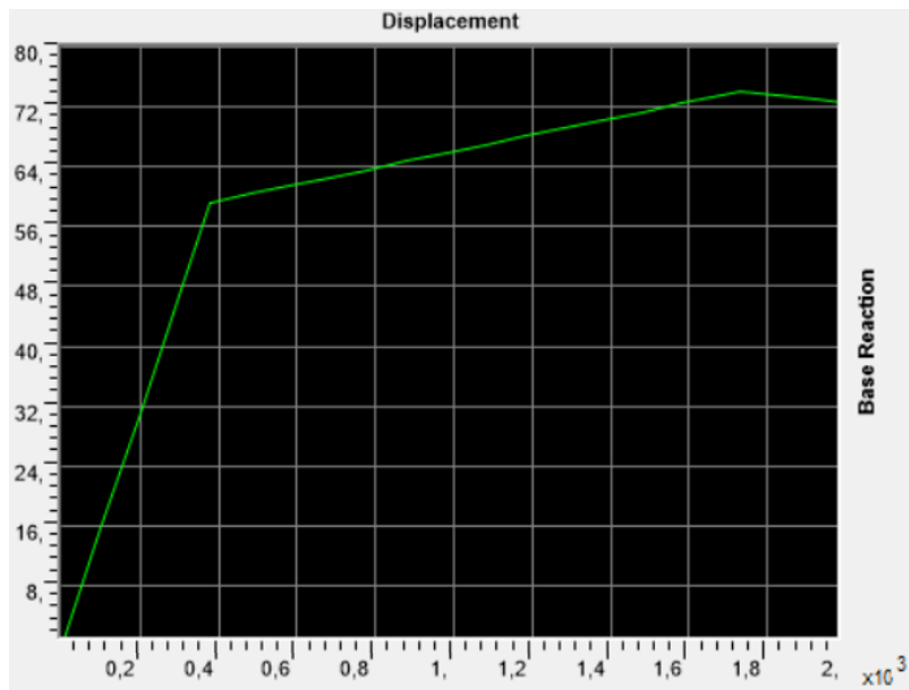


Figure 6-18, capacity curve obtained for rawland monopole tower case study

From the FEM model we can observe how the first plastic hinges are formed at the base of one of the 4 legs of the tower, after which those in the middle are generated and then gradually created in each membrane. *Figure 6-20* shows various successive steps in the formation of plastic hinges.



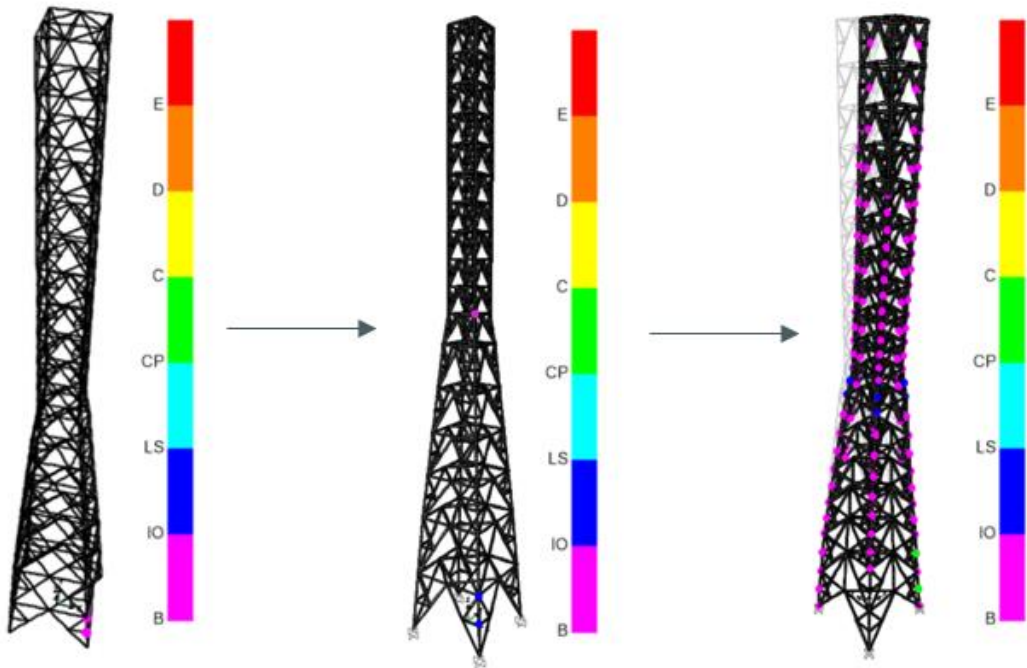


Figure 6-19, examples of different time steps of the hinges for the lattice tower case study

where B indicates yield condition, IO indicates Immediate Occupancy condition, LS indicates Life Safety condition and CP indicates Collapse Prevention condition, C indicates the collapse condition about the capacity curve. *Figure 6-21* explain these points on the capacity curve.

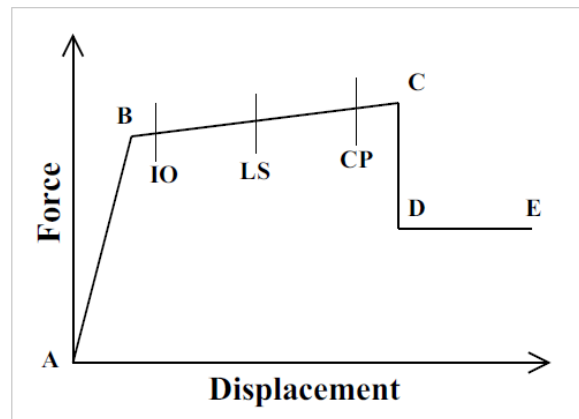


Figure 6-20, definition of the condition on the capacity curve

It is observed that the physical model proposed in the case of single-post towers simulates the overall capacity of the tower well, while for the lattice towers there is a greater discrepancy due to the simplifications made to define the parameters to describe the towers. Overall, the elastic behavior of the curve corresponds, lower values are observed for the ultimate capacity. *Figure 6-22* compares the curves obtained for the lattice tower, while *Figure 6-23* compares the curves obtained for the single-pole tower.

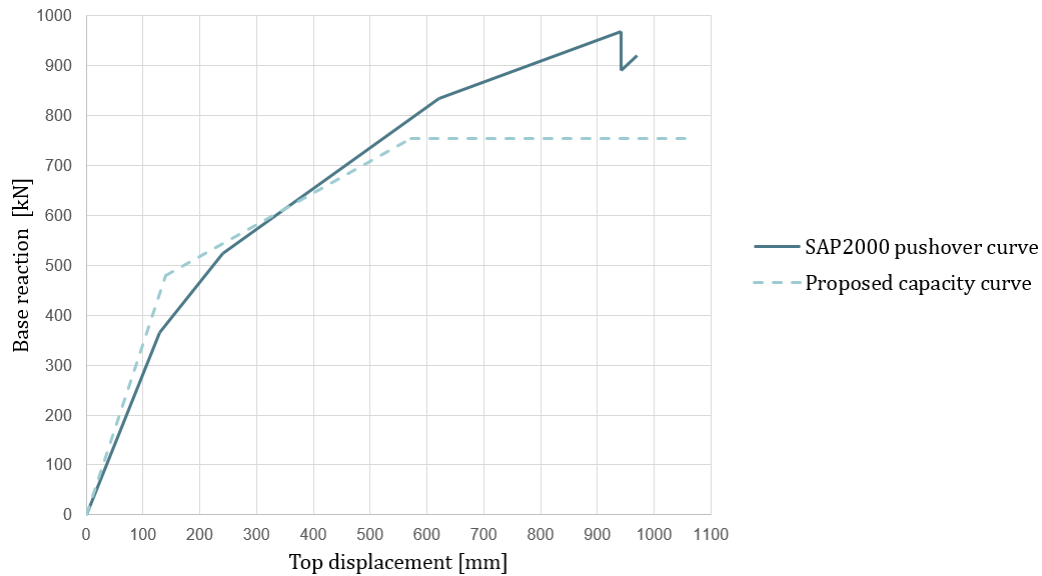


Figure 6-21, Comparison between the capacity curves from SAP2000 FEM model and SDOF equivalent model for the rawland lattice tower

In the case of the lattice tower, an imperfect correspondence is observed in the elastic section, this is since for the lattice towers a simplification has been assumed on the assignment of the mechanical properties. What was done was to assume the mechanical ownership of the legs for the whole tower. This leads to greater stiffness than the simplified SDOF model. While for the post-elastic part there is an underestimated behavior by the simplified model, but this is in favor of safety.

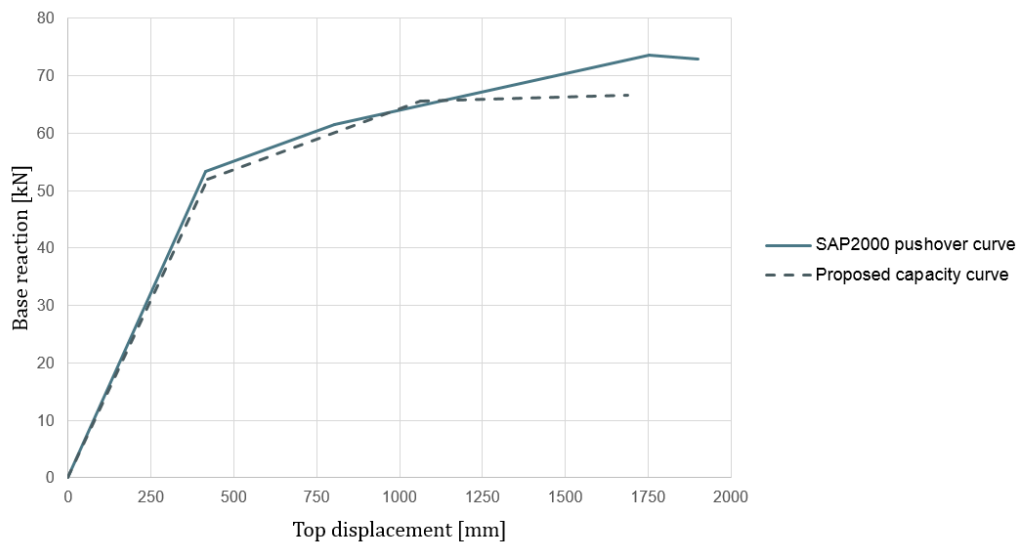


Figure 6-22, Comparison between the capacity curves from SAP2000 FEM model and SDOF equivalent model for the rawland monopole tower

In the case of the monopole tower, an excellent correspondence is observed in the elastic section, thanks to the greater simplicity in evaluating the properties of the

structure. Even for the second case study, the ultimate capacity is underestimated. While the simplified model proposed allows to represent with a good degree of reliability the post-elastic section for this type of tower.

## 6.4 Ideal City Buildings' Modelling:

For details on the modeling and definition of the physical properties of the residential and non-residential buildings that compose the virtual city of the Ideal City, refer to the work done by Marasco and Cimellaro (2018). Such work is essential as many BTS are located on the roofs of buildings.

# 7 Seismic Scenario's Features

## 7.1 Introduction

Since a detailed seismic characterization of the site is beyond the scope of this research, a simplified scenario-based approach is used to estimate the seismic input to be applied on IDEAL CITY proposed by Marasco and Cimellaro (2018) already for the building layer. Therefore, the seismic input was rescaled as a function of the distance from the epicenter set for the Ideal City. For more information on the approach used to mitigate the seismic input for each structural element present on the territory of the Ideal City, please refer to the work carried out by Marasco and Cimellaro (2018).

Concerning buildings, attenuation was available starting from the building portfolio layer. For towers on the ground having no possibility of calculating the attenuation of the seismic input in the exact point of where the tower is located, it was decided to apply the calculated attenuation of the building closest to the tower itself.

## 7.2 Definition of a Seismic scenario

The seismic scenario is assumed in terms of:

- seismic source;
- soil characteristics (geometrical attenuation);
- geometry of the fault rupture area;
- time history recorded in the epicenter (seismic action).

The seismic source is characterized by the fault type, expected moment magnitude of the seismic event, and localization of the hypocenter and epicenter. A simplified procedure is proposed to estimate the geometrical attenuation at any building location within the virtual city. The geometrical attenuation of the seismic excitation is estimated through the Boore-Atkinson attenuation law. For this purpose, the shear wave velocity in the upper most 30 m (VS30) for the city of Turin is assumed to model the soil characteristics. The VS30 map is obtained via USGS website.

For the details about the application of this model, please refer to the work proposed by Marasco and Cimellaro (2018).

## 8 Damage assessment

### 8.1 Introduction

Structural performance can be estimated using static or dynamic analysis methods. The choice of the analysis methods used in evaluating the performance of the structure depends on the degree of accuracy to be obtained, the availability of the starting data and the complexity of the model itself (Noori, Marasco et al. 2017). In this work a dynamic method is applied for the evaluation of the damage of the network components. A nonlinear dynamic analysis with acceleration time history is implemented. This is because this process is already used for the layers of the Ideal City defined previously. According to HAZUS (FEMA 2011) the seismic damage to structures can be classified into five levels (none, mild, moderate, extensive and complete).

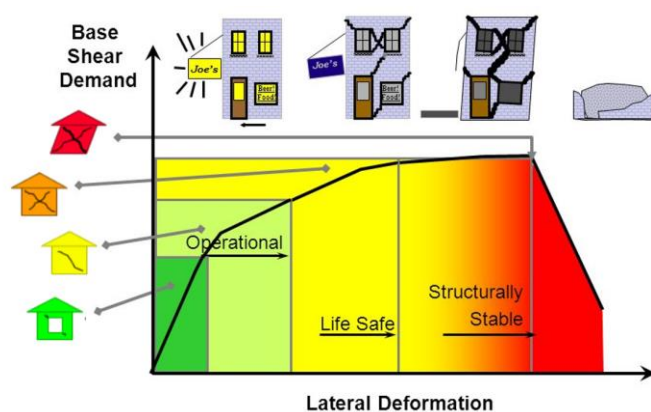


Figure 8-1, Damage states from HAZUS (FEMA 2011)

Based on this, various indicators can be used to quantify the damage to the various components of the network. These indicators are called Engineering Demand Parameters (EDP) and are used to predict the damage states (DS) of structural and non-structural components of different structures (Marasco and Cimellaro 2018). As for buildings and therefore also for BSCs, the maximum inter-story drift is widely adopted as EDP because it can characterize the dynamic response of a building (Marasco and Cimellaro 2018). In the case of support towers, top displacement and top rotation are indicators that can be adopted as EDP to define structural damage or service damage (Khedr 1998). As regards the buildings and therefore also the BSCs, the damage assessment takes place through analytical fragility curves developed by Marasco and Cimellaro (2018) for the built environment of the Ideal City. While about the support towers of the BTS, no fragility curve has been found in the literature that describes the damage based

on the seismic input. For this reason, the same procedure proposed by Cimellaro, Domaneschi et al. (2017) was applied to assign damage states to buildings based on the capacity curve of the structure. Strength-based damage criteria are used for "light" and "moderate" damage states, while strain-based criteria are used for "extensive" and "full" damage states. It is certainly a simplifying method, but given the computational burden, there is a need to reduce the calculation times. It must also be said that extensive damage to telecommunication towers due to seismic events has certainly been recorded in a much lower number than the damage suffered by buildings (Khedr 1998).

## 8.2 Nonlinear time history analysis

To evaluate the response of the various network components and the built environment direct integration time history analysis is performed in SAP2000 (figure 8-2). It is a dynamic analysis method in which the equilibrium equations of motion (equation 8-1) are fully integrated as a structure is subjected to dynamic loading (CSI. 2018). As dynamic loading the analysis uses the time history of the recorded accelerograms of known events shown in the previous chapters.

$$M\ddot{u}(t) + C\dot{u}(t) + Ku(t) = F(t) \quad (8-1)$$

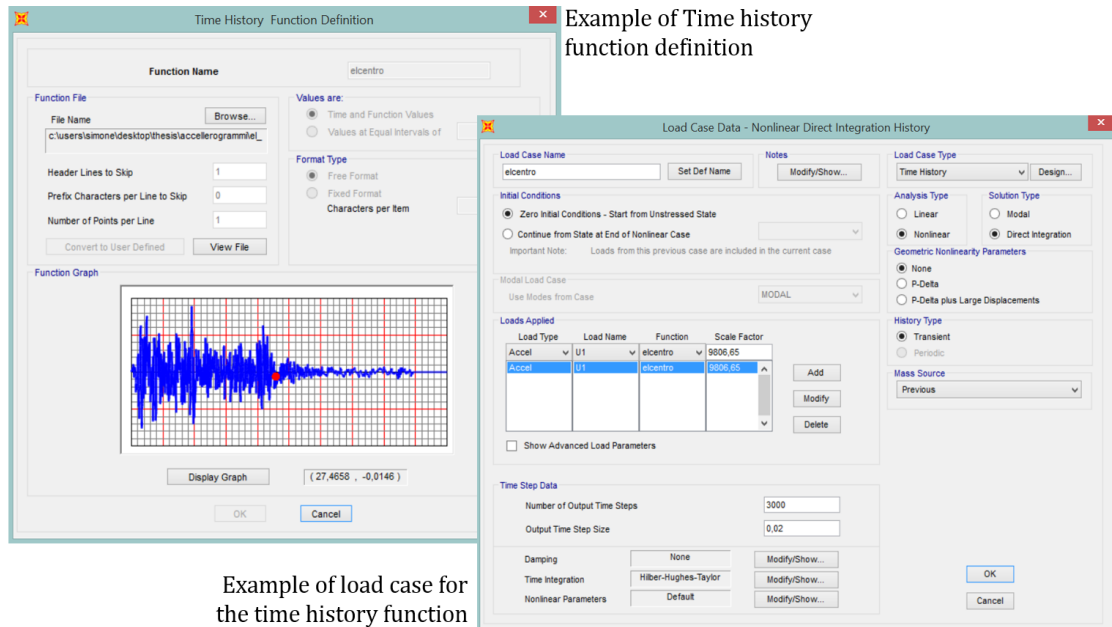


Figure 8-2, window to set the time history analysis in SAP2000 (CSI. 2018)

Therefore, the buildings (therefore also of the BSCs) and the BTSS' support towers were representatives of equivalent SDOFs. To perform the analysis these SDOFs are modeled through multilinear plastic link elements in SAP2000 (CSI. 2018).



Each link element represents a structure with its own physical properties defined through the physical model defined in chapter 6. *Figure 8-3* illustrates the the concept of passage from 3D MDOF elements to link elements for buildings.

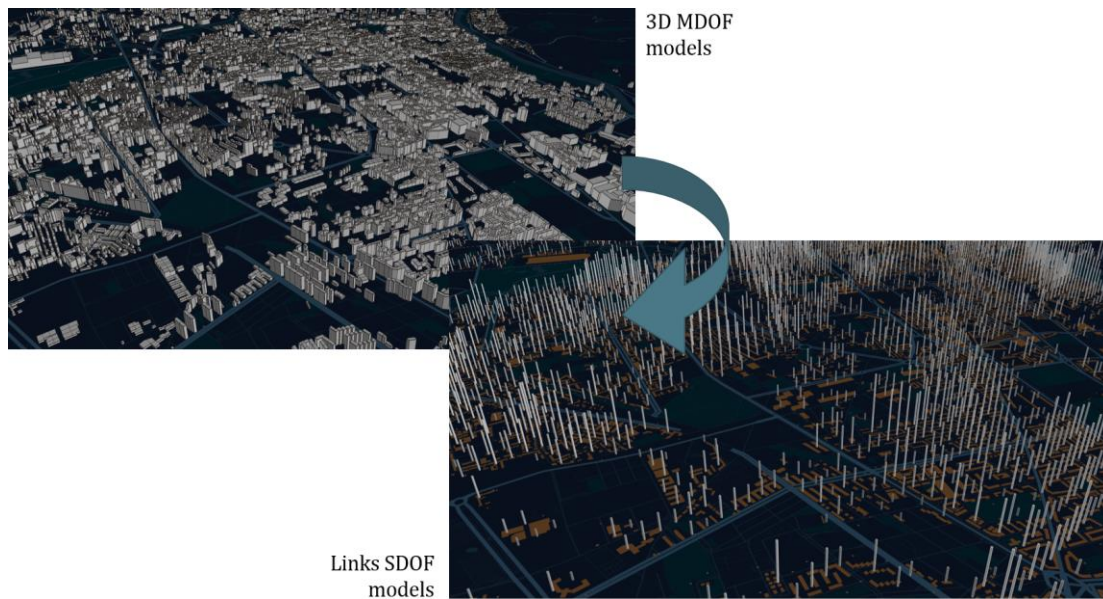


Figure 8-3, from 3D MDOF models to links SDOF elements

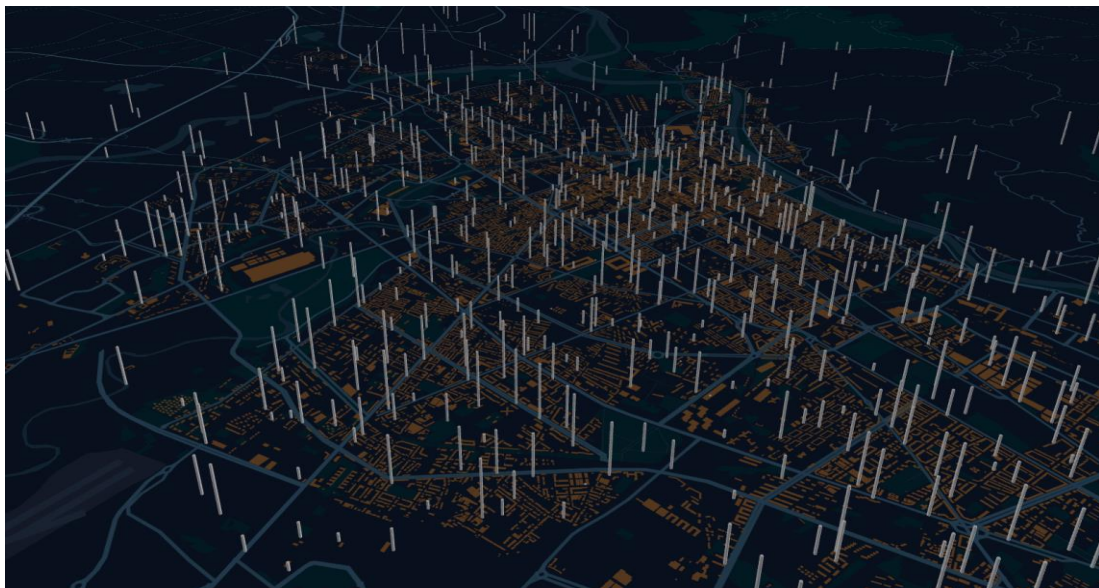










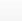
Figure 8-4, links elements for BTS towers (rawland towers + rooftop towers) discretized by the height

To carry out the analysis, it was necessary to insert each link element in the geographic position to which it belongs, in such a way as to also consider the attenuation of the seismic action being an analysis on an urban scale. To do this, the SAP2000 database editing was used where a geographic position was assigned to each link by means of geometric coordinates and distinct according to the height of the antenna (*figures 8-5*).



Interactive Database Editing - Joint Coordinates

File Excel Edit View Options

Joint Coordinates

	Joint	CoordSys	CoordType	XorR	Y	T Degrees	Z	Special	GUID
▶ 1	GLOBAL	Cartesian	399653.91	4994864...		5	No		aebe1ecb-6c2e-4baf-a16e-16dca34a83c8
2	GLOBAL	Cartesian	398397.28	4996838...		3.5	No		aebe1ecb-6c2e-4baf-a16e-16dca34a83c9
3	GLOBAL	Cartesian	400358.94	4993438...		3.5	No		aebe1ecb-6c2e-4baf-a16e-16dca34a83c10
4	GLOBAL	Cartesian	400244.31	4992631...		5	No		aebe1ecb-6c2e-4baf-a16e-16dca34a83c11
5	GLOBAL	Cartesian	399650.21	4991910...		3.5	No		aebe1ecb-6c2e-4baf-a16e-16dca34a83c12
6	GLOBAL	Cartesian	399359.78	4991198...		2.5	No		aebe1ecb-6c2e-4baf-a16e-16dca34a83c13
7	GLOBAL	Cartesian	398804.03	4991111...		3.5	No		aebe1ecb-6c2e-4baf-a16e-16dca34a83c14
8	GLOBAL	Cartesian	398187.42	4990638...		5	No		aebe1ecb-6c2e-4baf-a16e-16dca34a83c15
9	GLOBAL	Cartesian	397723.8	4990814...		4.5	No		aebe1ecb-6c2e-4baf-a16e-16dca34a83c16
10	GLOBAL	Cartesian	397235.57	4989887.5		5	No		aebe1ecb-6c2e-4baf-a16e-16dca34a83c17
11	GLOBAL	Cartesian	396126.66	4987870...		4.5	No		aebe1ecb-6c2e-4baf-a16e-16dca34a83c18
12	GLOBAL	Cartesian	396515.26	4987036...		3.5	No		aebe1ecb-6c2e-4baf-a16e-16dca34a83c19
13	GLOBAL	Cartesian	395909.54	4985873...		4	No		aebe1ecb-6c2e-4baf-a16e-16dca34a83c20
14	GLOBAL	Cartesian	397570.78	4995866...		5	No		aebe1ecb-6c2e-4baf-a16e-16dca34a83c21
15	GLOBAL	Cartesian	397933.71	4995605...		6.5	No		aebe1ecb-6c2e-4baf-a16e-16dca34a83c22
16	GLOBAL	Cartesian	397377.5	4995118...		5	No		aebe1ecb-6c2e-4baf-a16e-16dca34a83c23
17	GLOBAL	Cartesian	397831.6	4994806.2		7	No		aebe1ecb-6c2e-4baf-a16e-16dca34a83c24
18	GLOBAL	Cartesian	398643.25	4994380...		2.5	No		aebe1ecb-6c2e-4baf-a16e-16dca34a83c25
19	GLOBAL	Cartesian	396413.76	4995600...		2.5	No		aebe1ecb-6c2e-4baf-a16e-16dca34a83c26
20	GLOBAL	Cartesian	396060.5	4995582.3		5.5	No		aebe1ecb-6c2e-4baf-a16e-16dca34a83c27
21	GLOBAL	Cartesian	395526.09	4995408...		5	No		aebe1ecb-6c2e-4baf-a16e-16dca34a83c28
22	GLOBAL	Cartesian	394549.92	4995937...		2.5	No		aebe1ecb-6c2e-4baf-a16e-16dca34a83c29

Undo Last Apply Apply to Model Done

Figure 8-5, Editing database for assigning coordinates to links elements in SAP2000 (CSI. 2018)

Link/Support Type: MultiLinear Plastic

Property Name: 14\_RAW

Property Notes:

Total Mass and Weight

Mass: 18473

Weight: 181220

Rotational Inertia 1: 0

Rotational Inertia 2: 0

Rotational Inertia 3: 0

Factors For Line, Area and Solid Springs

Property is Defined for This Length in a Line Spring: 1

Property is Defined for This Area in Area and Solid Springs: 1

Directional Properties

Direction	Fixed	NonLinear	Properties
<input type="checkbox"/> U1	<input type="checkbox"/>	<input type="checkbox"/>	Modify/Show for U1...
<input checked="" type="checkbox"/> U2	<input type="checkbox"/>	<input checked="" type="checkbox"/>	Modify/Show for U2...
<input type="checkbox"/> U3	<input type="checkbox"/>	<input type="checkbox"/>	Modify/Show for U3...
<input type="checkbox"/> R1	<input type="checkbox"/>	<input type="checkbox"/>	Modify/Show for R1...
<input type="checkbox"/> R2	<input type="checkbox"/>	<input type="checkbox"/>	Modify/Show for R2...
<input type="checkbox"/> R3	<input type="checkbox"/>	<input type="checkbox"/>	Modify/Show for R3...

P-Delta Parameters

Advanced...

OK

Cancel

Figure 8-6, General setting window to define the SDOF links (CSI. 2018)

The analyzes of the various components are performed in different simulations. As for the BSCs, being their buildings, only the input file of the building portfolio layer of the Ideal City is updated. Once this was done using the work by Marasco and Cimellaro (2018) it was possible to obtain the results and consequently then

the level of damage to the buildings for the various case studies. While for the support towers of the BTS another input file has been created for the simulations. Each link element has been assigned the physical properties of the tower it represents. *Figure 8-6* illustrates the definition of the link elements. As a first step, the type of link element is defined, after which the equivalent mass calculated with the physical model is assigned and finally the elastic and plastic properties are set only for the directions that simulate the horizontal response of the structure to the external action. For this reason, since the towers are elements with double symmetry, it is sufficient to set the elastic-plastic parameters in a single horizontal direction U1, as the results would be the same in the other direction. The other DOFs are fixed. *Figure 8-7* shows the screen for setting the elastic and plastic parameters for the DOF selected to evaluate the response for the towers. It is necessary to fix the stiffness, the damping and the force-displacement relationship, this happens with the parameters determined by the physical model of chapter 6. Finally, it is necessary to select the hysteresis model to simulate the degradation. For towers the kinematic model is a fine model to describe the behave (Madugula 2001). In the case of buildings, the model used is that of Takeda (Marasco and Cimellaro 2018).

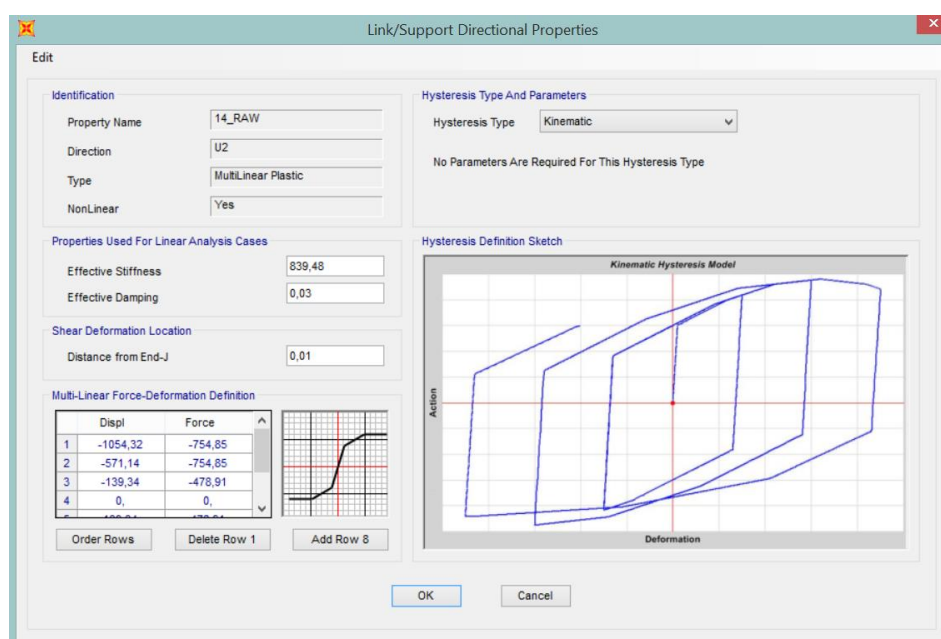


Figure 8-7, Setting physical proprierty window for the SDOF links for the BTS towers

As defined in the previous chapter, a time history function has been associated to each link element based on the distance of the epicenter hypothesized for each scenario within the territory of the Ideal City. Having to available the functions that have been applied to the buildings, what was done for the towers on the ground was to assign the time history function of the building closest to it to the tower. This is to save calculation time as the difference between the exact function and the one assigned to the building is more winey and minimal (*figure 8-8*).

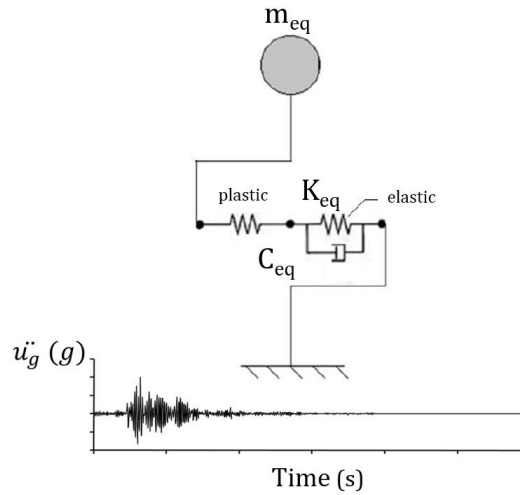


Figure 8-8, schematization of the time history application for rawland towers

Accurate modeling of the seismic amplification effects for a roof mounted tower typically requires a dynamic analysis of the combined tower and building structure to be built. Dynamic analysis methods such as a modal method or a time history of a combined model can be computationally labor-intensive and time-consuming, and often involve high design costs (Azeem and Aliya 2018). FEMA (FEMA 2011) classifies towers as NSE sensitive to seismic action. This means that the action must be countered by non-structural elements anchored to structural elements. A simplified procedure, it is that to consider the telecommunications towers of the non-structural elements (NSE) for buildings by modifying the seismic action by means of a multiplicative factor (*figure 8-9*).

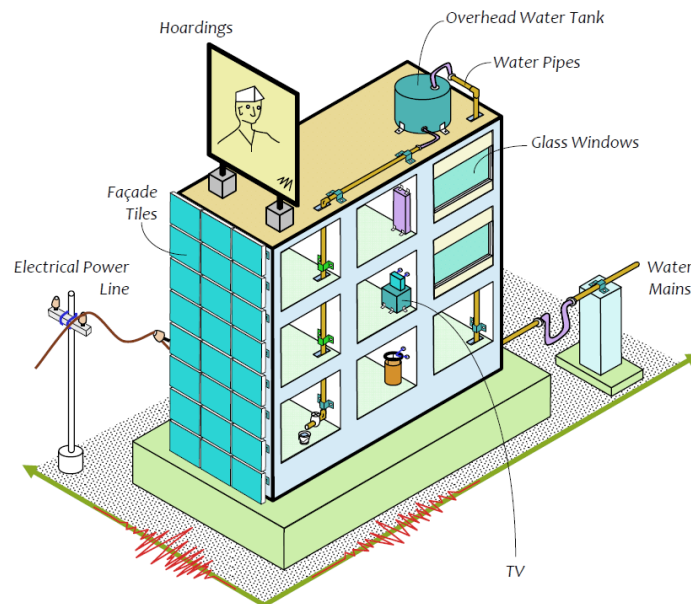


Figure 8-9, illustration of some NSE considered for a building (Murty, Goswami et al. 2012)

In specific condition, the NSE with specific characteristics should be studied in detail to understand if the mass and the level of connection between the NSE

element and the structural element (SE) becomes increasingly rigid. If this happened, then the NSE element would begin to influence the response of the structural element (SE) to which it is connected and consequently of the entire structure (Murty, Goswami et al. 2012). In this work, being an urban-scale study, the use of the simplified method with the amplification factor is widely accepted. So, to consider the effect of the motion of the building on the NSE, an acceleration amplification factor can be applied to the seismic action. The case of the building with the tower is decomposed into two sub-problems. One, that studies the behavior of the building considering it without a tower. The second one that studies the behavior of the tower without the interaction of the building by modifying only the input of the seismic action at the base of the tower. (Figure 8-10).

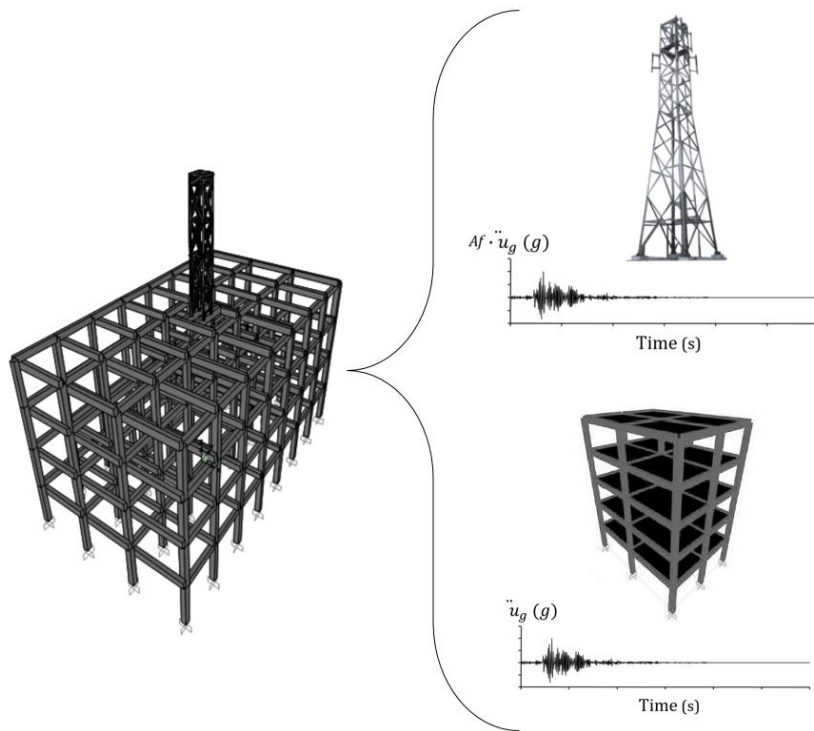


Figure 8-10, decomposition of the structure into the structural and non-structural component

There are various approaches to define the amplification factor, for example (Assi 2006) proposes an amplification factor that depends on the period of the building. Or (Azeem and Aliya 2018) proposes an amplification factor that depends on the relationship between the period of the tower and that of the structure. In accordance with the provisions of Eurocode 8 (Eurocode 2004), the amplification factor is determined through *equation 8-2*. This equation allows to obtain the amplification factor for any level of the building.

$$A_f = \frac{3 \cdot \left(1 + \frac{x}{h}\right)}{1 + \left(1 - \frac{T_t}{T_b}\right)} - 0,5 \quad (8-2)$$

Where,  $A_f$  is the amplification factor for the ground accelerations,  $h$  is the height of the building,  $x$  is a variable along the height of the building,  $T_t$  is the e fundamental vibration period of the tower,  $T_b$  e fundamental vibration period of the building (known from the building portfolio layer). Therefore, the acceleration on the roof is given by the product between the amplification factor  $A_f$  and the acceleration on the ground  $\ddot{u}_g(t)$ .

$$\ddot{u}(t)_{rooftop\ tower} = A_f \cdot \ddot{u}_g(t) \quad (8-3)$$

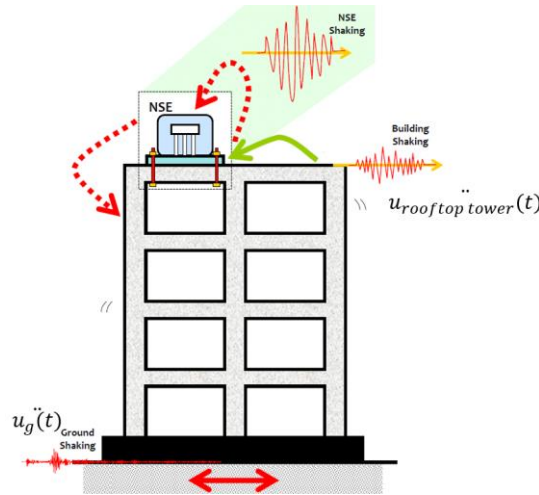


Figure 8-11, Various vibrations and interactions between SEs and NSE (Murty, Goswami et al. 2012)

Figure 8-12 illustrates the concept applied in the analysis of towers on roofs using the link element SDOF, subject to a time history modified by the amplification factor.

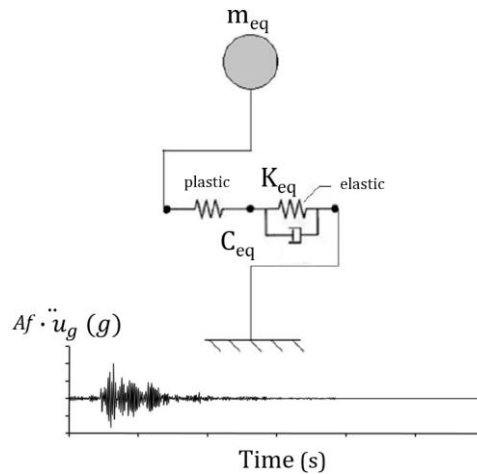


Figure 8-12, schematization of the time history application for rooftop towers

Both buildings and towers are analyzed in the two horizontal directions. Then, the absolute maximum top displacements of each link element in each direction are estimated. Finally, the absolute maximum displacement is considered as a seismic demand. *Figure 8-13* shows an example of the moving history for a rawland tower in the Northridge scenario. While *figure 8-14* shows the SAP2000 output table for the maximum and minimum top displacements for rawland towers.

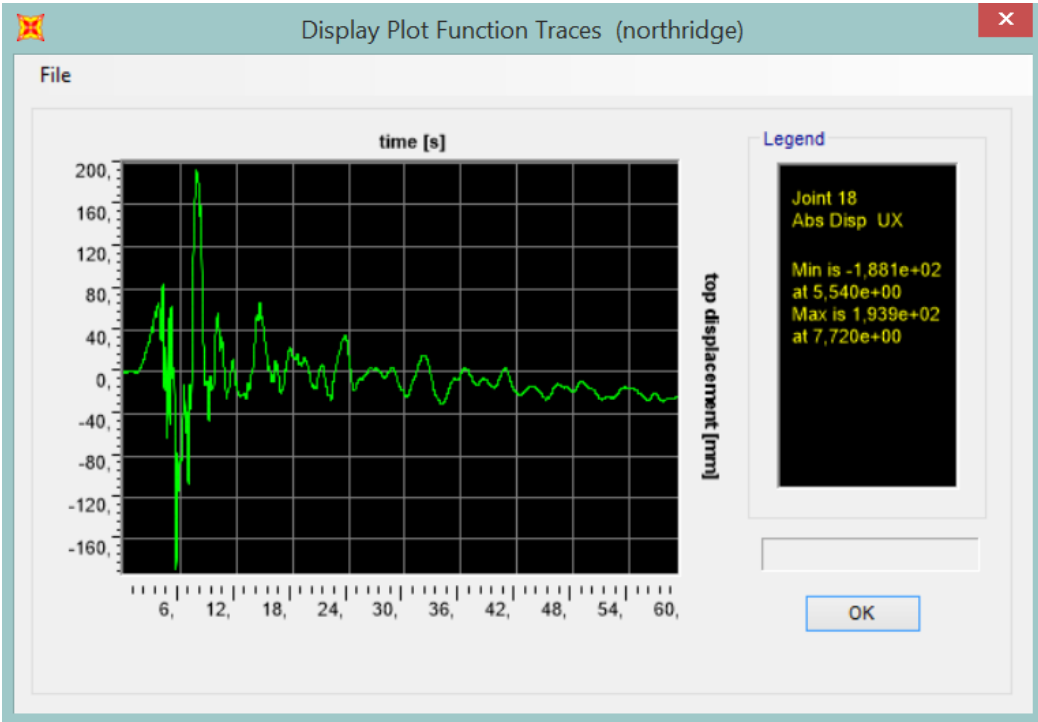


Figure 8-13, examples of the history of top displacement for a link element that represents a rawland tower in the Northridge case

Figure 8-14 is a screenshot of the 'Joint Displacements - Absolute' window. It displays a table with columns for Joint Text, OutputCase, CaseType Text, StepType Text, U1 mm, U2 mm, U3 mm, R1 Radians, R2 Radians, and R3 Radians. The table lists data for joints 1 through 8, each with maximum and minimum values for three directions (U1, U2, U3). The values are in millimeters (mm) for displacements and radians for rotations. The window includes a menu bar (File, View, Edit, Format-Filter-Sort, Select, Options), a status bar (Record: 1 of 690), and buttons for 'Add Tables...' and 'Done'.

Joint Text	OutputCase	CaseType Text	StepType Text	U1 mm	U2 mm	U3 mm	R1 Radians	R2 Radians	R3 Radians
1	northridge	NonModHist	Max	188,936138	0	0	0	0	0
1	northridge	NonModHist	Min	-132,355907	0	0	0	0	0
2	northridge	NonModHist	Max	189,19035	0	0	0	0	0
2	northridge	NonModHist	Min	-155,811655	0	0	0	0	0
3	northridge	NonModHist	Max	192,799843	0	0	0	0	0
3	northridge	NonModHist	Min	-182,201575	0	0	0	0	0
4	northridge	NonModHist	Max	188,941361	0	0	0	0	0
4	northridge	NonModHist	Min	-133,738825	0	0	0	0	0
5	northridge	NonModHist	Max	190,996154	0	0	0	0	0
5	northridge	NonModHist	Min	-172,378462	0	0	0	0	0
6	northridge	NonModHist	Max	45,239451	0	0	0	0	0
6	northridge	NonModHist	Min	-47,297107	0	0	0	0	0
7	northridge	NonModHist	Max	188,936138	0	0	0	0	0
7	northridge	NonModHist	Min	-132,355907	0	0	0	0	0
8	northridge	NonModHist	Max	188,936138	0	0	0	0	0
8	northridge	NonModHist	Min	-132,355907	0	0	0	0	0

Figure 8-14, view example of the window with the top absolute maximum and minimum displacement for direction 1 for the rawland towers



## 8.3 Damage Level for the Buildings

For the buildings of the virtual city once known the absolute maximum displacement in the head. It must then be converted into the maximum inter-story drift which allows to better characterize the responses of the building. That is, this conversion involves the passage from the global response (SDOF) to the local response (MDOF) through a simplified response model. This model is based on the definition of the lateral displacement distribution which identifies the response of the MDOF system which is evaluated as the sum of an elastic and plastic contribution. These contributions are defined starting from the elastic displacement  $u_{top,e}$  (given by the average capacity curve) and from the plastic displacement  $u_{top,p}$  (equal to the maximum top displacement recorded with the equivalent SDOF model). Once the distribution of displacements for the MDOF (the detailed model for the building) system is known, the maximum inter-story drift of the building itself is obtained. *Figure 8-15* shows an illustrative example of the estimation of the lateral absolute displacement distribution based on the calculated top displacement (Marasco and Cimellaro 2018).

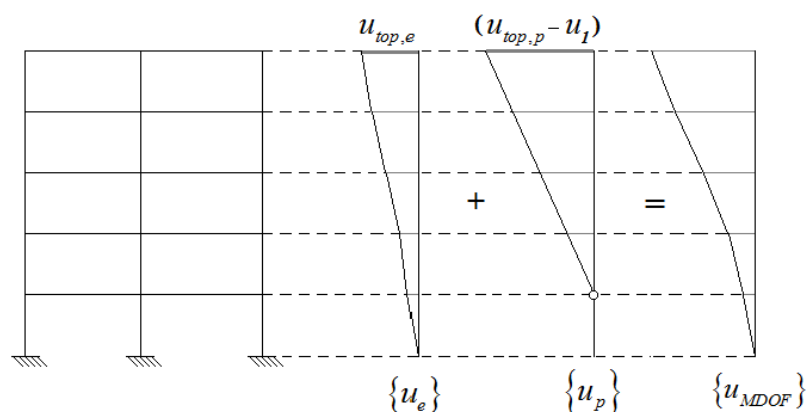


Figure 8-15, Elastic and plastic displacements distributions (Marasco and Cimellaro 2018)

When the maximum absolute inter-story drift is identified, it is compared with the thresholds values of inter-story drift proposed by Ghobarah (2004) to assess the damage level (*table 8-1*) (Marasco and Cimellaro 2018).

Damage State	Ductile MRF	Nonductile MRF	Ductile Walls	Nonductile Walls
No damage	<0.2%	<0.1%	<0.2%	<0.1%
Slight	0.4%	0.2%	0.4%	0.2%
Moderate	<1.0%	<0.5%	<0.8%	<0.4%
Extensive	1.8%	0.8%	1.8%	0.7%
Complete	>3.0%	>1.0%	>2.5%	>0.8%

Table 8-1, Threshold values of inter-story drift proposed by Ghobarah (2004) (Marasco and Cimellaro



Finally, the fragility curves in terms of PGA have been derived based on the threshold of inter-story drifts proposed by Ghobarah (2004). Figure 8-16 summarizes the process to define a damage level for the buildings of the Ideal City.

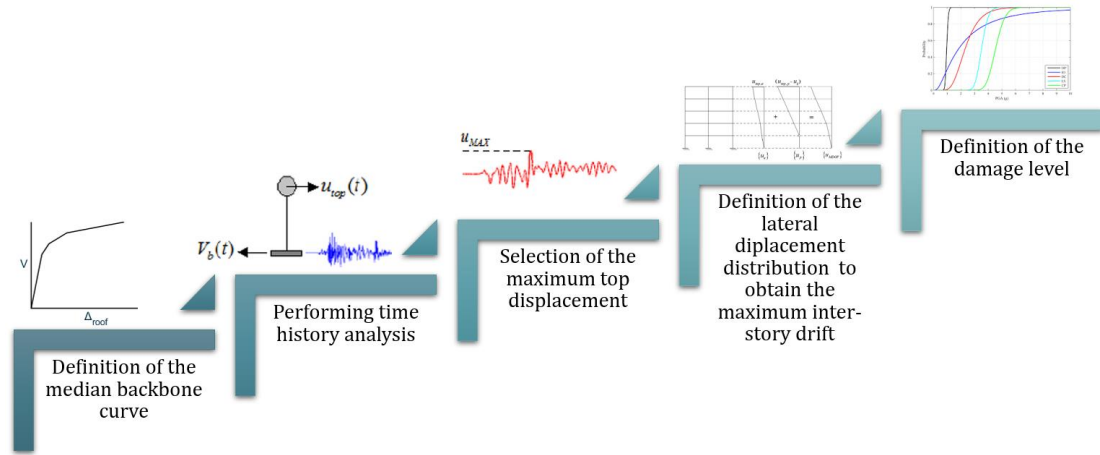


Figure 8-16, procedure proposed by (Marasco and Cimellaro 2018) to assess the damage to the buildings of the Ideal City

## 8.4 Damage Level for the BTS

In the case of the BTS support towers, contrary to what happened for the buildings, no works have been found in the literature that led to the definition of seismic fragility curves for them. This is since the telecommunication towers are more exposed to damage due to the action of the wind than the earthquake. In this work there was no possibility to develop seismic fragility curves for the towers, that's because the time required would have been excessive. For these reasons, the simplified procedure proposed by (Cimellaro, Domaneschi et al. 2017) for RC buildings was adopted for the definition of damage levels for the towers. This method involves defining the damage level on an urban scale using the characteristic points of the structure's capacity curve. It is certainly a simplification method, but at the same time it leads to reliable results, in favor of safety and there is a saving of calculation time. A criterion based on the deformation of the structure is used. Having defined the top displacement as the output value from the time history analysis, it makes the evaluation more immediate. Therefore, if the tower remains in the linear field it does not suffer damage, after which in the non-linear field, based on the displacement that is recorded, the structure can suffer slight, moderate or severe damage. Finally, if the structure exceeds the ultimate displacement defined through the simplified physical model of chapter 6, then the tower is considered to have suffered complete damage. Figure 8-17 summarizes the concept proposed by (Cimellaro, Domaneschi et al. 2017) for the definition of damage levels.

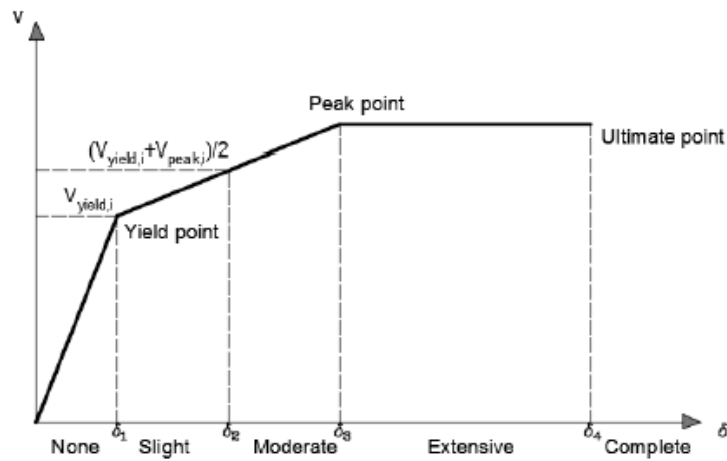


Figure 8-17, definition of damage levels for towers based on the capacity curve (Cimellaro, Domaneschi et al. 2017)

Damage State	top displacement $\delta_{top}$
No damage	$\delta_{top} < \delta_1$
Slight	$\delta_1 < \delta_{top} < \delta_2$
Moderate	$\delta_2 < \delta_{top} < \delta_3$
Extensive	$\delta_3 < \delta_{top} < \delta_4$
Complete	$\delta_{top} > \delta_4$

Table 8-2, Damage criteria for the towers

Figure 8-18 summarizes the process to define a damage level for the telecommunication network towers.

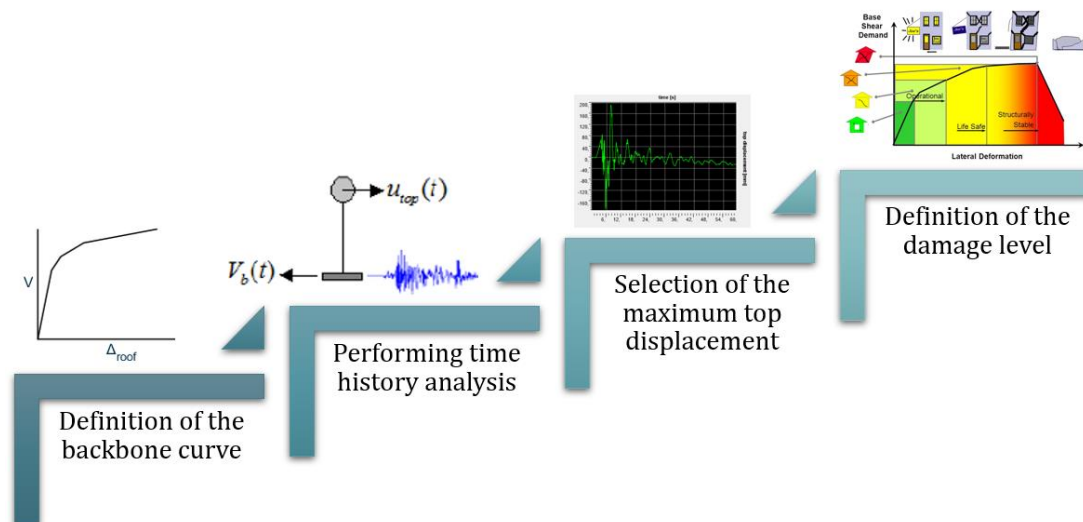


Figure 8-18, procedure proposed to assess the damage to the telecom towers of the Ideal City

## 9 Resilience Indices and Case Studies

### 9.1 Introduction

The objective of this work as stated in the introductory chapter is to try to assess the vulnerability of the communication infrastructure at the urban level to disastrous events. However, defining the vulnerability of a wireless communication network is a challenging task due to the large number of components and structures involved. In the literature there are few studies related to this enterprise, mainly because the networks are privately managed, making it difficult to find information. In fact, as we have seen in the previous chapters, many simplifying hypotheses have been introduced to characterize the various components of the network. The only proof of failure occurs after natural disasters. In many cases, the main reason for failures is due to various design errors, such as installing a BTS on an extremely vulnerable buildings (Travanca, Varum et al. 2013). As will be seen in the following paragraphs, different vulnerability indices will be introduced based on simple parameters such as the number of BTS out of service. Subsequently, in the second part of the chapter, the results obtained from some simulations carried out on the network in seismic events with different characteristics will be illustrated. All results of the simulations are made using one of the central server of the resilience lab of the DISEG department in Polytechnic of Turin.

### 9.2 Resilience Indices

In the literature no indices have been found that assess the vulnerability of a wireless network at urban level. For this reason, various indices are defined which allow to evaluate the robustness of the network. These indexes make it possible to assess the vulnerability of the physical part of the network quickly and easily, and of the quality of the service. These indices are then tested in different case studies later.

#### 9.2.1 BTS Towers Resilience Index ( $R_{\text{TOW}}$ )

The first index concerns the physical part of the network, and in particular the BTS towers that allow users to connect to the network. The BTS towers resilience

index ( $R_{TOW}$ ), it can be defined through the ratio between the BTS that still working after the event ( $N_{t,f}$ ) and the total BTS of the network in conditions of normal activity ( $N_t$ ) and the *equation 9-1* shows its.

$$R_{TOW} = \frac{N_{t,f}}{N_t} \quad (9-1)$$

Where, the number of functioning towers ( $N_{t,f}$ ) is given by *equation 9-2*.

$$N_{t,f} = N_t - N_{t,out} \quad (9-2)$$

Where,  $N_{t,out}$  is the number of towers out of order for the MNO network. A tower can be out of service for several reasons not just structural damage. *Figure 9-1* illustrates the various reasons that can lead to a rooftop BTS being out of service. While *Figure 9-2* illustrates the various reasons that can lead to a rawland BTS being out of service.

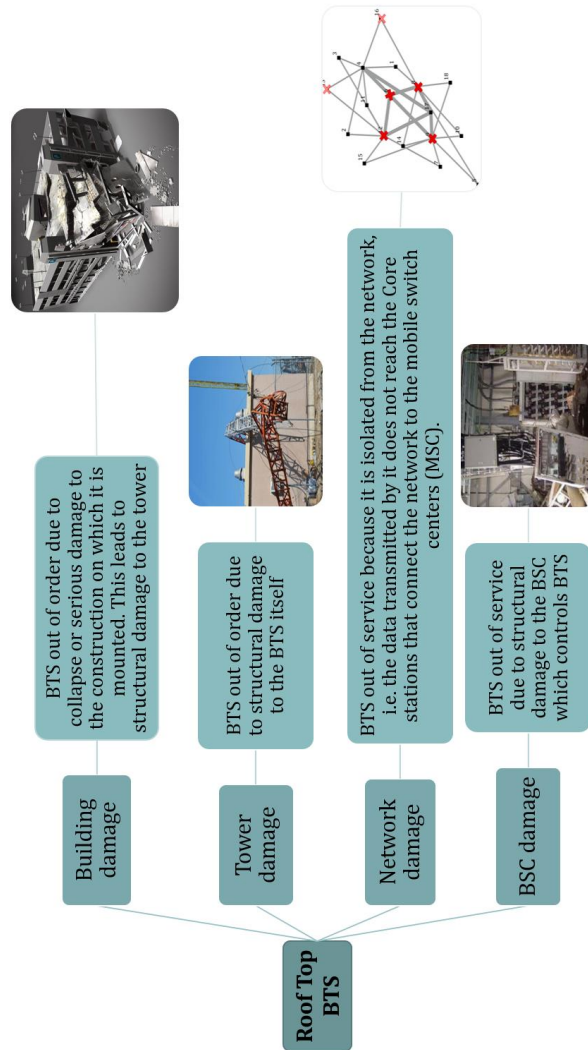


Figure 9-1, outline of the possible scenarios that can take a rooftop BTS out of service

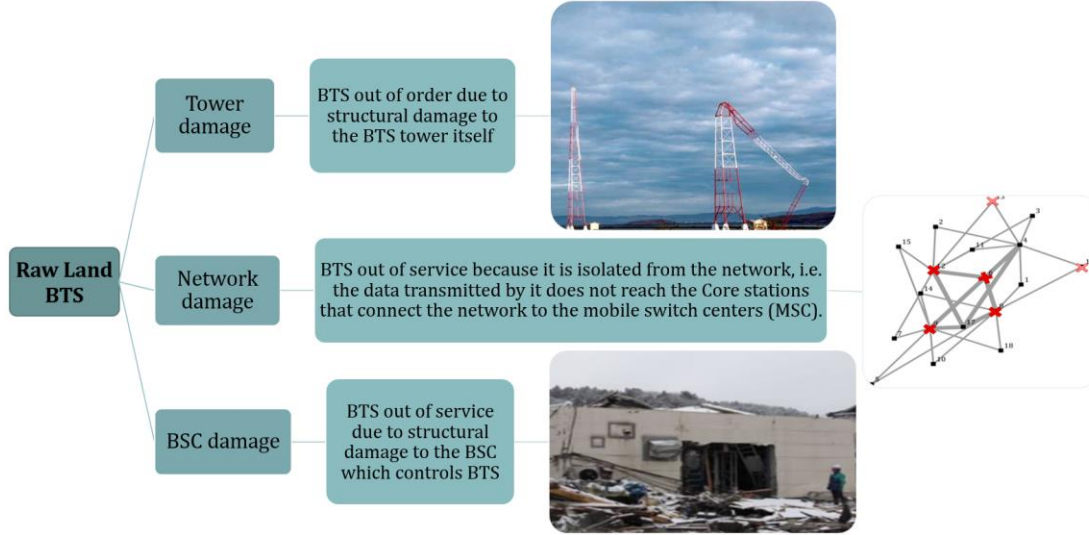


Figure 9-2, outline of the possible scenarios that can take a rawland BTS out of service

$R_{TOW}$  is a resilience index relative to the physical damage of the network. It allows you to quickly evaluate the robustness of the network. As a value close to 1 indicates that the network is robust, while low values indicate that strategic measures should be taken to increase robustness. This metric could be associated with an economic loss due to repair, replacement and downtime costs causing lost profits for companies. Typically, the more redundant the network, the more likely it is to get a high  $R_{TOW}$ . However, in large-scale networks, if many towers collapse, the economic loss could still be substantial and should be considered. A reliable solution would be to install the BTS on low vulnerable buildings identified during the design phase of the network in order to make the network more robust, as well as design the buildings that house the control stations with a low vulnerability to disasters.

### 9.2.2 Throughput Resilience Index ( $R_{THR}$ )

The second proposed resilience metric ( $R_{THR}$ ) is related to the quality of service. It therefore evaluates the difference in the quality of the service offered to users by each MNO between the condition of normal operation and post-disaster. The  $R_{THR}$  is calculated as the ratio between the post and pre-disaster weighted mean throughput ( $\langle THR \rangle$ ) (equation 9-3).

$$R_{THR} = \frac{\langle THR \rangle_{post-disaster}}{\langle THR \rangle_{pre-disaster}} \quad (9-3)$$

The throughput as detailed in Chapter 5 is calculated for each pair cluster user-BTS. Then to each cluster is assigned the best throughput available. Consequently, it is also known with which BTS the cluster connects. This is a purely theoretical

procedure in accordance with what is proposed by (Di Francesco, Malandrino et al. (2017)), as in reality it may happen that the user at a given moment does not connect to the BTS which in theory offers the best throughput for traffic issues at that given moment. In this work, not having available data on data traffic, the hypothesis of the best throughput for each cluster was therefore assumed. After that, to avoid any bias due to variance in throughput, the obtained values were weighted by the number of users in each cluster as shown in *equation 9-4*.

$$\langle THR \rangle = \frac{\sum_{i=1}^{nc} N_{UE,i} \cdot THR_i}{N_{UE}} \quad (9-4)$$

where:  $N_{UE,i}$  is the number of users in each cluster,  $nc$  is the number of clusters,  $THR_i$  is the highest throughput for the  $i$ -th cluster,  $N_{UE}$  is the total number of users served by the considered MNO. Low values of  $R_{THR}$  imply that the event causes a significant loss in the quality of the service, meaning several users experiencing slow data transfer. Considering the best throughput value obtained for each user cluster, it is possible to calculate the number of users per BTS. This is only a theoretical representation since depending on the actual demand and traffic, users might connect to other BTSs and have lower throughput. However, the number of users served by each BTS could be used as an indicator of critical conditions. If the  $R_{THR}$  index value is close to 1 then it means that the user clusters have substantially the same quality of service as they had before the disaster. This means having a greater possibility and speed to be able to communicate with the emergency services as the networks are not congested. On the contrary, when it tends to zero it can mean that the cluster is very far from the first free BTS and therefore it will have a weak signal so communication will need more time. Or it is in the case in which many BTS are out of service and the remaining suffer a peak of users which requires time for its management.

### 9.2.3 Serviced Clusters Resilience Index ( $R_{UE-BTS}$ )

The third index is defined through the number of users served by each BTS ( $R_{UE-BTS}$ ). As previously mentioned, it can be defined as an index for assessing the level of grid saturation in post-disaster emergency conditions. This is because the BTS associated with the user cluster takes place on the basis of the best throughput and not of the real traffic condition that can occur after a disaster, not having available, as mentioned, any data traffic recording. The index ( $R_{UE-BTS}$ ) is defined as the ratio of the average number of post-disaster and pre-disaster users for BTS ( $\langle UExBTS \rangle$ ), as shown in *equation 9-5*.

$$R_{UE-BTS} = \frac{\langle UE \times BTS \rangle_{post\ disaster}}{\langle UE \times BTS \rangle_{pre\ disaster}} \quad (9-5)$$

If you have a lot of BTS with several users to manage above a physical limit set by the technology, then surely the clusters managed by that BTS will suffer delays or loss of signal for communication. This affects the management of relief for example. By its definition,  $R_{BTS} > 1$  indicates that the load on the infrastructure has increased. In case of extreme events,  $R_{BTS}$  can assume values much greater than 1. While when its value is less than 1 then it means that the network is working with a safety margin to guarantee each cluster of users the best possible connection for them.

### 9.3 Application to the Study Cases and Validation of Resilient Indices

The proposed procedure with the various indices to assess resilience is tested on the wireless communication network of the Ideal City that has been built. To test the network's response to disastrous events, four seismic events that have marked world seismic history were chosen as input scenarios using Opensignal software (Cimellaro and Marasco 2015). They are the Northridge seismic event (Imar County Hospital parking lot in Sylmar, California, USA), the Kobe earthquake (Kobe Japanese Meteorological Agency station, Japan), the El Centro earthquake (Imperial Valley Irrigation District substation, California, USA), and the seismic scenario of Hachinohe (Hachinohe City, Japan). Northridge and Kobe records represent near-field earthquakes, whereas El Centro and Hachinohe are examples of far-field seismic scenarios. Once a seismic scenario is defined, a pair of horizontal orthogonal acceleration time histories have been applied to the components of the network and to the built environment by considering the geometrical attenuation.

#### 9.3.1 Characteristics of the four scenarios of the study cases

	El Centro	Kobe	Hachinohe	Northridge
Date	5/18/1940	1/17/1995	5/16/1968	1/17/1994
Region	Imperial Valley	Hyogoken Nanbu	Tokachi-oki	California
$M_w$	6.9	6.8	8.2	6.7
Depth [km]	16.00	17.60	26.00	11.30
PGA [g]	0.35	0.82	0.23	0.84

Table 9-1, Characteristics of the four scenarios selected



Northridge and Kobe records represent near-field earthquakes, whereas El Centro and Hachinohe are examples of far-field seismic scenarios. *Table 9-1* describes the main seismological characteristics of each event.

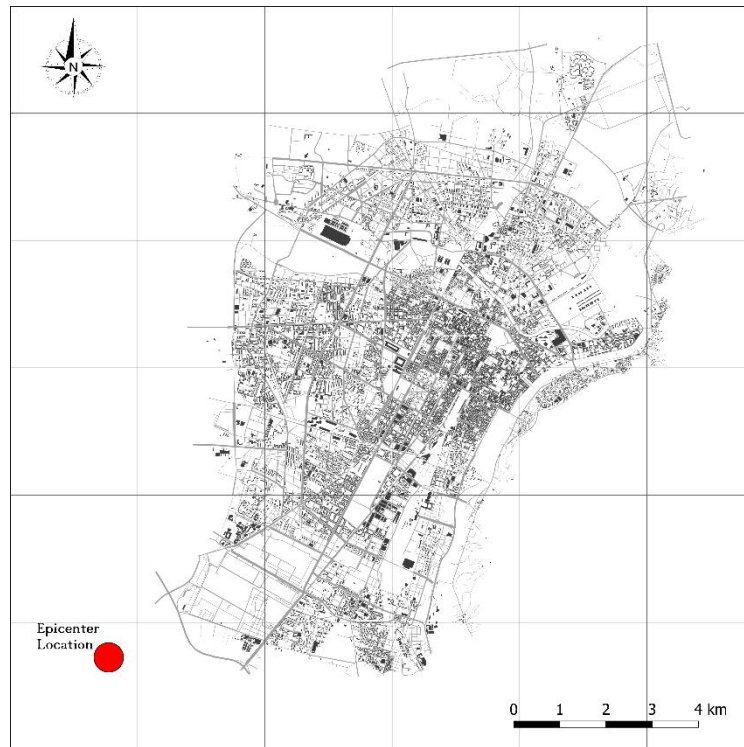


Figure 9-3, localitazion of the epicenter for the simulations

For simulations performed on the Ideal City, the seismic input definition has been set in terms of epicenter location, magnitude, and time history recorded in the epicenter. The epicenter distance associated with the center of gravity of the downtown is 9 km *Figure 9-3*. So, the location of the epicenter remains the same for each scenario, the other input parameters change.

### 9.3.2 Results for the First Scenario: El Centro

The first test field to assess the vulnerability of the Ideal City's telecommunications network was the El Centro scenario. Once the analysis has been performed, the estimate of the damage level of each component is obtained and finally, through a tool with Python code, the virtual city with the damage level of each component can be displayed. *Figure 9-4* illustrates a detail of the virtual city view window with the tool working with Python code. After performing the calculations and defining the damage states, looking at the results it can be seen that about 40% of buildings suffer moderate damage, around 20% suffer slight damage, less than one percent suffer no damage, and finally just under 15% and 30% of buildings suffer extensive or complete damage. The total percentages of

buildings associated with each DS have been calculated and illustrated into the *Figure 9-5*. Also, into *Figure 9-5*, it shows the damage suffered by buildings discretized according to the construction period.

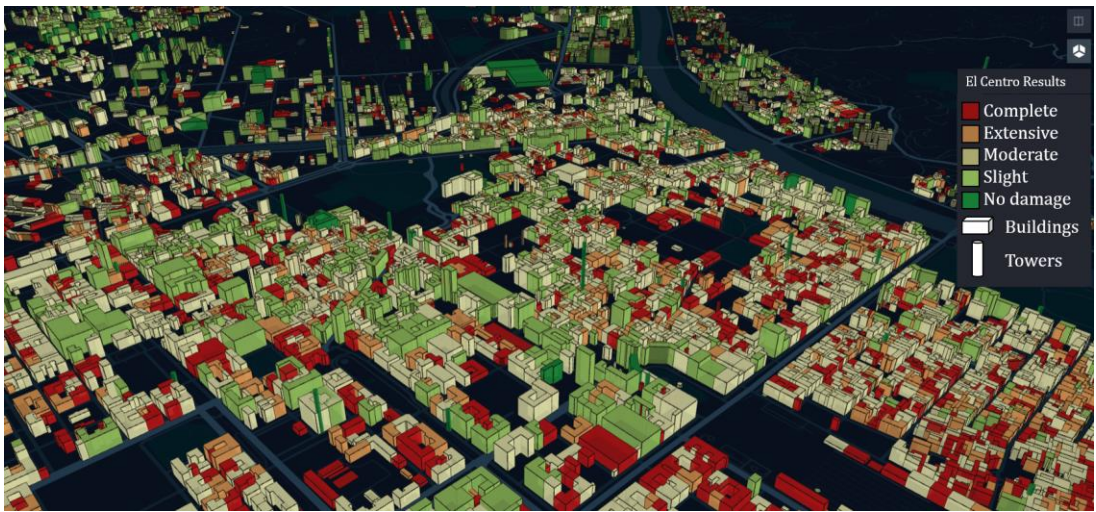


Figure 9-4, 3D damage visualization of the IDEAL CITY downtown after first scenario

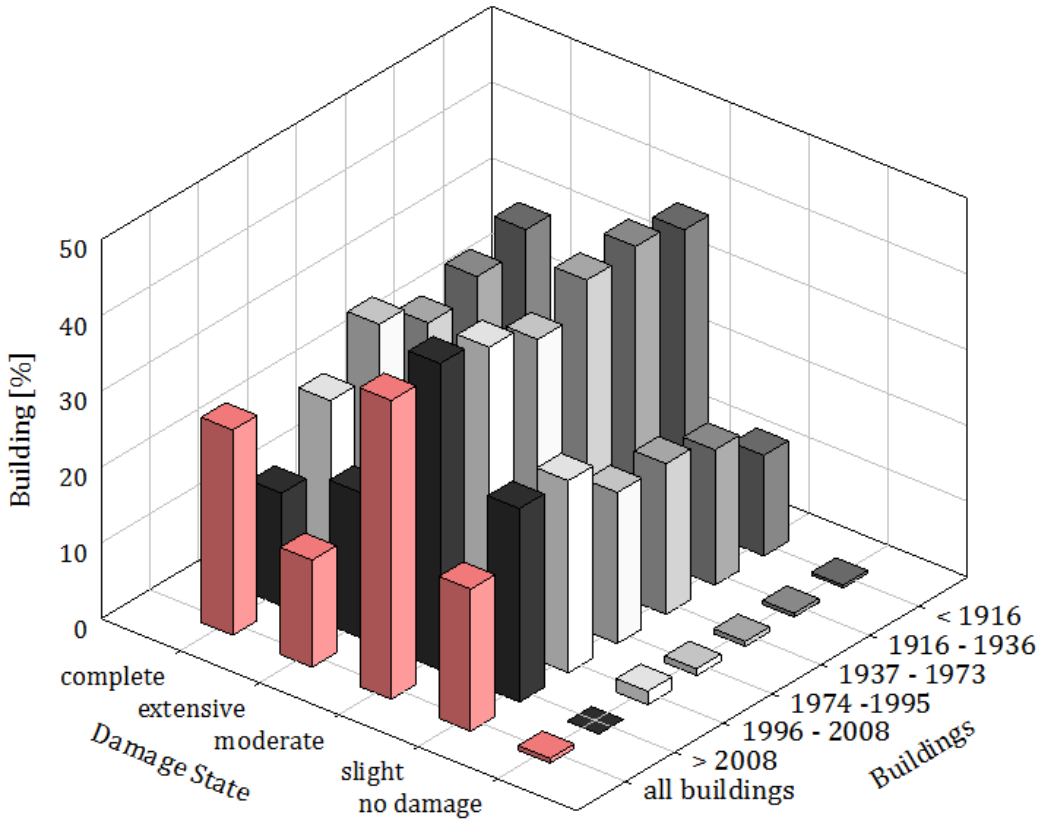


Figure 9-5, damage state for the buildings for the first scenario based on the year of costruction

From *Figure 9-5* it can be seen how the older buildings, therefore those of the category <1916 and 1916-1937, suffer greater damage than more recent buildings. In the city as a whole, the first scenario on the built environment causes minor and moderate damage. It is possible to observe that the highest percentage

of complete and extensive damaged buildings are found in the city center (downtown) and in the older neighborhoods. On the basis of the results obtained from the simulations on the building portfolio, the results concerning the level of damage suffered by the control stations of the telecommunication network (BSC) are obtained (Figure 9-6). A BSC can be considered out of service if it experiences severe structural damage or if it remains isolated from the grid. Regarding the structural damage the BSC is out of order when it suffers a "complete" damage. A BSC, on the other hand, is isolated when it no longer has a route to get to one of the two Core stations. Figure 9-7 shows the BSCs out of service regardless of the reason. It is observed that four BSCs suffer structural damage, while the other four are out of service because they do not have an intact path available to get to the core stations.

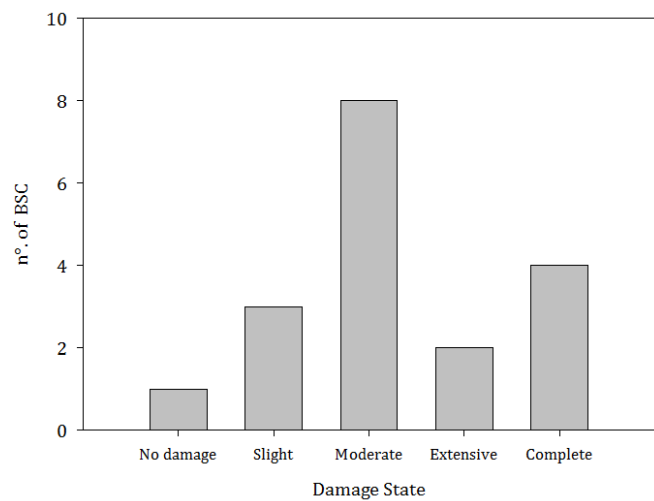


Figure 9-6 BSC' damage distribution within *IDEAL CITY* for El Centro scenario

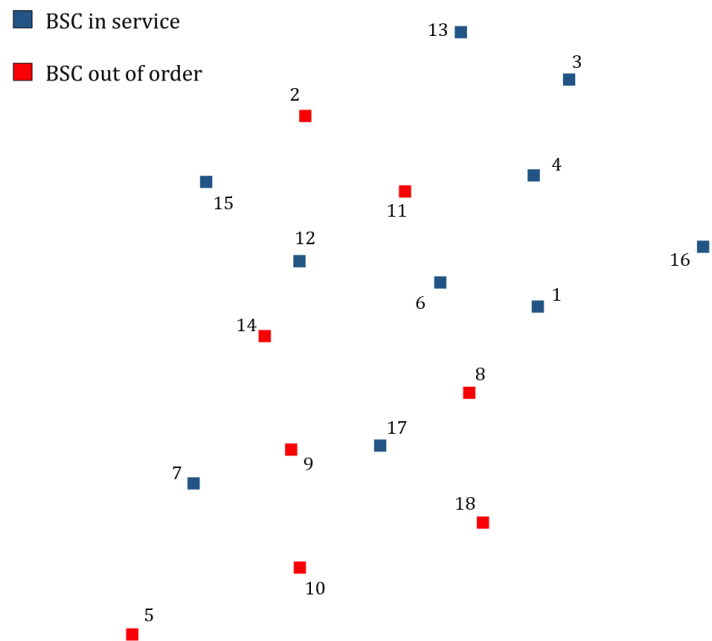


Figure 9-7, BSC state after El Centro scenario

BSC 2, 8, 9, and 11 stations suffer structural damage, while BSC 5, 10, 14, and 18 stations are out of service because they are isolated from the network. This because stations 8 and 9 are Aggregation stations, which also have 5, 10, 14, and 18 between the Edge stations to manage. Once the BSCs were out of service, and the results of the damage levels for the BTSs were known, it was possible to map which BTSs are still in service after the event, and which are not for each MNO. As defined in paragraph 9.2.1, a BTS can be considered out of service not only for structural damage it has suffered, but for various reasons. This concept is illustrated in detail in *Figure 9-8*.

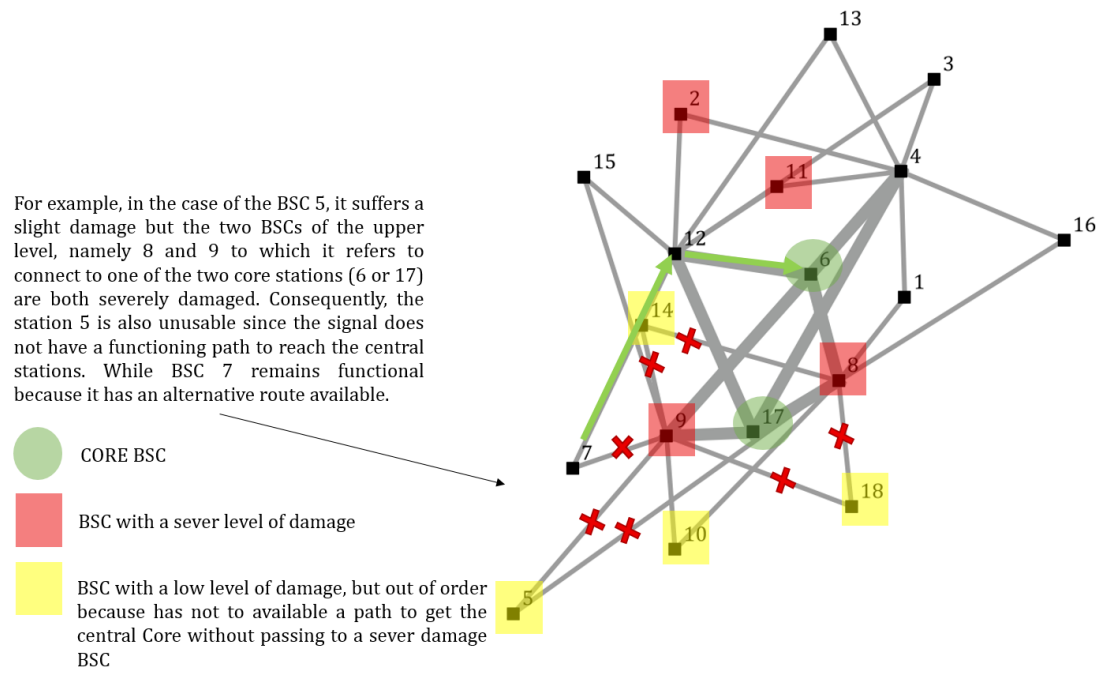


Figure 9-8, concept of why some BSCs are out of order even though their structure suffers minor damage

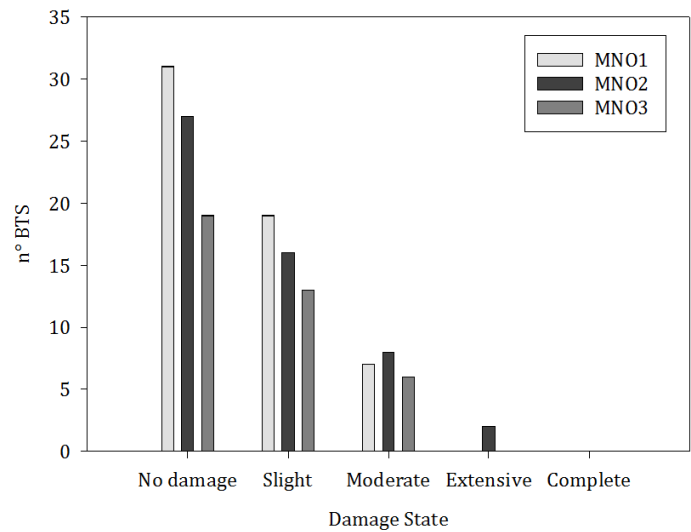


Figure 9-9, Damage State for the Raw land towers for the first scenario

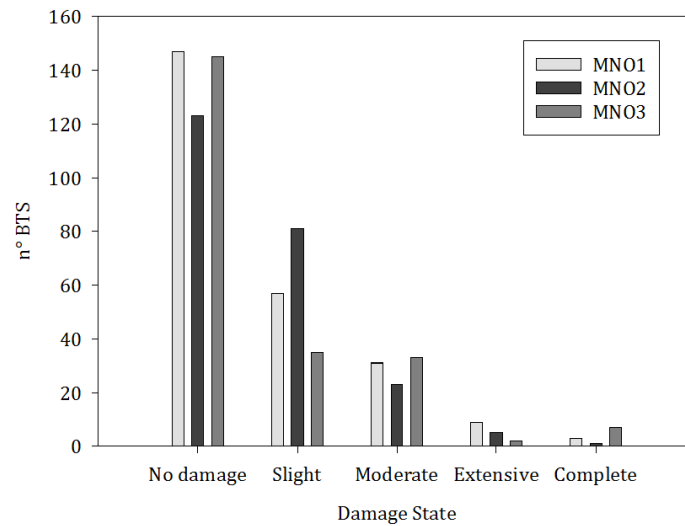


Figure 9-10 Damage State for the Roof top towers for the first scenario

Figure 9-9 and *Figure 9-10* show the results obtained for the damage status of the roof top towers and for the raw land towers. It is immediately observed that the towers that suffer severe structural damage are few units. Towers that undergo "extensive" or "complete" structural damage are considered out of service, because even if the tower does not collapse, excessive displacement overhead can cause misalignments to the antennas.

Figure 9-11 shows the BTS not working for the first MNO, Figure 9-12 shows the BTS not working for the second MNO, and finally, *Figure 9-13* shows the BTS not working for the third MNO.

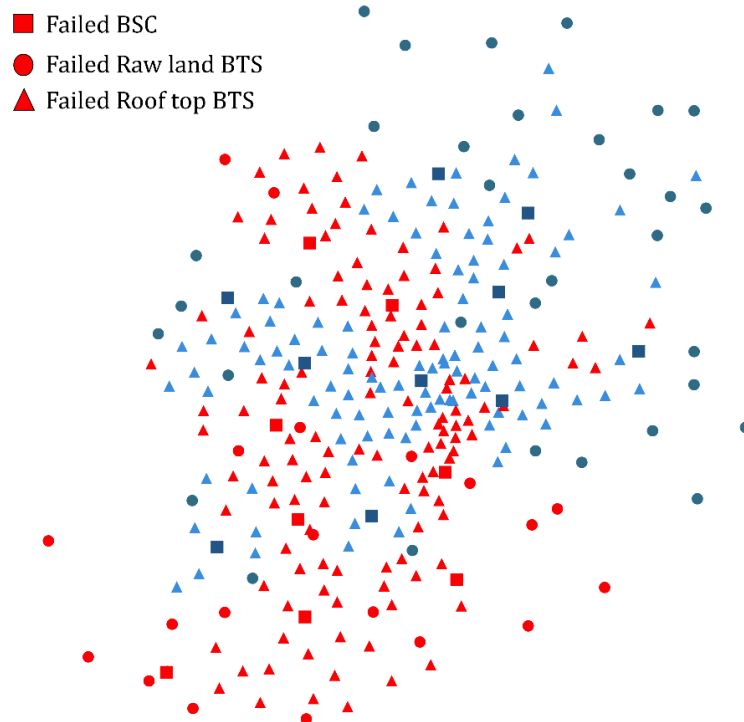


Figure 9-11, BTS out of order for the MNO1 for the first scenario

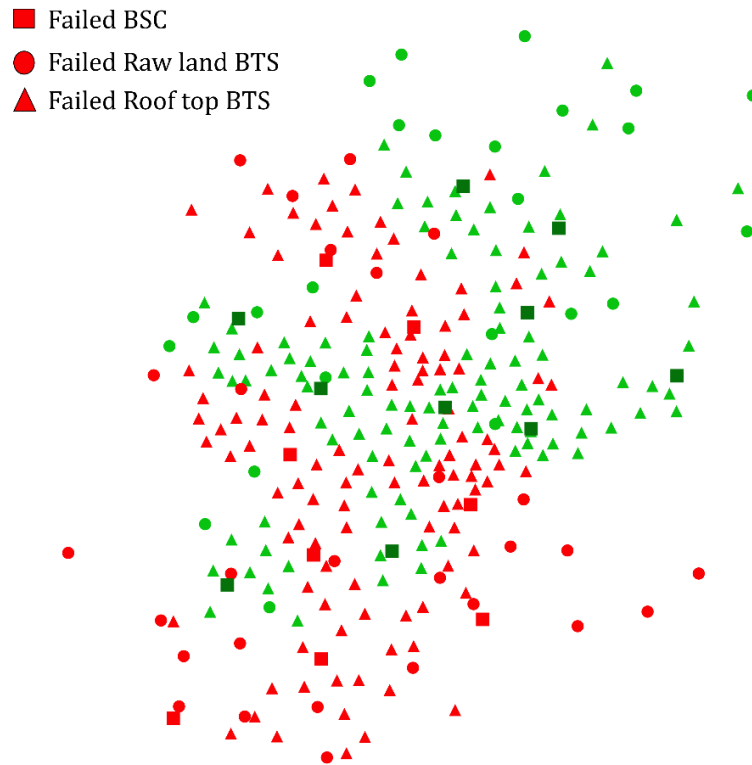


Figure 9-12, BTS out of order for MNO2 for the first scenario

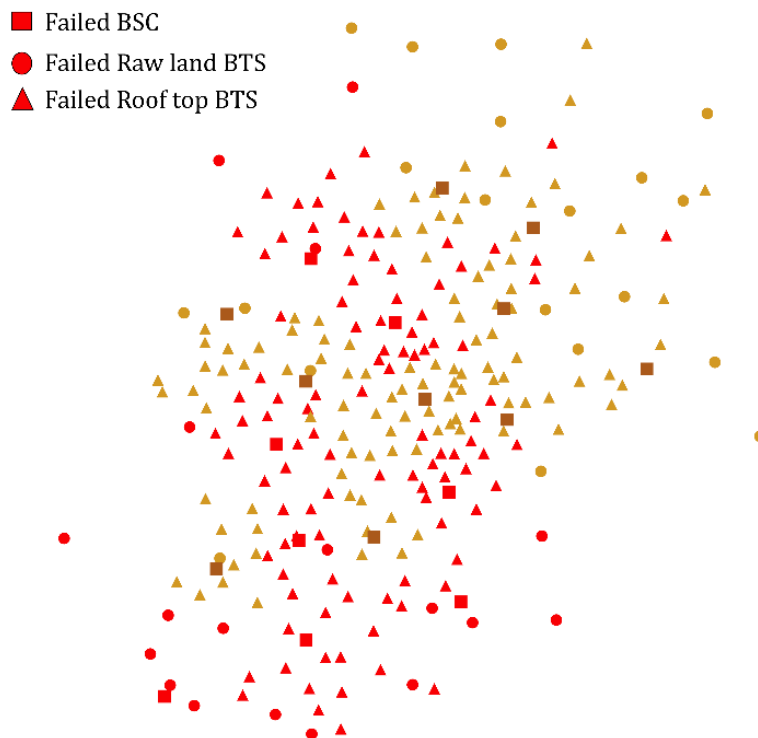


Figure 9-13, BTS out of order for MNO3 for the first scenario

Figure 9-14 summarizes the values for each MNO of the BTS out of order based on the condition leading to the BTS failure.

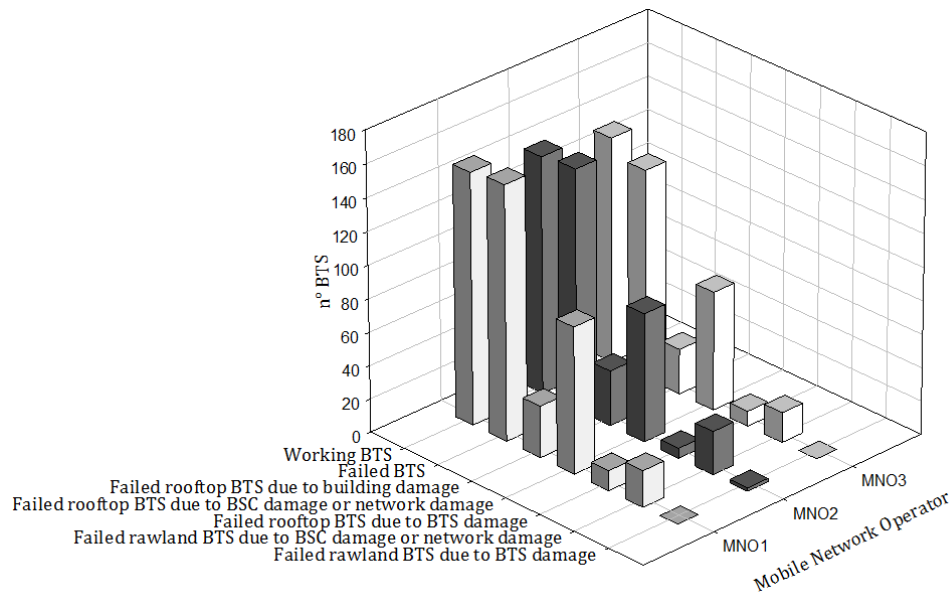


Figure 9-14, abstract of the damaged BTS values for each condition for the first scenario

Therefore, observing the results given by the first scenario, it is possible to notice how little less than half of the BSCs are lost, while just over half of the BTS are in service. The main cause of the non-functioning of the BTS is certainly the damage to the control stations, while it is observed that the structural damage suffered by the towers is very limited to a few cases. Once the BTS out of service after the event are known, the Throughput available for each user cluster can be recalculated.



Figure 9-15, THR value for user cluster given by the first MNO for a portion of Ideal City' downtown after first case scenario



Figure 9-15 reports the throughput of the same portion of the virtual city center that is illustrated in Chapter 5 by Figure 5-25, where throughput is reported under ordinary conditions.

### 9-3-3 Results for the Second Scenario: Kobe

The second test field to assess the vulnerability of the Ideal City's telecommunications network was the scenario due to the Kobe earthquake. Once the analysis has been performed, an estimate of the damage level of each component is obtained and finally, through a tool with Python code, the virtual city with the damage level of each component can be displayed. Figure 9-16 illustrates a detail of the virtual city view window with the tool working with Python code. In terms of damage to the building portfolio, there is a similar trend in case one. Just over 35% of buildings suffer moderate damage, just under 30% of buildings suffer full damage, 9% extensive damage, and finally, buildings that suffer little or no damage are approximately 23% and about 23% respectively. 2%. Figure 9-16 and Figure 9-17 show a 3D view of the damage suffered by the virtual city developed immediately after the Kobe event.

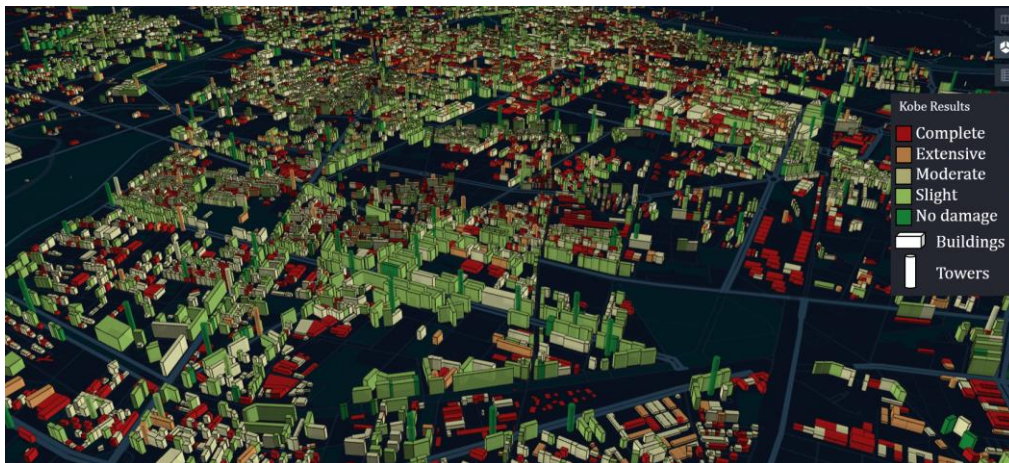


Figure 9-16, 3D damage visualization of the IDEAL CITY downtown for the second scenario



Figure 9-17, 3D damage visualization of the IDEAL CITY for the second scenario

Figure 9-18 summarizes the percentages of buildings damaged by damage status for all buildings and for buildings divided into categories by construction period.

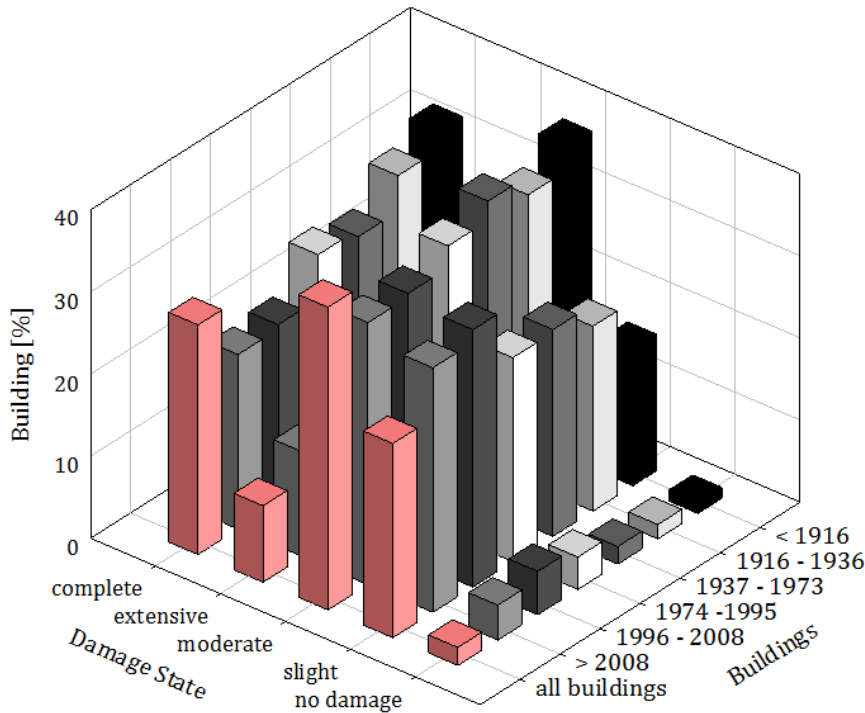


Figure 9-18, damage state for the buildings for the second scenario based on the year of construction

The results on the building portfolio show a general trend in damage levels like the El Centro scenario, but with slightly lower levels of serious damage. As specified in the first scenario after the analysis on buildings the damage levels for the control stations (BSC) can be determined. Figure 9-19 illustrates the number of BSCs based on the damage state.

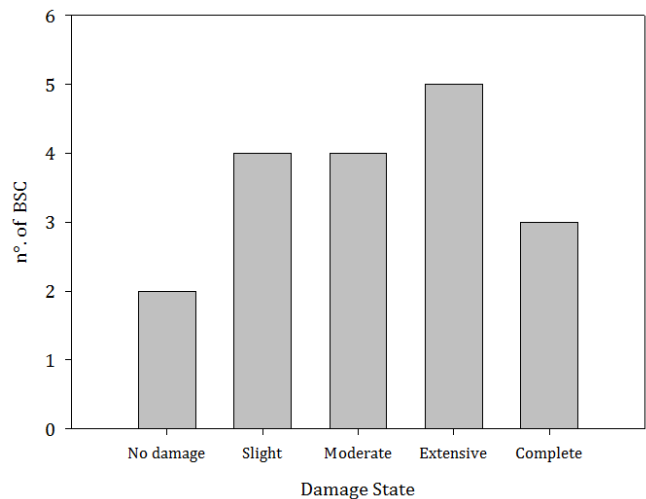


Figure 9-19, BSC' damage distribution within IDEAL CITY for Kobe scenario

Once the damage conditions of the BSCs were known, it was possible to know which stations are out of service and which ones continue to work after the

seismic event. *Figure 9-20* illustrates which BSCs are out of order after the seismic event of the second scenario.

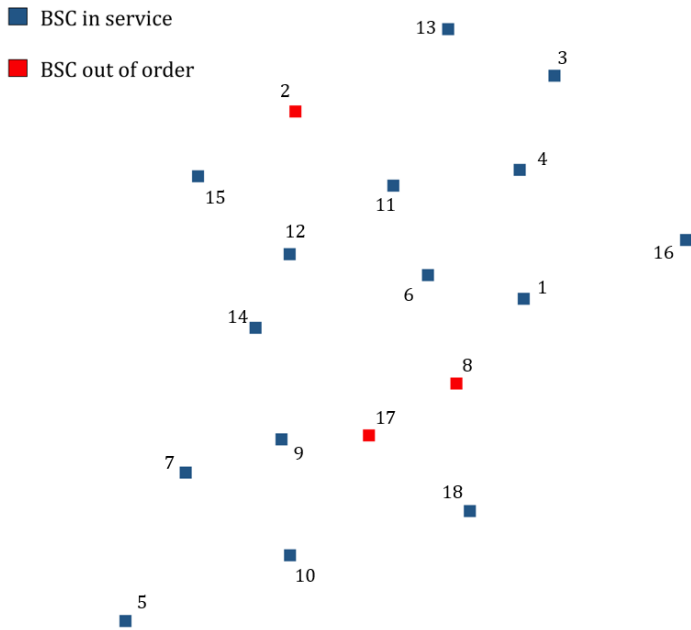


Figure 9-20, BSC state after Kobe scenario

It can be seen from *Figure 9-20* how three stations are out of order, so surely the BTS connected to these BSCs will be useless as the BTS-BSC connection is a "star" type. Once the non-functioning BSCs were known, the non-functioning BTSs were evaluated due to the structural damage that they have suffered. As in the previous case, towers which have an "extensive" or "complete" damage status are considered out of service. This is done, because an excessive displacement but which does not lead to the collapse of the tower can produce a misalignment of the antennas and getting the BTS useless anyway. *Figure 9-21* and show the results obtained for the damage status of the roof top towers and for the raw land towers.

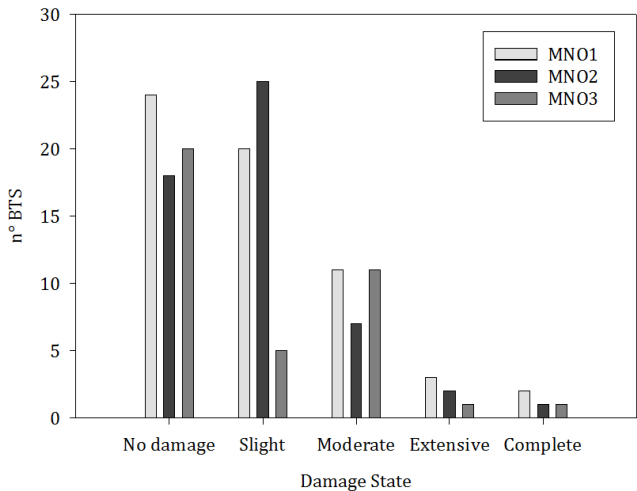


Figure 9-21, Damage State for the Raw land towers for second scenario

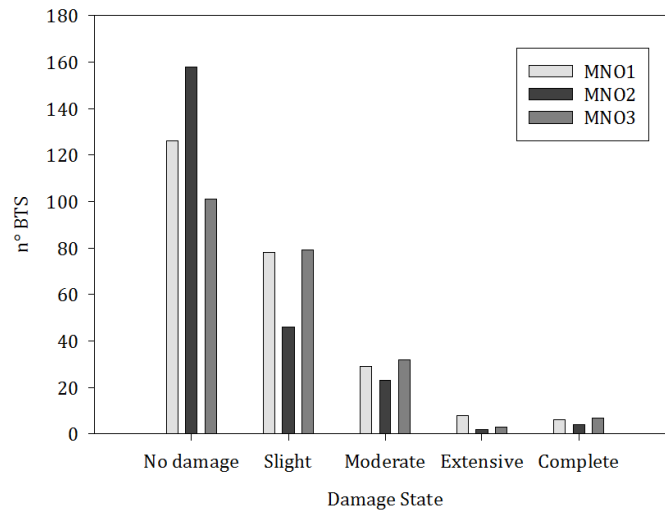


Figure 9-22, Damage State for the Roof top towers for second scenario

At this point it is possible to know the BTS that work even after the event for each MNO for case 2. *Figure 9-23*, *Figure 9-24* and *Figure 9-25* show the BTS that are out of service respectively for the first, second and third MNO.

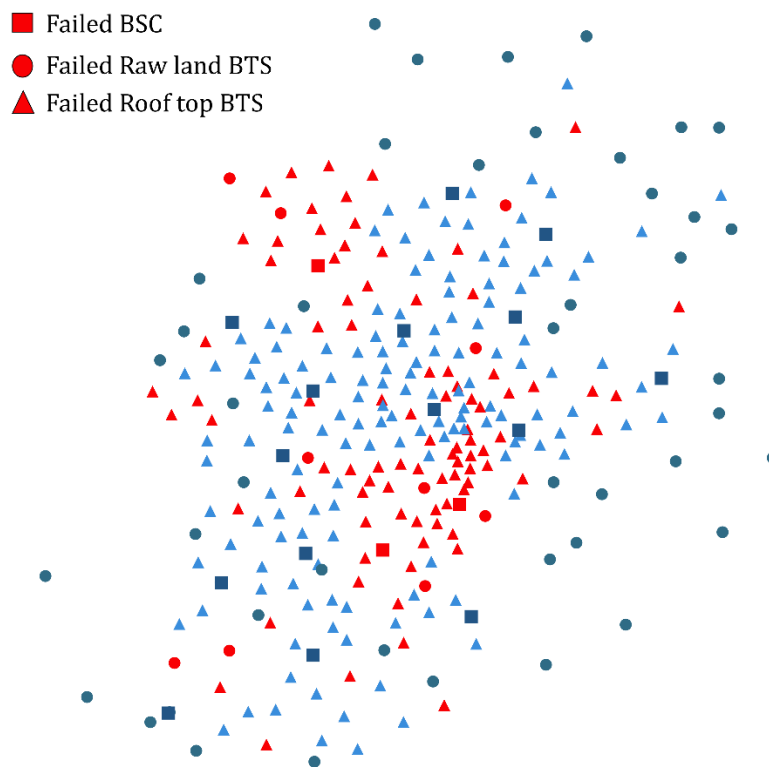


Figure 9-23, BTS out of order for the MNO1 for second scenario

As can be seen from *Figure 9-23* which shows the BTSs out of order for the first mobile network operator (MNO1), most of the BTSs are out of order due to damage to the station that manages the BTS. This means that having a wireless network with stations designed with good anti-seismic standards, this greatly reduces the lost BTS.

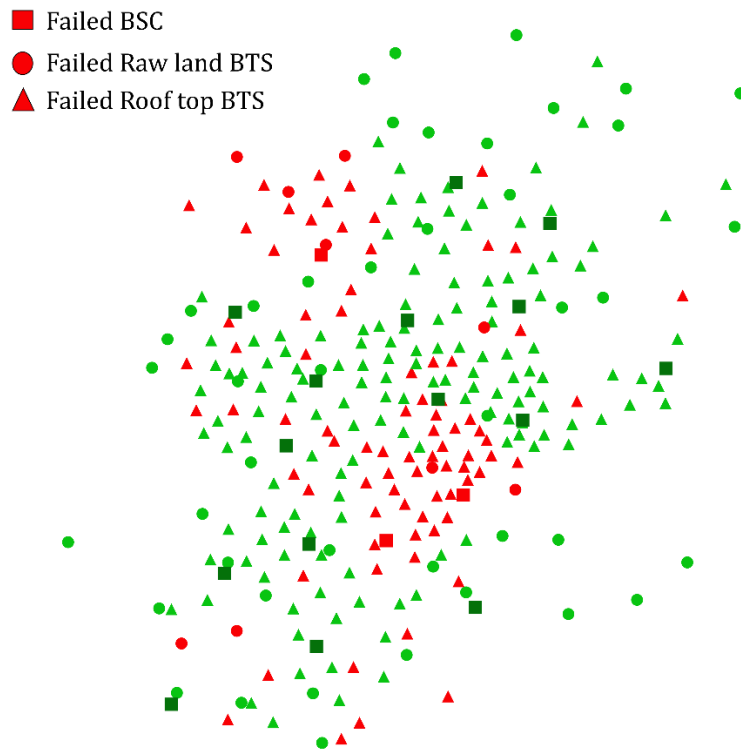


Figure 9-24, BTS out of order for the MNO2 for second scenario

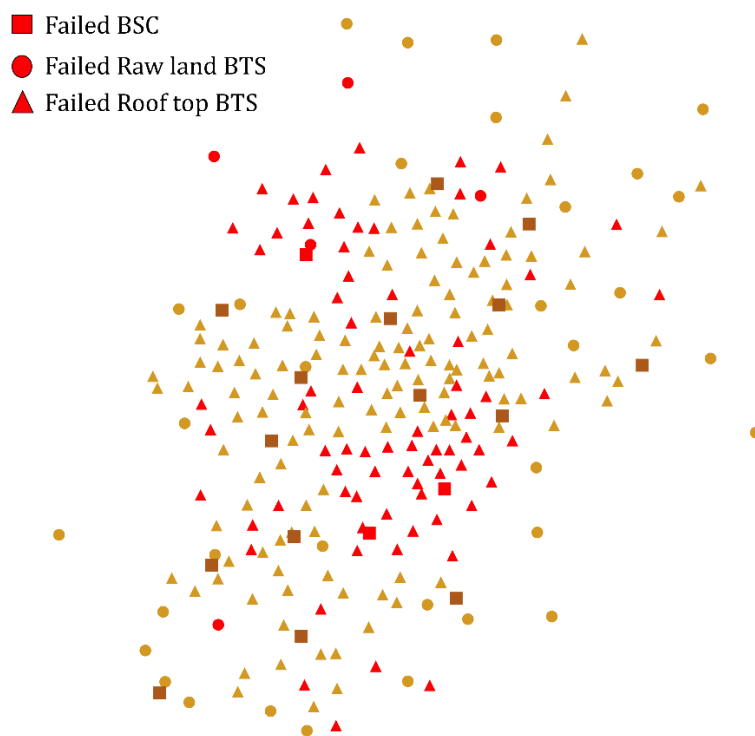


Figure 9-25, BTS out of order for the MNO3 for second scenario

Figure 9-26 summarizes the values for each MNO of the BTS out of order based on all the condition leading to the BTS failure.

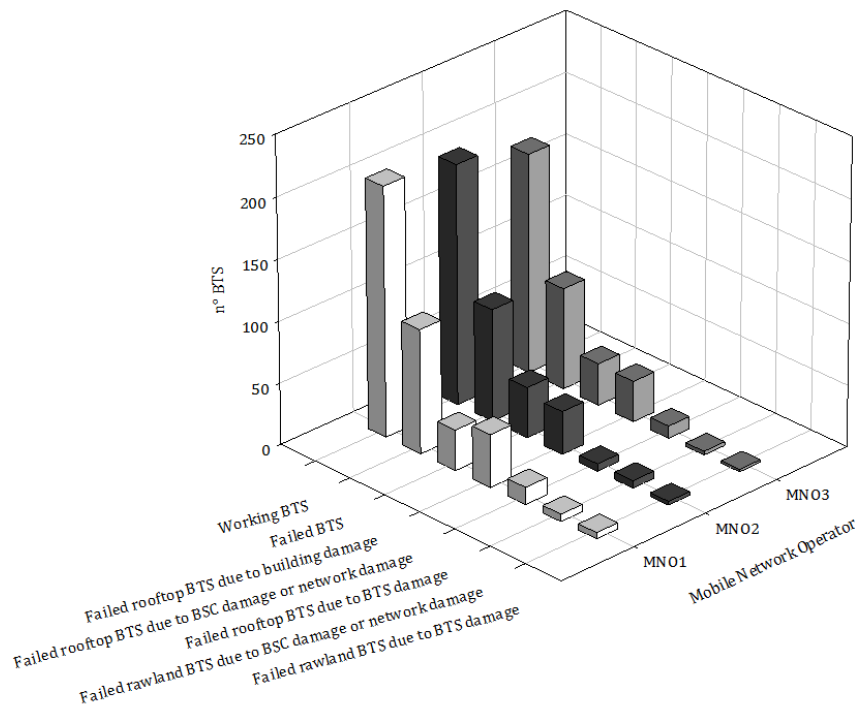


Figure 9-26, abstract of the damaged BTS values for each condition for the second scenario

For the second scenario, a lower number of BTS out of service is observed than in the first case. This is mainly because no BSC is excluded from the network for reasons of connection to the network itself. In that, observing the results regarding structural damage, similar results are found in order of magnitude. Once the distribution of the BTS still functioning after the event is known, the best Throughput available for each user cluster can be obtained.



Figure 9-27, THR value for user cluster given by the first MNO for a portion of Ideal City' downtown after second case scenario



Figure 9-27 reports the results of the THR after the second scenario as a disaster for the city center of the virtual city. It is observed that the THR is of slightly better quality than in the first scenario.

#### 9-3-4 Results for the Third Scenario: Hachinohe

The third test field to assess the vulnerability of the Ideal City's telecommunications network was the scenario due to the 1968 Hachinohe earthquake. Once the analysis is performed, an estimate of the damage level of each component is obtained and finally, through a tool with Python code, it can possible to view the virtual city with the damage level of each component. Figure 9 28 illustrates a detail of the results for the elements of the downtown of the city using the Python tool. While figure 9-29 shows the detail of a building with a tower always with the Python tool.

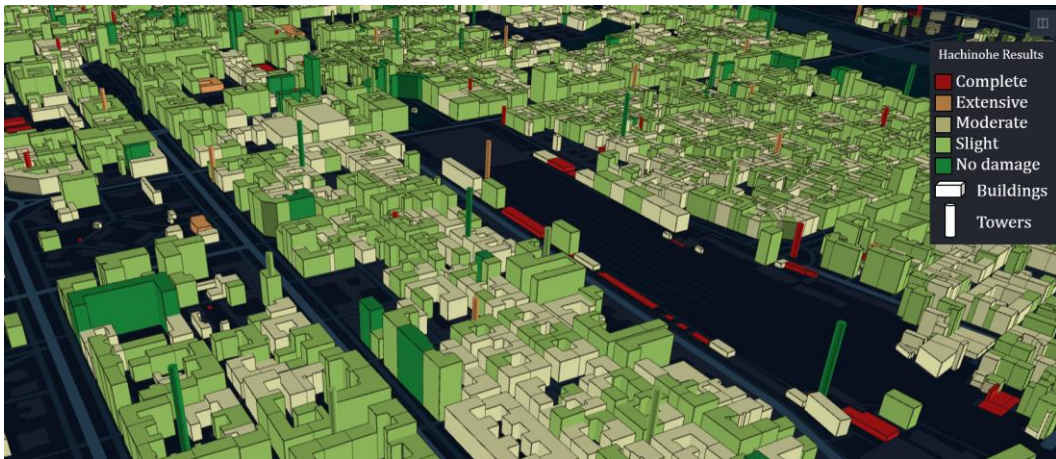


Figure 9-28, 3D damage visualization of the downtown for the third scenario with Python tool

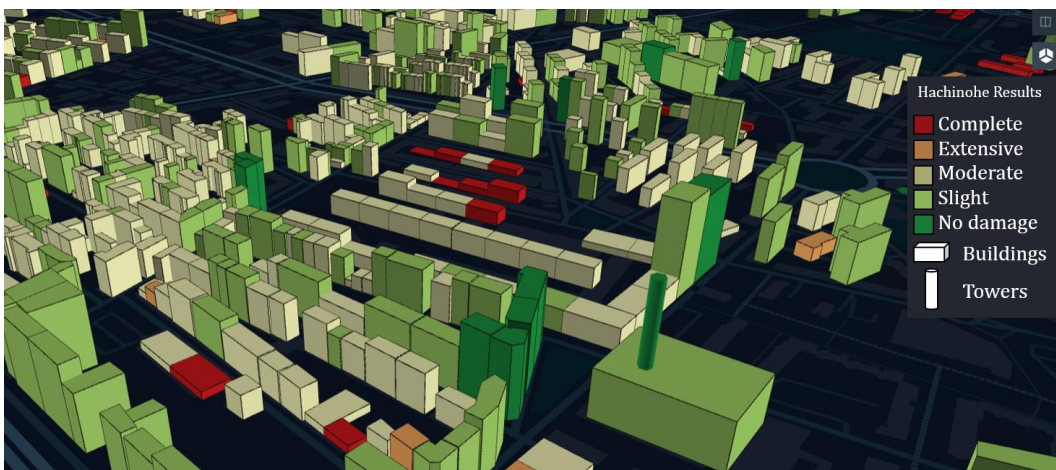


Figure 9-29, 3D damage visualization of a building with a tower for the third scenario with Python tool

Figure 9-30 summarizes the damage level results for the built environment. The results for buildings in general are grouped together, and damage to buildings by construction period is also shown.



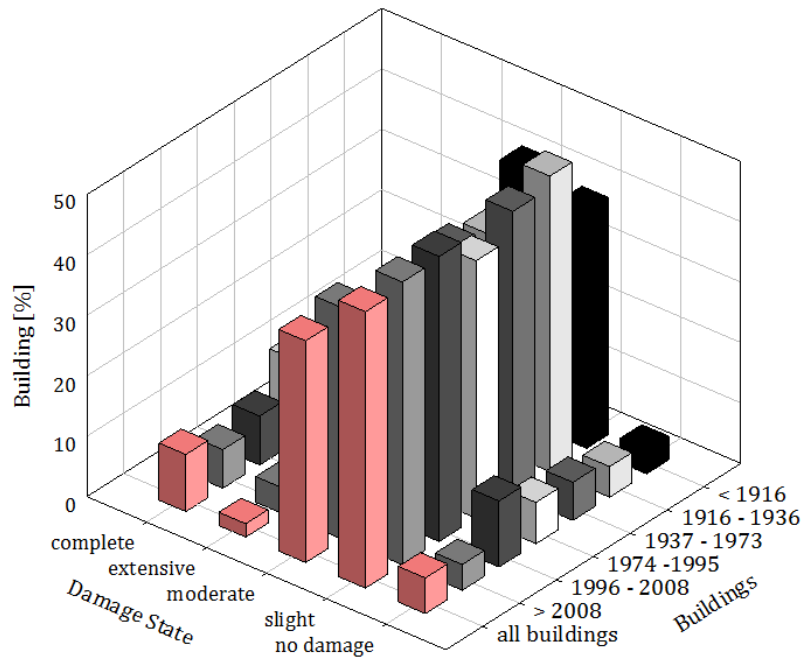


Figure 9-30, damage state for the buildings for the third scenario based on the year of construction

In the third case, a much lower overall damage to the structures is observed than in the first two cases. In fact, as can be seen from Figure 9-30, most of the buildings suffer light or moderate damage. About 45% of the buildings after applying the third event suffer mild damage, while about 36% suffer moderate damage. Buildings that suffer severe or extensive damage are 9% and 2% respectively. Finally, the buildings that do not suffer any damage are 6% of the total. From *Figure 9-30* Figure 9-30 even for the subdivision into categories based on the construction period, the trend that is observed is very similar to that seen for the all the buildings. As for the previous known cases the damage to buildings is known the damage to the control stations. *Figure 9-31* shows the number of BSCs with the related damage for the various damage categories.

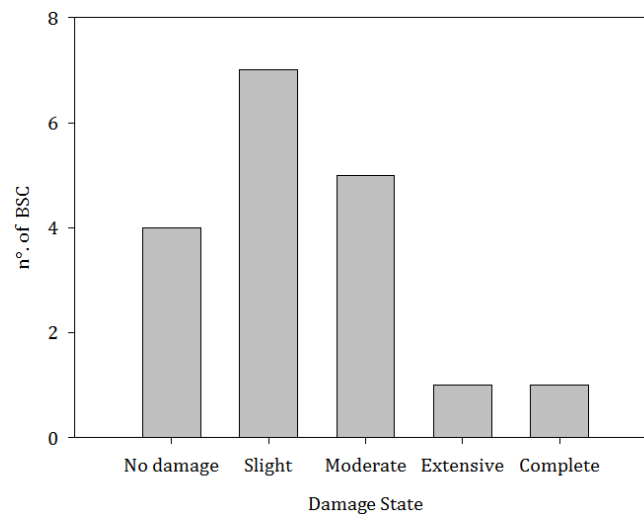


Figure 9-31, BSC' damage distribution within IDEAL CITY for Hachinohe scenario

Once the damage conditions of the BSCs were known, it was possible to know which stations are out of service and which ones continue to work after the seismic event. *Figure 9-32* illustrates which BSCs are out of order after the seismic event of the second scenario.

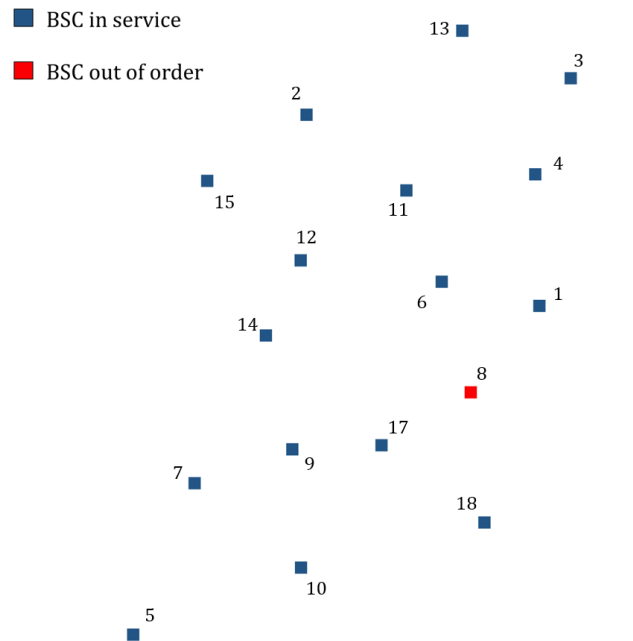


Figure 9-32, BSC state after Hachinohe scenario

Once the damaged BSCs are known, the out-of-service BTS can be known for each condition. It can be seen from *Figure 9-32* that only station 8 is out. Surely the BTS connected to it will be out of service. *Figure 9-33* shows for each level of structural damage the number of towers with that level of damage for towers on the ground. While *Figure 9-34* reports for each structural damage level the number of towers with that damage level for rooftop towers.

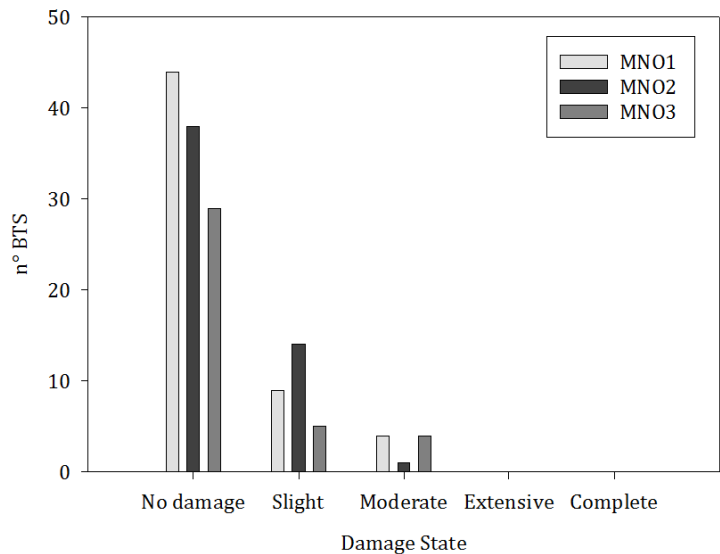


Figure 9-33, Damage State for the Raw land towers for third scenario

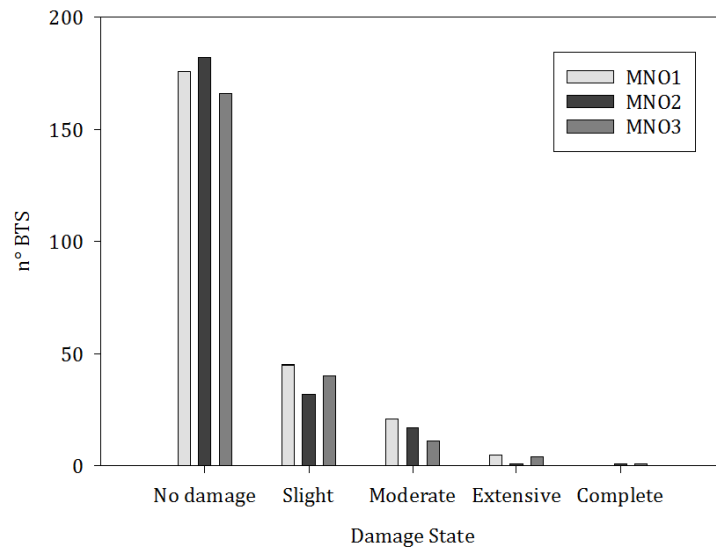


Figure 9-34, Damage State for the Roof top towers for third scenario

It can be observed from *Figure 9-33* and *Figure 9-34* that for the third scenario the structural damage to the BTS towers is generally minimal or absent. Once the structural damage levels are known also for the BTS towers, it is possible to know the BTS still functioning after the event and those are out of service for one of the possible conditions. *Figure 9-35* illustrates which BTSs are out of service for the first MNO, *Figure 9-36* shows the BTSs out of service for the second MNO, and finally *Figure 9-37* shows the BTSs out of service for the third MNO.

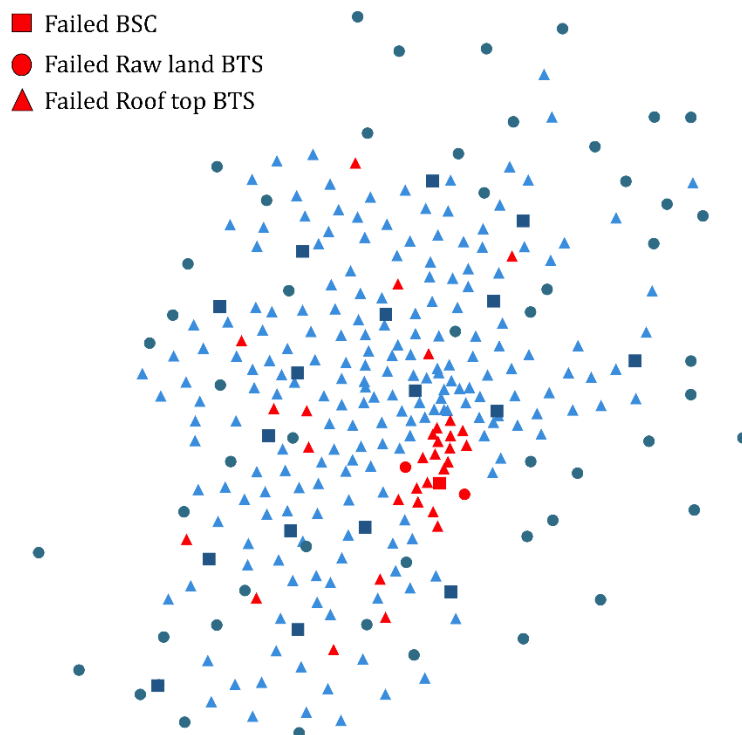


Figure 9-35, BTS out of order for the MNO1 for third scenario

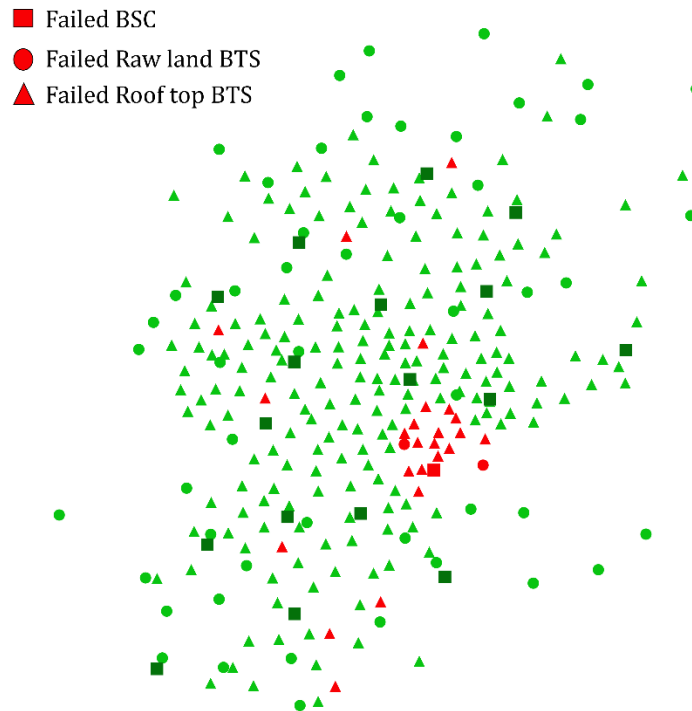


Figure 9-36, BTS out of order for the MNO2 for third scenario

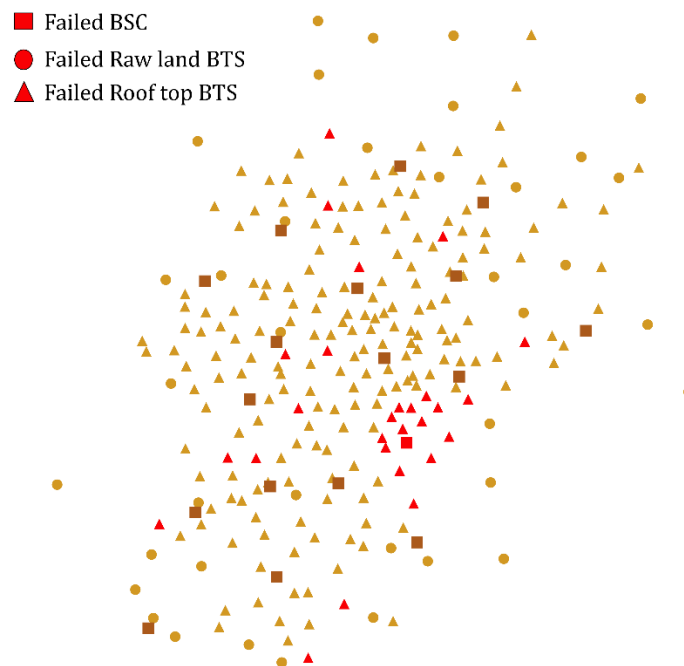


Figure 9-37, BTS out of order for the MNO3 for third scenario

From the figures showing the networks for each operator, it can be observed for the third case that the BTS out of use are mainly due to the damage to a BSC. This will lead to a reduction in the quality of service for the city center.

*Figure 9-38* summarizes the values for each MNO of the BTS out of order based on all the condition leading to the BTS failure.

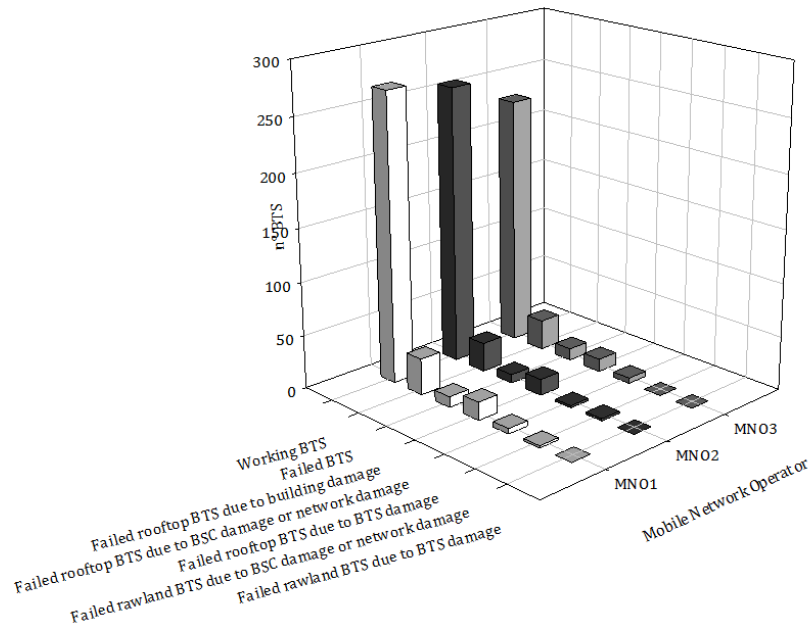


Figure 9-38, abstract of the damaged BTS values for each condition for the third scenario

The effects of the Hachinohe scenario on the network are limited to a few out of order BTS and a damaged BSC. Surely the network manages to guarantee a good quality service even after the event. This can also be seen thanks to Figure 9-39 which shows the detail of the THR quality for a portion of the downtown user clusters after the event. It does not differ much from the value in conditions of absence of damage to the network.



Figure 9-39, THR value for user cluster given by the first MNO for a portion of Ideal City' downtown after third case scenario

### 9-3-5 Results for the Fourth Scenario: Northridge

The latest test field where the Ideal City's wireless communication network vulnerability was tested is the scenario due to the 1994 Northridge, California earthquake. Once the analysis is performed, an estimate of the damage level of each component is obtained and finally, through a tool with Python code, it can possible to view the virtual city with the damage level of each component. Figure 9-40 illustrates a detail of the results for the elements of the downtown of the city using the Python tool. While Figure 9-41 shows a more general view of the southern area of the virtual city.

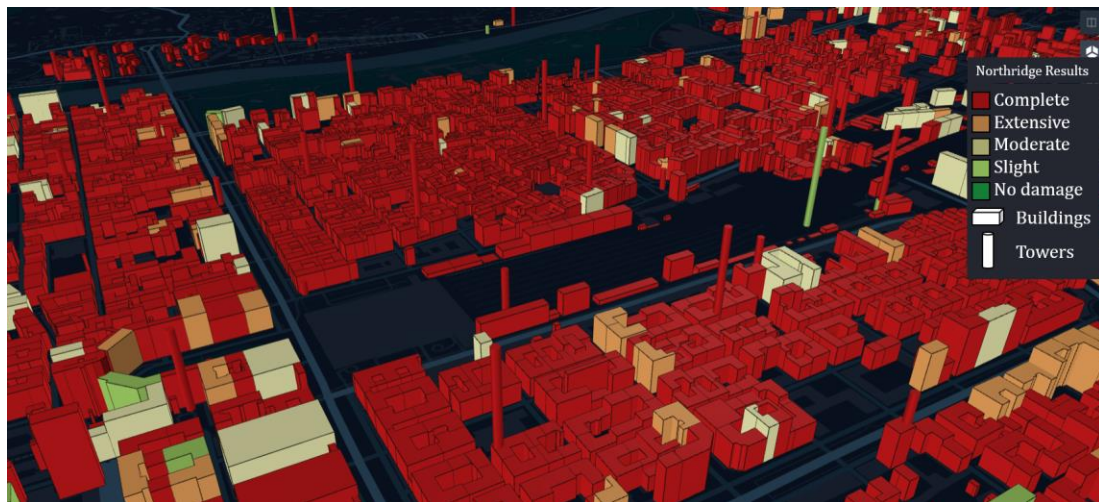


Figure 9-40, 3D damage visualization of the downtown for the fourth scenario with Python tool

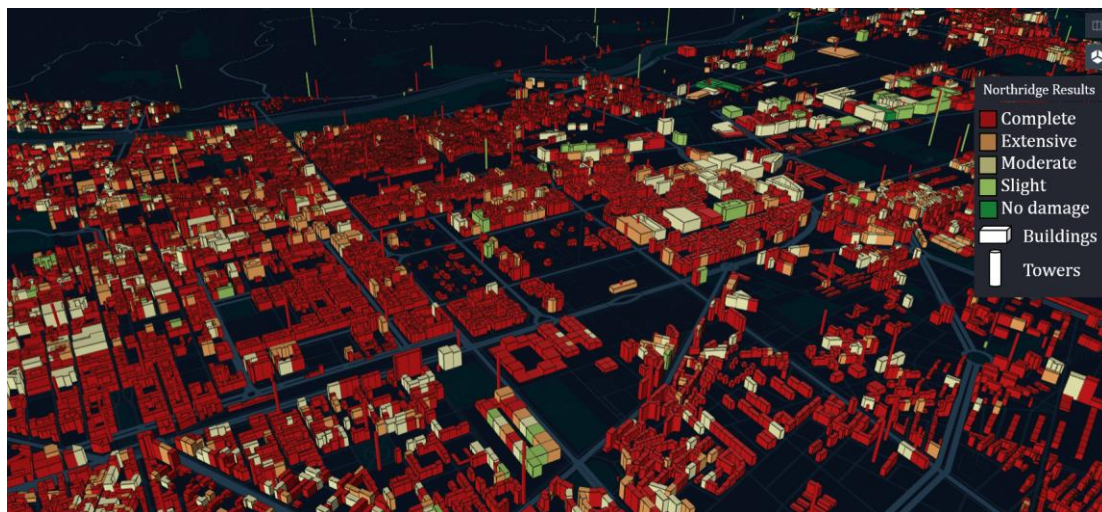


Figure 9-41, 3D damage visualization of the south of the city for the fourth scenario with Python tool

Figure 9-42 summarizes the damage level results for the built environment. The results for buildings in general are grouped together, and damage to buildings by construction period is also shown.



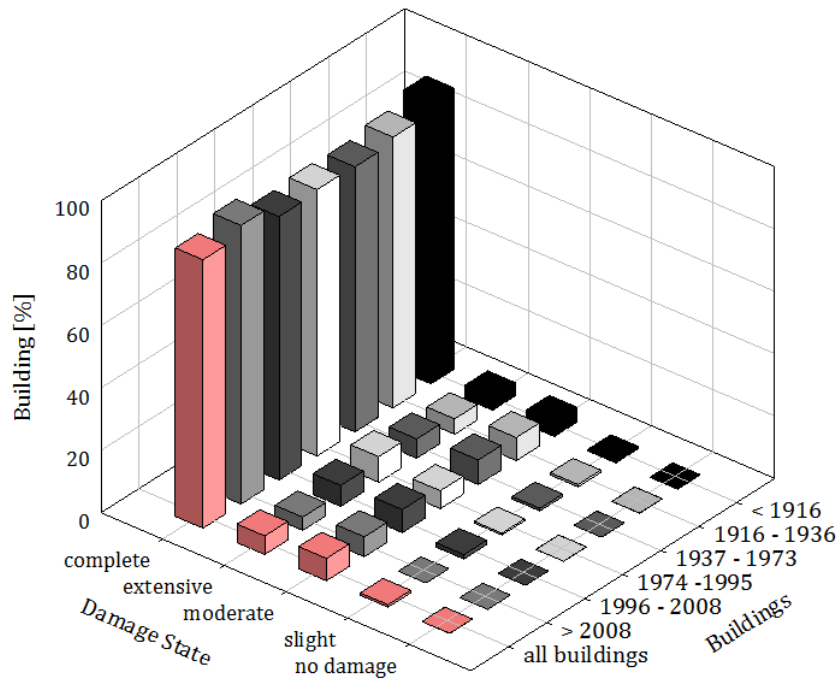


Figure 9-42, damage state for the buildings for the fourth scenario based on the year of construction

In this last case, as already observed from the Python visualization tool, *Figure 9-42* shows that most of the buildings suffer extensive or complete damage. More than 80% of buildings collapse, while 7% suffer extensive damage. The remaining buildings take moderate / minor damage. Observing the results of the damage suffered by the buildings, it is possible to guess that the communication network has suffered serious damage. *Figure 9-43* shows the number of BSCs with the related damage for the various damage categories for this last case.

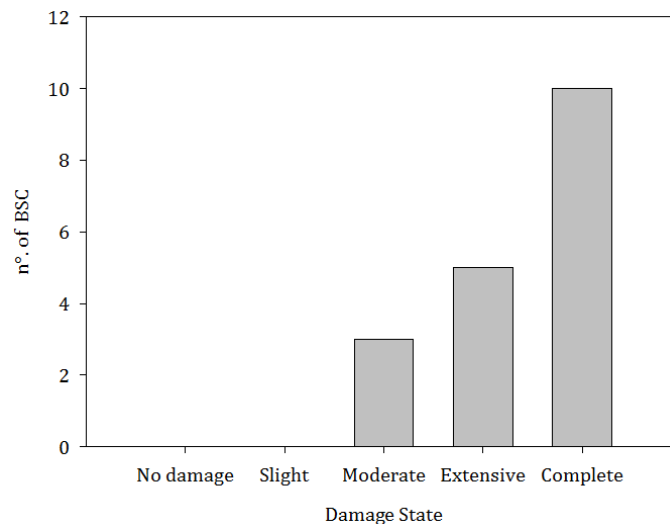


Figure 9-43, BSC' damage distribution within IDEAL CITY for Northridge scenario

Once the damage suffered by the BSC stations is known, based on the damage level and the network topology it is determined which BSCs are still in operation, and



which are not. BSCs 1, 2, 7, 8, 9, 10, 11, 12, 15, 16 and 17 suffer complete damage and are therefore out of order for structural reasons, while BSC 5, 14, and 18 do not suffer serious structural damage but are out of order. I use because they remain isolated from the network, i.e. there is no path available for them to get to a BSC CORE. *Figure 9-44* illustrates which BSCs are still running after the event, and which are not.

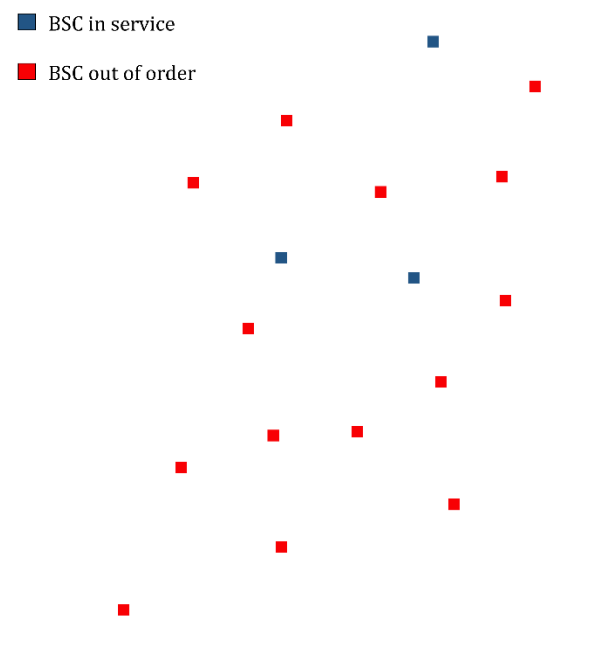


Figure 9-44, BSC state after Northridge scenario

Then we move on to observe the structural damage that the towers undergo. *Figure 9-45* shows the number of BTS on the ground for each damage state. While *Figure 9-46* shows the number of BTS on the roofs for each state of damage.

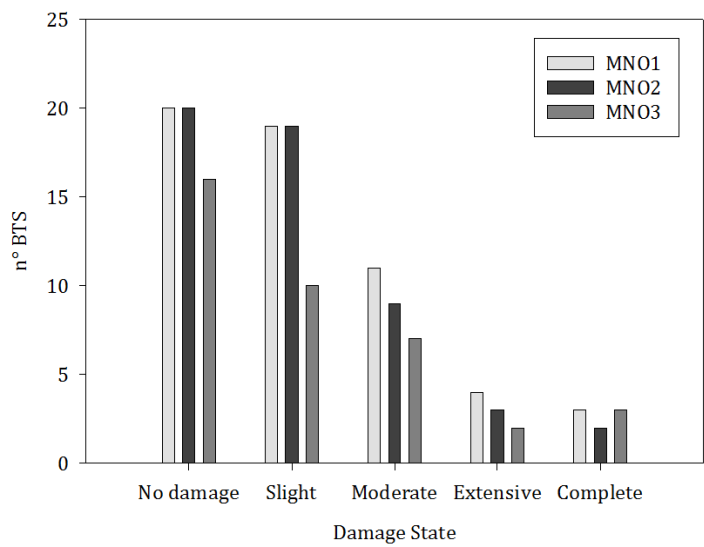


Figure 9-45, Damage State for the Raw land towers for fourth scenario

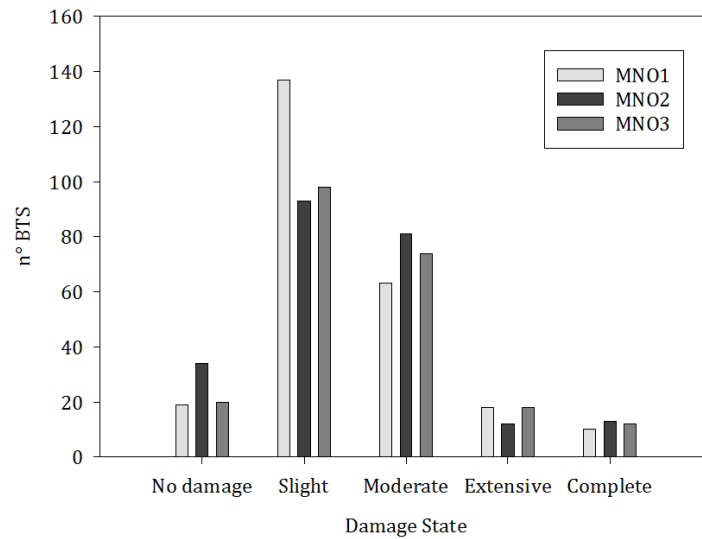


Figure 9-46, Damage State for the Roof top towers for fourth scenario

Once the structural damage levels are known also for the BTS towers, it is possible to know the BTS still functioning after the event and those are out of service for one of the possible conditions. *Figure 9-47* illustrates which BTSs are out of service for the first MNO, *Figure 9-48* shows the BTSs out of service for the second MNO, and finally *Figure 9-49* shows the BTSs out of service for the third MNO.

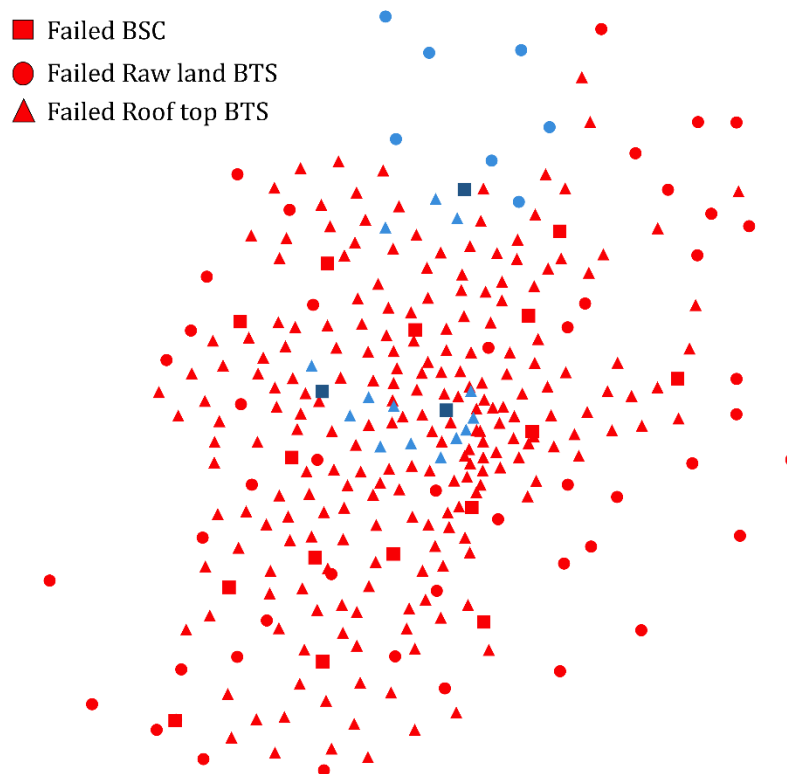


Figure 9-47, BTS out of order for the MNO1 for fourth scenario

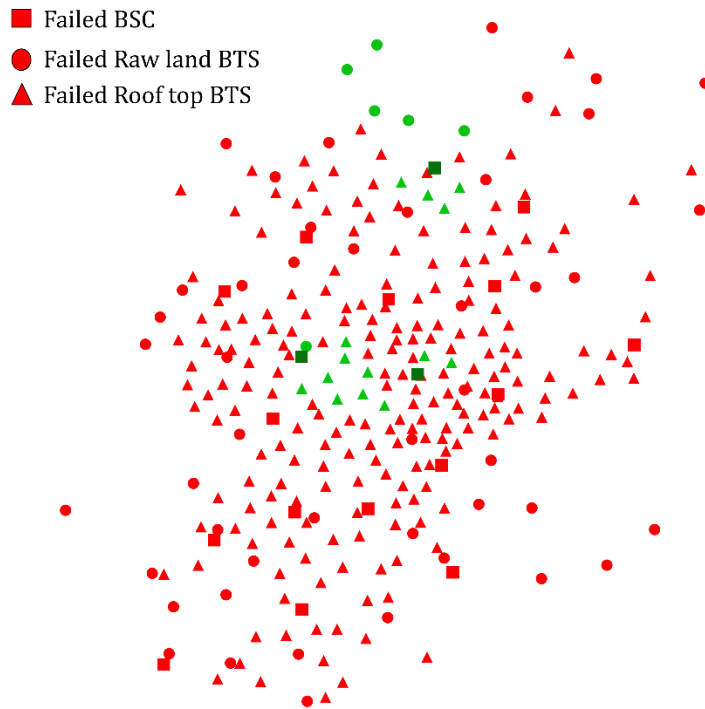


Figure 9-48, BTS out of order for the MNO2 for fourth scenario

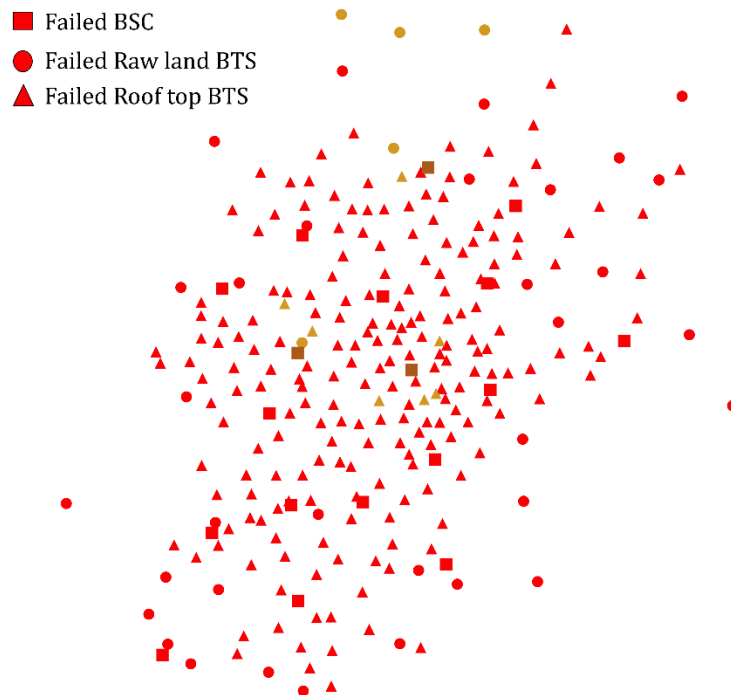


Figure 9-49, BTS out of order for the MNO3 for fourth scenario

Event four as can be seen from *Figure 9-47*, *Figure 9-48* and *Figure 9-49* causes almost total damage to the networks of each MNO. Certainly after this event the few remaining BTSs will be overloaded with traffic and this will cause

communication delays. *Figure 9-50* summarizes the values for each MNO of the BTS out of order based on all the condition leading to the BTS failure.

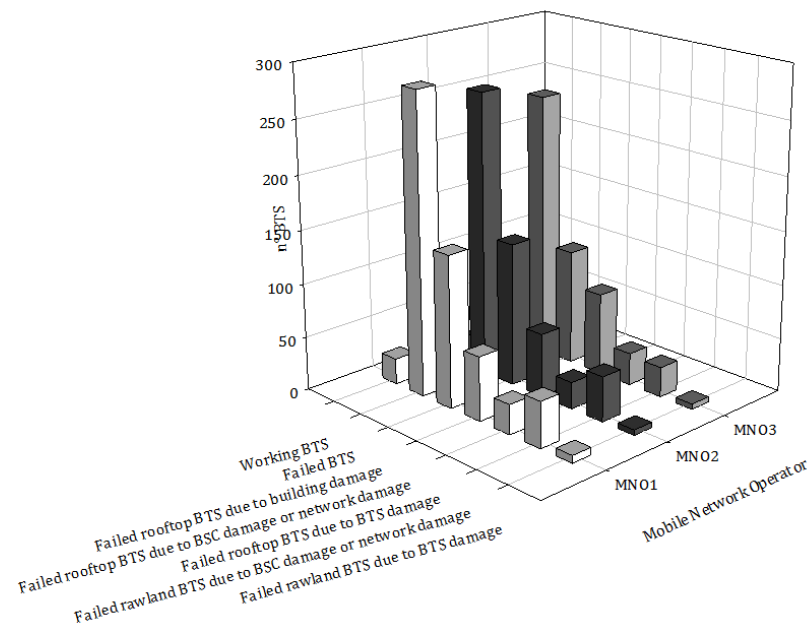


Figure 9-50, abstract of the damaged BTS values for each condition for the fourth scenario

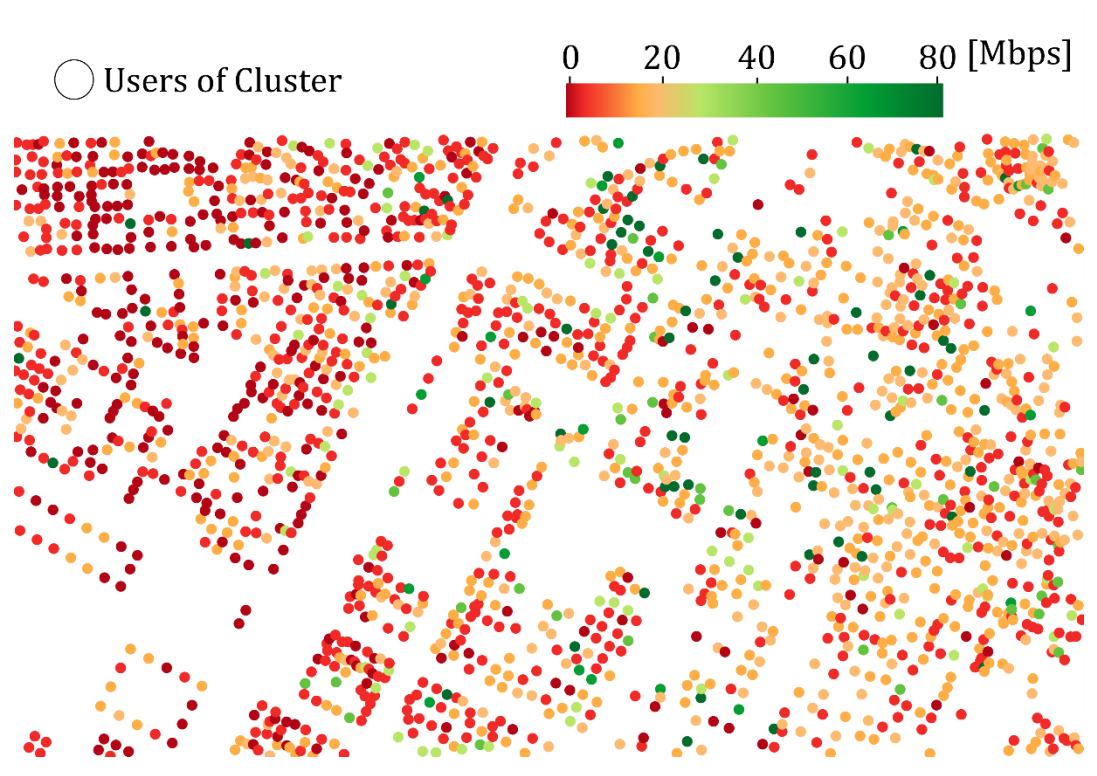


Figure 9-51, THR value for user cluster given by the first MNO for a portion of Ideal City' downtown after fourth case scenario

The effects of the Northridge scenario on the network are significant. Almost all BTS are out of order due to structural damage to buildings or damage suffered by

the BSCs. The towers that suffer extensive structural damage are, on the other hand, still limited, confirming the low vulnerability of these structures to dynamic seismic actions. Certainly, the high number of BTS out of order causes a delay and a noticeable reduction in quality for communications. It must also be said that many clusters of users will have no signal level in their position, this can be seen well from the calculation of the THR after the Northridge event which is shown in *Figure 9-51*.

#### 9.4 Assessment of the Resilience Indices for each scenario

Once the network structures of each MNO were known after each scenario (based on the remaining BSCs and BTSs), the resilience indexes defined in paragraph 9.2 were calculated.

MNO	N° BTS	1° scenario El Centro	2° scenario Kobe	3° scenario Hachinohe	4° scenario Northridge
MN01	BTS out of order	153	101	34	280
	BTS working	151	203	270	24
	$R_{TOW}$	0,497	0,668	0,888	0,079
MN02	BTS out of order	144	91	27	264
	BTS working	142	195	259	22
	$R_{TOW}$	0,496	0,681	0,906	0,077
MN03	BTS out of order	125	82	28	246
	BTS working	135	178	232	14
	$R_{TOW}$	0,519	0,685	0,892	0,054

Table 9-2, results for the  $R_{TOW}$  resilience index

From the results of the  $R_{TOW}$  index show in the *Table 9-2*, it can be seen that the networks of the individual MNOs have a similar level of resilience. It can be observed that the network of MN02 is more resilient than the others and, that of MN01 even if compared to the latter it has a lower number of BTS. This shows that to obtain a resilient network it is not necessary to have a great redundancy of the elements, but it is necessary in an urban environment to place the BTS on buildings with low vulnerability to disasters, in this way, in addition to saving the building from extensive damage, it is possible to indirectly create a benefit for the communication network. From the results on the number of BTSs who stop working, a large incidence is caused by the BSCs that are out of service. This implies that it is necessary to design the structures of the BSC with better anti-seismic criteria. On the basis of what was calculated in chapter 5 for the ordinary working conditions for each MNO it was possible to obtain the weighted mean

throughput in normal conditions ( $\langle \text{THR} \rangle_{\text{pre-disaster}}$ ). The results are show in the *Table 9-3*.

MNO	$\langle \text{THR} \rangle_{\text{pre-disaster}}$ [Mbps]
MNO1	21,39
MNO2	20,68
MNO3	21,03

Table 9-3, weighted mean throughput in normal condition for each MNO

Note the structure of the network after each event the same procedure was done to derive weighted mean throughput post disaster ( $\langle \text{THR} \rangle_{\text{post}}$ ). It is lower than normal conditions as fewer BTS means more traffic on the remaining antennas.

	El Centro	Kobe	Hachinohe	Northridge
MNO	$\langle \text{THR} \rangle_{\text{post-disaster}}$ [Mbps]	$\langle \text{THR} \rangle_{\text{post-disaster}}$ [Mbps]	$\langle \text{THR} \rangle_{\text{post-disaster}}$ [Mbps]	$\langle \text{THR} \rangle_{\text{post-disaster}}$ [Mbps]
MNO1	13,87	17,41	20,51	8,77
MNO2	14,32	17,37	20,02	9,32
MNO3	13,55	16,85	20,33	9,48

Table 9-4, weighted mean throughput for each scenario and for each MNO

	El Centro	Kobe	Hachinohe	Northridge
MNO	$R_{\text{THR}}$	$R_{\text{THR}}$	$R_{\text{THR}}$	$R_{\text{THR}}$
MNO1	0,648	0,814	0,959	0,410
MNO2	0,694	0,840	0,968	0,451
MNO3	0,644	0,801	0,967	0,451

Table 9-5,  $R_{\text{THR}}$  values

Overall, what you notice is that throughput tends to decrease as expected. However, some users who are close to functional BTS may experience a better connection due to reduced interference. In the case of Hachinohe where BTS are lost in a limited area, one might think that the clusters of that area suffer a loss of signal in reality this does not happen for two reasons, the first is that the technology that uses 3G and 4G allows you to connect to antennas even a few kilometers (3km) away. The second is that each BTS is capable of simultaneously managing a few tens of thousands of users. Since under normal network conditions each BTS would have to handle fewer than 1000 users if all users connected at the same time, this means that the network has a certain amount of

overhead. Finally, it evaluates the increase in traffic on the BTS which remain in operation after each scenario. To do this, the third proposed index is used. *Table 9-6* shows the average number of users for each BTS.

MNO	<UExBTS>
MNO1	935.76
MNO2	915.53
MNO3	702.64

Table 9-6, Users per BTS for each MNO in normal condition

	El Centro	Kobe	Hachinohe	Northridge
MNO	<UExBTS>	<UExBTS>	<UExBTS>	<UExBTS>
MNO1	2056,84	1014.13	961.03	13983,22
MNO2	1945,33	984,91	934,99	9372,97
MNO3	1803,65	773,29	734.28	11732,22

Table 9-7, Users per BTS for each MNO after each scenario

	El Centro	Kobe	Hachinohe	Northridge
MNO	$R_{UE-BTS}$	$R_{UE-BTS}$	$R_{UE-BTS}$	$R_{UE-BTS}$
MNO1	2,19	1,08	1,02	14,94
MNO2	2,23	1,07	1,02	10,23
MNO3	2,57	1,10	1,04	16,69

Table 9-8,  $R_{UE-BTS}$  values

Based on the results of the third index, it is first observed that the network of the third MNO is the most congested in each scenario. After that, we see that in cases where there are few BTS out of service, the network is able to redistribute the request on the BTS that remain in operation without losing too much quality in the speed of the connection offered.

Finally, an assessment is made of the possibility chosen by the MNOs to join their networks in the event of an emergency to be able to provide a connection to as wide a range of users as possible. *Table 9-9*, shows the results on Weighted Average Throughput after each scenario and the number of users per BTS.

	El Centro	Kobe	Hachinohe	Northridge
<THR> <sub>post-disaster</sub> [Mbps]	16,48	19,28	21,12	11,23
<UExBTS>	638,8	485,3	335,8	6194,5

Table 9-9, Average throughput and number of users per BTS after the combination of the MNO's networks

It can be seen from the results shown in *Table 9-9* that the union of the networks brings benefits to quality and coverage for users.



## 10 Analysis implementation

Having to work on a large-scale system, it is necessary to use methods that exploit code languages to carry out physical simulations. There are several algorithms for performing large-scale simulations. Each part of the Ideal City project is implemented through the same writing method. It means that each infrastructure is implemented using the same language. The writing language to do most of the work in this study was done using the Python language. That is the same language used to implement the other strategic infrastructures. This is because the goal of the Ideal City project is to create an integrated platform for assessing the resilience of a city with various levels of infrastructure. The SAP2000 GGG software was used to assess the damage, the results of which are then manipulated using Python. Finally, the results are displayed through two GIS tools that allow you to view the results given by the Python codes in a simpler way through the direct exchange of data by plug-ins.

Figure 10-1 resumes the proposed step-by-step procedure adopted for large scale seismic simulation.

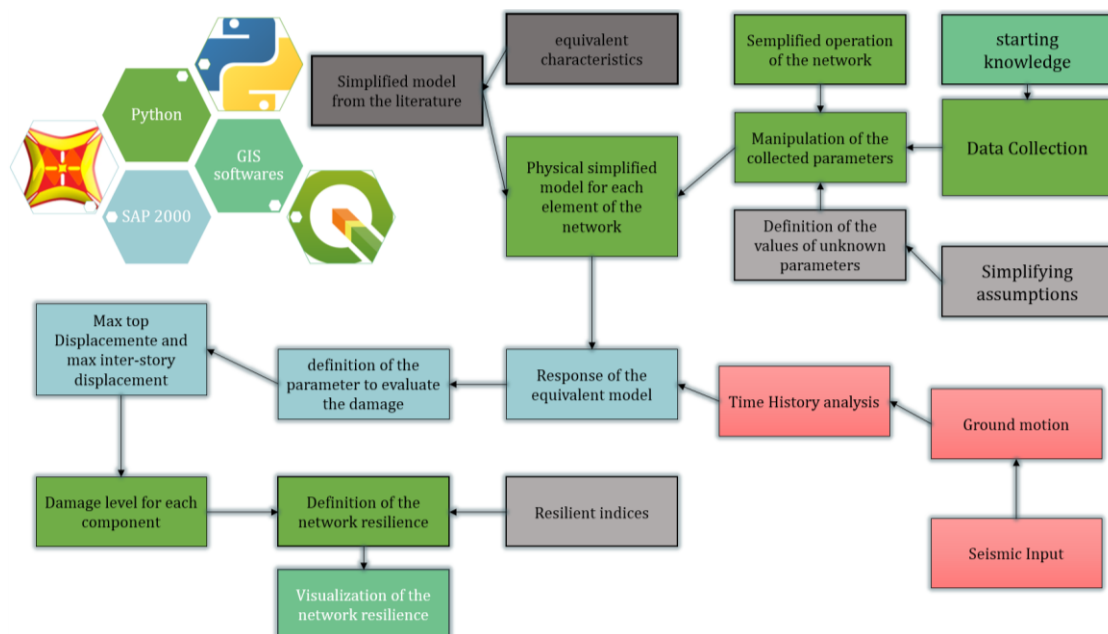


Figure 10-1, summary diagram of the analysis flow

The annexes section shows the codes written in Python that manage each step of the simulation.

# Conclusion

Today, the concept of virtual city is spreading more and more in the scientific community. Determining the damage suffered by a strategic infrastructure such as the communication network due to natural or man-made events represents a complex challenge. The complexity is given by the scale at which one works. In fact, a series of not indifferent components come into play. It brings with it uncertainties that must be managed with the assumption of simplifying hypotheses.

In this study, a method is proposed to assess the vulnerability to seismic events of a wireless communication network. The method is based on the construction of a network for a large city, characterizing the main components of the network (BTS and BSC) through different structural and non-structural parameters. A series of parameters were assigned based on collected data, some had to undergo some manipulations, while for others it was decided to follow a deterministic approach based on hypotheses defined on known parameters. The intense collection and processing of data led to the creation of a complete database of the exposure of the typical components of a new generation cellular network. The database represents a strong point of this work as it can be easily manipulated in order to allow the insertion of new parameters or components, for example to perform future interoperability studies with the electricity grid. The definition of the physical properties of each element takes place using simplified methods found in the literature. Then, the performance of the building was obtained through non-linear time history analyzes, in which each component was modeled as an equivalent SDOF system. The dynamic characteristics of each single component of the network were derived from the capacity curve. Furthermore, the dynamic degradation was modeled on the basis of the kinematic hysteretic model. The proposed modeling leads to limit the computational efforts without losing accuracy and consistency with the expected results even using a non-linear analysis. Note the response to the seismic input in terms of global displacements, for structures such as control stations it has then been converted into local terms of inter-storey displacement, while for elements such as towers the global response can be an already good compromise to evaluate the damage status of the element. Finally, the assignment of the damage level for buildings takes place through the use of fragility curves present in the literature, while for towers the damage is estimated as a function of the displacements that characterize the capacity curve. The reliability of the proposed simulation model was demonstrated by the results of the seismic simulation based on various scenarios. First of all, the results showed a direct proportionality between the damage

suffered by the elements and the intensity of the seismic action. The second observation made is that the vulnerability of the wireless network is closely related to the vulnerability of the built environment. This means that there is a high interoperability between the building portfolio and the network. An interesting result is also given by the results on merging networks after a disaster. It is noted that the emergency service is better than in the case of separate networks. It is a fundamental result as today this does not happen in reality. Future work may concern the study of the interdependence of the cellular network with the electricity grid that was developed for the Ideal City in order to observe whether there is a connection between the vulnerability of the electricity grid and the cellular network. Other future studies may concern the use of models to estimate data traffic for different moments in order to determine a more realistic distribution on the user network. This is because in the study proposed here a simplification on the functioning of the network has been assumed. That is, it was assumed that each user connects to the network (maximum load) and that this happens with respect to the BTS that offers him the best connection. In reality, the distribution of users on the network depends on the load that the network must manage at a given moment in time. The whole simulation model proposed has been implemented in Python environment. Furthermore, a simple visualization tool is used that provides a simple and immediate interaction with the results offered by the model.

# Bibliography

1. 3GPP (2014). "3GPP Long Term Evolution: System Overview, Product Development, and Test Challenges ".
2. Abu-Al-Saud, D. W. A. (2019). "Wireless & Mobile Communications."
3. Access, E. (2010). "Further advancements for E-UTRA physical layer aspects." 3GPP Technical Specification TR 36: V2.
4. Alves, R. J., M. M. Rodrigues, M. H. Paiva and M. E. Segatto (2017). A note on resilience of telecommunication networks. 2017 CHILEAN Conference on Electrical, Electronics Engineering, Information and Communication Technologies (CHILECON), IEEE.
5. Ambraseys, N. N., K. u. Simpson and J. J. Bommer (1996). "Prediction of horizontal response spectra in Europe." *Earthquake Engineering & Structural Dynamics* 25(4): 371-400.
6. Assi, R. (2006). "Seismic Analysis of Telecommunication Towers Mounted on Building Roof tops." Master degree thesis,( McGill University, Montreal, Canada).
7. Azeem, M. and I. Aliya (2018). "APPROXIMATION OF SEISMIC PLIFICATION EFFECTS ON ROOFTOP TELECOMMUNICATION TOWERS." *International Journal of Civil Engineering* 9(13).
8. Baho, D. L., C. R. Allen, A. S. Garmestani, H. B. Fried-Petersen, S. E. Renes, L. H. Gunderson and D. G. Angeler (2017). "A quantitative framework for assessing ecological resilience." *Ecology and society: a journal of integrative science for resilience and sustainability* 22(3): 1.
9. Balanis, C. A. and A. C. Polycarpou (2003). "Antennas." *Wiley Encyclopedia of Telecommunications*.
10. Bhosale, N., P. Kumar and A. Pandey (2012). "Influence of host structure characteristics on response of rooftop telecommunication towers." *International Journal of Civil and Structural Engineering* 2(3): 728.
11. Booker, G., J. Torres, S. Guikema, A. Sprintson and K. Brumbelow (2010). "Estimating cellular network performance during hurricanes." *Reliability Engineering & System Safety* 95(4): 337-344.
12. Brumbelow, K., J. Torres, S. Guikema, E. Bristow and L. Kanta (2007). Virtual cities for water distribution and infrastructure system research. World environmental and water resources congress 2007: Restoring our natural habitat.
13. Bruneau, M., S. E. Chang, R. T. Eguchi, G. C. Lee, T. D. O'Rourke, A. M. Reinhorn, M. Shinozuka, K. Tierney, W. A. Wallace and D. Von Winterfeldt (2003). "A framework to quantitatively assess and enhance the seismic resilience of communities." *Earthquake spectra* 19(4): 733-752.
14. Campanella, T. J. (2006). "Urban resilience and the recovery of New Orleans." *Journal of the American planning association* 72(2): 141-146.
15. Cardoni, A., G. Cimellaro, M. Domaneschi, S. Sordo and A. Mazza (2020). "Modeling the interdependency between buildings and the electrical distribution system for seismic resilience assessment." *International Journal of Disaster Risk Reduction* 42: 101315.
16. Cash, D. W., W. N. Adger, F. Berkes, P. Garden, L. Lebel, P. Olsson, L. Pritchard and O. Young (2006). "Scale and cross-scale dynamics: governance and information in a multilevel world." *Ecology and society* 11(2).
17. Cimellaro, G. P., M. Domaneschi, S. Mahin and G. Scutiero (2017). Exploring simulation tools for urban seismic analysis and resilience assessment. 6th

- International Conference on Computational Methods in Structural Dynamics and Earthquake Engineering (COMPDYN2017) 15-17, Rhodes Island Greece.
18. Cimellaro, G. P. and S. Marasco (2015). "A computer-based environment for processing and selection of seismic ground motion records: OPENSIGNAL." *Frontiers in Built Environment* 1: 17.
  19. Cimellaro, G. P. and S. Marasco (2018). *Introduction to dynamics of structures and earthquake engineering*, Springer.
  20. Cimellaro, G. P., A. M. Reinhorn and M. Bruneau (2010). "Framework for analytical quantification of disaster resilience." *Engineering structures* 32(11): 3639-3649.
  21. Cimellaro, G. P., A. M. Reinhorn and M. Bruneau (2010). "Seismic resilience of a hospital system." *Structure and Infrastructure Engineering* 6(1-2): 127-144.
  22. Cimellaro, G. P., C. Renschler, A. M. Reinhorn and L. Arendt (2016). "PEOPLES: a framework for evaluating resilience." *Journal of Structural Engineering* 142(10): 04016063.
  23. Corrado, V., I. Ballarini and S. P. Corgnati (2012). "National scientific report on the TABULA activities in Italy." Dipartimento di Energetica, Gruppo di Ricerca TEBE, Politecnico di Torino, Torino, Italy.
  24. COST, D. J. C., Thomas Kürner (1996). "Final report for COST Action 231, Chapter 4."
  25. CSI. (2018). "Integrated Finite Element Analysis and Design of Structures Basic Analysis Reference Manual Computers and Structures, Inc., Berkeley, California, USA.
  26. de Souza Couto, R., S. Secci, M. E. M. Campista and L. H. M. K. Costa (2016). "Reliability and survivability analysis of data center network topologies." *Journal of Network and Systems Management* 24(2): 346-392.
  27. Deidda, M., A. Pala and G. Sanna (2020). Modelling a cell tower using SFM: automated detection of structural elements from skeleton extraction on a point cloud. 2020 24th ISPRS Congress-Technical Commission II, International Society for Photogrammetry and Remote Sensing.
  28. Di Francesco, P., F. Malandrino and L. A. DaSilva (2017). "Assembling and using a cellular dataset for mobile network analysis and planning." *IEEE Transactions on Big Data* 4(4): 614-620.
  29. Dias, J. R. (2007). "Analysis and Design of Lattice Steel Towers for Electrical Energy Transport according with the EC3(EN) and the EN50341-1."
  30. Domaneschi, M., G. P. Cimellaro and G. Scutiero (2019). "A simplified method to assess generation of seismic debris for masonry structures." *Engineering Structures* 186: 306-320.
  31. Dong, W., J. Zhang, X. Gao, P. Zhang and Y. Wu (2007). Cluster identification and properties of outdoor wideband MIMO channel. 2007 IEEE 66th Vehicular Technology Conference, IEEE.
  32. Dudenhoeffer, D. D., M. R. Permann and M. Manic (2006). CIMS: A framework for infrastructure interdependency modeling and analysis. Proceedings of the 2006 winter simulation conference, IEEE.
  33. Edfors, O., M. Sandell, J.-J. van de Beek, D. Landström and F. Sjöberg (1996). "An introduction to orthogonal frequency-division multiplexing."
  34. Ellingwood, B. R., H. Cutler, P. Gardoni, W. G. Peacock, J. W. van de Lindt and N. Wang (2016). "The centerville virtual community: A fully integrated decision model of interacting physical and social infrastructure systems." *Sustainable and Resilient Infrastructure* 1(3-4): 95-107.
  35. Ellingwood, B. R., D. V. Rosowsky and W. Pang (2008). "Performance of light-frame wood residential construction subjected to earthquakes in regions of moderate seismicity." *Journal of structural engineering* 134(8): 1353-1363.
  36. Eurocode (2004). "Eurocode 8: Design of structures for earthquake resistance - Part 1: General
  37. rules, seismic actions and rules for buildings ".

38. Fan, J., Q. Yin, G. Y. Li, B. Peng and X. Zhu (2011). MCS selection for throughput improvement in downlink LTE systems. 2011 Proceedings of 20th international conference on computer communications and networks (ICCCN), IEEE.
39. FEMA (2011). "Hazus: FEMA's methodology for estimating potential losses from disasters."
40. Fujii, T. (2003). "Path loss prediction formula in mobile communication-an expansion of." SAKAGAMI" path loss prediction formula-," Trans. IEICE, Japan, J86-B 10: 2264-2267.
41. Galvez, C. and G. McClure (1995). A simplified method for aseismic design of self-supporting lattice telecommunication towers. 7th Canadian Conference on Earthquake Engineering, Montreal, Ca.
42. Gálvez, C. A. (1995). Static method for aseismic design of self-supporting towers, Department of Civil Engineering and Applied Mechanics, McGill University.
43. Ghobarah, A. (2004). On drift limits associated with different damage levels. International workshop on performance-based seismic design, Dept. of Civil Engineering, McMaster University, June 28–July 1.
44. Giovinazzi, S., A. Austin, R. Ruiter, C. Foster, M. Nayyerloo, N.-K. Nair and L. Wotherspoon (2017). "Resilience and fragility of the telecommunication network to seismic events." Bulletin of the New Zealand Society for Earthquake Engineering 50(2): 318-328.
45. Haenggi, M., J. G. Andrews, F. Baccelli, O. Dousse and M. Franceschetti (2009). "Stochastic geometry and random graphs for the analysis and design of wireless networks." IEEE journal on selected areas in communications 27(7): 1029-1046.
46. Hamutuk, L. "Civil society comments on infrastructure strategic sector." Timor-Leste: La'o Hamutuk, nd <https://www.laohamutuk.org/econ/14TLDPM/InfraCSOen.pdf>.
47. Hassan, E. M. and H. Mahmoud (2020). "An integrated socio-technical approach for post-earthquake recovery of interdependent healthcare system." Reliability Engineering & System Safety 201: 106953.
48. Hata, M. (1980). "Empirical formula for propagation loss in land mobile radio services." IEEE transactions on Vehicular Technology 29(3): 317-325.
49. Heinrichs, T. D., B. J. Jennings and N. E. Singer (2013). Motivating Business to Design a More Resilient Nation One Building at a Time, Sandia National Lab.(SNL-NM), Albuquerque, NM (United States).
50. ISTAT (2018). "Dati riguardanti trasporti e telecomunicazioni."
51. ITU (2009). "Guidelines for evaluation of radio interface technologies for IMT-Advanced."
52. ITU (2020). "Measuring digital development."
53. Jin, X., L. E. Li, L. Vanbever and J. Rexford (2013). Softcell: Scalable and flexible cellular core network architecture. Proceedings of the ninth ACM conference on Emerging networking experiments and technologies.
54. Ketonen, J., M. Juntti and J. R. Cavallaro (2010). "Performance—complexity comparison of receivers for a LTE MIMO–OFDM system." IEEE transactions on signal processing 58(6): 3360-3372.
55. Khedr, M. A. and G. McClure (2000). "A simplified method for seismic analysis of lattice telecommunication towers." Canadian Journal of Civil Engineering 27(3): 533-542.
56. Khedr, M. A. H. (1998). Seismic analysis of lattice towers, Citeseer.
57. Kwasinski, A. and A. K. Tang (2011). Telecommunications Performance in the M= 9.0 Off-shore East Coast of Japan Earthquake and Tsunami March 11 2011. Japan Society of Civil Engineers' International Symposium on Engineering Lessons Learned from the Giant Earthquake.

58. Kyung, D. and J. Lee (2015). "Load-carrying behavior of transmission-tower connected foundations subjected to different load directions." *Soils and Foundations* 55(3): 575-587.
59. Lanier, B., D. Schnierch and S. Rizkalla (2009). "Behavior of steel monopoles strengthened with high-modulus CFRP materials." *Thin-Walled Structures* 47(10): 1037-1047.
60. Lefort, T. (1998). "Comparison of wind and earthquake effects on self-supporting antenna towers."
61. Leiserson, C. E. (1985). "Fat-trees: universal networks for hardware-efficient supercomputing." *IEEE transactions on Computers* 100(10): 892-901.
62. Lyu, D.-S., J.-H. Hong, M.-S. Jang, D.-J. Shin, C.-K. Lee and H. Lee (1994). An Implementation of Transcoding/Selecting System in Base Station Controller for Digital Cellular Communication. ISITA'94: International Symposium on Information Theory & Its Applications 1994; Proceedings, Institution of Engineers, Australia.
63. Madugula, M. K. (2001). Dynamic response of lattice towers and guyed masts, ASCE Publications.
64. Malandrino, F., C.-F. Chiasserini and S. Kirkpatrick (2017). "Cellular network traces towards 5G: Usage, analysis and generation." *IEEE Transactions on Mobile Computing* 17(3): 529-542.
65. Marasco, S., A. Cardoni, A. Z. Noori, O. Kammouh, M. Domaneschi and G. P. Cimellaro (2020). "Integrated platform to assess seismic resilience at the community level." *Sustainable Cities and Society*: 102506.
66. Marasco, S. and G. P. Cimellaro (2018). "Large scale simulation of IDEAL CITY under seismic scenario." Ph.D. thesis Department of Structural, Building and Geotechnical Engineering, Politecnico di Torino: 1-188.
67. Mauthe, A., D. Hutchison, E. K. Cetinkaya, I. Ganchev, J. Rak, J. P. Sterbenz, M. Gunkelk, P. Smith and T. Gomes (2016). Disaster-resilient communication networks: Principles and best practices. 2016 8th International Workshop on Resilient Networks Design and Modeling (RNDM), IEEE.
68. McAllister, T. P. (2015). "Community resilience planning guide for buildings and infrastructure systems, volume i."
69. McClure, G., C. A. Gálvez and S. Zaugg (1997). Equivalent Static Load Method for Seismic Analysis of Lattice Telecommunication Towers. Building to Last, ASCE.
70. Mikus, J. (1994). Seismic Analysis of Self-Supporting Telecommunications Towers, Department of Civil Engineering and Applied Mechanics, McGill University.
71. Mishra, A. R. (2007). Advanced cellular network planning and optimisation: 2G/2.5 G/3G... evolution to 4G, John Wiley & Sons.
72. Mühleisen, M., D. Bültmann, R. Schoenen and B. Walke (2011). Analytical evaluation of an IMT-advanced compliant LTE system level simulator. 17th European Wireless 2011-Sustainable Wireless Technologies, VDE.
73. Murty, C., R. Goswami, A. Vijayanarayanan, R. P. Kumar and V. V. Mehta (2012). Earthquake Protection of Non-Structural Elements in Buildings, Gujarat State Disaster Management Authority, Government of Gujarat.
74. Noori, A. Z., S. Marasco, O. Kammouh, M. Domaneschi and G. Cimellaro (2017). Smart cities to improve resilience of communities. 8th International Conference on Structural Health Monitoring of Intelligent Infrastructure, SHMII Brisbane; Australia.
75. Opensignal (2017). "Global State of Mobile Networks."
76. Owada, Y., J. Byonpyo, H. Kumagai, Y. Takahashi, M. Inoue, G. Sato, K. Temma and T. Kuri (2018). Resilient mesh network system utilized in areas affected by the Kumamoto earthquakes. 2018 5th International Conference on Information and Communication Technologies for Disaster Management (ICT-DM), IEEE.
77. Pakdel-Lahiji, N., M. Bastami and M. Sadeghi (2016). "Seismic vulnerability assessment and risk modelling of telecommunication systems." *International Journal of Critical Infrastructures* 12(4): 295-310.



78. PRB.org (2020). "Urban Population."
79. Rao, N. P. and V. Kalyanaraman (2001). "Non-linear behaviour of lattice panel of angle towers." *Journal of Constructional Steel Research* 57(12): 1337-1357.
80. Rath, S., N. Malik, N. Chahal and S. Malik (2014). "Throughput for TDD and FDD 4 G LTE Systems." *International Journal of Innovative Technology and Exploring Engineering (IJITEE)*, ISSN: 2278-3075.
81. Sackmann, V. (1996). Prediction of natural frequencies and mode shapes of self-supporting lattice telecommunication towers, Department of Civil Engineering and Applied Mechanics, McGill University.
82. Sakano, T., Z. M. Fadlullah, T. Ngo, H. Nishiyama, M. Nakazawa, F. Adachi, N. Kato, A. Takahara, T. Kumagai and H. Kasahara (2013). "Disaster-resilient networking: a new vision based on movable and deployable resource units." *IEEE Network* 27(4): 40-46.
83. Sauter, M. (2010). "3.7. 1 mobility management in the cell-dch state." *From GSM to LTE: An Introduction to Mobile Networks and Mobile Broadband*: 160.
84. Shang, F., W. Su, Q. Wang, H. Gao and Q. Fu (2014). "A location estimation algorithm based on RSSI vector similarity degree." *International Journal of Distributed Sensor Networks* 10(8): 371350.
85. Smith, P., D. Hutchison, J. P. Sterbenz, M. Schöller, A. Fessi, M. Karaliopoulos, C. Lac and B. Plattner (2011). "Network resilience: a systematic approach." *IEEE Communications Magazine* 49(7): 88-97.
86. Sosinsky, B. (2009). *Networking bible*, John Wiley & Sons.
87. Steelman, J. S. and J. F. Hajjar (2009). "Influence of inelastic seismic response modeling on regional loss estimation." *Engineering Structures* 31(12): 2976-2987.
88. Sterbenz, J. P., E. K. Cetinkaya, M. A. Hameed, A. Jabbar and J. P. Rohrer (2011). Modelling and analysis of network resilience. 2011 Third International Conference on Communication Systems and Networks (COMSNETS 2011), IEEE.
89. Stojcev, M. (2005). Alberto Leon-Garcia, Indra Widjaja, *Communication Networks: Fundamental Concepts and Key Architectures*, McGraw Hill Higher Education, Boston, 2004, ISBN 0-07-119848-2. Hardcover, pp. 900, plus XXVII, Pergamon.
90. Stokey, W. F. (1988). "Vibration of systems having distributed mass and elasticity." *Shock and vibration Handbook*: 7.11-17.15.
91. Sun, W., P. Bocchini and B. D. Davison (2020). "Resilience metrics and measurement methods for transportation infrastructure: the state of the art." *Sustainable and Resilient Infrastructure* 5(3): 168-199.
92. Tah, A. M., K. M. Alsilevanai and M. Özakça (2017). "Comparison of Various Bracing System for Self-Supporting Steel Lattice Structure Towers." *American Journal of Civil Engineering* 5(2): 60-68.
93. Taurino, V., O. Kammouh, A. Cardoni and G. Paolo (2018). "RESILIENCE ASSESSMENT OF LARGE SCALE WATER DISTRIBUTION NETWORKS: A SIMULATION APPROACH."
94. Travanca, R., H. Varum and P. V. Real (2013). "The past 20 years of telecommunication structures in Portugal." *Engineering Structures* 48: 472-485.
95. Weatherspoon, H. (2014). "Data Center Network Topologies: FatTree."
96. Xu, D., J. Zhang, X. Gao, P. Zhang and Y. Wu (2007). Indoor office propagation measurements and path loss models at 5.25 GHz. 2007 IEEE 66th Vehicular Technology Conference, IEEE.
97. Yu, S. M. and S.-L. Kim (2013). Downlink capacity and base station density in cellular networks. 2013 11th international symposium and workshops on modeling and optimization in mobile, ad hoc and wireless networks (WiOpt), IEEE.
98. Zhang, J., D. Dong, Y. Liang, X. Nie, X. Gao, Y. Zhang, C. Huang and G. Liu (2008). Propagation characteristics of wideband MIMO channel in urban micro-and macrocells. 2008 IEEE 19th International Symposium on Personal, Indoor and Mobile Radio Communications, IEEE.

# Acknowledgment

At the end of this university path, I would like to express my sincere gratitude first, to my supervisor, Prof. Gian Paolo Cimellaro for having been close to me despite the critical situation of these times causing the impossibility of carrying out this work at the University of Berkeley with the research group of Prof Kenichi Soga, wisely accompanying me in my first real research experience and for allowing me to collaborate with a group of extraordinary people. A huge thank you I must do to an exceptional person, the one who followed me daily, taking time away from his research, the PhD student Alessandro Cardoni. To Dr. Eng. Francesco Malandrino without whom this work would never have started. Thanks to his patience in explaining to me concepts of fields unknown to me such as telecommunications and writing with new languages. Thanks, is a must to Sebastiano Marasco for his few but precious advice. Finally, thanks go to my family for giving me the opportunity to complete a prestigious university course, in an elite university.

# Annexes

## I.I Script to define the Throughput

```
#Definition of the libraries in use
import numpy as np
import pandas as pd
import json
import matplotlib.pyplot as plt
import scipy as sp
import pyproj as prj
import shapely as Shp
#import dask as dk
#import pandarallel
#pandarallel.initialize()
import time
import geopandas as gpd
#import geojson
import contextily as ctx
#import geoplot
import plotly.express as px
import plotly.graph_objects as go
import folium

start_time = time.time()

#Definition and import of input data about first provider's Base station

dataBs = pd.read_csv('BTS_wind3_Ma-o-Mi.txt', sep="\t", header=None, skiprows=1)
dataBs.columns = ["id_Bs", "Id_building", "Cx_Bs", "Cy_Bs", "band", "frequency", "type",
                  "typeofcell", "h_building", "h_Bs", "h_tot",
                  "material", "classofmaterial", "link_BSC", "structure", "section", "res
traint"]
#print(dataBs)

#Definition and import of input general data

type_h = {'id_Building':np.int32,'h':np.float64}
h_building = pd.read_csv('altezze.ed.txt', sep="\t", skiprows=1, converters = type_h)
h_building.columns = ["id_Building", "h"]
#print(h_building)
h_ed = h_building["h"]
h_ed = h_ed.astype(float)
#h_ed.dtype
#print(h_ed)
h_m = h_ed.mean()
#print("{0:.2f}".format(h_m))

street = pd.read_csv('strade.txt', sep="\t", converters={"width":float}, header=None, ski
prows=1)
```

```

street.columns = ["id_street", "width"]
#print(street)
w_street = street["width"]
w_street = w_street.astype(float)
#w_street.dtype
#print(w_street)
w_m = w_street.mean()
#print("{0:.2f}".format(w_m))

#Definition and import of input data about Cluster Users

users = pd.read_csv('utenti.wind3.txt', sep="\t", converters={'user_per_cluster': int}, header=None)
users.columns = ["id_cluster", "users_per_cluster", "Cx_Ue", "Cy_Ue"]
#print(users)

#-----STEPS-----
#1°: Compute the distances between the user selected and the all Base stations in meters

distances = pd.DataFrame()
dist_p1 = pd.DataFrame()

dataBs['key'] = 1
users['key'] = 1
left = dataBs[['id_Bs', 'Cx_Bs', 'Cy_Bs', 'key']]
right = users[['id_cluster', 'Cx_Ue', 'Cy_Ue', 'key']]
#print(left)
pairs = pd.merge(right, left, on = 'key').drop("key",1)
#print(pairs)

distances["distance [m]"] = np.sqrt((pow((pairs.Cx_Ue - pairs.Cx_Bs),2))+(pow((pairs.Cy_Ue - pairs.Cy_Bs),2)))
distances = distances.round(decimals = 2)
left1 = dataBs[['id_Bs', 'key']]
right1 = users[['id_cluster', 'key']]
pairs1 = pd.merge(right1, left1, on = 'key').drop("key",1)
dist_p1 = pd.concat([pairs1["id_cluster"], pairs1["id_Bs"], distances], axis = 1)
dist_p1.columns = ["id_Ue [-]", "id_Bs [-]", "distance [m]"]
#dist_p1.index = np.arange(1, len(dist_p1)+1)
#dist_p1.to_csv("distance_to_provider1.txt", index = False, sep="\t", header = True)
#print(dist_p1)

#2°: Compute the LOS probability for each couple UE-
Bs using the formulas provided by the ITU

freq_B = 0.8
freq_A = 1.8
left = dataBs[['id_Bs', 'frequency', 'h_tot', 'key']]
left["frequency"] = left["frequency"]/1000
right = users[['id_cluster', 'key']]
pairs = pd.merge(right, left, on = 'key').drop("key",1)
#pairs.index = np.arange(1, len(pairs)+1)
pairs = pd.concat([pairs, dist_p1["distance [m]"]], axis = 1)

```

```

pairs.columns = ["id_Ue [-]", "id_Bs [-",
                "frequency [GHz]", "h_tot [m]", "distance [m]"]
#print(pairs)

pairs.loc[pairs["frequency [GHz]"] == freq_B, 'P_LOS'] = (np.minimum(1, (18/pairs["distance [m]"]))) * (1 - np.exp(-(pairs["distance [m]"]/63))) + np.exp(-(pairs["distance [m]"]/63))).round(decimals = 5)
pairs.loc[pairs["frequency [GHz]"] == freq_A, 'P_LOS'] = (np.minimum(1, (18/pairs["distance [m]"]))) * (1 - np.exp(-(pairs["distance [m]"]/36))) + np.exp(-(pairs["distance [m]"]/36))).round(decimals = 5)
#print(pairs)

#3°: Compute the Path Loss in dB for each couple UE-
Bs using the formulas provided by the ITU,
# keeping in mind the difference between in LOS and in NLOS

h_UE = 1.5
cost1 = 161.04
cost2 = 28
cost3 = 22.7
cost4 = 7.8
lim_Mac = 0.2
lim_Mic = 0.23

pairs.loc[(pairs["frequency [GHz]"] == freq_B) & (pairs["P_LOS"] < lim_Mac), 'PL [dB]'] =
(cost1 - (7.1 * np.log10(w_m)) + 7.5 * np.log10(h_m) - ((24.37 -
(3.7 * (pow((h_m / pairs["h_tot [m]"), 2)))) * np.log10(pairs["h_tot [m]"]))) + (((43.42 -
(3.1 * np.log10(pairs["h_tot [m]"])))) * ((np.log10(pairs["distance [m]"]) - 3)) + (20
* np.log10(pairs["frequency [GHz]"]))) - ((3.2 * (pow((np.log10(11.75 * h_UE)), 2))) - 4.97
)).round(decimals = 2)
pairs.loc[(pairs["frequency [GHz]"] == freq_B) & (pairs["P_LOS"] >= lim_Mac), 'PL [dB]']
= (cost2 + (22 * np.log10(pairs["distance [m]"]))) + (20 * np.log10(pairs["frequency [GHz]
"]))).round(decimals = 2)
pairs.loc[(pairs["frequency [GHz]"] == freq_A) & (pairs["P_LOS"] < lim_Mic), 'PL [dB]'] =
(cost3 + (36.7 * np.log10(pairs["distance [m]"]))) + (26 * np.log10(pairs["frequency [GHz]
"]))).round(decimals = 2)
pairs.loc[(pairs["frequency [GHz]"] == freq_A) & (pairs["P_LOS"] >= lim_Mic), 'PL [dB]']
= (cost4 + (40 * np.log10(pairs["distance [m]"]))) - (18 * np.log10(pairs["h_tot [m]"]))) -
(18 * np.log10(h_UE)) + (2 * np.log10(pairs["frequency [GHz]"]))).round(decimals = 2)

#4°: Compute the received signal strength indicator (RSSI)

# We assume a transmission power of 43 dBm for macro-cells, and 30 dBm
# for micro-cells. Using such a model, we can then compute

Pt_micro = 30
Pt_macro = 43

pairs.loc[pairs["frequency [GHz]"] == freq_B, 'RSSI [dBm]'] = (Pt_macro - pairs["PL [dB]"]
]).round(decimals = 2)
pairs.loc[pairs["frequency [GHz]"] == freq_A, 'RSSI [dBm]'] = (Pt_micro - pairs["PL [dB]"]
]).round(decimals = 2)

# Now let's convert the RSSI index from dBm to Watt
pairs["RSSI [Watt]"] = (10 ** ((pairs["RSSI [dBm]"] - 30) / 10))

```

```

#pairs.to_csv("reslod.txt", index = False, sep="\t", header = True)

#5°: Now we compute the all Interference and the Noise
#sum_Interf = pd.DataFrame()
sum_RSSI = pairs.groupby(by=["id_Ue [-]"])[ "RSSI [Watt]"].sum()
sum_RSSI = sum_RSSI.to_frame()
sum_RSSI.columns = [ "sum_RSSI [Watt]" ]
sum_RSSI.rename_axis("id_Ue [-]", axis="columns")
#print(sum_RSSI)

pairs = pd.merge(pairs, sum_RSSI, on = 'id_Ue [-]')
pairs [ "Interference [Watt]" ] = pairs["sum_RSSI [Watt]" ] - pairs["RSSI [Watt]" ]

#6°: Compute the signal-to-interference-plus-noise ratio (SINR)

#pairs["SINR [Watt]" ] = pairs["RSSI [Watt]" ] / pairs["Interference [Watt]" ].round(decimal
s = 4)
pairs["SINR [dB]" ] = (10 * np.log10((pairs["RSSI [Watt]" ] / pairs["Interference [Watt]" ]
)).round(decimals = 2)

#7°: Define the ThroughPut from experimental data curve considering a 2x2 MIMO sysytem

RB = 50 # number of resarch block
xp = pd.Series([-25, -20, -10, -5, 0, 5, 10, 12, 15, 20, 25, 30, 35, 40, 45])
yp = pd.Series([0.000, 0.005, 0.010, 0.020, 0.100, 0.200, 0.340, 0.400, 0.520, 0.760, 1.0
00, 1.240, 1.340, 1.400, 1.440])
yp = yp * RB
#print(yp)

#plot the experimental cuve
#plt.xlabel('SINR (dB)')
#plt.ylabel('throughPut (Mbps)')
#plt.title("Experimental throughput curve [Mbps]", loc = "center", color = "darkred")
#plt.grid(color='grey', linestyle='-', linewidth=0.2)
#plt.plot(xp, yp, color='blue', marker='o', linestyle='-', linewidth=1.5, markersize=5)
#plt.savefig('throughput.png')
#plt.show()
#plt.close()

pairs["Throughput [Mbps]" ] = (np.interp(pairs["SINR [dB]" ], xp, yp)).round(decimals = 2)
#pairs.index = np.arange(1, len(pairs)+1)
#pairs.to_csv("reslod.txt", index = False, sep="\t", header = True)
print(pairs)

#8°: Definition of the use of each base station

Bs_cap = pd.DataFrame()
Bs_cap = pairs.loc[pairs.groupby(by=["id_Ue [-]"])[ "Throughput [Mbps]" ].idxmax()]
Bs_cap.index = np.arange(1, len(Bs_cap)+1)
Bs_cap = Bs_cap.drop(columns=[ 'frequency [GHz]', 'h_tot [m]', 'distance [m]', 'P_LOS', 'PL
[dB]', 'RSSI [dBm]',
                                'RSSI [Watt]', 'sum_RSSI [Watt]', 'Interference [Watt]',
                                'SINR [dB]' ])

```

```

Bs_cap.loc[Bs_cap["Throughput [Mbps]"] == 0, 'Throughput [Mbps]'] = 1
Bs_cap.to_csv("capacityBs.txt", index = False, sep="\t", header = True)
n_users = pd.DataFrame()
n_users["n_Ue_per_cluster [-]"] = users['users_per_cluster']
n_users.index = np.arange(1, len(Bs_cap)+1)
Bs_cap = pd.concat([Bs_cap, n_users], axis = 1)
#print(Bs_cap)

n_cluster_Bs = pd.DataFrame()
n_cluster_Bs["n of cluster per Bs [-]"] = Bs_cap['id_Bs [-]'].value_counts()
n_cluster_Bs["id_Bs [-]"] = n_cluster_Bs.index

n_cluster_Bs = n_cluster_Bs.sort_values(by=['id_Bs [-]'])
n_cluster_Bs.index = np.arange(0, len(n_cluster_Bs))
#print(n_cluster_Bs)

nUe_Bs = Bs_cap.groupby(by=["id_Bs [-]"])[["n_Ue_per_cluster [-]"]].sum()
nUe_Bs = nUe_Bs.to_frame()
nUe_Bs.columns = ["n_Ue_Bs [-]"]
nUe_Bs["id_Bs [-]"] = nUe_Bs.index
nUe_Bs.index = np.arange(0, len(nUe_Bs))
#print(nUe_Bs)

res_Bs = pd.merge(n_cluster_Bs, nUe_Bs, on = ['id_Bs [-]'])
res_Bs = res_Bs[['id_Bs [-]', 'n of cluster per Bs [-]', 'n_Ue_Bs [-]']]
#res_Bs.to_csv("res_Bs.txt", index = True, sep="\t", header = True)
#print(res_Bs)

right_res = dataBs[['id_Bs', 'Cx_Bs', 'Cy_Bs']]
right_res.columns = ["id_Bs [-]", "Cx_Bs [m]", "Cy_Bs [m]"]
#print(right_res)

df1 = pd.merge(right_res, res_Bs, on = "id_Bs [-]")
df1 = df1.set_index('id_Bs [-]')
print(df1)

df2 = pd.DataFrame({'id_Bs [-]':range(1,len(dataBs)+1), 'n of cluster per Bs [-]':0, 'n_Ue_Bs [-]':0 })
df2 = df2.set_index('id_Bs [-]')
df2["n of cluster per Bs [-]"] = df1["n of cluster per Bs [-]"]
df2["n_Ue_Bs [-]"] = df1["n_Ue_Bs [-]"]
df2= df2.fillna(0)
df2["id_Bs [-]"] = df2.index
df2.index = np.arange(0, len(df2))
res_Bs_fin = pd.merge(df2, right_res, on = "id_Bs [-]")
f = pd.DataFrame()
f["frequency [GHz]"] = dataBs["frequency"]/1000
res_Bs_fin = pd.concat([res_Bs_fin, f], axis = 1)
res_Bs_fin = res_Bs_fin[["id_Bs [-]", "Cx_Bs [m]", "Cy_Bs [m]", "frequency [GHz]", "n of cluster per Bs [-]", "n_Ue_Bs [-]"]]
res_Bs_fin.to_csv("res_Bs_fin.txt", index = True, sep="\t", header = True)
print(res_Bs_fin)
res_Bs_fin1 = res_Bs_fin.drop_duplicates(subset=['Cx_Bs [m]'], keep='first')

```

#9°: Plotting of results for Base Stations based of frequency's split



```

import matplotlib.ticker
from matplotlib.ticker import StrMethodFormatter
from matplotlib.ticker import ScalarFormatter
from matplotlib.ticker import FormatStrFormatter
from mpl_toolkits.axes_grid1 import make_axes_locatable

Turin = gpd.read_file("confine_tot.shp")
#print(Turin)
g_res_Bs_fin = gpd.GeoDataFrame(res_Bs_fin, geometry = gpd.points_from_xy(res_Bs_fin["Cx_
Bs [m]"], res_Bs_fin["Cy_Bs [m]"]))
gMacro_cell_res = g_res_Bs_fin[g_res_Bs_fin["frequency [GHz]"] == freq_B]
gMicro_cell_res = g_res_Bs_fin[g_res_Bs_fin["frequency [GHz]"] == freq_A]
#print(gMicro_cell_res)
#print(g_res_Bs_fin)

fig, (ax1, ax2) = plt.subplots(1, 2)
ax1.ticklabel_format(axis="x", style="sci", scilimits=(3.8,4), useMathText= True)
ax1.ticklabel_format(axis="y", style="sci", scilimits=(4.9,5), useMathText= True)
plt.setp(ax1.get_xticklabels(), rotation=90, ha='right')
ax1.set_xlabel('Est (mt)')
ax1.set_ylabel('North (mt)')
ax1.set_title('Macro_cell')
ax2.ticklabel_format(axis="x", style="sci", scilimits=(3.8,4), useMathText= True)
ax2.ticklabel_format(axis="y", style="sci", scilimits=(4.9,5), useMathText= True)
plt.setp(ax2.get_xticklabels(), rotation=90, ha='right')
ax2.set_xlabel('Est (mt)')
ax2.set_ylabel('North (mt)')
ax2.set_title('Micro_cell')
Turin.plot(ax=ax1, alpha = 1, color = "white", edgecolor = "black", linewidth = 1.5)
gMacro_cell_res.plot(ax=ax1, column="n of cluster per Bs [-
]", marker = "o", cmap="plasma", scheme='fisher_jenks', k = 6, markersize = 60, edgecolor
="black", legend = True, legend_kwds={ 'title': 'N° Ue cluster by Bs', 'loc': 'upper left
'})
Turin.plot(ax=ax2, alpha = 1, color = "white", edgecolor = "black", linewidth = 1.5)
gMicro_cell_res.plot(ax=ax2, column="n of cluster per Bs [-
]", marker = "o", cmap="plasma", scheme='fisher_jenks', k = 6, markersize = 60, edgecolo
r="black", legend = True, legend_kwds={ 'title': 'N° Ue cluster by Bs', 'loc': 'upper left'
})
plt.savefig('n.cluster.Bs.png', dpi = 600)
fig.suptitle("Number of cluster managed by each Base station [-]")
plt.show()
plt.close()

fig, (ax1, ax2) = plt.subplots(1, 2)
ax1.ticklabel_format(axis="x", style="sci", scilimits=(3.8,4), useMathText= True)
ax1.ticklabel_format(axis="y", style="sci", scilimits=(4.9,5), useMathText= True)
plt.setp(ax1.get_xticklabels(), rotation=90, ha='right')
ax1.set_xlabel('Est (mt)')
ax1.set_ylabel('North (mt)')
ax1.set_title('Macro_cell')
ax2.ticklabel_format(axis="x", style="sci", scilimits=(3.8,4), useMathText= True)
ax2.ticklabel_format(axis="y", style="sci", scilimits=(4.9,5), useMathText= True)
plt.setp(ax2.get_xticklabels(), rotation=90, ha='right')
ax2.set_xlabel('Est (mt)')
ax2.set_ylabel('North (mt)')

```

```

ax2.set_title('Micro_cell')
Turin.plot(ax=ax1, alpha = 1, color = "white", edgecolor = "black", linewidth = 1.5)
gMacro_cell_res.plot(ax=ax1, column="n_Ue_Bs [-]", marker = "o", cmap="plasma", scheme='fisher_jenks', k = 6, markersize = 60, edgecolor = "black", legend = True, legend_kwds={ 'title': 'N°.Ue by Bs', 'loc': 'upper left'})
Turin.plot(ax=ax2, alpha = 1, color = "white", edgecolor = "black", linewidth = 1.5)
gMicro_cell_res.plot(ax=ax2, column="n_Ue_Bs [-]", marker = "o", cmap="plasma", scheme='fisher_jenks', k = 6, markersize = 60, edgecolor = "black", legend = True, legend_kwds={ 'title': 'N°.Ue by Bs', 'loc': 'upper left'})
plt.savefig('n.users.Bs.png', dpi = 600)
fig.suptitle("Number of users managed by each Base station [-]")
plt.show()
plt.close()

```

```

#10°: Defining the Results for Base station based on their position (macro+micro)
Ue_per_Bs = pd.DataFrame()
Ue_per_Bs["sum per Bs [-]"] = res_Bs_fin.groupby(by=["Cx_Bs [m]"])[ "n_Ue_Bs [-]"].sum()
Ue_per_Bs["Cx_Bs [m]"] = Ue_per_Bs.index
Ue_per_Bs.index = np.arange(0, len(Ue_per_Bs))
#print(Ue_per_Bs)
Ue_per_Bs.to_csv("Ue_per_Bs.txt", index = True, sep="\t", header = True)
res_Bs_fin1.index = np.arange(0, len(res_Bs_fin1))
#print(res_Bs_fin1)
Bs_tot = pd.merge(res_Bs_fin1, Ue_per_Bs, on = 'Cx_Bs [m]')
Bs_tot = Bs_tot.drop(columns = ["frequency [GHz]", "n of cluster per Bs [-]", "n_Ue_Bs [-]"])
print(Bs_tot)
Bs_tot.to_csv("Bs_tot.txt", index = True, sep="\t", header = True)

g_Bs_tot = gpd.GeoDataFrame(Bs_tot, geometry = gpd.points_from_xy(Bs_tot["Cx_Bs [m]"], Bs_tot["Cy_Bs [m]"]))
print(g_Bs_tot)

ax = plt.axes()
plt.xticks(rotation='vertical')
plt.ticklabel_format(axis="x", style="sci", scilimits=(3.8,4), useMathText= True)
plt.ticklabel_format(axis="y", style="sci", scilimits=(4.9,5), useMathText= True)
plt.xlabel('Est (mt)')
plt.ylabel('North (mt)')
Turin.plot(ax = ax, alpha = 1, color = "white", edgecolor = "black", linewidth = 1.5)
g_Bs_tot.plot(ax = ax, alpha = 1, column="sum per Bs [-]", marker = "o", cmap="plasma", scheme='natural_breaks', k = 8, markersize = 60, edgecolor = "black", legend = True, legend_kwds={ 'title': 'Sum Ue by Bs', 'loc': 'upper left'})
plt.show()
plt.close()

```

```

#11°: Plotting the Results for the Ue Cluster based on the best Throughput that they have
u = pd.DataFrame()
u = users[["id_cluster", 'Cx_Ue', 'Cy_Ue']]
u.columns = ["id_Ue [-]", "Cx [m]", "Cy [m]"]
res_th_UE = pd.merge(u, Bs_cap, on = "id_Ue [-]")
#print(res_th_UE)

g_res_th_UE = gpd.GeoDataFrame(res_th_UE, geometry = gpd.points_from_xy(res_th_UE["Cx [m]"], res_th_UE["Cy [m]"]))

```

```

fig, ax = plt.subplots()
plt.xticks(rotation='vertical')
plt.ticklabel_format(axis="x", style="sci", scilimits=(3.8,4), useMathText= True)
plt.ticklabel_format(axis="y", style="sci", scilimits=(4.9,5), useMathText= True)
plt.xlabel('Est (mt)')
plt.ylabel('North (mt)')
divider = make_axes_locatable(ax)
cax = divider.append_axes("right", size="5%", pad=0.1)
Turin.plot(ax = ax, alpha = 1, color = "white", edgecolor = "black", linewidth = 1.5)
g_res_th_UE.plot(ax = ax, alpha = 1, column="Throughput [Mbps]", marker = "o", cmap="plasma", markersize = 30, edgecolor="black", legend = True, legend_kwds={'label': "Throughput [Mbps]"}, cax = cax)
plt.show()
plt.close()

print("--- %s seconds ---" % (time.time() - start_time))

```

## 1.2 Script to assessment of damage components

```

#Definition of the libraries in use
import numpy as np
import pandas as pd
import json
import matplotlib.pyplot as plt
import scipy as sp
import pyproj as prj
import shapely as Shp
import time
import geopandas as gpd
import contextily as ctx
import geoplots

#import plotly.express as px
#import plotly.graph_objects as go

start_time = time.time()

#Definition and import of input data about damage suffered by buildings
str_dam_buil = pd.read_csv('Damage_state_buildings.txt', sep="\t", header=None, skiprows=1)
str_dam_buil.columns = ["id_build", "el centro", "hachinoe", "kobe", "northridge"]
#print(str_dam_buil)

#Import the data about the central office control
bsc = pd.read_csv('BSC.txt', sep="\t", header=None, skiprows=1)
bsc.columns = ["id_BSC", "Cx", "Cy", "id_build", "n_story", "area",
               "h_building", "id_Bs", "Cx_Bs", "Cy_Bs", "stand_BTS",
               "CoveragBTS", "struct_BTS", "h_BTS", "link_core1", "link_core2",
               "link_agg1", "link_agg2" ]
#print(bsc)

#Import the data about the base stations on rooftop
bts_rooftop = pd.read_csv('BTS_tim_rooftop.txt', sep="\t", header=None, skiprows=1)

```

```

bts_rooftop.columns = ["id_bs", "id_build", "Cx_bs", "Cy_bs", "band", "frequency", "type",
    "typeofcell",
    "h_build", "h_bs", "h_tot", "material", "classofmaterial", "link_bsc",
    "structure", "section", "restrain"]
#print(bts_rooftop)

#Import the data about the base stations on ground
bts_rawland= pd.read_csv('BTS_tim_rawland.txt', sep="\t", header=None, skiprows=1)
bts_rawland.columns = ["id_bs", "id_build", "Cx_bs", "Cy_bs", "band", "frequency", "type",
    "typeofcell",
    "h_build", "h_bs", "h_tot", "material", "classofmaterial", "link_bsc",
    "structure", "section", "restrain"]
#print(bts_rawland)

#-----STEPS-----

#1°: Determine which switch centers are out of order
bsc_1 = bsc[["id_BSC", "id_build", "Cx", "Cy"]]
#print(bsc_1)
bsc_1 = pd.merge(bsc_1, str_dam_build, on = 'id_build')
bsc_2 = bsc_1
print(bsc_2)

import matplotlib.ticker
from matplotlib.ticker import StrMethodFormatter
from matplotlib.ticker import ScalarFormatter
from matplotlib.ticker import FormatStrFormatter
from mpl_toolkits.axes_grid1 import make_axes_locatable

Turin = gpd.read_file("confine_tot.shp")
Buildings = gpd.read_file("buildings.aggiornati.shp")
Build = Buildings[["ID", "geometry"]]
Build.columns = ["id_build", "geometry"]
Build['id_build'] = Build['id_build'].astype('int64')
#Build.info()
#print(Build)

g_bsc_1 = gpd.GeoDataFrame(bsc_1, geometry = gpd.points_from_xy(bsc_1["Cx"], bsc_1["Cy"])
)

ax = plt.axes()
plt.xticks(rotation='vertical')
plt.ticklabel_format(axis="x", style="sci", scilimits=(3.8,4), useMathText= True)
plt.ticklabel_format(axis="y", style="sci", scilimits=(4.9,5), useMathText= True)
plt.xlabel('Est (mt)')
plt.ylabel('North (mt)')
Turin.plot(ax = ax, alpha = 1, color = "white", edgecolor = "black", linewidth = 1.5)
g_bsc_1.plot(ax = ax, alpha = 1, column="hachinoe", marker = "s", cmap="plasma", markersize = 60, edgecolor="black", legend = True, legend_kwds={ 'title': 'Hachinohe Earthquake',
    'loc': 'upper left'})
plt.show()
plt.close()

#2°: Determine which residential buildings collapse so also the Bs are out of order

```

```

bts_1 = bts_rooftop[["id_bs", "id_build", "Cx_bs", "Cy_bs", "link_bsc"]]
bts_rawland_1 = bts_rawland[["id_bs", "id_build", "Cx_bs", "Cy_bs", "link_bsc"]]
bts_1 = pd.merge(bts_1, str_dam_build, on = 'id_build')
bts_1 = pd.concat([bts_1, bts_rawland_1])
bts_1.index = np.arange(0, len(bts_1))
bts_1.fillna('No_damage', inplace=True)
bts_1.columns = ["id_bs", "id_build", "Cx_bs", "Cy_bs", "id_BSC", "el centro", "hachinoe",
, "kobe", "northridge"]
bts_1.loc[bts_1["id_build"] == "No_damage", "id_build"] = "no_data"
print("\n", bts_1)

```

```

Turin = gpd.read_file("confine_tot.shp")
g_bts_1 = gpd.GeoDataFrame(bts_1, geometry = gpd.points_from_xy(bts_1["Cx_bs"], bts_1["Cy_bs"]))

```

```

ax = plt.axes()
plt.xticks(rotation='vertical')
plt.ticklabel_format(axis="x", style="sci", scilimits=(3.8,4), useMathText= True)
plt.ticklabel_format(axis="y", style="sci", scilimits=(4.9,5), useMathText= True)
plt.xlabel('Est (mt)')
plt.ylabel('North (mt)')
Turin.plot(ax = ax, alpha = 1, color = "white", edgecolor = "black", linewidth = 1.5)
g_bts_1.plot(ax = ax, alpha = 1, column="el centro", marker = "o", cmap="plasma", markersize = 60, edgecolor="black", legend = True, legend_kwds={ 'title': 'El Centro Earthquake', 'loc': 'upper left'})
plt.show()
plt.close()

```

#3°: Damage about buildings

```

#buildings_damage = pd.merge(Build, str_dam_build, on = 'id_build')
#print(buildings_damage)

```

```

#ax = plt.axes()
#plt.xticks(rotation='vertical')
#plt.ticklabel_format(axis="x", style="sci", scilimits=(3.8,4), useMathText= True)
#plt.ticklabel_format(axis="y", style="sci", scilimits=(4.9,5), useMathText= True)
#plt.xlabel('Est (mt)')
#plt.ylabel('North (mt)')
#Turin.plot(ax = ax, alpha = 1, color = "white", edgecolor = "black", linewidth = 1.5)
#buildings_damage.plot(ax = ax, alpha = 1, column="kobe", cmap="RdYlGn", edgecolor="black", legend = True, legend_kwds={ 'title': 'Northridge Earthquake', 'loc': 'upper left'})
#lt.show()
#plt.close()

```

#4°: Determinate the Bs that are out of order because of switch center is damage

```

bsc_2["el centro work"] = "in"
bsc_2.loc[(bsc_2["el centro"] == 'Complete') | (bsc_2["el centro"] == 'Extensive'), 'el centro work'] = "out"
bsc_2["hachinoe work"] = "in"
bsc_2.loc[(bsc_2["hachinoe"] == "Complete") | (bsc_2["hachinoe"] == 'Extensive'), 'hachinoe work'] = "out"
bsc_2["kobe work"] = "in"
bsc_2.loc[(bsc_2["kobe"] == "Complete") | (bsc_2["kobe"] == 'Extensive'), 'kobe work'] = "out"

```

```

bsc_2["northridge work"] = "in"
bsc_2.loc[(bsc_2["northridge"] == "Complete") | (bsc_2["northridge"] == 'Extensive'), 'northridge work'] = "out"
bsc_2.to_csv("BSC_out.txt", index = False, sep="\t", header = True)
print(bsc_2)
#bts_1.info()

bsc_3 = bsc_2[["id_BSC", "el centro work", "hachinoe work", "kobe work", "northridge work"]]

res = pd.merge(bts_1, bsc_3, on = 'id_BSC')
#print(res)

res["EL CENTRO WORK?"] = "YES"
res.loc[(res["el centro work"] == "out") | ((res["el centro"] == "Complete") | (res["el centro"] == "Extensive"))], 'EL CENTRO WORK?'] = "NO"
res["HACHINOE WORK?"] = "YES"
res.loc[(res["hachinoe work"] == "out") | ((res["hachinoe"] == "Complete") | (res["hachinoe"] == "Extensive"))], 'HACHINOE WORK?'] = "NO"
res["KOBE WORK?"] = "YES"
res.loc[(res["kobe work"] == "out") | ((res["kobe"] == "Complete") | (res["kobe"] == "Extensive"))], 'KOBE WORK?'] = "NO"
res["NORTHRIDGE WORK?"] = "YES"
res.loc[(res["northridge work"] == "out") | ((res["northridge"] == "Complete") | (res["northridge"] == "Extensive"))], 'NORTHRIDGE WORK?'] = "NO"
res.to_csv("funzionBS.txt", index = False, sep="\t", header = True)
#print(res)

res = res[["id_bs", "Cx_bs", "Cy_bs", "id_BSC", "EL CENTRO WORK?", "HACHINOE WORK?", "KOBE WORK?", "NORTHRIDGE WORK?"]]
g_res= gpd.GeoDataFrame(res, geometry = gpd.points_from_xy(res["Cx_bs"], res["Cy_bs"]))
print(g_res)

fig, ((ax1, ax2), (ax3, ax4)) = plt.subplots(2, 2)
ax1.ticklabel_format(axis="x", style="sci", scilimits=(3.8,4), useMathText= True)
ax1.ticklabel_format(axis="y", style="sci", scilimits=(4.9,5), useMathText= True)
plt.setp(ax1.get_xticklabels(), rotation=90, ha='right')
ax1.set_xlabel('Est (mt)')
ax1.set_ylabel('North (mt)')
ax1.set_title('El Centro Earthquake')
ax2.ticklabel_format(axis="x", style="sci", scilimits=(3.8,4), useMathText= True)
ax2.ticklabel_format(axis="y", style="sci", scilimits=(4.9,5), useMathText= True)
plt.setp(ax2.get_xticklabels(), rotation=90, ha='right')
ax2.set_xlabel('Est (mt)')
ax2.set_ylabel('North (mt)')
ax2.set_title('Hichinoe Earthquake')
ax3.ticklabel_format(axis="x", style="sci", scilimits=(3.8,4), useMathText= True)
ax3.ticklabel_format(axis="y", style="sci", scilimits=(4.9,5), useMathText= True)
plt.setp(ax3.get_xticklabels(), rotation=90, ha='right')
ax3.set_xlabel('Est (mt)')
ax3.set_ylabel('North (mt)')
ax3.set_title('Kobe Earthquake')
ax4.ticklabel_format(axis="x", style="sci", scilimits=(3.8,4), useMathText= True)
ax4.ticklabel_format(axis="y", style="sci", scilimits=(4.9,5), useMathText= True)
plt.setp(ax4.get_xticklabels(), rotation=90, ha='right')
ax4.set_xlabel('Est (mt)')
ax4.set_ylabel('North (mt)')

```

```

ax4.set_title('Northridge Earthquake')

Turin.plot(ax=ax1, alpha = 1, color = "white", edgecolor = "black", linewidth = 1.5)
g_res.plot(ax = ax1, alpha = 1, column="EL CENTRO WORK?", marker = "o", cmap="RdYlGn", markersize = 40, edgecolor="black", legend = True, legend_kwds={ 'title': 'Bs working or not', 'loc': 'upper left'})
Turin.plot(ax=ax2, alpha = 1, color = "white", edgecolor = "black", linewidth = 1.5)
g_res.plot(ax = ax2, alpha = 1, column="HACHINOE WORK?", marker = "o", cmap="RdYlGn", markersize = 40, edgecolor="black", legend = True, legend_kwds={ 'title': 'Bs working or not', 'loc': 'upper left'})
Turin.plot(ax=ax3, alpha = 1, color = "white", edgecolor = "black", linewidth = 1.5)
g_res.plot(ax = ax3, alpha = 1, column="KOBE WORK?", marker = "o", cmap="RdYlGn", markersize = 40, edgecolor="black", legend = True, legend_kwds={ 'title': 'Bs working or not', 'loc': 'upper left'})
Turin.plot(ax=ax4, alpha = 1, color = "white", edgecolor = "black", linewidth = 1.5)
g_res.plot(ax = ax4, alpha = 1, column="NORTHRIDGE WORK?", marker = "o", cmap="RdYlGn", markersize = 40, edgecolor="black", legend = True, legend_kwds={ 'title': 'Bs working or not', 'loc': 'upper left'})
plt.subplots_adjust(left=None, bottom=None, right=None, top=None, wspace=0.4, hspace=0.4)
plt.show()
plt.close()

```

#5°: Definition of the antennas in operation or not by dividing them according to the working frequency

```

#Import the data about the base stations divided by type of cell
bts_MaoMi= pd.read_csv('BTS_tim_Ma-o-Mi.txt', sep="\t", header=None, skiprows=1)
bts_MaoMi.columns = ["id_bs", "id_build", "Cx_bs", "Cy_bs", "band", "frequency", "type", "typeofcell",
                    "h_build", "h_bs", "h_tot", "material", "classofmaterial", "link_bsc", "structure", "section", "restrain"]
print(bts_MaoMi)

df_app = res[["Cx_bs", "EL CENTRO WORK?", "HACHINOE WORK?", "KOBE WORK?", "NORTHRIDGE WORK?"]]
bts_output = pd.merge(bts_MaoMi, df_app, on = 'Cx_bs')
bts_output.to_csv("BTS_output.txt", index = False, sep="\t", header = True)
print(bts_output)

print("--- %s seconds ---" % (time.time() - start_time))

```

## I.3 Script to display the virtual city

#Definition of the libraries in use

```

import numpy as np
import pandas as pd
import json
import matplotlib.pyplot as plt
import scipy as sp
import pyproj as prj
import shapely as Shp
import time

```



```

import geopandas as gpd
import contextily as ctx
import geoplot
#import plotly.express as px
#import plotly.graph_objects as go

start_time = time.time()

# import of input data about layer arlady did
Building = pd.read_csv('buildings.txt', sep="\t", header=None, skiprows=1)
Roads = pd.read_csv('roads.txt', sep="\t", header=None, skiprows=1)
PW = pd.read_csv('power_network.txt', sep="\t", header=None, skiprows=1)
water = pd.read_csv('water.txt', sep="\t", header=None, skiprows=1)

import matplotlib.ticker
from matplotlib.ticker import StrMethodFormatter
from matplotlib.ticker import ScalarFormatter
from matplotlib.ticker import FormatStrFormatter
from mpl_toolkits.axes_grid1 import make_axes_locatable

Turin = gpd.read_file("confine_tot.shp")
Buildings = gpd.read_file("buildings.aggiornati.shp")
Build = Buildings[["ID", "h_building", "geometry"]]
Build.columns = ["id_build", "h_building", "geometry"]
Build['id_build'] = Build['id_build'].astype('int64')
#Build.info()
telecom1 = gdp.read_file("teleocm1", sep = "\t", header = none)
telecom2 = gdp.read_file("teleocm2", sep = "\t", header = none)
telecom3 = gdp.read_file("teleocm3", sep = "\t", header = none)
print(Build)

union = pd.merge(Build, Roads, PW, water, on = 'id_build')
print(union)
union.to_file('build_res.shp')

fig(fig1)
plt.ticklabel_format(axis="x", style="sci", scilimits=(3.8,4), useMathText= True)
plt.ticklabel_format(axis="y", style="sci", scilimits=(4.9,5), useMathText= True)
plt.xlabel('Est (mt)')
plt.ylabel('North (mt)')
divider = make_axes_locatable(ax)
cax = divider.append_axes("right", size="5%", pad=0.1)
IDEALCITY.plot(ax = ax, alpha = 1, color = "white", edgecolor = "black", linewidth = 1.5)
Telecom.plot(ax = ax, alpha = 1, column="Throughput [Mbps]", marker = "o", cmap="plasma",
    markersize = 30, edgecolor="black", legend = True, legend_kwds={'label': "Throughput [M
bps]"}, cax = cax)
plt.show()
plt.close()
print("--- %s seconds ---" % (time.time() - start_time))

```

## 1.4 script for input data after the scenario

```
#Definition of the libraries in use
import numpy as np
import pandas as pd
import json
import matplotlib.pyplot as plt
import scipy as sp
import pyproj as prj
import shapely as Shp
import time

start_time = time.time()

#Definition and import of input data about provider's Base stations

dataBs = pd.read_csv('BTS_wind3_Ma-o-
Mi_complete_after_earthquakes.txt', sep="\t", header=None, skiprows=1)
dataBs.columns = ["id_Bs", "Id_building", "Cx_Bs", "Cy_Bs", "band", "frequency", "type",
"typeofcell", "h_building", "h_Bs", "h_tot",
"material", "classofmaterial", "link_BSC", "structure", "section", "res
traint", "ELCENTRO", "HACHINOHE", "KOBE", "NORTHRIDGE"]
print(dataBs)

#EL CENTRO input data

DataELCENTRO=dataBs[dataBs.ELCENTRO != "NO"]

DataELCENTRO = DataELCENTRO.drop(columns=['ELCENTRO', 'HACHINOHE', 'KOBE', 'NORTHRIDGE'])
DataELCENTRO.to_csv("ELCENTRO_complete.txt", index = False, sep="\t", header = True)
print(DataELCENTRO)

#HACHINOHE input data

DataHACHINOHE=dataBs[dataBs.HACHINOHE != "NO"]

DataHACHINOHE = DataHACHINOHE.drop(columns=['ELCENTRO', 'HACHINOHE', 'KOBE', 'NORTHRIDGE'
])
DataHACHINOHE.to_csv("HACHINOHE_complete.txt", index = False, sep="\t", header = True)
print(DataHACHINOHE)

#KOBE input data

DataKOBE=dataBs[dataBs.KOBE != "NO"]

DataKOBE = DataKOBE.drop(columns=['ELCENTRO', 'HACHINOHE', 'KOBE', 'NORTHRIDGE'])
DataKOBE.to_csv("KOBE_complete.txt", index = False, sep="\t", header = True)
print(DataKOBE)

#KOBE input data

DataNORTHRIDGE=dataBs[dataBs.NORTHRIDGE != "NO"]

DataNORTHRIDGE = DataNORTHRIDGE.drop(columns=['ELCENTRO', 'HACHINOHE', 'KOBE', 'NORTHRIDG
E'])
```

```
DataNORTHBRIDGE.to_csv("NORTHBRIDGE_complete.txt", index = False, sep="\t", header = True)
print(DataNORTHBRIDGE)
```

```
print("--- %s seconds ---" % (time.time() - start_time))
```

## 1.5 script to define the condition after each scenario

```
#Definition of the libraries in use
import numpy as np
import pandas as pd
import json
import matplotlib.pyplot as plt
import scipy as sp
import pyproj as prj
import shapely as Shp
#import dask as dk
#import pandarallel
#pandarallel.initialize()
import time
import geopandas as gpd
#import geojson
import contextily as ctx
#import geoplots
import plotly.express as px
import plotly.graph_objects as go
#import folium

start_time = time.time()

#Definition and import of input data about first provider's Base station

dataBsin = pd.read_csv('BTS_wind3_Ma-o-
Mi_extensive+complete_after_earthquakes.txt', sep="\t", header=None, skiprows=1)
dataBsin.columns = ["id_Bs", "Id_building", "Cx_Bs", "Cy_Bs", "band", "frequency", "type",
"typeofcell", "h_building", "h_Bs", "h_tot",
"material", "classofmaterial", "link_BSC", "structure", "section", "res
traint", "ELCENTRO", "HACHINOHE", "KOBE", "NORTHBRIDGE"]
print(dataBsin)

#Selecting just the Bs that still work after earthquakes

dataBs=dataBsin[dataBsin.KOBE != "NO"]

dataBs = dataBs.drop(columns=['ELCENTRO', 'HACHINOHE', 'KOBE', 'NORTHBRIDGE'])
dataBs.to_csv("provaBs.txt", index = False, sep="\t", header = True)
print(dataBs)

df = pd.DataFrame()
df["id_Bs"] = dataBs["id_Bs"]
df.index = np.arange(0, len(df))
print(df)
#Definition and import of input general data
```

```

type_h = {'id_Building':np.int32,'h':np.float64}
h_building = pd.read_csv('altezze.ed.txt', sep="\t", skiprows=1, converters = type_h)
h_building.columns = ["id_Building", "h"]
#print(h_building)
h_ed = h_building["h"]
h_ed = h_ed.astype(float)
#h_ed.dtype
#print(h_ed)
h_m = h_ed.mean()
#print("{0:.2f}".format(h_m))

street = pd.read_csv('strade.txt', sep="\t", converters={"width":float}, header=None, skiprows=1)
street.columns = ["id_street", "width"]
#print(street)
w_street = street["width"]
w_street = w_street.astype(float)
#w_street.dtype
#print(w_street)
w_m = w_street.mean()
#print("{0:.2f}".format(w_m))

#Definition and import of input data about Cluster Users

users = pd.read_csv('utenti.wind3.txt', sep="\t", converters={'user_per_cluster': int}, header=None)
users.columns = ["id_cluster", "users_per_cluster", "Cx_Ue", "Cy_Ue"]
#print(users)

#-----STEPS-----
#1°: Compute the distances between the user selected and the all Base stations in meters

distances = pd.DataFrame()
dist_p1 = pd.DataFrame()

dataBs['key'] = 1
users['key'] = 1
left = dataBs[['id_Bs', 'Cx_Bs', 'Cy_Bs', 'key']]
right = users[['id_cluster', 'Cx_Ue', 'Cy_Ue', 'key']]
#print(left)
pairs = pd.merge(right, left, on = 'key').drop("key",1)
#print(pairs)

distances["distance [m]"] = np.sqrt((pow((pairs.Cx_Ue - pairs.Cx_Bs),2))+(pow((pairs.Cy_Ue - pairs.Cy_Bs),2)))
distances = distances.round(decimals = 2)
left1 = dataBs[['id_Bs', 'key']]
right1 = users[['id_cluster', 'key']]
pairs1 = pd.merge(right1, left1, on = 'key').drop("key",1)
dist_p1 = pd.concat([pairs1["id_cluster"], pairs1["id_Bs"], distances], axis = 1)
dist_p1.columns = ["id_Ue [-]", "id_Bs [-]", "distance [m]"]
#dist_p1.index = np.arange(1, len(dist_p1)+1)
#dist_p1.to_csv("distance_to_provider1.txt", index = False, sep="\t", header = True)
#print(dist_p1)

```

#2°: Compute the LOS probability for each couple UE-Bs using the formulas provided by the ITU

```
freq_B = 0.8
freq_A = 1.8
left = dataBs[['id_Bs','frequency', 'h_tot', 'key']]
left["frequency"] = left["frequency"]/1000
right = users[['id_cluster', 'key']]
pairs = pd.merge(right, left, on = 'key').drop("key",1)
#pairs.index = np.arange(1, len(pairs)+1)
pairs = pd.concat([pairs, dist_p1["distance [m]"]], axis = 1)
pairs.columns = ["id_Ue [-]", "id_Bs [-]", "frequency [GHz]", "h_tot [m]", "distance [m]"]
#print(pairs)

pairs.loc[pairs["frequency [GHz]"] == freq_B, 'P_LOS'] = (np.minimum(1,(18/pairs["distance [m]"]))) * (1 - np.exp(-(pairs["distance [m]"]/63))) + np.exp(-(pairs["distance [m]"]/63))).round(decimals = 5)
pairs.loc[pairs["frequency [GHz]"] == freq_A, 'P_LOS'] = (np.minimum(1,(18/pairs["distance [m]"]))) * (1 - np.exp(-(pairs["distance [m]"]/36))) + np.exp(-(pairs["distance [m]"]/36))).round(decimals = 5)
#print(pairs)
```

#3°: Compute the Path Loss in dB for each couple UE-Bs using the formulas provided by the ITU,  
# keeping in mind the difference between in LOS and in NLOS

```
h_UE = 1.5
cost1 = 161.04
cost2 = 28
cost3 = 22.7
cost4 = 7.8
lim_Mac = 0.2
lim_Mic = 0.23

pairs.loc[(pairs["frequency [GHz]"] == freq_B) & (pairs["P_LOS"] < lim_Mac), 'PL [dB]'] = (cost1 - (7.1 * np.log10(w_m)) + 7.5 * np.log10(h_m) - ((24.37 - (3.7 * (pow((h_m / pairs["h_tot [m]"),2)))) * np.log10(pairs["h_tot [m]"]))) + (((43.42 - (3.1 * np.log10(pairs["h_tot [m]"])))) * ((np.log10(pairs["distance [m]"]) - 3)) + (20 * np.log10(pairs["frequency [GHz]"]))) - ((3.2 * (pow((np.log10(11.75 * h_UE)),2))) - 4.97)).round(decimals = 2)
pairs.loc[(pairs["frequency [GHz]"] == freq_B) & (pairs["P_LOS"] >= lim_Mac), 'PL [dB]'] = (cost2 + (22 * np.log10(pairs["distance [m]"]))) + (20 * np.log10(pairs["frequency [GHz]"]))).round(decimals = 2)
pairs.loc[(pairs["frequency [GHz]"] == freq_A) & (pairs["P_LOS"] < lim_Mic), 'PL [dB]'] = (cost3 + (36.7 * np.log10(pairs["distance [m]"]))) + (26 * np.log10(pairs["frequency [GHz]"]))).round(decimals = 2)
pairs.loc[(pairs["frequency [GHz]"] == freq_A) & (pairs["P_LOS"] >= lim_Mic), 'PL [dB]'] = (cost4 + (40 * np.log10(pairs["distance [m]"]))) - (18 * np.log10(pairs["h_tot [m]"]))) - (18 * np.log10(h_UE)) + (2 * np.log10(pairs["frequency [GHz]"]))).round(decimals = 2)
```

#4°: Compute the received signal strength indicator (RSSI)

```

# We assume a transmission power of 43 dBm for macro-cells, and 30 dBm
# for micro-cells. Using such a model, we can then compute

Pt_micro = 30
Pt_macro = 43

pairs.loc[pairs["frequency [GHz]"] == freq_B, 'RSSI [dBm]'] = (Pt_macro - pairs["PL [dB]"
]).round(decimals = 2)
pairs.loc[pairs["frequency [GHz]"] == freq_A, 'RSSI [dBm]'] = (Pt_micro - pairs["PL [dB]"
]).round(decimals = 2)

# Now let's convert the RSSI index from dBm to Watt
pairs["RSSI [Watt]"] = (10 ** ((pairs["RSSI [dBm]"] - 30) / 10))
#pairs.to_csv("reslod.txt", index = False, sep="\t", header = True)

#5°: Now we compute the all Interference and the Noise
#sum_Interf = pd.DataFrame()
sum_RSSI = pairs.groupby(by=["id_Ue [-]"])[ "RSSI [Watt]"].sum()
sum_RSSI = sum_RSSI.to_frame()
sum_RSSI.columns = [ "sum_RSSI [Watt]" ]
sum_RSSI.rename_axis("id_Ue [-]", axis="columns")
#print(sum_RSSI)

pairs = pd.merge(pairs, sum_RSSI, on = 'id_Ue [-]')
pairs [ "Interference [Watt]" ] = pairs["sum_RSSI [Watt]" ] - pairs["RSSI [Watt]" ]

#6°: Compute the signal-to-interference-plus-noise ratio (SINR)

#pairs["SINR [Watt]"] = pairs["RSSI [Watt]" ] / pairs["Interference [Watt]"].round(decimal
s = 4)
pairs["SINR [dB]"] = (10 * np.log10((pairs["RSSI [Watt]" ] / pairs["Interference [Watt]" ]
)).round(decimals = 2)

#7°: Define the ThroughPut from experimental data curve considering a 2x2 MIMO sysstem

RB = 50 # number of resarch block
xp = pd.Series([-25, -20, -10, -5, 0, 5, 10, 12, 15, 20, 25, 30, 35, 40, 45])
yp = pd.Series([0.000, 0.005, 0.010, 0.020, 0.100, 0.200, 0.340, 0.400, 0.520, 0.760, 1.0
00, 1.240, 1.340, 1.400, 1.440])
yp = yp * RB
#print(yp)

#plot the experimental cuve
#plt.xlabel('SINR (dB)')
#plt.ylabel('throughPut (Mbps)')
#plt.title("Experimental throughput curve [Mbps]", loc = "center", color = "darkred")
#plt.grid(color='grey', linestyle='--', linewidth=0.2)
#plt.plot(xp, yp, color='blue', marker='o', linestyle='--', linewidth=1.5, markersize=5)
#plt.savefig('throughput.png')
#plt.show()
#plt.close()

pairs["Throughput [Mbps]"] = (np.interp(pairs["SINR [dB]"], xp, yp)).round(decimals = 2)
#pairs.index = np.arange(1, len(pairs)+1)

```

```

#pairs.to_csv("reslod.txt", index = False, sep="\t", header = True)
print(pairs)

#8°: Definition of the user of each base station

Bs_cap = pd.DataFrame()
Bs_cap = pairs.loc[pairs.groupby(by=["id_Ue [-]"])[["Throughput [Mbps]"].idxmax()]]
Bs_cap.index = np.arange(1, len(Bs_cap)+1)
Bs_cap = Bs_cap.drop(columns=['frequency [GHz]', 'h_tot [m]', 'distance [m]', 'P_LOS', 'PL
[dB]', 'RSSI [dBm]',
                                'RSSI [Watt]', 'sum_RSSI [Watt]', 'Interference [Watt]',
                                'SINR [dB]'])
n_users = pd.DataFrame()
n_users["n_Ue_per_cluster [-]"] = users['users_per_cluster']
n_users.index = np.arange(1, len(Bs_cap)+1)
Bs_cap = pd.concat([Bs_cap, n_users], axis = 1)
Bs_cap.loc[Bs_cap["Throughput [Mbps]"] == 0, 'n_Ue_per_cluster [-]'] = 0
Bs_cap.to_csv("Bs_cap.txt", index = True, sep="\t", header = True)
Bs_cap.to_csv("throughput_miglioreUE.txt", index = False, sep="\t", header = True)
print(Bs_cap)

n_cluster_Bs = pd.DataFrame()
n_cluster_Bs["n of cluster per Bs [-]"] = Bs_cap['id_Bs [-]'].value_counts()
n_cluster_Bs["id_Bs [-]"] = n_cluster_Bs.index

n_cluster_Bs = n_cluster_Bs.sort_values(by=['id_Bs [-]'])
n_cluster_Bs.index = np.arange(0, len(n_cluster_Bs))
print(n_cluster_Bs)

nUe_Bs = Bs_cap.groupby(by=["id_Bs [-]"])[["n_Ue_per_cluster [-]"].sum()
nUe_Bs = nUe_Bs.to_frame()
nUe_Bs.columns = ["n_Ue_Bs [-]"]
nUe_Bs["id_Bs [-]"] = nUe_Bs.index
nUe_Bs.index = np.arange(0, len(nUe_Bs))
print(nUe_Bs)

res_Bs = pd.merge(n_cluster_Bs, nUe_Bs, on = ['id_Bs [-]'])
res_Bs = res_Bs[['id_Bs [-]', 'n of cluster per Bs [-]', 'n_Ue_Bs [-]']]
res_Bs.columns = ["id_Bs", "n of cluster per Bs [-]", "n_Ue_Bs [-]"]
res_Bs.to_csv("res_Bs.txt", index = True, sep="\t", header = True)
print(res_Bs)

right_res = dataBs[['id_Bs', 'Cx_Bs', 'Cy_Bs']]
right_res.columns = ["id_Bs", "Cx_Bs [m]", "Cy_Bs [m]"]
#print(right_res)

df1 = pd.merge(right_res, res_Bs, on = "id_Bs")
#df1 = df1.set_index('id_Bs [-]')
#print(df1)

df2 = pd.DataFrame({'col1':range(0,len(dataBs)), 'n of cluster per Bs [-]':0, 'n_Ue_Bs [-]':0})
#print(df2)
df3 = pd.concat([df, df2], axis = 1)
df3 = df3.drop(columns=["col1"])
df3.columns = ["id_Bs", "n of cluster per Bs [-]", "n_Ue_Bs [-]"]

```



```

print(df3)
df3.to_csv("df3.txt", index = True, sep="\t", header = True)

df4 = pd.concat([res_Bs, df3], axis = 0)
df4.index = np.arange(0, len(df4))
print(df4)
df4 = df4.drop_duplicates(subset=['id_Bs'], keep='first')
df4 = df4.sort_values(by = ['id_Bs'])
df4.index = np.arange(0, len(df4))
print(df4)
df4.to_csv("df4.txt", index = True, sep="\t", header = True)

res_Bs_fin = pd.merge(df4, right_res, on = "id_Bs")
res_Bs_fin.to_csv("res_Bs_fin.txt", index = True, sep="\t", header = True)
print(res_Bs_fin)

f = pd.DataFrame()
f["frequency [GHz]"] = dataBs["frequency"]/1000
f.index = np.arange(0, len(f))
print(f)
res_Bs_fin = pd.concat([res_Bs_fin, f], axis = 1)
#res_Bs_fin = res_Bs_fin[["id_Bs [-", "Cx_Bs [m]", "Cy_Bs [m]", "frequency [GHz]", "n of cluster per Bs [-", "n_Ue_Bs [-", "]]]]
res_Bs_fin.to_csv("res_Bs_fin.txt", index = True, sep="\t", header = True)
print(res_Bs_fin)
#res_Bs_fin1 = res_Bs_fin.drop_duplicates(subset=['Cx_Bs [m]'], keep='first')

#9°: Plotting of results for Base Stations based of frequency's split

import matplotlib.ticker
from matplotlib.ticker import StrMethodFormatter
from matplotlib.ticker import ScalarFormatter
from matplotlib.ticker import FormatStrFormatter
from mpl_toolkits.axes_grid1 import make_axes_locatable

Turin = gpd.read_file("confine_tot.shp")
#print(Turin)
g_res_Bs_fin = gpd.GeoDataFrame(res_Bs_fin, geometry = gpd.points_from_xy(res_Bs_fin["Cx_Bs [m]"], res_Bs_fin["Cy_Bs [m]"]))
gMacro_cell_res = g_res_Bs_fin[g_res_Bs_fin["frequency [GHz]"] == freq_B]
gMicro_cell_res = g_res_Bs_fin[g_res_Bs_fin["frequency [GHz]"] == freq_A]
#print(gMicro_cell_res)
#print(g_res_Bs_fin)

fig, (ax1, ax2) = plt.subplots(1, 2)
ax1.ticklabel_format(axis="x", style="sci", scilimits=(3.8,4), useMathText= True)
ax1.ticklabel_format(axis="y", style="sci", scilimits=(4.9,5), useMathText= True)
plt.setp(ax1.get_xticklabels(), rotation=90, ha='right')
ax1.set_xlabel('Est (mt)')
ax1.set_ylabel('North (mt)')
ax1.set_title('Macro_cell')
ax2.ticklabel_format(axis="x", style="sci", scilimits=(3.8,4), useMathText= True)

```

```

ax2.ticklabel_format(axis="y", style="sci", scilimits=(4.9,5), useMathText= True)
plt.setp(ax2.get_xticklabels(), rotation=90, ha='right')
ax2.set_xlabel('Est (mt)')
ax2.set_ylabel('North (mt)')
ax2.set_title('Micro_cell')
Turin.plot(ax=ax1, alpha = 1, color = "white", edgecolor = "black", linewidth = 1.5)
#gMacro_cell_res.plot(ax=ax1, column="n of cluster per Bs [-
]", marker = "o", cmap="plasma", scheme='fisher_jenks', k = 6, markersize = 60, edgecolor
="black", legend = True, legend_kwds={ 'title': 'N°.Ue cluster by Bs', 'loc': 'upper left
'})
Turin.plot(ax=ax2, alpha = 1, color = "white", edgecolor = "black", linewidth = 1.5)
gMicro_cell_res.plot(ax=ax2, column="n of cluster per Bs [-
]", marker = "o", cmap="plasma", scheme='fisher_jenks', k = 6, markersize = 60, edgecolo
r="black", legend = True, legend_kwds={ 'title': 'N°.Ue cluster by Bs', 'loc': 'upper left'
})
plt.savefig('n.cluster.Bs.png', dpi = 600)
fig.suptitle("Number of cluster managed by each Base station [-]")
plt.show()
plt.close()

```

```

fig, (ax1, ax2) = plt.subplots(1, 2)
ax1.ticklabel_format(axis="x", style="sci", scilimits=(3.8,4), useMathText= True)
ax1.ticklabel_format(axis="y", style="sci", scilimits=(4.9,5), useMathText= True)
plt.setp(ax1.get_xticklabels(), rotation=90, ha='right')
ax1.set_xlabel('Est (mt)')
ax1.set_ylabel('North (mt)')
ax1.set_title('Macro_cell')
ax2.ticklabel_format(axis="x", style="sci", scilimits=(3.8,4), useMathText= True)
ax2.ticklabel_format(axis="y", style="sci", scilimits=(4.9,5), useMathText= True)
plt.setp(ax2.get_xticklabels(), rotation=90, ha='right')
ax2.set_xlabel('Est (mt)')
ax2.set_ylabel('North (mt)')
ax2.set_title('Micro_cell')
Turin.plot(ax=ax1, alpha = 1, color = "white", edgecolor = "black", linewidth = 1.5)
#gMacro_cell_res.plot(ax=ax1, column="n_Ue_Bs [-
]", marker = "o", cmap="plasma", scheme='fisher_jenks', k = 6, markersize = 60, edgecolor
="black", legend = True, legend_kwds={ 'title': 'N°.Ue by Bs', 'loc': 'upper left'})
Turin.plot(ax=ax2, alpha = 1, color = "white", edgecolor = "black", linewidth = 1.5)
gMicro_cell_res.plot(ax=ax2, column="n_Ue_Bs [-
]", marker = "o", cmap="plasma", scheme='fisher_jenks', k = 6, markersize = 60, edgecolo
r="black", legend = True, legend_kwds={ 'title': 'N°.Ue by Bs', 'loc': 'upper left'})
plt.savefig('n.users.Bs.png', dpi = 600)
fig.suptitle("Number of users managed by each Base station [-]")
plt.show()
plt.close()

```

```

#10°: Defining the Results for Base station based on their position (macro+micro)
Ue_per_Bs = pd.DataFrame()
Ue_per_Bs["sum per Bs [-]"] = res_Bs_fin.groupby(by=["Cx_Bs [m]"])[ "n_Ue_Bs [-]"].sum()
Ue_per_Bs["Cx_Bs [m]"] = Ue_per_Bs.index
Ue_per_Bs.index = np.arange(0, len(Ue_per_Bs))
print(Ue_per_Bs)
#Ue_per_Bs.to_csv("Ue_per_Bs.txt", index = True, sep="\t", header = True)
res_Bs_fin.index = np.arange(0, len(res_Bs_fin))

Bs_tot = pd.merge(res_Bs_fin, Ue_per_Bs, on = 'Cx_Bs [m]')

```

```

Bs_tot = Bs_tot.drop(columns = ["frequency [GHz]", "n of cluster per Bs [-]", "n_Ue_Bs [-]"])
Bs_tot = Bs_tot.drop_duplicates(subset=['Cx_Bs [m]'], keep='first')
Bs_tot.index = np.arange(0, len(Bs_tot))
print(Bs_tot)
Bs_tot.to_csv("Bs_tot.txt", index = True, sep="\t", header = True)

g_Bs_tot = gpd.GeoDataFrame(Bs_tot, geometry = gpd.points_from_xy(Bs_tot["Cx_Bs [m]"], Bs_tot["Cy_Bs [m]"]))
print(g_Bs_tot)

ax = plt.axes()
plt.xticks(rotation='vertical')
plt.ticklabel_format(axis="x", style="sci", scilimits=(3.8,4), useMathText= True)
plt.ticklabel_format(axis="y", style="sci", scilimits=(4.9,5), useMathText= True)
plt.xlabel('Est (mt)')
plt.ylabel('North (mt)')
Turin.plot(ax = ax, alpha = 1, color = "white", edgecolor = "black", linewidth = 1.5)
g_Bs_tot.plot(ax = ax, alpha = 1, column="sum per Bs [-]", marker = "o", cmap="plasma", scheme='natural_breaks', k = 8, markersize = 60, edgecolor="black", legend = True, legend_kwds={ 'title': 'Sum Ue by Bs', 'loc': 'upper left'})
plt.show()
plt.close()

#11°: Plotting the Results for the Ue Cluster based on the best Throughput that they have
u = pd.DataFrame()
u = users[['id_cluster', 'Cx_Ue', 'Cy_Ue']]
u.columns = ["id_Ue [-]", "Cx [m]", "Cy [m]"]
res_th_UE = pd.merge(u, Bs_cap, on = "id_Ue [-]")
res_th_UE.to_csv("res_th_UE.txt", index = True, sep="\t", header = True)
print(res_th_UE)

g_res_th_UE = gpd.GeoDataFrame(res_th_UE, geometry = gpd.points_from_xy(res_th_UE["Cx [m]"], res_th_UE["Cy [m]"]))
fig, ax = plt.subplots()
plt.xticks(rotation='vertical')
plt.ticklabel_format(axis="x", style="sci", scilimits=(3.8,4), useMathText= True)
plt.ticklabel_format(axis="y", style="sci", scilimits=(4.9,5), useMathText= True)
plt.xlabel('Est (mt)')
plt.ylabel('North (mt)')
divider = make_axes_locatable(ax)
cax = divider.append_axes("right", size="5%", pad=0.1)
Turin.plot(ax = ax, alpha = 1, color = "white", edgecolor = "black", linewidth = 1.5)
g_res_th_UE.plot(ax = ax, alpha = 1, column="Throughput [Mbps]", marker = "o", cmap="plasma", markersize = 30, edgecolor="black", legend = True, legend_kwds={'label': "Throughput [Mbps]"}, cax = cax)
plt.show()
plt.close()

print("--- %s seconds ---" % (time.time() - start_time))

```

## 1.6 script for evaluate the resilience indices

```
#Definition of the libraries in use
import numpy as np
import pandas as pd
import json
import matplotlib.pyplot as plt
import scipy as sp
import pyproj as prj
import shapely as Shp
#import dask as dk
#import pandarallel
#pandarallel.initialize()
import time
import geopandas as gpd
#import geojson
import contextily as ctx
#import geoplot
import plotly.express as px
import plotly.graph_objects as go
import folium

start_time = time.time()

#Definition and import of input data about first provider's Base station

dataBsin = pd.read_csv('BTS_retunite_Ma-o-
Mi_complete_after_earthquakes.txt', sep="\t", header=None, skiprows=1)
dataBsin.columns = ["id_Bs", "Id_building", "Cx_Bs", "Cy_Bs", "band", "frequency", "type"
, "typeofcell", "h_building", "h_Bs", "h_tot",
                    "material", "classofmaterial", "link_BSC", "structure", "section", "res
traint", "ELCENTRO", "HACHINOHE", "KOBE", "NORTHRIDGE", "provider", "location"]
print(dataBsin)

#Selecting just the Bs that still work after earthquakes

dataBs=dataBsin[dataBsin.NORTHRIDGE != "NO"]

dataBs = dataBs.drop(columns=['ELCENTRO', 'HACHINOHE', 'KOBE', 'NORTHRIDGE'])
dataBs.to_csv("provaBs.txt", index = False, sep="\t", header = True)
print(dataBs)

df = pd.DataFrame()
df["id_Bs"] = dataBs["id_Bs"]
df.index = np.arange(0, len(df))
print(df)
#Definition and import of input general data

type_h = {'id_Building':np.int32,'h':np.float64}
h_building = pd.read_csv('altezze.ed.txt', sep="\t", skiprows=1, converters = type_h)
h_building.columns = ["id_Building", "h"]
#print(h_building)
h_ed = h_building["h"]
h_ed = h_ed.astype(float)
#h_ed.dtype
#print(h_ed)
```

```

h_m = h_ed.mean()
#print("{0:.2f}".format(h_m))

street = pd.read_csv('strade.txt', sep="\t", converters={"width":float}, header=None, skiprows=1)
street.columns = ["id_street", "width"]
#print(street)
w_street = street["width"]
w_street = w_street.astype(float)
#w_street.dtype
#print(w_street)
w_m = w_street.mean()
#print("{0:.2f}".format(w_m))

#Definition and import of input data about Cluster Users

users = pd.read_csv('utenti.totali.txt', sep="\t", converters={'user_per_cluster': int}, header=None)
users.columns = ["id_cluster", "users_per_cluster", "Cx_Ue", "Cy_Ue"]
#print(users)

#-----STEPS-----
#1°: Compute the distances between the user selected and the all Base stations in meters

distances = pd.DataFrame()
dist_p1 = pd.DataFrame()

dataBs['key'] = 1
users['key'] = 1
left = dataBs[['id_Bs', 'Cx_Bs', 'Cy_Bs', 'key']]
right = users[['id_cluster', 'Cx_Ue', 'Cy_Ue', 'key']]
#print(left)
pairs = pd.merge(right, left, on = 'key').drop("key",1)
#print(pairs)

distances["distance [m]"] = np.sqrt((pow((pairs.Cx_Ue - pairs.Cx_Bs),2))+(pow((pairs.Cy_Ue - pairs.Cy_Bs),2)))
distances = distances.round(decimals = 2)
left1 = dataBs[['id_Bs', 'key']]
right1 = users[['id_cluster', 'key']]
pairs1 = pd.merge(right1, left1, on = 'key').drop("key",1)
dist_p1 = pd.concat([pairs1["id_cluster"], pairs1["id_Bs"], distances], axis = 1)
dist_p1.columns = ["id_Ue [-]", "id_Bs [-]", "distance [m]"]
#dist_p1.index = np.arange(1, len(dist_p1)+1)
#dist_p1.to_csv("distance_to_provider1.txt", index = False, sep="\t", header = True)
#print(dist_p1)

#2°: Compute the LOS probability for each couple UE-
Bs using the formulas provided by the ITU

freq_B = 0.8
freq_A = 1.8
left = dataBs[['id_Bs', 'frequency', 'h_tot', 'key']]

```

```

left["frequency"] = left["frequency"]/1000
right = users[['id_cluster', 'key']]
pairs = pd.merge(right, left, on = 'key').drop("key",1)
#pairs.index = np.arange(1, len(pairs)+1)
pairs = pd.concat([pairs, dist_p1["distance [m]"]], axis = 1)
pairs.columns = ["id_Ue [-]", "id_Bs [-",
]", "frequency [GHz]", "h_tot [m]", "distance [m]"]
#print(pairs)

pairs.loc[pairs["frequency [GHz]"] == freq_B, 'P_LOS'] = (np.minimum(1,(18/pairs["distance [m]"]))) * (1 - np.exp(-(pairs["distance [m]"]/63))) + np.exp(-(pairs["distance [m]"]/63))).round(decimals = 5)
pairs.loc[pairs["frequency [GHz]"] == freq_A, 'P_LOS'] = (np.minimum(1,(18/pairs["distance [m]"]))) * (1 - np.exp(-(pairs["distance [m]"]/36))) + np.exp(-(pairs["distance [m]"]/36))).round(decimals = 5)
#print(pairs)

#3°: Compute the Path Loss in dB for each couple UE-
Bs using the formulas provided by the ITU,
# keeping in mind the difference between in LOS and in NLOS

h_UE = 1.5
cost1 = 161.04
cost2 = 28
cost3 = 22.7
cost4 = 7.8
lim_Mac = 0.2
lim_Mic = 0.23

pairs.loc[(pairs["frequency [GHz]"] == freq_B) & (pairs["P_LOS"] < lim_Mac), 'PL [dB]'] =
(cost1 - (7.1 * np.log10(w_m)) + 7.5 * np.log10(h_m) - ((24.37 -
(3.7 * (pow((h_m / pairs["h_tot [m]"),2)))) * np.log10(pairs["h_tot [m]"]))) + (((43.42 -
(3.1 * np.log10(pairs["h_tot [m]"])))) * ((np.log10(pairs["distance [m]"]))) - 3)) + (20
* np.log10(pairs["frequency [GHz]"]))) - ((3.2 * (pow((np.log10(11.75 * h_UE)),2))) - 4.97
)).round(decimals = 2)
pairs.loc[(pairs["frequency [GHz]"] == freq_B) & (pairs["P_LOS"] >= lim_Mac), 'PL [dB]']
= (cost2 + (22 * np.log10(pairs["distance [m]"]))) + (20 * np.log10(pairs["frequency [GHz]
"]))).round(decimals = 2)
pairs.loc[(pairs["frequency [GHz]"] == freq_A) & (pairs["P_LOS"] < lim_Mic), 'PL [dB]'] =
(cost3 + (36.7 * np.log10(pairs["distance [m]"]))) + (26 * np.log10(pairs["frequency [GHz]
"]))).round(decimals = 2)
pairs.loc[(pairs["frequency [GHz]"] == freq_A) & (pairs["P_LOS"] >= lim_Mic), 'PL [dB]']
= (cost4 + (40 * np.log10(pairs["distance [m]"]))) - (18 * np.log10(pairs["h_tot [m]"]))) -
(18 * np.log10(h_UE)) + (2 * np.log10(pairs["frequency [GHz]"]))).round(decimals = 2)

#4°: Compute the received signal strength indicator (RSSI)

# We assume a transmission power of 43 dBm for macro-cells, and 30 dBm
# for micro-cells. Using such a model, we can then compute

Pt_micro = 30
Pt_macro = 43

pairs.loc[pairs["frequency [GHz]"] == freq_B, 'RSSI [dBm]'] = (Pt_macro - pairs["PL [dB]"]
]).round(decimals = 2)

```

```
pairs.loc[pairs["frequency [GHz]"] == freq_A, 'RSSI [dBm]'] = (Pt_micro - pairs["PL [dB]"
]).round(decimals = 2)
```

```
# Now let's convert the RSSI index from dBm to Watt
pairs["RSSI [Watt]"] = (10 ** ((pairs["RSSI [dBm]"] - 30) / 10))
#pairs.to_csv("reslod.txt", index = False, sep="\t", header = True)
```

```
#5°: Now we compute the all Interference and the Noise
#sum_Interf = pd.DataFrame()
sum_RSSI = pairs.groupby(by=["id_Ue [-]"])[ "RSSI [Watt]"].sum()
sum_RSSI = sum_RSSI.to_frame()
sum_RSSI.columns = ["sum_RSSI [Watt]"]
sum_RSSI.rename_axis("id_Ue [-]", axis="columns")
#print(sum_RSSI)
```

```
pairs = pd.merge(pairs, sum_RSSI, on = 'id_Ue [-]')
pairs ["Interference [Watt]"] = pairs["sum_RSSI [Watt]"] - pairs["RSSI [Watt]"]
```

```
#6°: Compute the signal-to-interference-plus-noise ratio (SINR)
```

```
#pairs["SINR [Watt]"] = pairs["RSSI [Watt]"] / pairs["Interference [Watt]"].round(decimal
s = 4)
pairs["SINR [dB]"] = (10 * np.log10((pairs["RSSI [Watt]"] / pairs["Interference [Watt]"]
)).round(decimals = 2)
```

```
#7°: Define the ThroughPut from experimental data curve considering a 2x2 MIMO sysytem
```

```
RB = 50 # number of resarch block
xp = pd.Series([-25, -20, -10, -5, 0, 5, 10, 12, 15, 20, 25, 30, 35, 40, 45])
yp = pd.Series([0.000, 0.005, 0.010, 0.020, 0.100, 0.200, 0.340, 0.400, 0.520, 0.760, 1.0
00, 1.240, 1.340, 1.400, 1.440])
yp = yp * RB
#print(yp)
```

```
#plot the experimental cuve
#plt.xlabel('SINR (dB)')
#plt.ylabel('throughPut (Mbps)')
#plt.title("Experimental throughput curve [Mbps]", loc = "center", color = "darkred")
#plt.grid(color='grey', linestyle='-', linewidth=0.2)
#plt.plot(xp, yp, color='blue', marker='o', linestyle='-', linewidth=1.5, markersize=5)
#plt.savefig('throughput.png')
#plt.show()
#plt.close()
```

```
pairs["Throughput [Mbps]"] = (np.interp(pairs["SINR [dB]"], xp, yp)).round(decimals = 2)
#pairs.index = np.arange(1, len(pairs)+1)
#pairs.to_csv("reslod.txt", index = False, sep="\t", header = True)
print(pairs)
```

```
#8°: Definition of the user of each base station
```

```
Bs_cap = pd.DataFrame()
Bs_cap = pairs.loc[pairs.groupby(by=["id_Ue [-]"])[ "Throughput [Mbps]"].idxmax()]
```



```

Bs_cap.index = np.arange(1, len(Bs_cap)+1)
Bs_cap = Bs_cap.drop(columns=['frequency [GHz]', 'h_tot [m]', 'distance [m]', 'P_LOS', 'PL
[dB]', 'RSSI [dBm]',
                                'RSSI [Watt]', 'sum_RSSI [Watt]', 'Interference [Watt]',
                                'SINR [dB]'])
n_users = pd.DataFrame()
n_users["n_Ue_per_cluster [-]"] = users['users_per_cluster']
n_users.index = np.arange(1, len(Bs_cap)+1)
Bs_cap = pd.concat([Bs_cap, n_users], axis = 1)
Bs_cap.loc[Bs_cap["Throughput [Mbps]"] == 0, 'n_Ue_per_cluster [-]'] = 0
Bs_cap.to_csv("Bs_cap.txt", index = True, sep="\t", header = True)
Bs_cap.to_csv("throughput_miglioreUE.txt", index = False, sep="\t", header = True)
print(Bs_cap)

n_cluster_Bs = pd.DataFrame()
n_cluster_Bs["n of cluster per Bs [-]"] = Bs_cap['id_Bs [-]'].value_counts()
n_cluster_Bs["id_Bs [-]"] = n_cluster_Bs.index

n_cluster_Bs = n_cluster_Bs.sort_values(by=['id_Bs [-]'])
n_cluster_Bs.index = np.arange(0, len(n_cluster_Bs))
print(n_cluster_Bs)

nUe_Bs = Bs_cap.groupby(by=["id_Bs [-]"])[["n_Ue_per_cluster [-]"]].sum()
nUe_Bs = nUe_Bs.to_frame()
nUe_Bs.columns = ["n_Ue_Bs [-]"]
nUe_Bs["id_Bs [-]"] = nUe_Bs.index
nUe_Bs.index = np.arange(0, len(nUe_Bs))
print(nUe_Bs)

res_Bs = pd.merge(n_cluster_Bs, nUe_Bs, on = ['id_Bs [-]'])
res_Bs = res_Bs[['id_Bs [-]', 'n of cluster per Bs [-]', 'n_Ue_Bs [-]']]
res_Bs.columns = ["id_Bs", "n of cluster per Bs [-]", "n_Ue_Bs [-]"]
res_Bs.to_csv("res_Bs.txt", index = True, sep="\t", header = True)
print(res_Bs)

right_res = dataBs[['id_Bs', 'Cx_Bs', 'Cy_Bs']]
right_res.columns = ["id_Bs", "Cx_Bs [m]", "Cy_Bs [m]"]
#print(right_res)

df1 = pd.merge(right_res, res_Bs, on = "id_Bs")
#df1 = df1.set_index('id_Bs [-]')
#print(df1)

df2 = pd.DataFrame({'col1':range(0,len(dataBs)), 'n of cluster per Bs [-]':0, 'n_Ue_Bs [-]':0})
#print(df2)
df3 = pd.concat([df, df2], axis = 1)
df3 = df3.drop(columns=["col1"])
df3.columns = ["id_Bs", "n of cluster per Bs [-]", "n_Ue_Bs [-]"]
print(df3)
df3.to_csv("df3.txt", index = True, sep="\t", header = True)

df4 = pd.concat([res_Bs, df3], axis = 0)
df4.index = np.arange(0, len(df4))
print(df4)
df4 = df4.drop_duplicates(subset=['id_Bs'], keep='first')
df4 = df4.sort_values(by = ['id_Bs'])

```

```

df4.index = np.arange(0, len(df4))
print(df4)
df4.to_csv("df4.txt", index = True, sep="\t", header = True)

res_Bs_fin = pd.merge(df4, right_res, on = "id_Bs")
res_Bs_fin.to_csv("res_Bs_fin.txt", index = True, sep="\t", header = True)
print(res_Bs_fin)

f = pd.DataFrame()
f["frequency [GHz]"] = dataBs["frequency"]/1000
f.index = np.arange(0, len(f))
print(f)
res_Bs_fin = pd.concat([res_Bs_fin, f], axis = 1)
#res_Bs_fin = res_Bs_fin[["id_Bs [-]", "Cx_Bs [m]", "Cy_Bs [m]", "frequency [GHz]", "n of cluster per Bs [-]", "n_Ue_Bs [-]"]]
res_Bs_fin.to_csv("res_Bs_fin.txt", index = True, sep="\t", header = True)
print(res_Bs_fin)
#res_Bs_fin1 = res_Bs_fin.drop_duplicates(subset=['Cx_Bs [m]'], keep='first')

import matplotlib.ticker
from matplotlib.ticker import StrMethodFormatter
from matplotlib.ticker import ScalarFormatter
from matplotlib.ticker import FormatStrFormatter
from mpl_toolkits.axes_grid1 import make_axes_locatable

Turin = gpd.read_file("confine_tot.shp")
#print(Turin)
g_res_Bs_fin = gpd.GeoDataFrame(res_Bs_fin, geometry = gpd.points_from_xy(res_Bs_fin["Cx_Bs [m]"], res_Bs_fin["Cy_Bs [m]"]))
#gMacro_cell_res = g_res_Bs_fin[g_res_Bs_fin["frequency [GHz]"] == freq_B]
#gMicro_cell_res = g_res_Bs_fin[g_res_Bs_fin["frequency [GHz]"] == freq_A]
#print(gMicro_cell_res)
#print(g_res_Bs_fin)

#9°: Defining the Results for Base station based on their position (macro+micro)
Ue_per_Bs = pd.DataFrame()
Ue_per_Bs["sum per Bs [-]"] = res_Bs_fin.groupby(by=["Cx_Bs [m]"])[["n_Ue_Bs [-]"]].sum()
Ue_per_Bs["Cx_Bs [m]"] = Ue_per_Bs.index
Ue_per_Bs.index = np.arange(0, len(Ue_per_Bs))
print(Ue_per_Bs)
#Ue_per_Bs.to_csv("Ue_per_Bs.txt", index = True, sep="\t", header = True)
res_Bs_fin.index = np.arange(0, len(res_Bs_fin))

Bs_tot = pd.merge(res_Bs_fin, Ue_per_Bs, on = 'Cx_Bs [m]')
Bs_tot = Bs_tot.drop(columns = ["frequency [GHz]", "n of cluster per Bs [-]", "n_Ue_Bs [-]"])
Bs_tot = Bs_tot.drop_duplicates(subset=['Cx_Bs [m]'], keep='first')
Bs_tot.index = np.arange(0, len(Bs_tot))
print(Bs_tot)
Bs_tot.to_csv("Bs_tot.txt", index = True, sep="\t", header = True)

```

```

g_Bs_tot = gpd.GeoDataFrame(Bs_tot, geometry = gpd.points_from_xy(Bs_tot["Cx_Bs [m]"], Bs_tot["Cy_Bs [m]"]))
print(g_Bs_tot)

ax = plt.axes()
plt.xticks(rotation='vertical')
plt.ticklabel_format(axis="x", style="sci", scilimits=(3.8,4), useMathText= True)
plt.ticklabel_format(axis="y", style="sci", scilimits=(4.9,5), useMathText= True)
plt.xlabel('Est (mt)')
plt.ylabel('North (mt)')
Turin.plot(ax = ax, alpha = 1, color = "white", edgecolor = "black", linewidth = 1.5)
g_Bs_tot.plot(ax = ax, alpha = 1, column="sum per Bs [-]", marker = "o", cmap="plasma", scheme='natural_breaks', k = 8, markersize = 60, edgecolor="black", legend = True, legend_kwds={ 'title': 'Sum Ue by Bs', 'loc': 'upper left'})
plt.show()
plt.close()

#10°: Plotting the Results for the Ue Cluster based on the best Throughput that they have
u = pd.DataFrame()
u = users[['id_cluster', 'Cx_Ue', 'Cy_Ue']]
u.columns = ["id_Ue [-]", "Cx [m]", "Cy [m]"]
res_th_Ue = pd.merge(u, Bs_cap, on = "id_Ue [-]")
res_th_Ue.to_csv("res_th_Ue.txt", index = True, sep="\t", header = True)
print(res_th_Ue)

print("--- %s seconds ---" % (time.time() - start_time))

```

## 1.7 script to define the physical parameters for the equivalent models

```

#Definition of the libraries in use
import numpy as np
import pandas as pd
import json
import matplotlib.pyplot as plt
import scipy as sp
import pyproj as prj
import shapely as Shp
import time
import sympy as spy
import scipy.integrate as integrate
import scipy.special as special

start_time = time.time()

import scipy.integrate
from numpy import exp
from math import sqrt
import scipy.integrate
from numpy import exp

```

```

#get the derivate
x = spy.Symbol('x')
L = spy.Symbol('L')
y = (((x**2)/(2*(L**2)))*(3-(x/L)))
yd1 = spy.diff(y,x)
print("\n", yd1)
y1 = yd1
yd2 = spy.diff(y1,x)
print(yd2)

#import raw data for raw land towers
rawlandData = pd.read_csv('BTS_rawland_dati_input_per_M_e_K.txt', sep="\t", header=None,
skiprows=1)
rawlandData.columns = ["id_Bs", "Id_building", "Cx_Bs", "Cy_Bs", "link_BSC2", "struct", "
sect", "restrain", "provider", "Bbott", "Btop",
                        "h", "t", "Qant", "var_h", "SC", "MC", "P_V_bra", "S_V_bra", "H_br
ac", "found", "conn", "P-frame", "loadearthq",
                        "P_sec", "S_sec", "T_sec", "Yg", "yp", "ys", "yt", "A_Psec", "A_S
sec", "A_Tsec", "I_Psec", "I_Ssec", "I_Tsec",
                        "m_Psec", "m_Ssec", "m_Tsec"]

print(rawlandData)

struct_conf = rawlandData["SC"]
Mi = pd.DataFrame()
Ki = pd.DataFrame()
Wi = pd.DataFrame()
Ti = pd.DataFrame()

for i in range(len(struct_conf)):
    if (struct_conf[i] == "SC4") or (struct_conf[i] == "SC5"):
        #1_MONOPOLE RAW LAND TOWERS-----
        #data input
        t = rawlandData.loc[i].at['t']
        Dbott = rawlandData.loc[i].at['B_bott']
        Rbott = Dbott/2
        rbott = Rbott-t
        Abott = np.pi*((Rbott**2)-(rbott**2))
        Ibott = (np.pi/64)*(((Dbott)**4)-((Dbott-(2*t))**4))
        Dtop = rawlandData.loc[i].at['B_top']
        Rtop = Dtop/2
        rtop = Rtop-t
        Atop = np.pi*((Rtop**2)-(rtop**2))
        Itop = (np.pi/64)*(((Dtop)**4)-((Dtop-(2*t))**4))
        E = 210000
        gamma = 7.85*(10**(-8))
        L = rawlandData.loc[i].at['h']

        #definition of the constant
        a = Abott*gamma
        b = ((Atop*gamma)*(Abott*gamma))/L
        c = Ibott
        q = (Itop-Ibott)/L

        #calculution of general Mass and Stiffness
        f = lambda x : (a-b*x)*(((x**2)/(2*(L**2)))*(3-x/L))**2)
        i = scipy.integrate.quad(f, 0, L)
        print("\n",i)

```

```

g = lambda x : 0.0015*(((x**2)/(2*(L**2)))*(3-x/L))**2)
j = scipy.integrate.quad(g, 0, L)
print("\n",j)
G1 = i[0]*101.97
G2 = j[0]*101.97
G3 = 1*101.97
Mi = G1+G2+G3
print("\n",Mi)
Mi[i].to_csv("Mrawland.txt", index = False, sep="\t", header = False)
k = lambda x : E*(c-q*x)*(((3/L**2)-(3*x/(L**3)))**2)
Ki = scipy.integrate.quad(k, 0, L)
print("\n",Ki)
Ki[i].to_csv("Krawland.txt", index = False, sep="\t", header = False)

Wi[i] = Ki[i]/(Mi[i]*9.81)
Wi[i].to_csv("Krawland.txt", index = False, sep="\t", header = False)

Ti[i] = (2*np.pi)/Wi[i]

else:
    #2_LATTICE RAW LAND TOWERS-----
    #data input
    Bbott = rawlandData.loc[i].at['B_bott']
    Btop = rawlandData.loc[i].at['B_top']
    const = rawlandData.loc[i].at['var_h']
    Ygbott = Bbott/2
    Ygtop = Btop/2
    yp = rawlandData.loc[i].at['yp']
    ys = rawlandData.loc[i].at['ys']
    Isecp = rawlandData.loc[i].at['I_Psec']
    Asecp = rawlandData.loc[i].at['A_Psec']
    Isecs = rawlandData.loc[i].at['I_Ssec']
    Asecs = rawlandData.loc[i].at['A_Ssec']
    mPsec = rawlandData.loc[i].at['m_Psec']
    mSsec = rawlandData.loc[i].at['m_Ssec']
    mTsec = rawlandData.loc[i].at['m_Tsec']
    alfa = 0.5
    mbott = ((1/np.sin(0.52))*(4*mPsec))+(8*(1/np.sin(0.785))*Bbott*mSsec)+(4*(1/np.s
in(0.785))*Bbott*mTsec)+(4*Bbott*mTsec)+(4*(Bbott/2)*mSsec)
    mtop = (4*mPsec)+(8*Btop*mSsec)+(4*Btop*mSsec)+(4*Btop*mSsec)+(4*(Btop/2)*mSsec)
    Ibott = 4*(Isecp + Asecp*((yp-
Ygbott)**2)) + (alfa**(2/3))*np.sin(0.785)*(8*(Isecs + Asecs*((ys+Ygbott)**2)))
    Itop = 4*(Isecp + Asecp*((yp-
Ygtop)**2)) + (alfa**(2/3))*np.sin(0.785)*(8*(Isecs + Asecs*((ys+Ygtop)**2)))
    L1 = rawlandData.loc[i].at['h']

    #definition of the constant
    a1 = mbott
    b1 = (mtop - mbott)/(L1)
    c1 = mtop

    #calculation of general Mass
    fl1 = lambda x : (a1-b1*x)*(((x**2)/(2*(L1**2)))*(3-x/L1))**2)
    il1 = scipy.integrate.quad(fl1, 0, const*L1)
    print("\n",il1)
    fl2 = lambda x : (c1)*(((x**2)/(2*(L1**2)))*(3-x/L1))**2)
    il2 = scipy.integrate.quad(fl2, const*L1, L1)

```

```

print("\n",il2)
gl = lambda x : 1.5*(((x**2)/(2*(L1**2)))*(3-x/L1))**2)
j1 = scipy.integrate.quad(gl, 0, L1)
print("\n",j1)
G1 = il1[0]+il2[0]
G2 = j1[0]*101.97
G3 = 3*101.97
Mil = G1+G2+G3
print("\n",Mil)
Mi[i].to_csv("Mrawland.txt", index = False, sep="\t", header = False)

#definition of the constant
E = 210000
c1 = 1.0433*(10**11)
q1 = 5.0194*(10**6)
z1 = 3.942*(10**9)
L1 = L1*1000

#calculation of general Stiffness
k11 = lambda x : E*(c1-q1*x)*(((3/L1**2)-(3*x/(L1**3))))**2)
Kil1 = scipy.integrate.quad(k11, 0, const*L1)
print("\n",Kil1)
k12 = lambda x : E*z1*(((3/L1**2)-(3*x/(L1**3))))**2)
Kil2 = scipy.integrate.quad(k12, const*L1, L1)
print("\n",Kil2)
Kil = Kil1[0]/10 + Kil2[0]
print("\n",Kil)
Ki[i].to_csv("Krawland.txt", index = False, sep="\t", header = False)

Wi[i] = Ki[i]/(Mi[i]*9.81)
Wi[i].to_csv("Krawland.txt", index = False, sep="\t", header = False)

Ti[i] = (2*np.pi)/Wi[i]

print("--- %s seconds ---" % (time.time() - start_time))

```

## 1.8 script to assign the parameters to the towers

```

#Definition of the libraries in use
import numpy as np
import pandas as pd
import json
import matplotlib.pyplot as plt
import scipy as sp
import pyproj as prj
import shapely as Shp
import time
import sympy as spy
import scipy.integrate as integrate
import scipy.special as special

start_time = time.time()

```

```

import scipy.integrate
from numpy import exp
from math import sqrt
import scipy.integrate
from numpy import exp

#1_ Data Input
Primary_sec_Data = pd.read_csv('primary_sec_types_rawland_towers', sep="\t", header=None,
    skiprows=1)
Primary_sec_Data.columns = ["P_section", "A_Psec", "I_Psec", "m_Psec", "y_Psec"]
print(Primary_sec_Data)

Secondary_sec_Data = pd.read_csv('secondary_sec_types_rawland_towers', sep="\t", header=None,
    skiprows=1)
Secondary_sec_Data.columns = ["S_section", "A_Ssec", "I_Ssec", "m_Ssec", "y_Ssec"]
print(Primary_sec_Data)

Tertiary_sec_Data = pd.read_csv('tertiary_sec_types_rawland_towers', sep="\t", header=None,
    skiprows=1)
Tertiary_sec_Data.columns = ["T_section", "A_Tsec", "I_Tsec", "m_Tsec", "y_Tsec"]
print(Primary_sec_Data)

Horizontal_sec_Data = pd.read_csv('tertiary_sec_types_rawland_towers', sep="\t", header=None,
    skiprows=1)
Tertiary_sec_Data.columns = ["H_section", "A_Hsec", "m_Tsec"]
print(Primary_sec_Data)

Material_Data = pd.read_csv('material_data.txt', sep="\t", header=None, skiprows=1)
Material_Data.columns = ["MC", "type"]

RawData1 = pd.read_csv('RawData_rawland_tower.txt', sep="\t", header=None, skiprows=1)
RawData1.columns = ["id_Bs", "Id_building", "Cx_Bs", "Cy_Bs", "link_BSC", "structure", "se
c_v", "restrain", "type", "provider",
                    "Bbott_BTS", "Btop_BTS", "h_BTS", "t", "SC", "h_var_coeff", "Qant", "
PV_brac", "STV_brac", "H_brac",
                    "found", "conn", "PF", "coat", "earthq"]
print(RawData1)

#2_assignment of characteristics rawland
struct_conf = pd.DataFrame()
struct_conf = RawData1["SC"]
Par_rawland_tower = pd.DataFrame()
for i in range(len(struct_conf)):
    if (struct_conf[i] == "SC1"):
        Par_rawland_tower["MC"] == Material_Data[0]
        Par_rawland_tower["type"] == Material_Data[0]
        if((RawData1["h_BTS"][i] <= 25 and RawData1["Bbott_BTS"][i] <= 3500) or RawData1
["Qant"][i] == 1.5):
            Par_rawland_tower["Psec"] = Primary_sec_Data["P_section"][4]
            Par_rawland_tower["Ssec"] = Secondary_sec_Data["S_section"][4]
            Par_rawland_tower["Tsec"] = Tertiary_sec_Data["T_section"][4]
            Par_rawland_tower["Tsec"] = Horizontal_sec_Data["H_section"][4]
            if((RawData1["h_BTS"][i] <= 30 and RawData1["Bbott_BTS"][i] <= 4000) or RawData1
["Qant"][i] == 3):
                Par_rawland_tower["Psec"] = Primary_sec_Data["P_section"][3]

```



```

        Par_rawland_tower["Ssec"] = Secondary_sec_Data["S_section"][3]
        Par_rawland_tower["Tsec"] = Tertiary_sec_Data["T_section"][3]
        Par_rawland_tower["Tsec"] = Horizontal_sec_Data["H_section"][3]
        if((RawData1["h_BTS"][i] <= 35 and RawData1["Bbott_BTS"][i] <= 4500) or RawData1
["Qant"][i] == 4.5):
            Par_rawland_tower["Psec"] = Primary_sec_Data["P_section"][2]
            Par_rawland_tower["Ssec"] = Secondary_sec_Data["S_section"][2]
            Par_rawland_tower["Tsec"] = Tertiary_sec_Data["T_section"][2]
            Par_rawland_tower["Tsec"] = Horizontal_sec_Data["H_section"][2]
            if((RawData1["h_BTS"][i] <= 40 and RawData1["Bbott_BTS"][i] <= 5000) or RawData1
["Qant"][i] == 6):
                Par_rawland_tower["Psec"] = Primary_sec_Data["P_section"][1]
                Par_rawland_tower["Ssec"] = Secondary_sec_Data["S_section"][1]
                Par_rawland_tower["Tsec"] = Tertiary_sec_Data["T_section"][1]
                Par_rawland_tower["Tsec"] = Horizontal_sec_Data["H_section"][1]
                if((RawData1["h_BTS"][i] <= 45 and RawData1["Bbott_BTS"][i] <= 5500) or RawData1
["Qant"][i] == 7.5):
                    Par_rawland_tower["Psec"] = Primary_sec_Data["P_section"][0]
                    Par_rawland_tower["Ssec"] = Secondary_sec_Data["S_section"][0]
                    Par_rawland_tower["Tsec"] = Tertiary_sec_Data["T_section"][0]
                    Par_rawland_tower["Tsec"] = Horizontal_sec_Data["H_section"][0]
                if (struct_conf[i] == "SC2"):
                    Par_rawland_tower["MC"] == Material_Data[1]
                    Par_rawland_tower["type"] == Material_Data[1]
                    if((RawData1["h_BTS"][i] <= 25 and RawData1["Bbott_BTS"][i] <= 2000) or RawData1
["Qant"][i] == 1.5):
                        Par_rawland_tower["Psec"] = Primary_sec_Data["P_section"][5]
                        Par_rawland_tower["Ssec"] = Secondary_sec_Data["S_section"][5]
                        Par_rawland_tower["Tsec"] = Tertiary_sec_Data["T_section"][5]
                        Par_rawland_tower["Tsec"] = Horizontal_sec_Data["H_section"][5]
                        if((RawData1["h_BTS"][i] <= 30 and RawData1["Bbott_BTS"][i] <= 2500) or RawData1
["Qant"][i] == 3):
                            Par_rawland_tower["Psec"] = Primary_sec_Data["P_section"][4]
                            Par_rawland_tower["Ssec"] = Secondary_sec_Data["S_section"][4]
                            Par_rawland_tower["Tsec"] = Tertiary_sec_Data["T_section"][4]
                            Par_rawland_tower["Tsec"] = Horizontal_sec_Data["H_section"][4]
                            if((RawData1["h_BTS"][i] <= 35 and RawData1["Bbott_BTS"][i] <= 3000) or RawData1
["Qant"][i] == 4.5):
                                Par_rawland_tower["Psec"] = Primary_sec_Data["P_section"][3]
                                Par_rawland_tower["Ssec"] = Secondary_sec_Data["S_section"][3]
                                Par_rawland_tower["Tsec"] = Tertiary_sec_Data["T_section"][3]
                                Par_rawland_tower["Tsec"] = Horizontal_sec_Data["H_section"][3]
                            if (struct_conf[i] == "SC3"):
                                Par_rawland_tower["MC"] == Material_Data[1]
                                Par_rawland_tower["type"] == Material_Data[1]
                                if((RawData1["h_BTS"][i] <= 20 and RawData1["Bbott_BTS"][i] <= 1000) or RawData1
["Qant"][i] == 1.5):
                                    Par_rawland_tower["Psec"] = Primary_sec_Data["P_section"][6]
                                    Par_rawland_tower["Ssec"] = Secondary_sec_Data["S_section"][6]
                                    Par_rawland_tower["Tsec"] = Tertiary_sec_Data["T_section"][6]
                                    Par_rawland_tower["Tsec"] = Horizontal_sec_Data["H_section"][6]
                                    if((RawData1["h_BTS"][i] <= 25 and RawData1["Bbott_BTS"][i] <= 1500) or RawData1
["Qant"][i] == 3):
                                        Par_rawland_tower["Psec"] = Primary_sec_Data["P_section"][5]
                                        Par_rawland_tower["Ssec"] = Secondary_sec_Data["S_section"][5]
                                        Par_rawland_tower["Tsec"] = Tertiary_sec_Data["T_section"][5]
                                        Par_rawland_tower["Tsec"] = Horizontal_sec_Data["H_section"][5]

```

```

        if((RawData1["h_BTS"][i] <= 30 and RawData1["Bbott_BTS"][i] <= 2000) or RawData1
["Qant"][i] == 4.5):
            Par_rawland_tower["Psec"] = Primary_sec_Data["P_section"][4]
            Par_rawland_tower["Ssec"] = Secondary_sec_Data["S_section"][4]
            Par_rawland_tower["Tsec"] = Tertiary_sec_Data["T_section"][4]
            Par_rawland_tower["Tsec"] = Horizontal_sec_Data["H_section"][4]

rawlandData = pd.DataFrame()
rawlandData = pd.merge(RawData1, Primary_sec_Data, on = 'Psection')
rawlandData = pd.merge(RawData1, Secondary_sec_Data, on = 'Ssection')
rawlandData = pd.merge(RawData1, Tertiary_sec_Data, on = 'Tsection')
rawlandData = pd.merge(RawData1, Horizontal_sec_Data, on = 'Hsection')
rawlandData = pd.merge(RawData1, Material_Data, on = 'MC')

rawlandData.to_csv("BTS_rawland_dati_input_per_M_e_K.txt", index = False, sep="\t", heade
r = False)

#3_assignment of characteristics rooftop
struct_conf = pd.DataFrame()
struct_conf = Rooftop1["SC"]
Par_rooftop_tower = pd.DataFrame()
for i in range(len(struct_conf)):
    if (struct_conf[i] == "SC1"):
        Par_rooftop_tower["MC"] == Material_Data[0]
        Par_roofotp_tower["type"] == Material_Data[0]
        if((rooftop1["h_BTS"][i] <= 25 and RawData1["Bbott_BTS"][i] <= 3500) or RawData
1["Qant"][i] == 1.5):
            Par_rooftop_tower["Psec"] = Primary_sec_Data["P_section"][4]
            Par_rooftop_tower["Ssec"] = Secondary_sec_Data["S_section"][4]
            Par_rooftop_tower["Tsec"] = Tertiary_sec_Data["T_section"][4]
            Par_rooftop_tower["Tsec"] = Horizontal_sec_Data["H_section"][4]
        if((RawData1["h_BTS"][i] <= 30 and RawData1["Bbott_BTS"][i] <= 4000) or RawData1
["Qant"][i] == 3):
            Par_rooftop_tower["Psec"] = Primary_sec_Data["P_section"][3]
            Par_rooftop_tower["Ssec"] = Secondary_sec_Data["S_section"][3]
            Par_rooftop_tower["Tsec"] = Tertiary_sec_Data["T_section"][3]
            Par_rooftop_tower["Tsec"] = Horizontal_sec_Data["H_section"][3]
        if((RawData1["h_BTS"][i] <= 35 and RawData1["Bbott_BTS"][i] <= 4500) or RawData1
["Qant"][i] == 4.5):
            Par_rooftop_tower["Psec"] = Primary_sec_Data["P_section"][2]
            Par_rooftop_tower["Ssec"] = Secondary_sec_Data["S_section"][2]
            Par_rooftop_tower["Tsec"] = Tertiary_sec_Data["T_section"][2]
            Par_rooftop_tower["Tsec"] = Horizontal_sec_Data["H_section"][2]
        if((RawData1["h_BTS"][i] <= 40 and RawData1["Bbott_BTS"][i] <= 5000) or RawData1
["Qant"][i] == 6):
            Par_rooftop_tower["Psec"] = Primary_sec_Data["P_section"][1]
            Par_rooftop_tower["Ssec"] = Secondary_sec_Data["S_section"][1]
            Par_rooftop_tower["Tsec"] = Tertiary_sec_Data["T_section"][1]
            Par_rooftop_tower["Tsec"] = Horizontal_sec_Data["H_section"][1]
        if((RawData1["h_BTS"][i] <= 45 and RawData1["Bbott_BTS"][i] <= 5500) or RawData1
["Qant"][i] == 7.5):
            Par_rooftop_tower["Psec"] = Primary_sec_Data["P_section"][0]
            Par_rooftop_tower["Ssec"] = Secondary_sec_Data["S_section"][0]
            Par_rooftop_tower["Tsec"] = Tertiary_sec_Data["T_section"][0]
            Par_rooftop_tower["Tsec"] = Horizontal_sec_Data["H_section"][0]
    if (struct_conf[i] == "SC2"):
        Par_rooftop_tower["MC"] == Material_Data[1]

```

```

        Par_rooftop_tower["type"] == Material_Data[1]
        if((RawData1["h_BTS"][i] <= 25 and RawData1["Bbott_BTS"][i] <= 2000) or RawData1
["Qant"][i] == 1.5):
            Par_rooftop_tower["Psec"] = Primary_sec_Data["P_section"][5]
            Par_rooftop_tower["Ssec"] = Secondary_sec_Data["S_section"][5]
            Par_rooftop_tower["Tsec"] = Tertiary_sec_Data["T_section"][5]
            Par_rooftop_tower["Tsec"] = Horizontal_sec_Data["H_section"][5]
            if((RawData1["h_BTS"][i] <= 30 and RawData1["Bbott_BTS"][i] <= 2500) or RawData1
["Qant"][i] == 3):
                Par_rooftop_tower["Psec"] = Primary_sec_Data["P_section"][4]
                Par_rooftop_tower["Ssec"] = Secondary_sec_Data["S_section"][4]
                Par_rooftop_tower["Tsec"] = Tertiary_sec_Data["T_section"][4]
                Par_rooftop_tower["Tsec"] = Horizontal_sec_Data["H_section"][4]
                if((RawData1["h_BTS"][i] <= 35 and RawData1["Bbott_BTS"][i] <= 3000) or RawData1
["Qant"][i] == 4.5):
                    Par_rooftop_tower["Psec"] = Primary_sec_Data["P_section"][3]
                    Par_rooftop_tower["Ssec"] = Secondary_sec_Data["S_section"][3]
                    Par_rooftop_tower["Tsec"] = Tertiary_sec_Data["T_section"][3]
                    Par_rooftop_tower["Tsec"] = Horizontal_sec_Data["H_section"][3]
            if (struct_conf[i] == "SC3"):
                Par_rooftop_tower["MC"] == Material_Data[1]
                Par_rooftop_tower["type"] == Material_Data[1]
                if((RawData1["h_BTS"][i] <= 20 and RawData1["Bbott_BTS"][i] <= 1000) or RawData1
["Qant"][i] == 1.5):
                    Par_rooftop_tower["Psec"] = Primary_sec_Data["P_section"][6]
                    Par_rooftop_tower["Ssec"] = Secondary_sec_Data["S_section"][6]
                    Par_rooftop_tower["Tsec"] = Tertiary_sec_Data["T_section"][6]
                    Par_rooftop_tower["Tsec"] = Horizontal_sec_Data["H_section"][6]
                    if((RawData1["h_BTS"][i] <= 25 and RawData1["Bbott_BTS"][i] <= 1500) or RawData1
["Qant"][i] == 3):
                        Par_rooftop_tower["Psec"] = Primary_sec_Data["P_section"][5]
                        Par_rooftop_tower["Ssec"] = Secondary_sec_Data["S_section"][5]
                        Par_rooftop_tower["Tsec"] = Tertiary_sec_Data["T_section"][5]
                        Par_rooftop_tower["Tsec"] = Horizontal_sec_Data["H_section"][5]
                        if((RawData1["h_BTS"][i] <= 30 and RawData1["Bbott_BTS"][i] <= 2000) or RawData1
["Qant"][i] == 4.5):
                            Par_rooftop_tower["Psec"] = Primary_sec_Data["P_section"][4]
                            Par_rooftop_tower["Ssec"] = Secondary_sec_Data["S_section"][4]
                            Par_rooftop_tower["Tsec"] = Tertiary_sec_Data["T_section"][4]
                            Par_rooftop_tower["Tsec"] = Horizontal_sec_Data["H_section"][4]

rooftopData = pd.DataFrame()
rooftopData = pd.merge(RoofData1, Primary_sec_Data, on = 'Psection')
rooftopData = pd.merge(RoofData1, Secondary_sec_Data, on = 'Ssection')
rooftopData = pd.merge(RoofData1, Tertiary_sec_Data, on = 'Tsection')
rooftopData = pd.merge(RoofData1, Horizontal_sec_Data, on = 'Hsection')
rooftopData = pd.merge(RoofData1, Material_Data, on = 'MC')

rooftopData.to_csv("BTS_rawland_dati_input_per_M_e_K.txt", index = False, sep="\t", heade
r = False)

print("--- %s seconds ---" % (time.time() - start_time))

```

## 1.9 script to display the indices results

```
#Definition of the libraries in use
import numpy as np
import pandas as pd
import matplotlib.pyplot as plt
import scipy as sp
import pyproj as prj
import shapely as Shp
import geopandas as gpd
import contextily as ctx

#Definition and import of input data about first provider's Base station
dataBs = pd.read_csv('BTS_tim_DEFINITIVA.txt', sep=";", header=None)
dataBs.columns = ["id_Bs", "Id_building", "Cx", "Cy", "band", "typeofBs", "Typeofstruc",
                 "frequency", "material", "typeofcell",
                 "link_BSC", "h_building", "h_Bs", "h_tot"]

#print(dataBs)
#plot the experimental cuve
plt.xlabel('SINR (dB)')
plt.ylabel('throughPut (Mbps)')
plt.title("Experimental throughput curve [Mbps]", loc = "center", color = "darkred")
plt.grid(color='grey', linestyle='-', linewidth=0.2)
plt.plot(xp, yp, color='blue', marker='o', linestyle='-', linewidth=1.5, markersize=5)
plt.savefig('throughput.png')
plt.show()
plt.close()
Throughput = np.interp(SINR_dB, xp, yp)
Throughput = pd.Series(Throughput)
Throughput = Throughput.round(decimals=4)
print(Throughput)
Throughput.to_csv("throughput.txt", index = False, sep="\t", header = False)
ind_maxBs = Throughput.idxmax()
Bs_max = dataBs.iloc[[ind_maxBs]]
print(ind_maxBs)

#Data merging
result_UE = pd.concat([id_Bs, PL, RSSI, SINR_dB, Throughput, Cell, Cx_Bs, Cy_Bs], axis =
1, keys = ["id_Bs [-]", "Path Loss [dB]", "RSSI [dB]",
          "SINR [dB]", "Throughput [Mbps]", "type.of.cell [-]",
          "Cx_Bs [m]", "Cy_Bs [m]"])
print(result_UE)
#Now we save the results in a .txt file
result_UE.to_csv("Result.txt", index = False, sep="\t", header = True)
import matplotlib.ticker
from matplotlib.ticker import StrMethodFormatter
from matplotlib.ticker import ScalarFormatter
from matplotlib.ticker import FormatStrFormatter
```

```

from mpl_toolkits.axes_grid1 import make_axes_locatable
#plot the borders of Turin city
Turin = gpd.read_file("confine_tot.shp")
#Turin = Turin.to_crs(epsg=3857)
#ax = Turin.plot(alpha = 0.5, facecolor="none", edgecolor="darkblue", linewidth=2.5)
#ctx.add_basemap(ax, url = ctx.providers.OpenStreetMap.Mapnik)
#plt.ylabel('coordinate y (mt)')
#plt.xticks(rotation='vertical')
#plt.title("City borders", loc = "center", color = "darkred")
#plt.ticklabel_format(axis="x", style="sci", scilimits=(3.8,4), useMathText= True)
#plt.ticklabel_format(axis="y", style="sci", scilimits=(4.9,5), useMathText= True)
#ax.set_axis_off()
#plt.savefig('turin_try.png', dpi = 1000)
#lt.show()
#plt.close()

#plot the Base stations and the user chosen
gdf = gpd.GeoDataFrame(dataBs, geometry = gpd.points_from_xy(dataBs.Cx, dataBs.Cy))
gUE = gpd.GeoDataFrame(user, geometry = gpd.points_from_xy(user.Cx, user.Cy))
#print(gUE)
bounding_box = [gdf["geometry"].x.min(), gdf["geometry"].x.max(), gdf["geometry"].y.min(),
, gdf["geometry"].y.max()]
Macro_cell = gdf[gdf["typeofcell"] == "Macro_cell"]
Micro_cell = gdf[gdf["typeofcell"] == "Micro_cell"]
ax = plt.axes()
Turin = Turin.to_crs(epsg=32632)
plt.xticks(rotation='vertical')
plt.ticklabel_format(axis="x", style="sci", scilimits=(3.8,4), useMathText= True)
plt.ticklabel_format(axis="y", style="sci", scilimits=(4.9,5), useMathText= True)
plt.xlabel('Est (mt)')
plt.ylabel('Nord (mt)')
ax.set_xlim(bounding_box[0]-1000, bounding_box[1]+2000)
ax.set_ylim(bounding_box[2]-1000, bounding_box[3]+2000)
Turin.plot(ax = ax, alpha = 1, color = "white", edgecolor = "black", linewidth = 1.5)
Macro_cell.plot(ax = ax, alpha = 0.8, color = "deepskyblue", marker = "o", markersize = 40, edgecolor="black" )
Micro_cell.plot(ax = ax, alpha = 1, color = "blue", marker = "o", markersize = 8, edgecolor="black" )
gUE.plot(ax = ax, alpha = 1, color = "orange", marker = "X", markersize = 50, edgecolor="black")
plt.legend(('Macro_cell', 'Micro_cell', 'User Cluster'))
plt.savefig('Bs.png', dpi = 300)
plt.show()
plt.close()

#plot the Results for the user chosen
gresult_UE = gpd.GeoDataFrame(result_UE, geometry = gpd.points_from_xy(dataBs.Cx, dataBs.Cy))
Macro_cell_Res = gresult_UE[gresult_UE["type.of.cell [-]"] == "Macro_cell"]
Micro_cell_Res = gresult_UE[gresult_UE["type.of.cell [-]"] == "Micro_cell"]

```

```

# print(Macro_cell_Res)

fig, (ax1, ax2) = plt.subplots(1, 2)

ax1.ticklabel_format(axis="x", style="sci", scilimits=(3.8,4), useMathText= True)
ax1.ticklabel_format(axis="y", style="sci", scilimits=(4.9,5), useMathText= True)
plt.setp(ax1.get_xticklabels(), rotation=90, ha='right')
ax1.set_xlabel('Est (mt)')
ax1.set_ylabel('Nord (mt)')
# ax1.axis('off')
ax1.set_title('BTS Macro cell')
ax2.ticklabel_format(axis="x", style="sci", scilimits=(3.8,4), useMathText= True)
ax2.ticklabel_format(axis="y", style="sci", scilimits=(4.9,5), useMathText= True)
plt.setp(ax2.get_xticklabels(), rotation=90, ha='right')
ax2.set_xlabel('Est (mt)')
ax2.set_ylabel('Nord (mt)')
# ax2.axis('off')
ax2.set_title('BTS Micro cell')
divider1 = make_axes_locatable(ax1)
divider2 = make_axes_locatable(ax2)
cax1 = divider1.append_axes("right", size="5%", pad=0.1)
cax2 = divider2.append_axes("right", size="5%", pad=0.1)
# Turin.plot(ax=ax1, alpha = 1, color = "white", edgecolor = "black", linewidth = 1.5)
Macro_cell_Res.plot(ax=ax1, column="Path Loss [dB]", marker = "o", cmap="plasma", marker
size = 10, legend = True, legend_kwds={'label': "[dB]"}, cax = cax1)
gUE.plot(ax = ax1, alpha = 1, color = "green", marker = "x", markersize = 30)
# ax1.legend([U], ('user cluster position'), loc = 'upper left')
# Turin.plot(ax=ax2, alpha = 1, color = "white", edgecolor = "black", linewidth = 1.5)
Micro_cell_Res.plot(ax=ax2, column="Path Loss [dB]", marker = "o", cmap="plasma", marker
size = 10, legend = True, legend_kwds={'label': "[dB]"}, cax = cax2)
gUE.plot(ax = ax2, alpha = 1, color = "green", marker = "x", markersize = 30)
plt.subplots_adjust(left=None, bottom=None, right=None, top=None, wspace=0.3, hspace=None
)
fig.suptitle("Path Loss Results [dB]")
ax1.legend(loc='upper left', shadow=True, fontsize='x-large')
plt.savefig('PathLossResult.tif', dpi = 300)
plt.show()
plt.close()

fig, (ax1, ax2) = plt.subplots(1, 2)
ax1.ticklabel_format(axis="x", style="sci", scilimits=(3.8,4), useMathText= True)
ax1.ticklabel_format(axis="y", style="sci", scilimits=(4.9,5), useMathText= True)
plt.setp(ax1.get_xticklabels(), rotation=90, ha='right')
ax1.set_xlabel('Est (mt)')
ax1.set_ylabel('Nord (mt)')
ax1.set_title('Macro_cell')
ax2.ticklabel_format(axis="x", style="sci", scilimits=(3.8,4), useMathText= True)
ax2.ticklabel_format(axis="y", style="sci", scilimits=(4.9,5), useMathText= True)
plt.setp(ax2.get_xticklabels(), rotation=90, ha='right')

```

```

ax2.set_xlabel('Est (mt)')
ax2.set_ylabel('Nord (mt)')
ax2.set_title('Micro_cell')
divider1 = make_axes_locatable(ax1)
divider2 = make_axes_locatable(ax2)
cax1 = divider1.append_axes("right", size="5%", pad=0.1)
cax2 = divider2.append_axes("right", size="5%", pad=0.1)
Turin.plot(ax=ax1, alpha = 1, color = "white", edgecolor = "black", linewidth = 1.5)
Macro_cell_Res.plot(ax=ax1, column="RSSI [dB]", marker = "o", cmap="plasma", markersize
= 60, edgecolor="black", legend = True, legend_kwds={'label': "[dBm]"}, cax = cax1)
gUE.plot(ax = ax1, alpha = 1, color = "green", marker = "X", markersize = 80, edgecolor="
black")
Turin.plot(ax=ax2, alpha = 1, color = "white", edgecolor = "black", linewidth = 1.5)
Micro_cell_Res.plot(ax=ax2, column="RSSI [dB]", marker = "o", cmap="plasma", markersize
= 60, edgecolor="black", legend = True, legend_kwds={'label': "[dBm]"}, cax = cax2)
gUE.plot(ax = ax2, alpha = 1, color = "green", marker = "X", markersize = 80, edgecolor="
black")
plt.subplots_adjust(left=None, bottom=None, right=None, top=None, wspace=0.3, hspace=None
)
plt.savefig('RSSIResult.png', dpi = 600)
fig.suptitle("RSSI Results [dBm]")
plt.show()
plt.close()

```

```

fig, (ax1, ax2) = plt.subplots(1, 2)
ax1.ticklabel_format(axis="x", style="sci", scilimits=(3.8,4), useMathText= True)
ax1.ticklabel_format(axis="y", style="sci", scilimits=(4.9,5), useMathText= True)
plt.setp(ax1.get_xticklabels(), rotation=90, ha='right')
ax1.set_xlabel('Est (mt)')
ax1.set_ylabel('Nord (mt)')
ax1.set_title('Macro_cell')
ax2.ticklabel_format(axis="x", style="sci", scilimits=(3.8,4), useMathText= True)
ax2.ticklabel_format(axis="y", style="sci", scilimits=(4.9,5), useMathText= True)
plt.setp(ax2.get_xticklabels(), rotation=90, ha='right')
ax2.set_xlabel('Est (mt)')
ax2.set_ylabel('Nord (mt)')
ax2.set_title('Micro_cell')
divider1 = make_axes_locatable(ax1)
divider2 = make_axes_locatable(ax2)
cax1 = divider1.append_axes("right", size="5%", pad=0.1)
cax2 = divider2.append_axes("right", size="5%", pad=0.1)
Turin.plot(ax=ax1, alpha = 1, color = "white", edgecolor = "black", linewidth = 1.5)
Macro_cell_Res.plot(ax=ax1, column="SINR [dB]", marker = "o", cmap="plasma", markersize
= 60, edgecolor="black", legend = True, legend_kwds={'label': "[dB]"}, cax = cax1)
gUE.plot(ax = ax1, alpha = 1, color = "green", marker = "X", markersize = 80, edgecolor="
black")
Turin.plot(ax=ax2, alpha = 1, color = "white", edgecolor = "black", linewidth = 1.5)

```



```

Micro_cell_Res.plot(ax=ax2, column="SINR [dB]", marker = "o", cmap="plasma", markersize
= 60, edgecolor="black", legend = True, legend_kwds={'label': "[dB]"}, cax = cax2)
gUE.plot(ax = ax2, alpha = 1, color = "green", marker = "X", markersize = 80, edgecolor="
black")
plt.subplots_adjust(left=None, bottom=None, right=None, top=None, wspace=0.3, hspace=None
)
plt.savefig('SINRResult.png', dpi = 600)
fig.suptitle("SINR Results [dB]")
plt.show()
plt.close()

```

```

fig, (ax1, ax2) = plt.subplots(1, 2)
ax1.ticklabel_format(axis="x", style="sci", scilimits=(3.8,4), useMathText= True)
ax1.ticklabel_format(axis="y", style="sci", scilimits=(4.9,5), useMathText= True)
plt.setp(ax1.get_xticklabels(), rotation=90, ha='right')
ax1.set_xlabel('Est (mt)')
ax1.set_ylabel('Nord (mt)')
ax1.set_title('Macro_cell')
ax2.ticklabel_format(axis="x", style="sci", scilimits=(3.8,4), useMathText= True)
ax2.ticklabel_format(axis="y", style="sci", scilimits=(4.9,5), useMathText= True)
plt.setp(ax2.get_xticklabels(), rotation=90, ha='right')
ax2.set_xlabel('Est (mt)')
ax2.set_ylabel('Nord (mt)')
ax2.set_title('Micro_cell')
divider1 = make_axes_locatable(ax1)
divider2 = make_axes_locatable(ax2)
cax1 = divider1.append_axes("right", size="5%", pad=0.1)
cax2 = divider2.append_axes("right", size="5%", pad=0.1)
Turin.plot(ax=ax1, alpha = 1, color = "white", edgecolor = "black", linewidth = 1.5)
Macro_cell_Res.plot(ax=ax1, column="Throughput [Mbps]", marker = "o", cmap="PiYG", marke
rsize = 60, edgecolor="black", legend = True, legend_kwds={'label': "[Mbps]"}, cax = cax1
)
gUE.plot(ax = ax1, alpha = 1, color = "red", marker = "X", markersize = 80, edgecolor="bl
ack")
Turin.plot(ax=ax2, alpha = 1, color = "white", edgecolor = "black", linewidth = 1.5)
Micro_cell_Res.plot(ax=ax2, column="Throughput [Mbps]", marker = "o", cmap="PiYG", marke
rsize = 60, edgecolor="black", legend = True, legend_kwds={'label': "[Mbps]"}, cax = cax2
)
gUE.plot(ax = ax2, alpha = 1, color = "red", marker = "X", markersize = 80, edgecolor="bl
ack")
plt.subplots_adjust(left=None, bottom=None, right=None, top=None, wspace=0.3, hspace=None
)
plt.savefig('ThroughputResult.png', dpi = 600)
fig.suptitle("Throughput Results [Mbps]")
plt.show()
plt.close()

```

```

gBs_max = gpd.GeoDataFrame(Bs_max, geometry = gpd.points_from_xy(Bs_max.Cx, Bs_max.Cy))

```

```

ax = plt.axes()
Turin = Turin.to_crs(epsg=32632)
plt.xticks(rotation='vertical')
plt.ticklabel_format(axis="x", style="sci", scilimits=(3.8,4), useMathText= True)
plt.ticklabel_format(axis="y", style="sci", scilimits=(4.9,5), useMathText= True)
plt.xlabel('Est (mt)')
plt.ylabel('Nord (mt)')
ax.set_xlim(bounding_box[0]-1000, bounding_box[1]+2000)
ax.set_ylim(bounding_box[2]-1000, bounding_box[3]+2000)
Turin.plot(ax = ax, alpha = 1, color = "white", edgecolor = "black", linewidth = 1.5)
gBs_max.plot(ax = ax, alpha = 1, color = "Blue", marker = "o", markersize = 120, edgecolor=
r="black")
gUE.plot(ax = ax, alpha = 1, color = "orange", marker = "X", markersize = 100, edgecolor=
"black")
plt.savefig('Bs_collegata.png', dpi = 300)
plt.show()
plt.close()

```



*“Intelligence is the ability to  
adapt to change.”*

*Stephen Hawking*

